NASA TECHNICAL MEMORANDUM

NASA TM X-2278

ATLAS-CENTAUR AC-19 AND AC-20 PERFORMANCE FOR THE 1969 MARINER MARS MISSIONS

by Lewis Research Center Staff

Lewis Research Center
Cleveland, Ohio 44135

NATIONAL AERONAUTICS AND SPACE ADMINISTRATION • WASHINGTON, D. C. • JULY 1971

1. Report No.	2. Government Accession No.	3. Recipient's Catalog No.
NASA TM X-2278		

4. Title and Subtitle	5. Report Date
ATLAS-CENTAUR AC-19 AND AC-20 PERFORMANCE FOR THE 1969 MARINER MARS MISSIONS	July 1971
	6. Performing Organization Code
7. Author(s)	8. Performing Organization Report No.
Lewis Research Center	E-6013
	10. Work Unit No.
9. Performing Organization Name and Address	491-02
Lewis Research Center National Aeronautics and Space Administration Cleveland, Ohio 44135	11. Contract or Grant No.
	13. Type of Report and Period Covered
12. Sponsoring Agency Name and Address	Technical Memorandum
National Aeronautics and Space Administration Washington, D.C. 20546	14. Sponsoring Agency Code

15. Supplementary Notes

16. Abstract

Atlas-Centaur launch vehicles AC-20 and AC-19, using a direct (one burn) mode of ascent, successfully placed Mariners VI and VII, respectively, into heliocentric transfer trajectories to the planet Mars in the first calendar quarter of 1969. Mariner VI flew by Mars on an equatorial pass of the planet on July 31, 1969. Five days later, on August 5, Mariner VII passed by the south pole of the planet Mars. This report discusses the flight performance of the AC-20 and AC-19 launch vehicles from lift-off through the Centaur maneuvers following spacecraft separation.

17. Key Words (Suggested by Author(s))	18. Distribution Statement
	Unclassified - unlimited

19. Security Classif. (of this report)	20. Security Classif. (of this page)	21. No. of Pages	22. Price*
Unclassified	Unclassified	165	$3.00

*For sale by the National Technical Information Service, Springfield, Virginia 22151

CONTENTS

ATLAS-CENTAUR AC-19 AND AC-20 PERFORMANCE FOR THE 1969 MARINER MARS MISSIONS

I. SUMMARY

by Edwin T. Muckley

Atlas-Centaur vehicle AC-20 successfully launched the Mariner VI spacecraft from Eastern Test Range (ETR) Complex 36B on February 24, 1969, at 2029:02 hours eastern standard time. Its companion spacecraft, Mariner VII, was successfully launched by AC-19 from ETR Complex 36A on March 27, 1969, at 1722:01 hours eastern standard time. Both vehicles utilized the direct-ascent mode to inject the spacecraft into type I heliocentric transfer trajectories to the planet Mars. Orbital insertion was accurate for both Mariner VI and Mariner VII and only a small midcourse correction was required for each spacecraft. For the Mariner VI spacecraft, a midcourse correction of 2.18 meters per second (at 10 days, miss plus time of flight) would have been required to meet the target specification conditions at encounter. The Mariner VII spacecraft would have required a correction of 2.01 meters per second to meet the encounter target specification conditions. Mariners VI and VII were targeted for a flyby of Mars on July 31 and August 5, 1969, respectively. The spacecraft missions were successful.

The AC-20 and AC-19 vehicles were the first Atlas-Centaur vehicles to be used in a planetary mission.

This report evaluates the flight performance of the Atlas-Centaur launch vehicles for the Mariner Mars 1969 missions, from lift-off through Centaur deflection maneuvers after spacecraft separation. The two flights were so similar that they are combined into one report.

II. INTRODUCTION

The purpose of the Mariner Mars 1969 missions was to obtain scientific data on the physical characteristics of the planet Mars and the composition of the Martian atmosphere. Previous Mariners (I to V) were launched by Atlas-Agena vehicles. Mariners I and II were launched toward Venus in 1962. Mariner I was unsuccessful due to a booster malfunction. Mariner II performed the first successful flyby of Venus in December 1962. Mariners III and IV were launched toward Mars in November 1964. Mariner III was unsuccessful due to failure of the nose fairing to separate. Mariner IV performed a successful flyby of Mars in July 1965. Mariner V was launched toward Venus in June 1967 and performed a successful flyby of Venus in October 1967.

The AC-20 and AC-19 launch vehicles were the 10th and 11th operational Centaurs and the first vehicles of this class to fly planetary missions. The vehicles were launched in February and March 1969 into direct-ascent trajectories to place the Mariner VI and Mariner VII into their proper heliocentric transfer orbits. Post-spacecraft-separation maneuvers were accomplished to decrease the probability of the launch vehicle impacting Mars and also to minimize contamination of the Mariner spacecraft from the vehicle exhaust products. It was planned for Mariner VI to fly by the Martian equator and for Mariner VII to fly by the southern polar ice cap of Mars in order to obtain data as different as possible from the standpoint of geography and climate. The spacecraft were targeted to fly by Mars in late July and early August 1969, within 5 days of each other.

This report evaluates the flight performance of the Atlas-Centaur (AC-20 and AC-19) launch vehicles, for the Mariner Mars 1969 missions, from lift-off through the Centaur maneuvers after spacecraft separation.

III. LAUNCH VEHICLE DESCRIPTION

by Eugene E. Coffey and Edwin T. Muckley

The Atlas-Centaur is a two-stage launch vehicle consisting of an Atlas first stage and a Centaur second stage connected by an interstage adapter. Both stages are 3.05 meters (10 ft) in diameter and the composite vehicle is 35.6 meters (117 ft) in length. The AC-20 vehicle weight at lift-off was approximately 145 380 kilograms (320 504 lbm). The basic structure of the Atlas and the Centaur stages utilizes thin-wall, pressure-stabilized, main propellant tank sections of monocoque construction. Figure III-1 shows the AC-20 lifting off with the Mariner VI spacecraft.

The first-stage SLV-3C Atlas (fig. III-2) is 21.03 meters (69 ft) long. It is powered by an MA-5 propulsion system consisting of a booster engine with two thrust chambers and with a total sea-level-rated thrust of 1494×10^3 newtons (336×10^3 lbf), a sustainer engine with a sea-level-rated thrust of 258×10^3 newtons (58×10^3 lbf), and two vernier engines with a sea-level-rated thrust of 2980 newtons (670 lbf) each. All engines use liquid oxygen and RP-1 (kerosene) as propellants and are ignited prior to lift-off. The booster engine thrust chambers are gimbaled for pitch, yaw, and roll control during the booster engine phase of the flight. This phase is completed at booster engine cutoff, which occurs when the vehicle acceleration reaches about 5.7 g's. The booster engine section is jettisoned 3.1 seconds later. The sustainer engine and the vernier engines continue to burn for the Atlas sustainer phase of the flight. During this phase the sustainer engine is gimbaled for pitch and yaw control, while the vernier engines are gimbaled for roll control only. The sustainer and vernier engines provide thrust until propellant depletion. The Atlas is severed from the Centaur by the firing of a shaped charge system located on the forward end of the Atlas-Centaur interstage adapter. The firing of a retrorocket system then separates the Atlas/interstage adapter from the Centaur.

The Centaur second stage with forward and aft payload adapters is shown in figure III-3. This stage, not including the payload adapters, is about 9.1 meters (30 ft) long. It is a high-performance stage (design specific impulse, 442 sec) powered by two RL10A-3-3 engines which generate a total rated thrust of approximately 133.45×10^3 newtons (30 000 lbf). These engines use liquid hydrogen and liquid oxygen as propellants. The Centaur main engines are gimbaled to provide pitch, yaw, and roll control during Centaur powered flight. Fourteen hydrogen peroxide engines, mounted on the aft periphery of the tank, provide thrust for attitude control after Centaur main engine cutoff,

for Centaur/spacecraft reorientation prior to spacecraft separation, and for the vehicle maneuvers after spacecraft separation.

The Centaur hydrogen tank is shielded with four insulation panel sections, each 2.54 centimeters (1 in.) thick. Each section consists of a polyurethane-foam-filled honeycomb core, covered with fiber-glass lamination. A fiber-glass nose fairing is used to provide an aerodynamic shield for the Mariner Mars 1969 spacecraft, for the Centaur guidance equipment, and for the Centaur electronic equipment during ascent. The insulation panels and the nose fairing are jettisoned during the Atlas sustainer phase. The Mariner Mars 1969 spacecraft is shown in figure III-4.

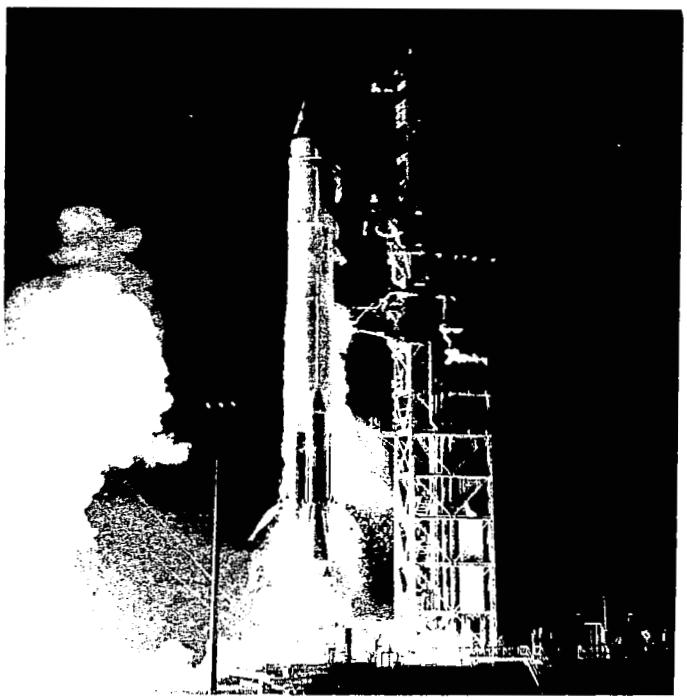

Figure III-1. - Atlas-Centaur lifting off with Mariner VI.

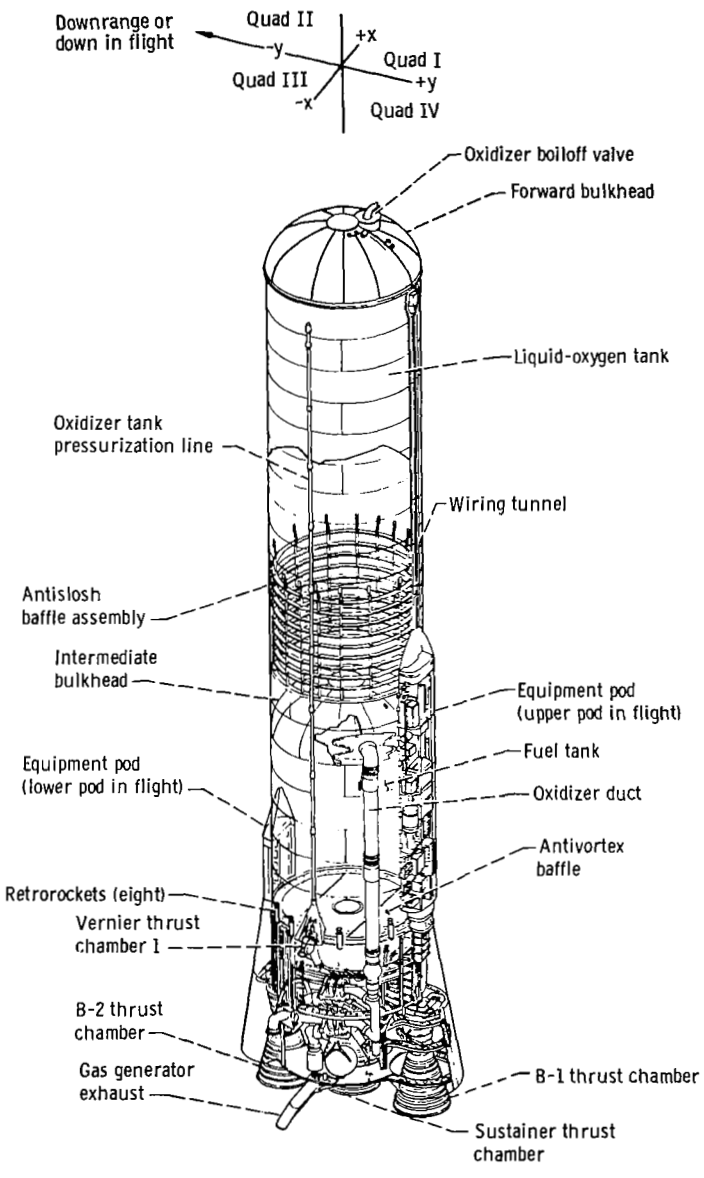

Figure III-2.- General arrangement of Atlas launch vehicle, AC-20 and AC-19.

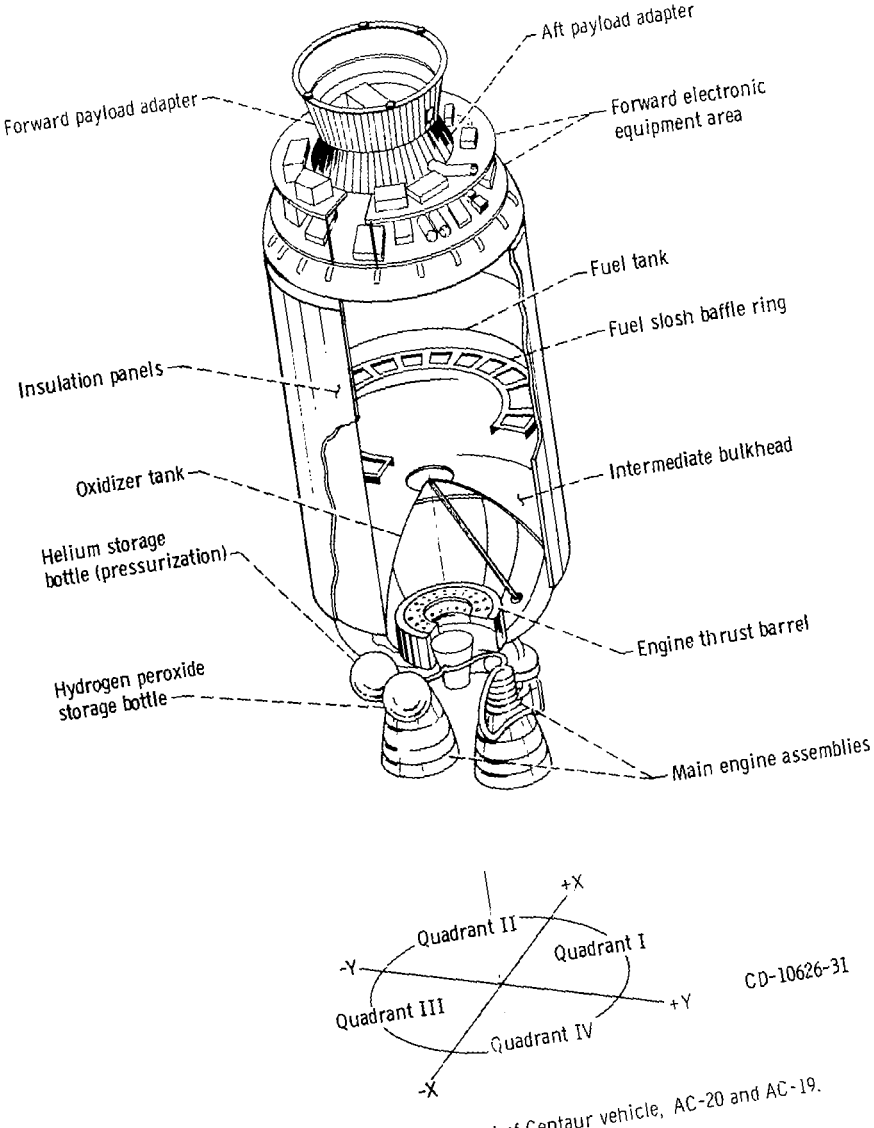

Figure III-3. - General arrangement of Centaur vehicle, AC-20 and AC-19.

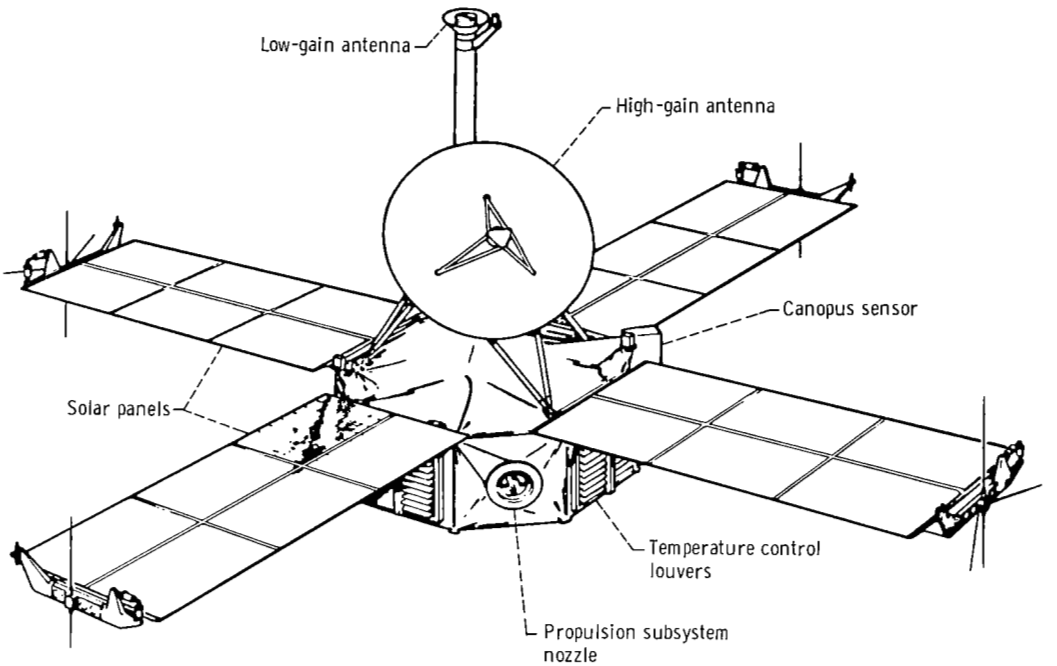

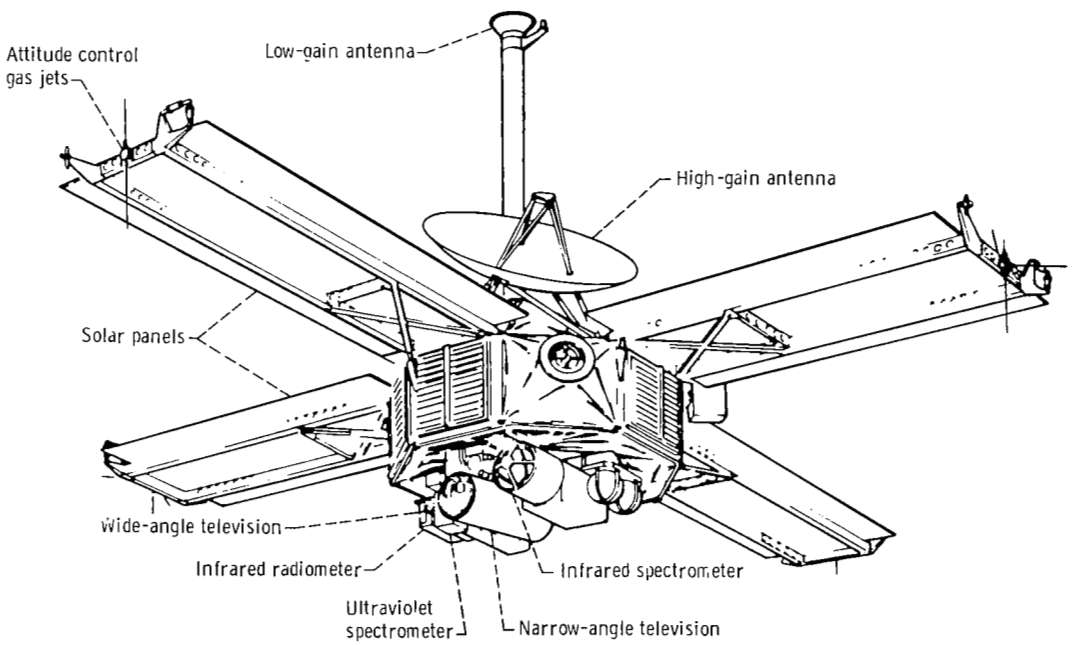

Figure III-4. - General arrangement of Mariner Mars 1969 spacecraft.

IV. MISSION PERFORMANCE

by Edwin T. Muckley

The 10th operational Atlas-Centaur vehicle, AC-20, with the Mariner VI spacecraft, was successfully launched from Eastern Test Range Complex 36B on February 24, 1969, at 2029:02 hours eastern standard time. The 11th operational Atlas-Centaur vehicle, AC-19, with the companion spacecraft Mariner VII, was successfully launched from Complex 36A on March 27, 1969, at 1722:01 hours eastern standard time. Both vehicles utilized the direct-ascent mode. All launch vehicle programmed objectives on both missions were successfully achieved.

A compendium of the mission profile and the heliocentric transfer trajectory are shown in figures IV-1 and IV-2. The AC-20 and AC-19 Atlas-Centaur flights were so similar that the following discussion is centered around the AC-20 flight performance as being typical of both. However, mission-peculiar events of the AC-19 flight are included when appropriate.

ATLAS FLIGHT PHASE

Ignition and thrust buildup of the Atlas engines on AC-20 were normal, and the vehicle lifted off (T + 0) with a combined vehicle and spacecraft weight of 145 380 kilograms (320 504 lbm) and a thrust-weight ratio of 1.22. Two seconds after lift-off, the vehicle initiated a programmed roll from the launcher fixed-azimuth to the required flight azimuth. The flight azimuth of AC-20 was 108° and that of AC-19 was 102.79°. At T + 15 seconds, the vehicle had rolled to the flight azimuth and began a preprogrammed pitch-over maneuver (commanded by the Centaur) which lasted through booster engine cutoff. The Centaur inertial guidance system was functioning during this time, but steering commands to correct for actual in-flight trajectory variations were not admitted to the Atlas flight control systems until after booster engine section jettison.

The pitch program used to command the vehicle during the booster flight was provided by the Centaur guidance system. This pitch program, one of a series selected on the basis of trajectory requirements and measured prelaunch upper-air soundings, was stored in the Centaur airborne computer. Booster engine gimbal angles for thrust vector control did not exceed 2.4° during the booster phase of flight.

Atlas booster engine cutoff, on AC-20, occurred when the vehicle acceleration reached 5.35 g's, at T + 147.1 seconds. The acceleration level was lower than the 5.7±0.113 g's required for initiation of the normal booster engine cutoff sequence. This was due to a malfunction of the booster engine cutoff backup accelerometer switch. This switch, which actuates at 5.9±0.2 g's and serves to back up the guidance system, had closed prematurely when the vehicle acceleration reached 5.02 g's. Consequently, booster engine cutoff occurred immediately when the booster engine cutoff enable signal was issued at T + 147.1 seconds. This resulted in booster engine cutoff occurring 4.9 seconds earlier than expected.

Because of the early booster engine cutoff, less propellants were consumed during the booster phase of flight. As a result, the sustainer engine was required to burn longer in order to attain propellant depletion, and consequently sustainer engine cutoff occurred approximately 18.5 seconds late. This had no adverse effect on vehicle performance, however.

The maximum vehicle angular rate resulting from booster engine section jettison was 7.17 degrees per second in pitch. Normal low-amplitude "slosh" of liquid oxygen was excited in the Atlas liquid-oxygen tank but was damped within a few seconds.

Vehicle acceleration during the Atlas boost phase on AC-19 was according to the mission plan. Centaur guidance issued the booster engine cutoff signal when the vehicle acceleration reached 5.68 g's. About 3 seconds later at T + 153.5 seconds, the Atlas programmer issued the staging command, causing separation of the booster engine section from the vehicle.

When guidance steering by the inertial guidance system was enabled, at about 8 seconds following Atlas booster engine section jettison, the resolver chain outputs indicated that the AC-20 vehicle was approximately 8^{o} nose high and 3^{o} nose left of the desired steering vector. These dispersions were within the expected limits, and the guidance system issued commands to correct the error and to continue the pitchover maneuver during the Atlas sustainer flight phase. On AC-20, the first part of a yaw (dogleg) maneuver was initiated at booster engine cutoff plus 8 seconds and the vehicle was yawed to the right. The second phase of the dogleg maneuver was started at Centaur main engine start (MES) plus 4 seconds. The purpose of the maneuver was to minimize flight over land masses (in accordance with range safety restrictions) and still attain the required orbital inclination conditions at Centaur main engine cutoff. The yaw (dogleg) maneuver was not required for the AC-19 flight since its planar flightpath did not violate range safety criteria.

Insulation panels were jettisoned during the sustainer flight phase at T + 191.7 seconds. The insulation panel assembly was completely severed into four sections by a shaped charge and the sections rotated away from the vehicle. Nose fairing unlatch was commanded at T + 228.5 seconds, and 0.5 second later the thruster bottles were actua-

ted, causing the fairing halves to rotate away from the vehicle. Vehicle angular rates resulting from insulation panel jettison were 3. 14 degrees per second, and those resulting from nose fairing jettison were 5. 16 degrees per second. These high-frequency pitch rates were damped in less than 2 seconds.

Atlas sustainer and vernier engine system performance was satisfactory throughout the flight. Sustainer engine cutoff (SECO) and vernier engine cutoff (VECO) were initiated simultaneously due to liquid-oxygen depletion, as planned. This occurred at T + 270. 8 seconds on AC-20 and at T + 255. 0 seconds on AC-19. On AC-20, the longer firing time to SECO resulted from the premature booster engine cutoff, as described previously.

Coincident with sustainer engine cutoff and vernier engine cutoff, the Centaur guidance steering commands to the Atlas flight control system were inhibited. This allowed the vehicle to coast in a free-flight mode until Atlas-Centaur separation, and also centered the Centaur engines. The Atlas staging command was issued by the Atlas flight programmer at T + 272. 8 seconds. A shaped charge was fired to sever the interstage adapter and separate the two stages. Eight retrorockets on the Atlas were then ignited to decelerate the Atlas stage. Only minor disturbances were noted during the staging sequences and these were damped in less than 0. 2 second.

CENTAUR FLIGHT PHASE

The main engine start sequence for the Centaur stage was initiated prior to sustainer engine cutoff. Propellant boost pumps were started by the Atlas programmer at T + 209. 5 seconds, which permitted the pumps to attain operating speed for main engine start. The required net positive suction pressure was provided by a helium pressure pulse to the propellant tanks to prevent boost pump cavitation during the near-zero-gravity period from sustainer engine cutoff (T + 270. 8 sec) until main engine start (T + 282. 3 sec). Eight seconds prior to main engine start, the Centaur timer issued prestart commands for engine firing. Centaur main engines were gimbaled to the null position. Engine prestart valves were opened to flow liquid hydrogen through the lines and thereby chill down the engine turbopumps. Chilldown of the turbopumps prevented cavitation during turbopump acceleration and made possible a uniform and rapid thrust build-up after engine ignition. At T + 282. 3 seconds, the ignition command was issued by the Centaur timer and engine thrust increased to flight levels.

Guidance steering commands were discontinued during the engine start sequence. This prevented engine gimbaling, which could cause excessive vehicle angular rates during the engine start transient. The total residual angular rates and disturbing torques induced subsequent to sustainer engine cutoff resulted in only a slight vehicle drift off the steering vector. The attitude error (AC-20) was corrected by the time guidance steering

began. Guidance steering was enabled at T + 286.3 seconds, 4 seconds after main engine start.

Through the remainder of the Centaur main engine firing, the guidance steering commands were required to provide the necessary pitch and yaw rate to achieve the velocity vector conditions for orbital injection.

All systems performed properly during the Centaur powered flight. At T + 725.5 seconds the required injection velocity was attained and the guidance system issued the command to shut down the engines. Shutdown transients (5.77 deg/sec - high frequency in pitch) at main engine cutoff were well within the predicted range of dispersions. On AC-20 the duration of the Centaur powered phase was 7.4 seconds longer than expected.

SPACECRAFT SEPARATION

Coincident with main engine cutoff, the guidance steering commands were temporarily discontinued. Immediately after main engine cutoff, the vehicle attitude control system was commanded to reorient the spacecraft separation pointing vector to 87^{o} (primarily nose down) in the pitch plane, measured from the vehicle's position at main engine cutoff. (See section V. TRAJECTORY AND PERFORMANCE for an explanation of this maneuver.) Spacecraft separation was commanded at T + 820.6 seconds, about 95 seconds after main engine cutoff. Angular rates of the vehicle just prior to spacecraft separation were approximately 0.1 degree per second. These rates were well below the maximum allowable (0.7 deg/sec). After spacecraft separation the spacecraft solar panels were deployed and the spacecraft acquired the Sun and the star Canopus for attitude reference. The spacecraft then stabilized in attitude.

CENTAUR DEFLECTION MANEUVER

During the 270 seconds that followed spacecraft separation, the relative separation velocity of the Centaur and the spacecraft was 0.61 meter per second (2 ft/sec). Attitude control of the Centaur was maintained during this period. The Centaur then began another reorientation, at T + 1091.2 seconds, to a vector approximately 71^{o} nose up and to the left of the separation vector.

At T + 1185.6 seconds, two 222-newton (50-lbf) thrust hydrogen peroxide engines were fired for a period of 40 seconds, thereafter two 13.3-newton (3.0-lbf) thrust hydrogen peroxide engines were commanded on for a period of 350 seconds. Separation distance between the spacecraft and Centaur was further increased, while hydrogen peroxide was consumed at a lower rate. This increased separation distance was necessary to

minimize the possible impingement of frozen particles on the spacecraft during the discharge of residual Centaur propellants ("blowdown") through the main engines. Nearly nominal disturbing moments in yaw and roll were observed during this period.

At T + 1575.6 seconds, just following the hydrogen peroxide engine firing sequence, the main engine blowdown phase was commanded. Disturbing torques on the vehicle resulting from the start of propellant discharge (blowdown) were well within the control limits. At T + 1629 seconds the Centaur programmer was stopped and the vehicle continued to coast in the existing mode. The Centaur deflection maneuver satisfied the constraints relative to spacecraft contamination and more than satisfied the planetary quarantine constraint.

MARS TRANSFER TRAJECTORY

Both Mariners VI and VII were accurately injected into heliocentric transfer trajectories to the planet Mars. The trajectories were targeted prior to launch such that encounter at Mars would occur on July 31, 1969, for Mariner VI and on August 5, 1969, for Mariner VII.

The launch vehicle injection accuracy can be measured by the magnitude of midcourse velocity correction required of the spacecraft at launch plus 10 days to meet the target specification conditions (miss distance and time of arrival) at Mars. This midcourse correction was not to exceed 13.5 meters per second. A change in velocity of 2.18 meters per second on Mariner VI and of 2.01 meters per second on Mariner VII would have been required to meet the target specifications. An actual midcourse correction of 3.06 meters per second was completed by Mariner VI on March 1, 1969, at 00:54.44 Greenwich mean time to correct for AC-20 launch vehicle injection errors and final target selection. For this mission the trajectory was designed for the Mariner VI to fly by the Martian equator at an altitude of approximately 3200 kilometers.

Similarly, an actual midcourse correction of 4.29 meters per second was completed by Mariner VII on April 8, 1969, at 2022:09 Greenwich mean time. For this mission the trajectory was designed for Mariner VII to fly by the Martian southern polar ice cap at an altitude of approximately 3100 kilometers.

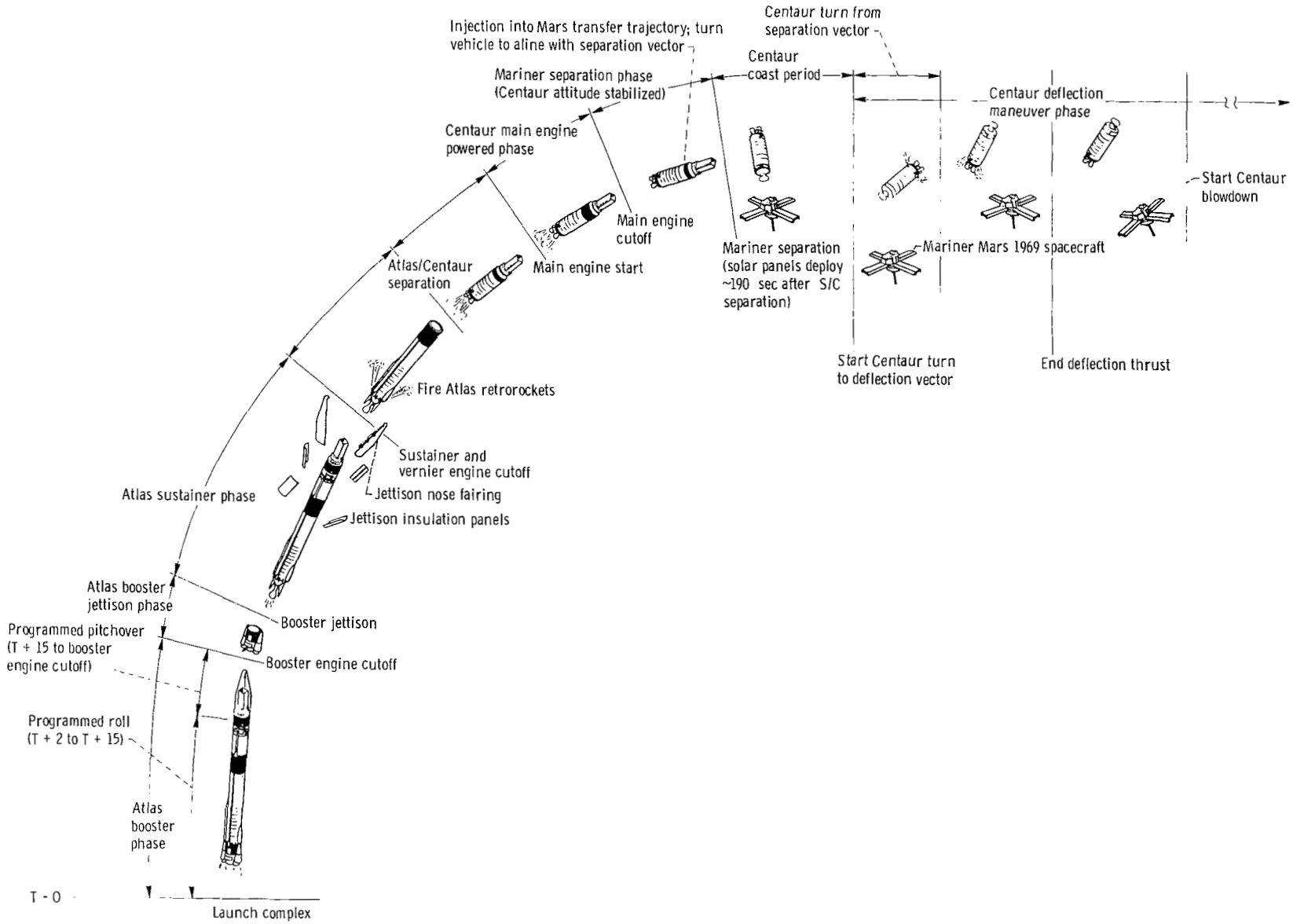

Figure IV-1. - Atlas-Centaur flight profile, AC-20 and AC-19. (All times are in seconds; all times are approximate.)

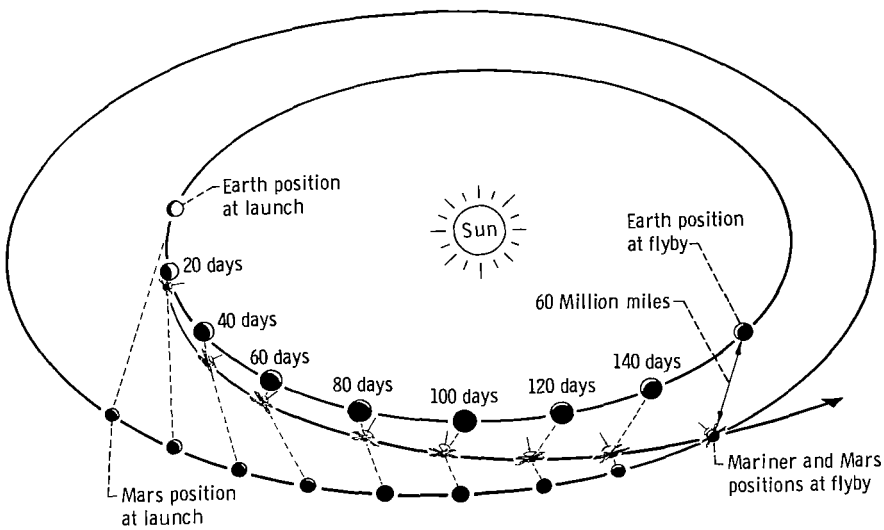

Figure IV-2. - Typical heliocentric transfer trajectory for a Mars mission.

V. TRAJECTORY AND PERFORMANCE

by John J. Nieberding

MISSION PLAN

The AC-20 and AC-19 missions were designed to achieve injection of the Mariner VI and VII spacecraft, respectively, into the trajectories required for a Mariner VI flyby of the Martian equator on July 31, 1969, and for a Mariner VII flyby of the Martian southern polar ice cap on August 5, 1969. AC-20 was the first Atlas-Centaur vehicle used to place a spacecraft on an interplanetary trajectory.

For both missions (AC-20 and AC-19), the launch vehicle was required to use the direct mode of ascent; that is, the Atlas and Centaur employed a nearly continuous powered phase with the Centaur main engines firing only once. In order to attain the proper Earth orbital inclination and comply with the Air Force Range Safety constraint that land overflight be minimized, AC-20 was required to perform a double yaw maneuver (dogleg) to the south. The first portion of this yaw was to be accomplished during the Atlas sustainer phase, while the second portion was to be performed during the Centaur powered phase. No yaw maneuver was required of AC-19, since the flightpath over land did not violate Air Force Range Safety requirements.

Following shutdown of the Centaur main engines, the spacecraft for each mission was separated from the Centaur. Each Centaur then performed a retromaneuver to minimize the contamination of the spacecraft by Centaur exhaust products and also to minimize the probability that the Centaur stage would impact and thereby contaminate the planet Mars.

TRAJECTORY RESULTS

The discussion in this section is generally centered around the trajectory and performance data of AC-20. AC-19 data are discussed in those cases where the AC-20 trajectory and performance data were not typical. Altitude against wind speed and wind direction data for AC-20 are presented in figures V-1 and V-2. Inertial velocity and axial load factor against time data are presented in figures V-3 and V-4, while altitude against time and ground range data are shown in figures V-5 and V-6. Corresponding data for

AC-19 are presented in figures V-7 to V-12. The predicted and the actual event times for both AC-19 and AC-20 are compared in table V-I. The predicted and the actual spacecraft orbital parameters for both flights are shown in table V-II. Centaur post-retromaneuver orbital parameters for both flights are presented in table V-III, and a postflight weights summary is presented in table V-IV.

Lift-off Through Atlas Booster Phase

Atmospheric conditions near the launch site were determined by a series of weather balloons sent aloft beginning about 18 hours prior to launch. Actual wind speed and wind direction data as a function of altitude are compared with predicted data in figures V-1 and V-2. Predicted data for AC-20 are based on statistically probable winds for the month of February for the Cape Kennedy region. Similar data for AC-19 are based on winds for the month of March. Wind direction is defined as the direction from which the wind is blowing; that is, a wind direction of 90^{o} indicates a wind from the east. In order to minimize the vehicle aerodynamic loading during the booster phase of flight, the wind data were evaluated and the appropriate booster pitch and yaw programs were selected. (The pitch and yaw programs used on AC-20 were PP211 and YP0, and those on AC-19 were PP181 and YP6.)

Radar tracking and Centaur guidance data indicated that the AC-20 flightpath during the booster phase was very close to the predicted path (see figs. V-5 and V-6). The transonic region, or the time span when the vehicle passes through Mach 1, occurred from about T + 60 to T + 64 seconds. During this 4-second period, the axial load factor (thrust acceleration in g's) was nearly constant (see fig. V-4), reflecting the high aerodynamic drag during this period. The maximum value of dynamic pressure, 4.09×10^{4} N/m^{2} (856 lbf/ft^{2}), occurred at T + 80 seconds, as expected. Atlas booster engine cutoff occurred at T + 147.1 seconds, 4.9 seconds earlier than predicted, due to a failure of the autopilot backup staging accelerometer (See the section GUIDANCE AND FLIGHT CONTROL SYSTEM for a more detailed explanation of the cause of this failure.) The effect of this early booster engine cutoff (BECO) on the time history of inertial velocity and axial acceleration can be seen from figures V-3 and V-4. The peak axial acceleration at BECO was 5.35 g's, instead of the predicted 5.7 g's. Actual inertial velocities were very close to the predicted value until BECO. At BECO, however, because the vehicle did not have sufficient time to achieve the predicted velocity, the actual inertial velocity was 0.21 kilometer per second (689 ft/sec) lower than expected. The vehicle altitude at BECO was about 3 kilometers (9840 ft) lower than it would have been if BECO had occurred at the predicted time; the ground range was about 9 kilometers (29 520 ft)

shorter than predicted (see figs. V-5 and V-6). These variations are in contrast to the close agreement of AC-19 data in figures V-9 to V-12.

Atlas Sustainer Phase

An abrupt decrease in acceleration occurred at BECO and is shown in figure V-4 and also in figure V-3, where a change in slope indicates a change in acceleration. A small but sudden increase in acceleration occurred at T + 150.1 seconds when the booster engine section, weighing 2848 kilograms (6279 lbm) was jettisoned. Following booster jettison, the axial acceleration increased smoothly until sustainer and vernier engine cutoff at T + 270.8 seconds, except for small perturbations caused by jettisoning the Centaur insulation panels (518 kg, 1142 lbm) at T + 191.7 seconds and the nose fairing (970 kg, 2139 lbm) at T + 228.5 seconds. (The increase in axial acceleration occurs because vehicle thrust increases as atmospheric pressure decreases, and also because the vehicle weight is constantly decreasing.) These small perturbations can be seen in the plot of predicted data because in this curve every data point is plotted. In the actual data, not every point is plotted, so that the effect is not seen.

The actual flight azimuth for AC-20 was 108°, the most southerly azimuth for which Range Safety would approve a launch. During the sustainer phase for AC-20 a 4° yaw maneuver to the right, or south, was performed beginning at BECO + 8 seconds, resulting in an equivalent flight azimuth of 115°. However, the equivalent flight azimuth required to yield the proper orbital inclination at Centaur main engine cutoff (MECO) was 124°. Because of land overflight problems, Range Safety would only permit a partial yaw maneuver during the sustainer phase. The remaining required yaw was performed during the Centaur powered phase. No yaw maneuver was required for AC-19 because a launch at the required flight azimuth, 102.79°, was acceptable to Range Safety since the land overflight at this azimuth was minimal.

Because of the early BECO, the Atlas booster consumed less fuel than expected during the booster phase. Since the booster and sustainer engines are supplied by the same propellant tanks, and since the sustainer fires until the propellant is depleted, the sustainer phase of flight lasted 23.4 seconds longer than predicted. This long sustainer firing caused the vehicle altitude at sustainer engine cutoff (SECO) to be approximately 7.5 kilometers (4.05 n mi) higher than expected and the vehicle ground range to be about 44 kilometers (23.8 n mi) greater than predicted. As can be seen from figure V-3, the vehicle velocity at SECO was very nearly as predicted. At SECO, the axial acceleration dropped to zero, indicating the loss of all thrust.

Centaur Main Engine Firing Phase

Centaur main engine start (MES) is timed to occur 11.5 seconds after SECO. Therefore, because SECO was late, so was MES. The increase in velocity and acceleration at MES can be seen in figures V-3 and V-4. At MES + 4 seconds, a 10^{o} yaw right was performed to the effective azimuth of 124^{o}. After MES, the uniformly decreasing Centaur propellant weight caused the axial acceleration to increase smoothly until Centaur main engine cutoff (MECO) at T + 725.5 seconds. Because of the late MES and the low Centaur thrust, the velocity and acceleration at any given time are lower than predicted for the duration of the Centaur powered phase. Although MECO occurred at 25.9 seconds later than predicted, 18.5 seconds of this delay was caused by the late SECO. Thus, the duration of the Centaur powered phase was only 7.4 seconds longer than predicted. Since extended Centaur firing durations of this magnitude have been observed on other flights (such as AC-19, see figs. V-9 and V-10) where BECO did occur when predicted, it is therefore concluded that the premature BECO on AC-20 had little effect on the Centaur firing duration. Based on trajectories reconstructed from tracking data and Centaur guidance data, at MECO the Centaur inertial velocity was 16.4 meters per second (54.0 ft/sec) lower than predicted, the altitude was 23.4 kilometers (12.7 n mi) high, and the ground range was 79 kilometers (43 n mi) farther than predicted. These position and velocity dispersions are consistent with the requirement for the proper orbital energy and angular momentum at cutoff.

Spacecraft Separation and Centaur Retromaneuver Phase

To ensure that the Centaur tank would not impact Mars, the MECO velocity vector was biased away from the planet so that the Centaur stage would miss Mars even if the retrothrust during the retromaneuver was significantly less than expected. If the Mariner VII spring separation velocity (0.61 m/sec, 2 ft/sec) had been imparted along this biased MECO velocity vector rather than along the desired separation vector, the premidcourse encounter point would have been altered by about 13 000 kilometers. This distance is also representative of the effect of the Mariner VI preseparation reorientation. Thus a separation vector which reoriented the spacecraft back towards the planet and which met the spacecraft antenna orientation requirements was required. Consequently, 2 seconds after MECO, the Centaur began to orient to the desired altitude vector for spacecraft separation. In order to attain the proper attitude, the Centaur was commanded to pitch down and yaw to the right. This resulted in a Centaur/Mariner attitude change of 88^{o} This new attitude pointed the vehicle more toward the Earth, biased 28^{o} forward of the local vertical in the direction of motion. The spacecraft was success-

fully separated from Centaur at T + 820.6 seconds at a relative velocity of 0.61 meter per second (2.0 ft/sec).

The Centaur then coasted for about 270 seconds alined to the separation vector before reorienting to its retromaneuver vector. This coast period allowed for increased separation distance between the spacecraft and Centaur stage to preclude Centaur exhaust products from impinging on the spacecraft during the retromaneuver. At T + 1091.2 seconds, the Centaur began to orient to the required retromaneuver vector by changing its attitude by about 74°. This maneuver was primarily a nose-up maneuver in the trajectory plane and resulted in a vehicle attitude of about 38° nose up with respect to the local horizontal. The maneuver was performed to further ensure that the vehicle would not impact Mars. At T + 1185.6 seconds, two 222-newton (50-lbf) thrust hydrogen peroxide engines were fired for 40 seconds, followed by the firing of two 13.3-newton (3-lbf) thrust hydrogen peroxide engines at T + 1225.6 for 350 seconds. The purpose of firing these 222- and 13.3-newton (50- and 13-lbf) thrust engines was to maximize the distance between the spacecraft and Centaur before the start of propellant blowdown. At T + 1575.6 seconds the Centaur main engine prestart valves were opened and residual propellants were discharged, the liquid oxygen through the main thrust chambers and the liquid hydrogen through the engine chilldown valves. Postflight analysis of the energy of the postretromaneuver orbits of the Centaur stages for AC-19 and AC-20 showed that on AC-20 the blowdown impulse was about 50 percent higher than predicted, while on AC-19 it was about 36 percent higher than predicted. These results are not unusual since high dispersions on blowdown impulse have been observed in other flights. The resulting orbits of the Centaur stages are defined in table V-3.

Spacecraft Midcourse Velocity Correction

The midcourse velocity correction is a ground-commanded maneuver performed in flight by the spacecraft to ensure arrival at the desired target at the desired time. The target coordinate system is defined in the following sketch:

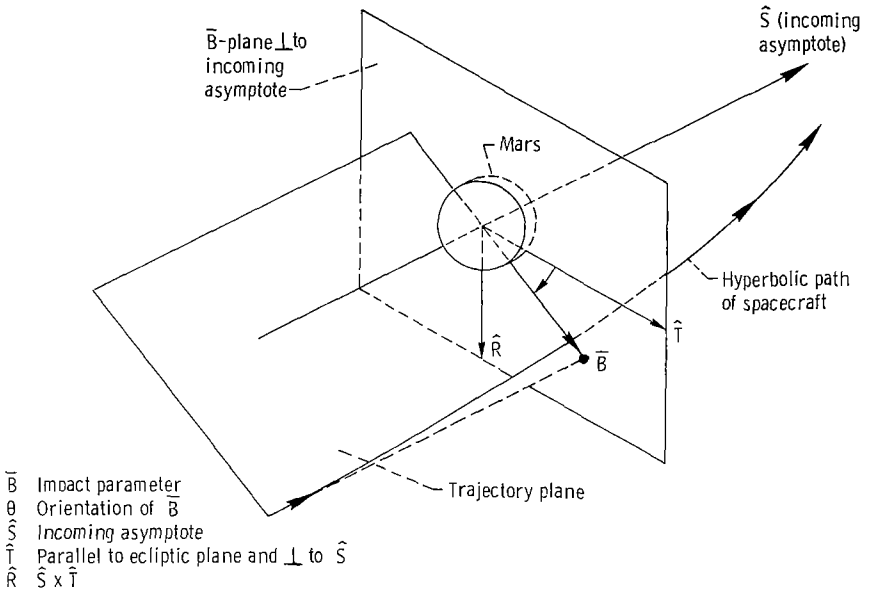

Encounter R, S, T coordinate system

The impact parameter $\bar{B}$ is defined as the radial distance from the center of the target planet, in a plane ($\bar{B}$ plane) normal to the incoming trajectory asymptote, at which the spacecraft would pass if the target planet had no gravity, that is, if the target planet did not deflect the trajectory. The projections of the vector $\bar{B}$ onto the $\bar{R}$ axis, $\bar{B} \cdot \hat{R}$, and onto the $\hat{T}$ axis, $\bar{B} \cdot \hat{T}$, define a unique position in the $\bar{B}$ plane. When the time of arrival or time of closest approach is specified, the target parameters are defined. The following table summarizes the midcourse velocity corrections and target parameters for Mariners VI and VII:

Mariner VI, AC-20					Mariner VII, AC-19				
Time of correction, Gmt									
00:54:44, March 1, 1969					20:22:09, April 8, 1969				
Midcourse correction (miss only)									
2.039 m/sec (6.689 ft/sec)					4.237 m/sec (13.901 ft/sec)				
Midcourse correction (miss plus time of flight)									
3.068 m/sec (10.065 ft/sec)					4.292 m/sec (14.081 ft/sec)				
$\bar{B} \cdot \hat{R}$		$\bar{B} \cdot \hat{T}$		Time of closest approach, Gmt	$\bar{B} \cdot \hat{R}$		$\bar{B} \cdot \hat{T}$		Time of closest approach, Gmt
km	n mi	km	n mi		km	n mi	km	n mi	
Final target parameters									
-643	-347	7317	3951	05:17:26, July 31, 1969	3440	1857	6468	3492	05:01:08, August 5, 1969
Actual encounter parameters									
-336	-181	7596	4101	05:19:07, July 31, 1969	3631	1960	6713	3625	05:00:50, August 5, 1969

The time of correction is the time at which the midcourse maneuver was completed. The miss-only midcourse correction is the velocity correction required to hit the final spacecraft target. Hence, it is called the "miss only" correction. In order to ensure the proper arrival time as well as arrival at the final target, a "miss plus time of flight" correction is required. This velocity correction, the total correction performed, is given below the miss-only correction. This correction is performed to achieve the final target parameters. The actual encounter coordinates and encounter times are included below the final parameters.

The miss-only and miss-plus-time-of-flight corrections quoted in the table are different corrections than the miss-only and miss-plus-time-of-flight corrections used to evaluate the accuracy with which the Centaur injected the spacecraft into the trajectory designed prior to launch. Prior to launch, a particular spacecraft target and associated arrival time are selected to be biased from Mars by a sufficient distance to ensure that the spacecraft will not impact the planet and thereby violate the planetary quarantine constraint. The spacecraft trajectory is then designed to meet these target conditions. Centaur injection accuracy is measured by the amount of the miss-only and miss-plus-time-of-flight corrections required by the spacecraft to achieve these conditions. The

final spacecraft target is, however, considerably closer to Mars than this biased target. The coordinates of this final target are presented under "Final target parameters." The midcourse corrections associated with this new target are those presented at the top of the table. The midcourse corrections required to achieve the biased target conditions (those used to evaluate Centaur injection accuracy) are quoted in the section GUIDANCE AND FLIGHT CONTROL SYSTEMS.

TABLE V-I. - FLIGHT EVENTS RECORD, AC-20 AND AC-19

Event	Programmer time, sec	AC-20		AC-19	
		Predicted time, sec	Actual time, sec	Predicted time, sec	Actual time, sec
Lift-off, 2-in. motion	T + 0.0	T + 0.0	T + 0.0	T + 0.0	T + 0.0
Start roll program	T + 2.0	T + 2.0	T + 2.0	T + 2.0	T + 2.0
End roll program	T + 15.0	T + 15.0	T + 15.0	T + 15.0	T + 15.0
Start pitch program	T + 15.0	T + 15.0	T + 15.0	T + 15.0	T + 15.0
Booster engine cutoff	BECO	T + 152.0	T + 147.1	T + 152.5	T + 150.4
Booster engine jettison	BECO + 3.1	T + 155.1	T + 150.1	T + 155.6	T + 153.5
Insulation panel jettison	BECO + 45	T + 197.0	T + 191.7	T + 197.5	T + 195.1
Nose fairing jettison	BECO + 82	T + 234.0	T + 228.5	T + 234.5	T + 231.9
Sustainer engine cutoff	SECO	T + 252.3	T + 270.8	T + 253.1	T + 255.0
Atlas/Centaur separation	SECO + 1.9	T + 254.2	T + 272.8	T + 255.0	T + 256.9
Centaur main engine start	SECO + 11.5	T + 263.8	T + 282.3	T + 264.5	T + 266.5
Centaur main engine cutoff	MECO	T + 699.6	T + 725.5	T + 701.5	T + 712.2
Start reorientation to spacecraft separation vector	MECO	T + 699.6	T + 728.0	T + 701.5	T + 715.0
Separate spacecraft	MECO + 95	T + 794.6	T + 820.6	T + 796.5	T + 807.4
Start reorientation to retromaneuver vector	MECO + 365	T + 1064.6	T + 1091.2	T + 1066.5	T + 1078.8
V-engines half on	MECO + 460	T + 1159 6	T + 1185.6	T + 1161.5	T + 1172.3
V-engines half off; S-engines half on	MECO + 500	T + 1199.6	T + 1225.6	T + 1201.5	T + 1212.3
S-engines half off; start blowdown	MECO + 850	T + 1549.6	T + 1575.6	T + 1551.5	T + 1562.4

TABLE V-II. - SPACECRAFT ORBIT PARAMETERS

Parameter	Units	Predicted		Actual			
		Mariner VI	Mariner VII	Guidance[a]		Tracking[b]	
				Mariner VI	Mariner VII	Mariner VI	Mariner VII
Epoch	sec from lift-off	794.6	796.5	820.6	807.4	820.6	807.4
Perigee altitude[c]	km	90.93	111.04	91.02	110.73	91.12	110.62
	n mi	49.10	59.96	49.15	59.79	49.20	59.73
Inclination	deg	43.369	30.983	43.365	30.997	43.363	31.012
Eccentricity	--------	1.181519	1.274817	1.181525	1.27489	1.18634	1.27480
Energy, C_3	$(km/sec)^2$	11.18459	16.88076	11.18468	16.88605	11.19129	16.88085
	$(ft/sec)^2$	1.20390×10^8	1.81703×10^8	1.20391×10^8	1.81760×10^8	1.20462×10^8	1.81704×10^8
Angular momentum	km^2/sec	7.50016×10^4	7.67076×10^4	7.50022×10^4	7.67070×10^4	7.50046	7.67047×10^4
	ft^2/sec	8.07310×10^{11}	8.25674×10^{11}	8.07317×10^{11}	8.25667×10^{11}	8.07343×10^{11}	8.25643×10^{11}

[a]Guidance reconstructed trajectory (GRT) obtained from telemetered Centaur guidance data.

[b]Jet Propulsion Laboratory data obtained from Deep Space Net Tracking data.

[c]Referenced to a mean equatorial altitude.

TABLE V-III. - CENTAUR POSTRETROMANEUVER

ORBIT PARAMETERS, AC-20 AND AC-19

Parameter[a]	Units	AC-20	AC-19
Epoch	sec from lift-off	3691.0	3608.8
Semimajor axis	km	-32586.3	-22205.5
	n mi	-17595.2	-11990.0
Eccentricity	--------	1.1996651	1.29748
Inclination	deg	43.23999	31.149
Energy, C_3	$(km/sec)^2$	12.23196	17.95046
	$(ft/sec)^2$	1.31664×10^8	1.932×10^8
Perigee radius	km	6506.3	6605.7
	n mi	3513.2	3566.8

[a]All parameters are based on tracking data.

TABLE V-IV. - POSTFLIGHT VEHICLE WEIGHT SUMMARY.

AC-20 AND AC-19

(a) Atlas

Item	AC-20		AC-19	
	Weight		Weight	
	kg	lbm	kg	lbm
Booster jettison weight:				
Booster dry weight	2 848	6 279	2 863	6 312
Booster residuals	472	1 041	472	1 041
Unburned lubrication oil	18	39	18	39
Total	3 338	7 359	3 353	7 392
Sustainer jettison weight:				
Sustainer dry weight	2 719	5 994	2 712	5 979
Sustainer residuals	241	531	300	661
Interstage adapter	481	1 060	474	1 044
Unburned lubrication oil	7	15	7	15
Total	3 448	7 600	3 493	7 699
Flight expendables:				
Main impulse fuel (RP-1)	37 653	83 010	37 675	83 060
Main impulse oxygen	83 168	183 353	83 126	183 261
Helium panel purge	2	5	2	5
Oxygen vent loss	141	311	141	311
Lubrication oil	83	184	83	184
Total	121 047	266 863	121 027	266 821
Ground expendables:				
Fuel (RP-1)	248	546	242	533
Oxygen	839	1 849	819	1 805
Lubrication oil	1	3	1	3
Exterior ice	24	54	24	54
Liquid nitrogen in helium shrouds	113	250	113	250
Pre-ignition gaseous oxygen loss	204	450	204	450
Total	1 429	3 152	1 403	3 095
Total Atlas tanked weight	129 262	284 974	129 276	285 007
Minus ground expendables	1 429	3 152	1 403	3 095
Total Atlas weight at lift-off	127 833	281 822	127 873	281 912

TABLE V-IV. - Concluded. POSTFLIGHT VEHICLE WEIGHT SUMMARY,

AC-20 AND AC-19

(b) Centaur

Item	AC-20		AC-19	
	Weight		Weight	
	kg	lbm	kg	lbm
Basic hardware:				
Body	514	1 133	516	1 138
Propulsion group	503	1 110	503	1 110
Guidance group	143	315	143	315
Fluid systems group	130	286	130	286
Electrical group	124	274	124	274
Separation group	36	79	36	79
Basic instrumentation equipment	109	240	109	240
Mission-peculiar equipment	78	172	78	173
Total	1 637	3 609	1 639	3 615
Jettisonable hardware:				
Nose fairing	970	2 139	969	2 136
Insulation panels	518	1 142	524	1 156
Ablated ice	23	50	23	50
Total	1 511	3 331	1 516	3 342
Centaur residuals at main engine cutoff:				
Liquid hydrogen	78	173	77	169
Liquid oxygen	250	551	246	542
Gaseous hydrogen	38	85	38	85
Gaseous oxygen	77	169	77	169
Hydrogen peroxide	58	128	59	130
Helium	4	8	4	8
Ice	5	12	5	12
Total	510	1 126	506	1 115
Centaur expendables:				
Main impulse hydrogen	2 212	4 876	2 212	4 876
Main impulse oxygen	11 142	24 563	11 124	24 525
Gas boiloff on ground, hydrogen	12	26	12	26
Gas boiloff on ground, oxygen	10	23	10	23
In-flight chill, hydrogen	10	23	10	23
In-flight chill, oxygen	14	31	14	31
Booster phase vent, hydrogen	24	53	24	53
Booster phase vent, oxygen	30	66	30	66
Sustainer phase vent, hydrogen	14	30	14	30
Sustainer phase vent, oxygen	27	60	27	60
Engine shutdown loss, hydrogen	3	6	3	6
Engine shutdown loss, oxygen	6	13	6	13
Hydrogen peroxide	20	44	19	42
Helium	1	1	1	1
Total	13 525	29 815	13 506	29 775
Total tanked weight	17 183	37 881	17 167	37 847
Minus ground vent	22	49	22	49
Total Centaur weight at lift-off	17 161	37 832	17 145	37 798
Spacecraft	386	850	385	848
Total Atlas-Centaur-spacecraft lift-off weight	145 380	320 504	145 403	320 558

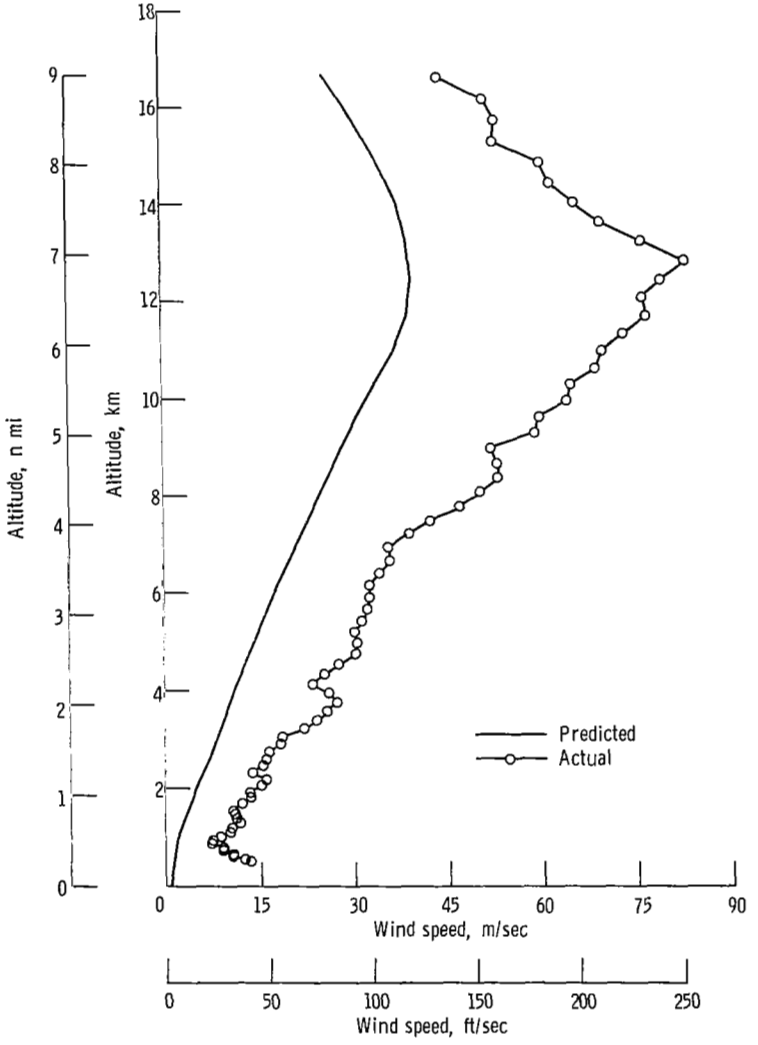

Figure V-1. - Altitude as function of wind speed, AC-20.

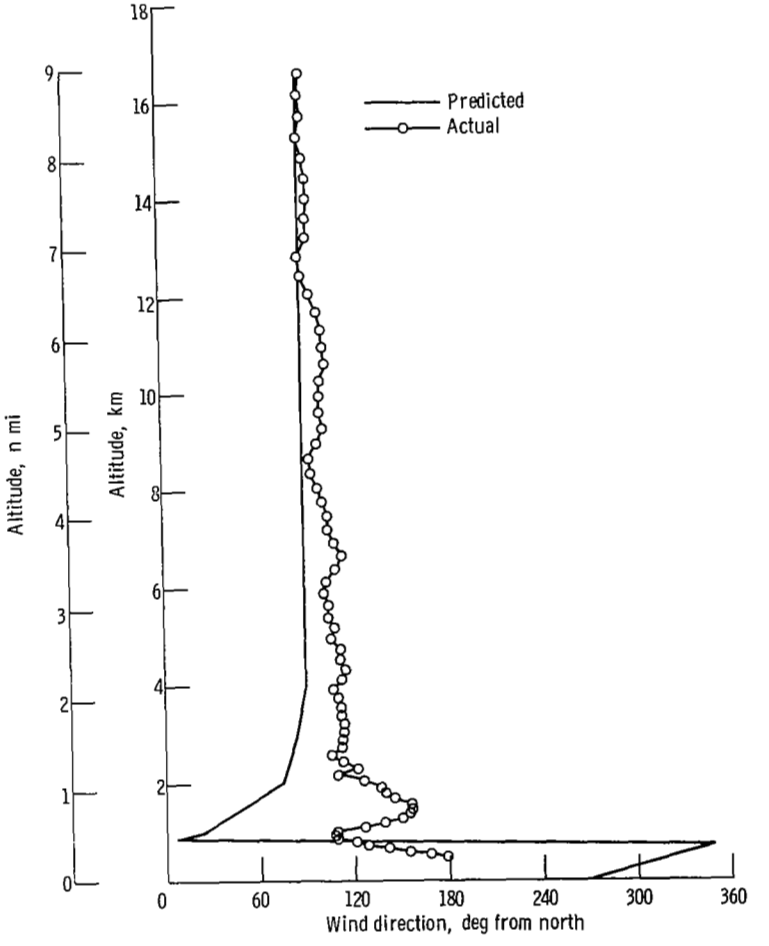

Figure V-2. - Altitude as function of wind direction, AC-20.

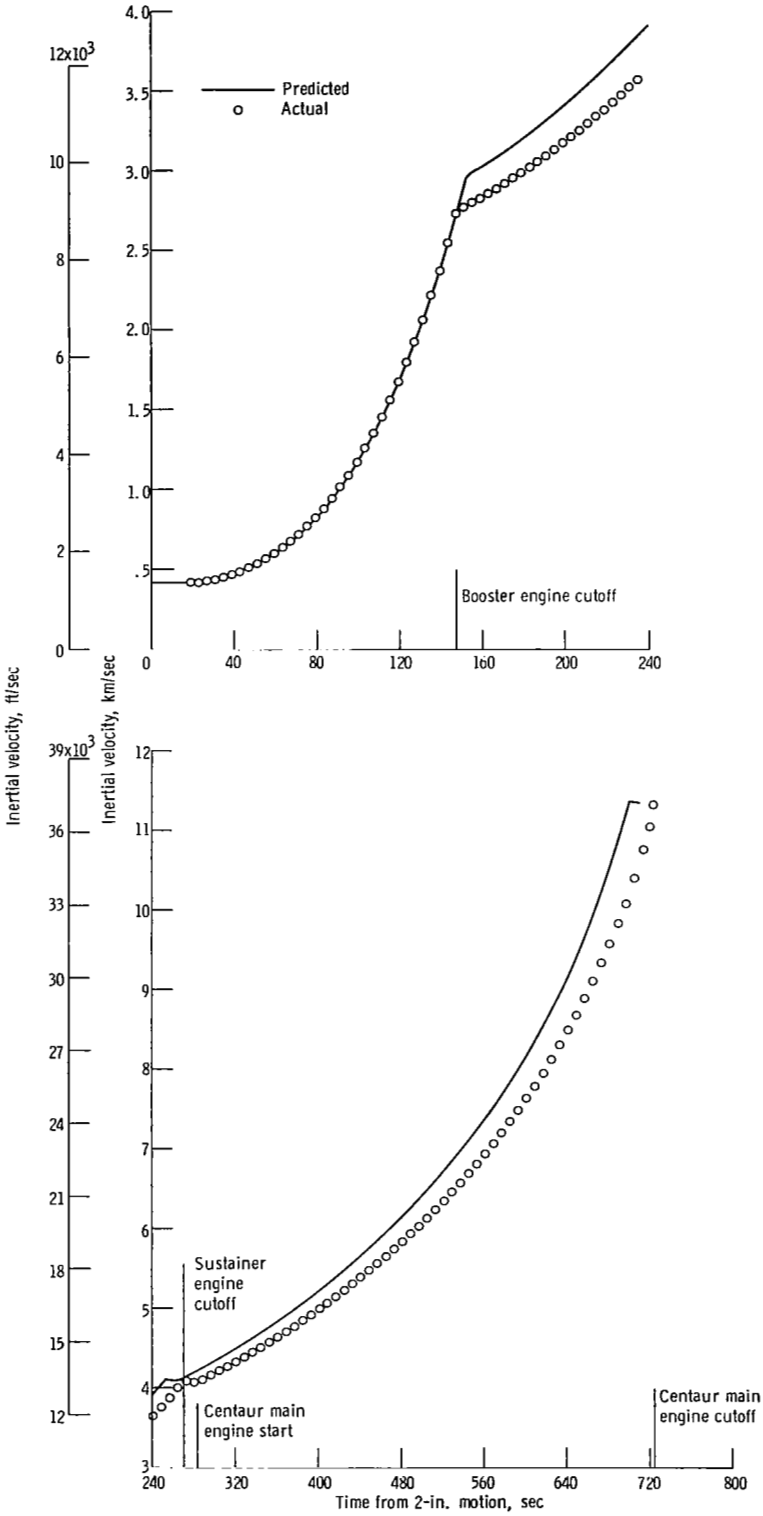

Figure V-3. - Inertial velocity as function of time, AC-20.

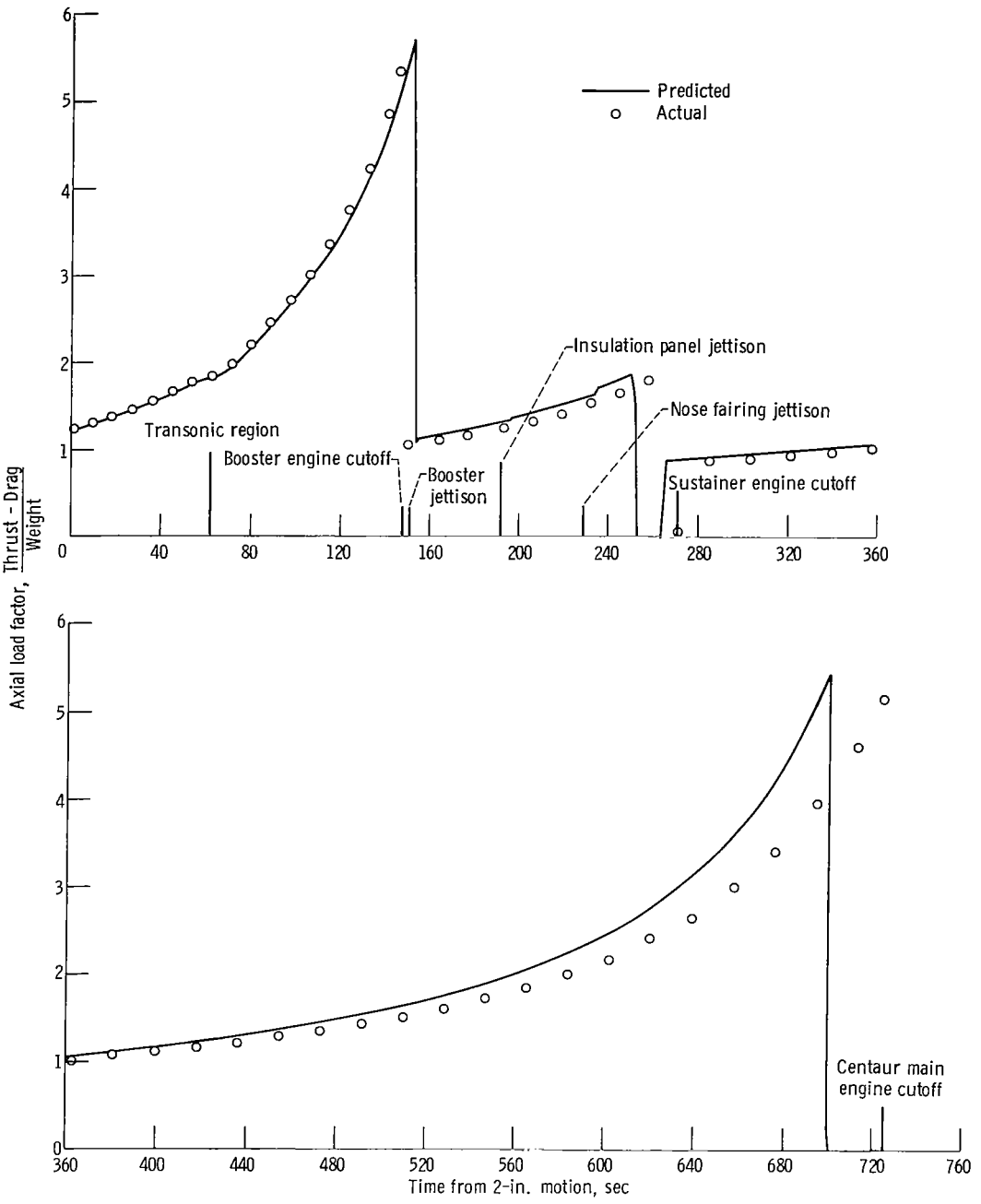

Figure V-4. - Axial load factor as function of time, AC-20.

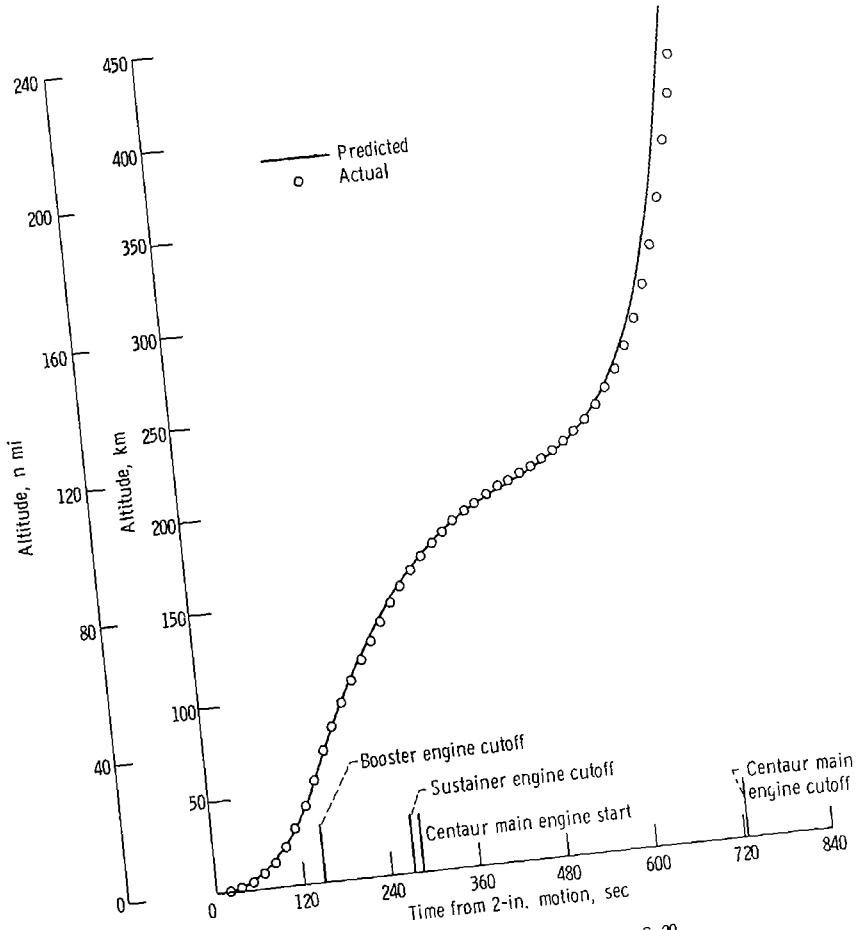

Figure V-5. - Altitude as function of time, AC-20.

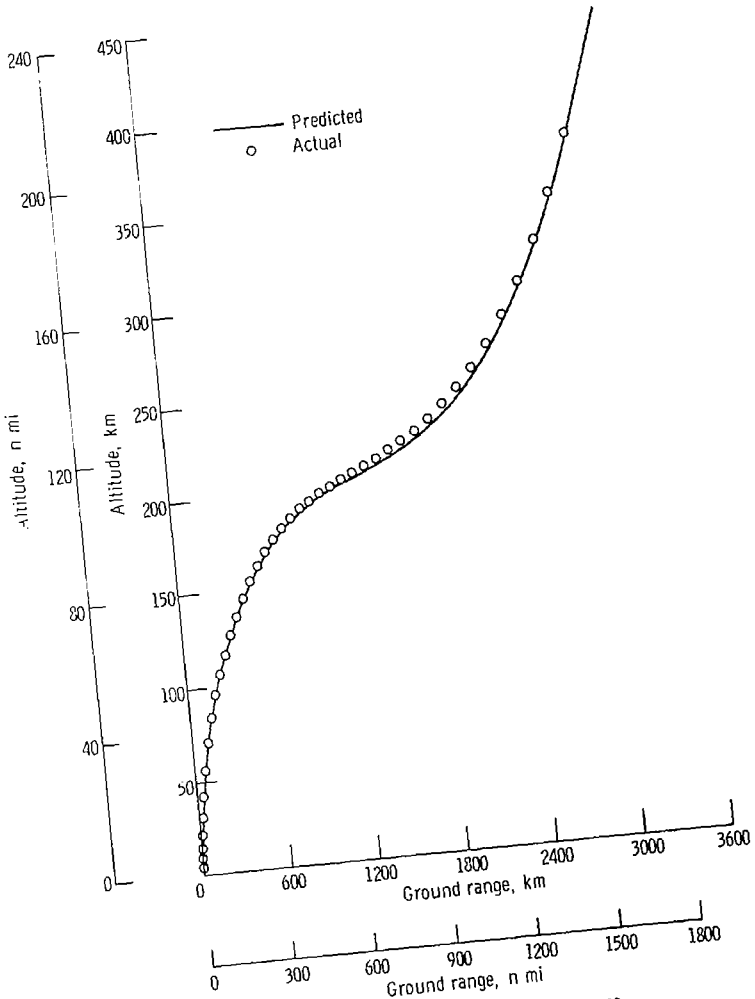

Figure V-6. - Altitude against ground range, AC-20.

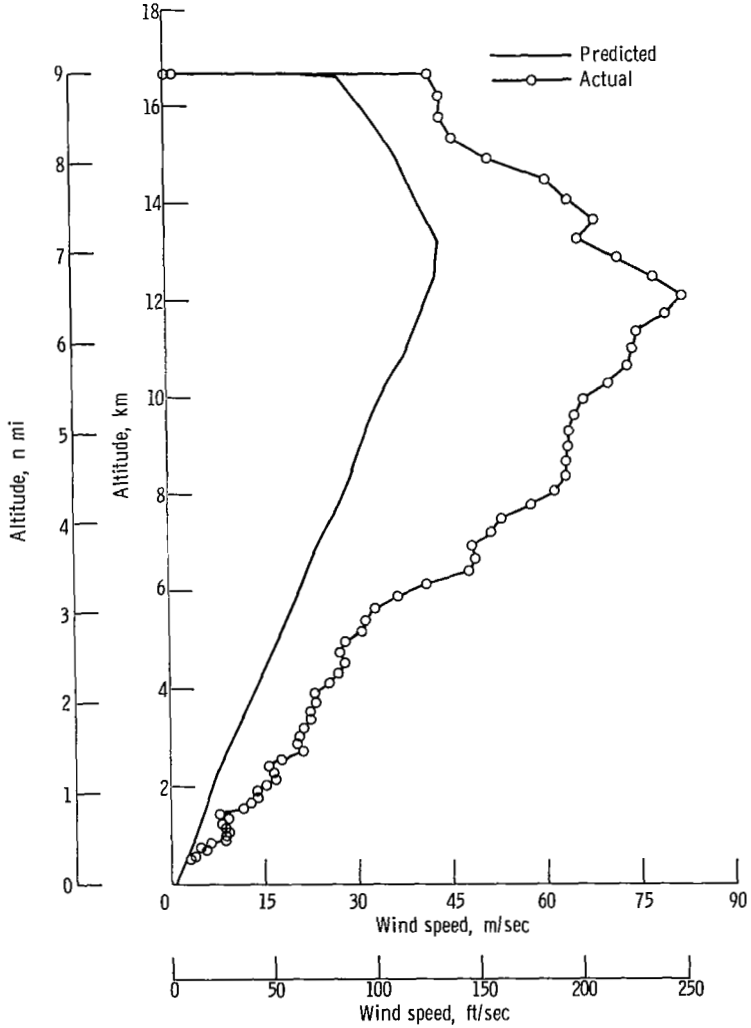

Figure V-7. - Altitude as function of wind speed, AC-19.

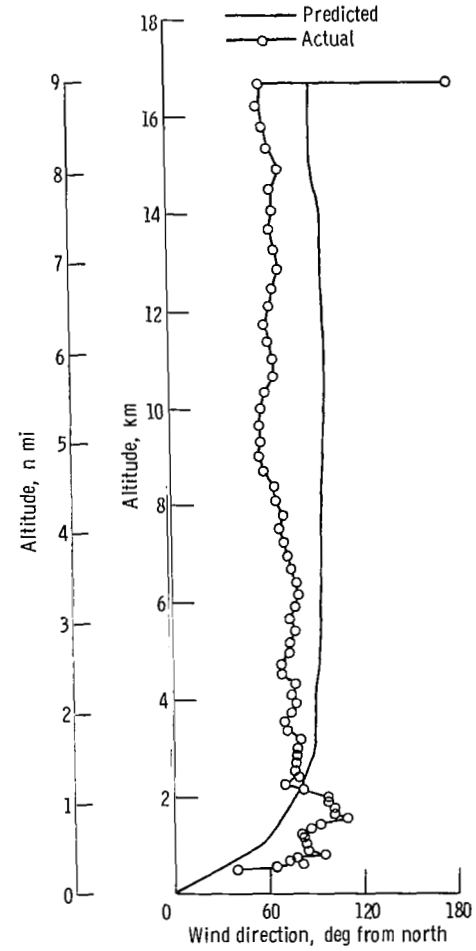

Figure V-8. - Altitude as function of wind direction, AC-19.

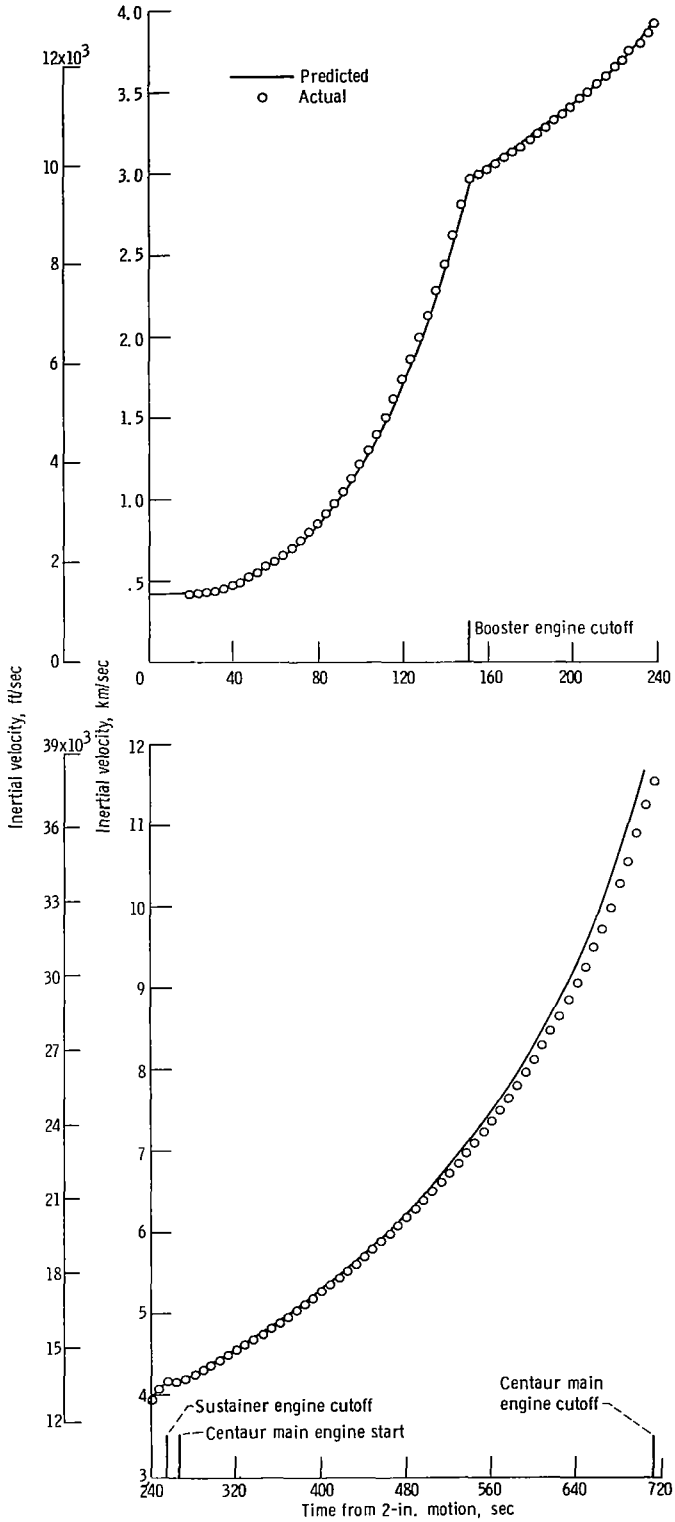

Figure V-9. - Inertial velocity as function of time, AC-19.

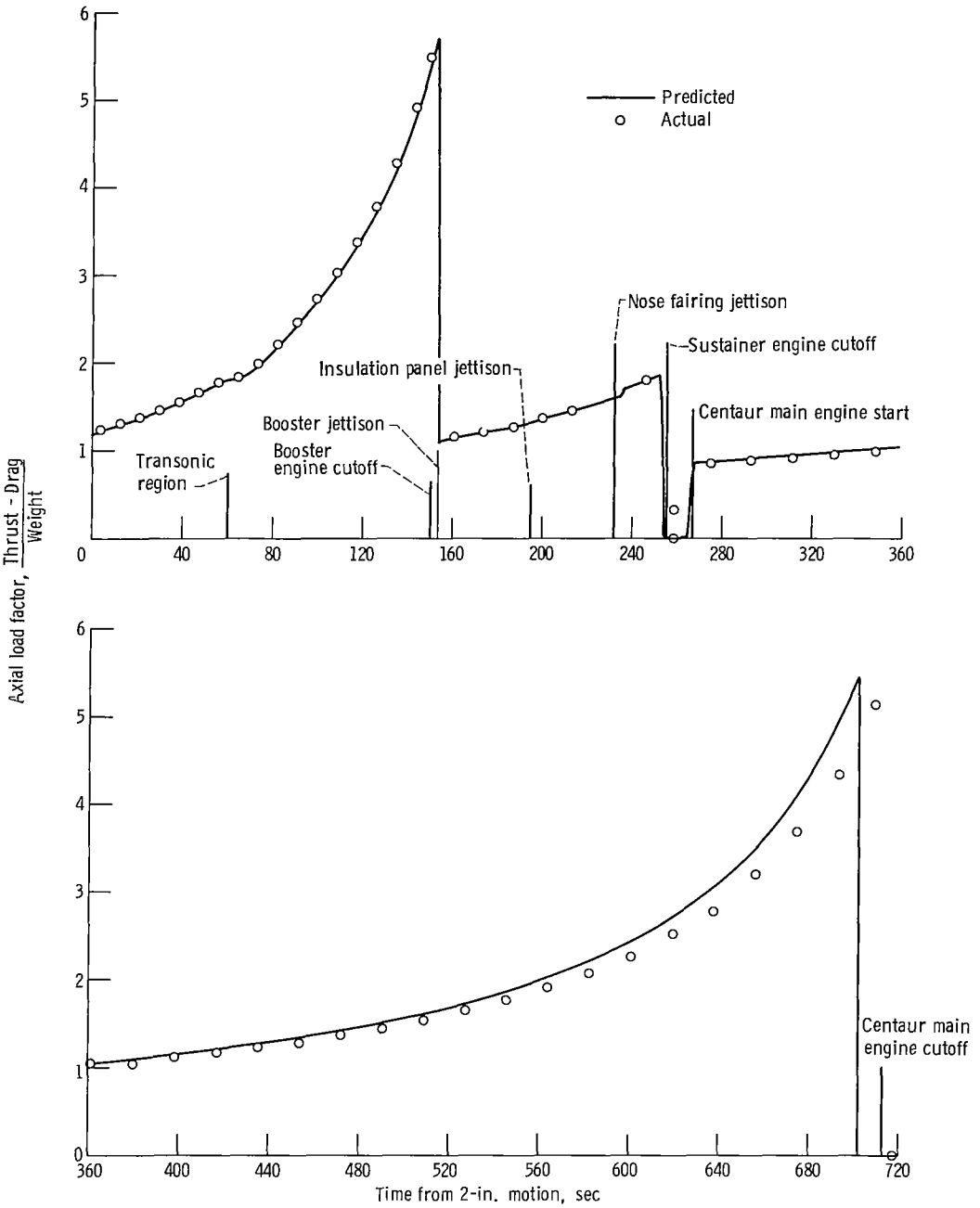

Figure V-10. - Axial load factor, AC-19.

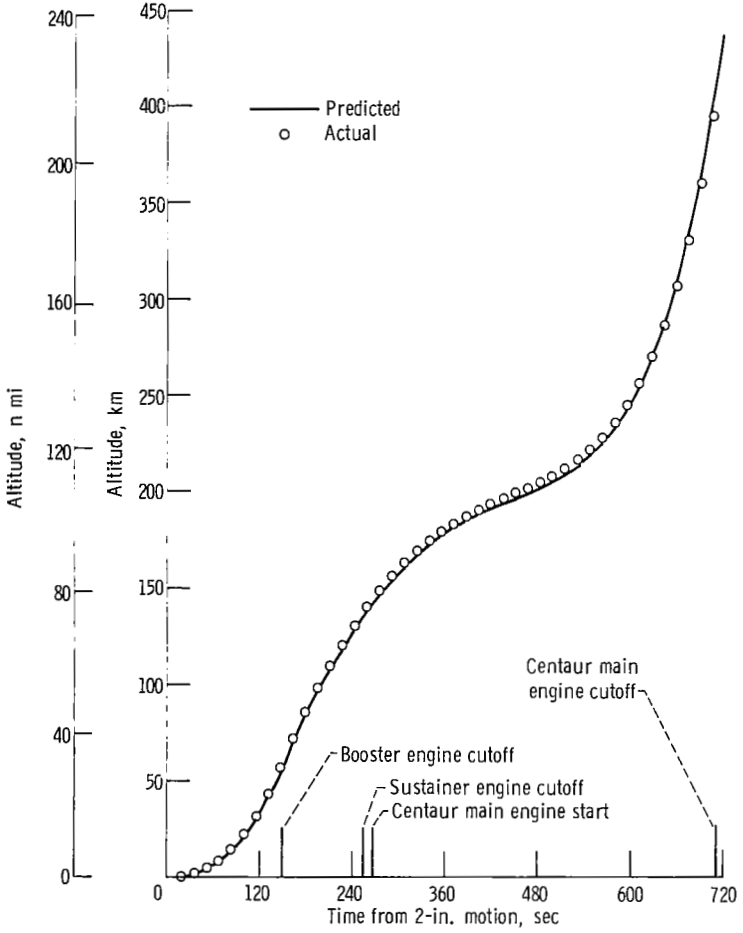

Figure V-11. - Altitude as function of time, AC-19.

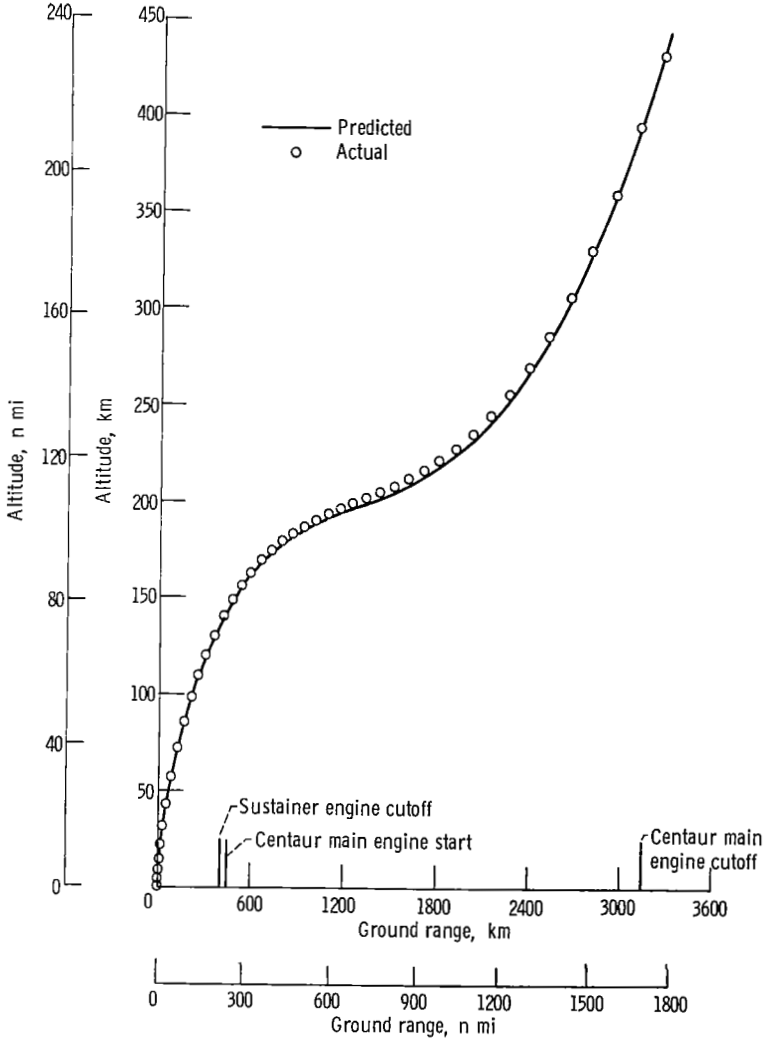

Figure V-12. - Altitude against ground range, AC-19.

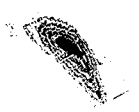

VI. LAUNCH VEHICLE SYSTEMS ANALYSIS

PROPULSION SYSTEM

by Kenneth W. Baud, Charles H. Kerrigan, and Donald B. Zelten

Atlas

System description. - The Atlas engine system (fig. VI-1) consists of a booster engine, a sustainer engine, two vernier engines, an engine start tank system, and an electrical control system. The engines use liquid oxygen and RP-1 (kerosene) for propellants. During engine start, electrically fired pyrotechnic igniters are used to ignite the gas generator propellants for driving the turbopumps; and hypergolic igniters are used to ignite the propellants in the thrust chambers of the booster, sustainer, and vernier engines. The pneumatic control of the engine system is discussed in the section PNEUMATIC SYSTEMS.

The booster engine, rated at 1494×10^3 newtons (336×10^3 lbf) thrust at sea level, consists of two gimbaled thrust chambers, propellant valves, two oxidizer and two fuel turbopumps driven by one gas generator, a lubricating oil system, and a heat exchanger. The sustainer engine, rated at 258×10^3 newtons (58×10^3 lbf) thrust at sea level, consists of a thrust chamber, propellant valves, one oxidizer and one fuel turbopump driven by a gas generator, and a lubricating oil system. The entire sustainer engine system gimbals. Each vernier engine is rated at 2.98×10^3 newtons (670 lbf) thrust at sea level and propellants are supplied from the sustainer turbopump. The vernier engines gimbal for roll control.

The engine start tank system consists of two spherical helium-pressurized propellant tanks for liquid oxygen and RP-1 (kerosene), each approximately 51 centimeters (20 in.) in diameter. This system supplies starting propellants (oxidizer and fuel) for the gas generators and the vernier engines, and fuel only for the booster and sustainer engines, for a period of approximately 2 seconds; thereafter, the turbopumps provide the propellants to sustain the engines.

System performance. - The performance of the Atlas propulsion system was satisfactory on each of the Mariner missions VI and VII. During the engine start phase for each vehicle, engine valve opening times and starting sequence events were within tolerances. The Atlas engine performance for the AC-20 and AC-19 flights was evaluated by

comparing measured parameters with the expected values. The data are tabulated in table VI-I.

On AC-20, booster engine cutoff (BECO) occurred 4.9 seconds earlier than expected because of a faulty backup staging accelerometer. (Refer to the section GUIDANCE AND FLIGHT CONTROL SYSTEMS for additional information on the faulty staging accelerometer.) Because of the premature BECO, sustainer and vernier engine cutoff (SECO/VECO) occurred approximately 18.5 seconds later than expected. SECO/VECO occurred at T + 270.8 seconds and resulted from liquid-oxygen depletion, the planned shutdown mode.

An apparent instrumentation anomaly occurred on AC-20 wherein the sustainer fuel pump inlet and discharge pressure data each showed a gradual decrease during sustainer engine operation. However, sustainer engine performance did not reflect an actual pressure decay. It is hypothesized that liquid oxygen leaking onto the transducer pressure sensing line caused the fuel in the sensing lines to freeze or partially freeze. This would cause the sustainer fuel pump pressure data to falsely reflect a pressure decay.

On AC-19, BECO occurred as planned when vehicle acceleration reached 5.68 g's (specification is 5.7±0.113 g's). SECO/VECO occurred at T + 255 seconds and was due to liquid-oxygen depletion as planned.

Centaur Main Engines

System description. - Two RL10A-3-3 engines (identified as C-1 and C-2) are used to provide thrust for the Centaur stage. Each engine (fig. VI-2) has a thrust chamber and is regeneratively cooled and turbopump fed. Propellants are liquid oxygen and liquid hydrogen. Engine rated thrust is 66 700 newtons (15 000 lbf) at an altitude of 61 000 meters (200 000 ft).

Starting and stopping of the engines is controlled by pneumatically operated valves which receive helium control pressure from engine-mounted solenoid valves. Discrete commands from the vehicle control system operate these solenoid valves. Ignition is accomplished by a spark igniter recessed in the propellant injector face. These engines operated by a "bootstrap" process: pumped fuel is circulated through the thrust chamber tubes and is than expanded through a turbine which drives the propellant pumps. This routing of fuel through the thrust chamber tubes serves the dual purpose of cooling the thrust chamber walls and adding energy to the fuel prior to expansion through the turbine. After passing through the turbine, the fuel is injected into the combustion chamber. The pumped oxidizer is supplied directly to the combustion chamber after passing through the propellant utilization (mixture ratio control) valve. The thrust level is maintained by regulating the amount of fuel bypassed around the turbine as a function of combustion chamber pressure.

System performance. - In-flight turbopump chilldown was commanded 8.0 seconds prior to main engine start for both flights. This chilldown was accomplished by opening both the oxidizer and the fuel pump inlet valves. The oxidizer passed through the pump and into the combustion chamber; the fuel flowed through the pump and discharged overboard through separate cooldown valves, one located downstream of each pump stage. The chilldown successfully prevented cavitation of the turbopumps during the start transients.

Main engine start was commanded at T + 282.3 and T + 266.5 seconds for AC-20 and AC-19, respectively. (Refer to the section GUIDANCE AND FLIGHT CONTROL SYSTEMS for details on the cause of the late engine start of AC-20.) The engine start transients were normal.

Fuel and oxidizer pump inlet temperatures and pressures indicated that the propellants remained above saturation at all times during engine operation. This condition ensured satisfactory net positive suction pressure (i.e., total pressure minus saturation pressure) throughout the engine firing periods.

Steady-state operating performance of the engines was evaluated by comparing measured parameters with the expected values. These data are tabulated in table VI-II. On AC-19 telemetry data indicated that the values of thrust chamber pressure for the C-1 and C-2 engines were lower than expected; however, the other related parameters for the engines indicated normal levels. It is therefore assumed that these low thrust chamber pressure values were falsely indicated. Similar data have been noted on a number of previous flights, and the cause of this data anomaly is not known.

Main engine cutoff was commanded by the guidance system at T + 725.5 and T + 712.2 seconds for AC-20 and AC-19, respectively. Engine shutdown sequences were normal The main engine firing durations were 7.4 and 8.8 seconds longer than expected for AC-20 and AC-19, respectively. No explanation is available for the longer-than-predicted firing time of AC-20 and AC-19. However, the longer-than-expected Centaur firing duration did not affect the performance of the Centaur stage.

A retrothrust operation was initiated at T + 1575.5 seconds for AC-20 and at T + 1562.4 seconds for AC-19. This operation was performed by commanding the pump inlet valves to open and allowing the propellants in the tanks to discharge through the main engine system.

Centaur Boost Pumps

System description. - A single boost pump is used for each propellant tank to supply propellants to the main engine turbopumps at the required inlet pressures. Each boost pump is a mixed-flow centrifugal type, and is powered by a hot-gas-driven turbine. The hot gas consists of superheated steam and oxygen from the catalytic decomposition of

90-percent-concentration hydrogen peroxide. Constant power is maintained on each turbine by metering the hydrogen peroxide through fixed orifices upstream of the catalyst bed. A speed-limiting control system is provided on each turbine; however, on these flights they were disconnected. The complete boost pump and hydrogen peroxide supply systems are shown in figures VI-3 to VI-6.

System performance. - Performance of the boost pumps was satisfactory for both the AC-20 and the AC-19 flights. Boost pump start occurred at T + 209.5 seconds for AC-20, and at T + 213.0 seconds for AC-19. Boost pump cutoff occurred at T + 725.5 seconds for AC-20, and at T + 712.2 seconds for AC-19. The relatively long boost pump operating time for AC-20 compared to AC-19 was caused by an early booster engine cutoff on AC-20. The early booster engine cutoff resulted in a long sustainer engine firing, and therefore a delayed Centaur engine start. Since the boost pump start signal is a programmed function referenced to booster engine cutoff, the AC-20 boost pumps were operating for a relatively long time period before the Centaur main engines were started. The turbine inlet pressure delay time (time from boost pump start signal to time of first indication of turbine inlet pressure rise) was less than 1 second for both turbines on the AC-20 and the AC-19 vehicles. A comparison of the expected and actual flight values for steady-state turbine inlet pressures is shown in table VI-III. Plots of turbine speed against time are shown in figures VI-7 to VI-10. The relatively long AC-20 boost pump operating period before start of the Centaur main engines may be seen by comparing AC-20 and AC-19 turbine speed curves. A comparison of the expected and actual flight values for steady-state turbine speeds is shown in table VI-IV. In general, the actual flight turbine speeds were from 600 to 1700 rpm higher than the expected values; however, their increase had no adverse effect on boost pump performance. Boost pump turbine speeds have been consistently higher than the acceptance test values on virtually all previous Centaur flights. These differences are due to the inability to accurately simulate the flight conditions during acceptance tests.

Turbine bearing temperatures for the fuel and oxidizer boost pumps are shown in figure VI-11 for AC-20, and in figure VI-12 for AC-19. The maximum values were comparable to values recorded on previous single-powered-phase flights.

Hydrogen Peroxide Engine and Supply System

System description. - The hydrogen peroxide engine and supply system (figs. VI-13 and VI-4) is identical on both AC-20 and AC-19. The system consists of 14 thruster engines, a supply bottle, and interconnecting tubing to the engines and boost pump turbines. These engines are used after main engine cutoff. Four 222.4-newton (50-lbf) thrust engines (V engines) and four 13.3-newton (3-lbf) thrust engines (S engines) are

used primarily for propellant settling and retention and for retromaneuver. Two clusters, each of which consists of two 15.6-newton (3.5-lbf) thrust engines (A engines) and one 26.7-newton (6-lbf) thrust engine (P engine), are used for attitude control (see table VI-XVII, GUIDANCE AND FLIGHT CONTROL SYSTEMS section for mode of operation). Propellant is supplied to the engines from a positive-expulsion, bladder-type storage tank which is pressurized with helium to an absolute pressure of about 210 N/cm^2 (305 psi) by the pneumatic system. The hydrogen peroxide is decomposed in the engine catalyst beds, and the hot decomposition products are expanded through converging-diverging nozzles to provide thrust. Hydrogen peroxide is also provided to drive the boost pump turbines. All the hydrogen peroxide supply lines are equipped with heaters; but on AC-20 and AC-19, and all other single-powered-phase vehicles, the heaters were not required on the boost pump feedlines and they were electrically disconnected.

Vehicle configuration changes were made on AC-20 and AC-19 as a result of suspected cryogenic leakage during the AC-17 flight. All the openings in the liquid-oxygen-tank radiation shield were covered in the vicinity of the hydrogen peroxide bottle to shield the hydrogen peroxide system from any leakage from the liquid-oxygen tank. A fiber-glass shield was also installed on the hydrogen peroxide bottle support yoke to protect the system from possible leakage from the liquid-oxygen-tank sump flanges and the liquid-oxygen-supply ducting. In addition to these changes, which were incorporated on both AC-20 and AC-19, two more shields were installed on AC-19. The liquid-oxygen sump-to-tank flange and the sump-to-pump flange were enclosed in shields to collect any liquid-oxygen leakage and direct it away from the hydrogen peroxide system.

System performance. - The location of the hydrogen peroxide system instrumentation is shown in figure VI-14. Four of the engine chamber surfaces were instrumented for temperature, three of the measurements being common to both AC-20 and AC-19 (two of the 13.3-N (3-lbf) thrust engines (S1 and S3), and one of the 26.7-N (6-lbf) thrust engines (P1)). The fourth engine measurement on each vehicle was on a 15.6-newton (3.5-lbf) thrust engine (A1 on AC-20 and A2 on AC-19). The S3 engine chamber temperature measurement reacted abnormally on both AC-20 and AC-19. During the V-half-on firing mode (see table VI-XVII, GUIDANCE AND FLIGHT CONTROL SYSTEMS section for details on this mode), which starts at main engine cutoff + 460 seconds, the S3 engine temperature increased rapidly, indicative of engine firing. The attitude control engine firing logic precludes the S engines firing during the V-half-on firing mode; therefore, there should not have been any increase in temperature. Investigation of the problem revealed an instrumentation installation error. Preflight photographs of the AC-20 vehicle showed that the thermocouple was clamped to the V3 engine rather than to the S3 engine. Photographs of this particular area on AC-19 are not available but it is assumed the same installation error was made on it. The increase in temperature was therefore a normal response to the V3 engine firing. All other engine temperature data indicated

normal performance. Temperature changes verified engine firing as programmed and as required to maintain vehicle control.

Two hydrogen peroxide supply system temperatures displayed unexpected cooling during the launch countdown of AC-20 (fig. VI-15). Shortly after the start of liquid-oxygen tanking, measurement CP351T (hydrogen peroxide feedline tee temperature) decreased from 311 K (101° F) to 265 K (17° F) within a period of about 16 minutes. The temperature then gradually decreased to 258 K (6° F) at lift-off. In a similar manner, measurement CP347T (hydrogen peroxide line between the boost pump feed valve and tee) decreased from 308 K (95° F) to 281 K (47° F) in about 14 minutes and then gradually decayed to 266 K (20° F) at lift-off. These two temperatures were considerably colder than the other hydrogen peroxide system temperatures on AC-20. They were considerably colder than the temperatures experienced during the integrated propellant tanking test, and they were colder than the same measurements on AC-19. The data tend to indicate a cryogenic leak but there is no conclusive proof of this hypothesis. After vehicle launch the two measurements reacted normally.

All other system temperatures were normal at lift-off on AC-20 (fig. VI-16). Shortly after the hydrogen peroxide bottle was pressurized at T - 180 seconds, the temperature measurement (CP346T) of the line between the bottle and the boost pump feed valve showed a sharp increase. This was the result of warm hydrogen peroxide being forced from the bottle and into the line. Immediately after lift-off all line temperatures decreased due to termination of the warm gas conditioning supply to the Centaur thrust section. On AC-20 starting at T + 115 seconds the temperature measurement (CP349T) of the line between the liquid-oxygen boost pump speed-limiting valve and the catalyst bed increased about 6 K. A more pronounced increase of 15 K was noted on AC-19 at T + 97 seconds. The same measurement on AC-16 responded like that on AC-20. On all previous vehicles the temperature of this particular line was not recorded. There is no reasonable explanation for the temperature of this line to increase as it did prior to boost pump start. However, it does appear to be a common phenomenon since it has occurred on all three flights where data were recorded.

At boost pump start, all hydrogen peroxide supply line temperatures rose abruptly as the relatively warmer hydrogen peroxide from the supply bottle flowed through the lines (fig. VI-16). During boost pump operation all the supply line temperatures stabilized at values near the temperature of the hydrogen peroxide in the supply bottle, which was 300 K (80° F). At main engine cutoff the flow of hydrogen peroxide was terminated in the boost pump feedlines, and all the line temperature measurements except CP348T and CP349T began a gradual cooling trend as the lines radiated heat to the space environment. Measurements CP348T and CP349T, which record the temperature of the line between the speed-limiting valve and catalyst bed of the liquid-hydrogen and liquid-oxygen boost pumps, respectively, showed a pronounced warming trend. This was expected,

and resulted from the close proximity of these lines to the hot boost pump turbines.

With the exception of the specific deviations previously noted, the hydrogen peroxide supply line temperatures shown in figures VI-15 and VI-16 for AC-20 are representative for both flights.

TABLE VI-I. - ATLAS PROPULSION SYSTEM PERFORMANCE, AC-20 AND AC-19

Parameter	Units	Expected operating range	T + 10 seconds		Booster engine cutoff		Sustainer/vernier engine cutoff[a]	
			AC-20	AC-19	AC-20	AC-19	AC-20	AC-19
Booster engine number 1 thrust chamber:								
Pressure, absolute	N/cm^2	386 to 410	397	398	399	400	(b)	(b)
	psi	560 to 595	575	577	579	580	(b)	(b)
Turbopump speed	rpm	6225 to 6405	6340	6370	6340	6350	(b)	(b)
Booster engine number 2 thrust chamber:								
Pressure, absolute	N/cm^2	386 to 410	397	400	402	405	(b)	(b)
	psi	560 to 595	575	580	583	587	(b)	(b)
Turbopump speed	rpm	6165 to 6345	6334	6330	6342	6330	(b)	(b)
Booster engine gas generator pressure, absolute	N/cm^2	351 to 382	368	371	365	371	(b)	(b)
	psi	510 to 555	534	538	529	538	(b)	(b)
Sustainer engine:								
Thrust chamber pressure, absolute	N/cm^2	469 to 493	496	493	489	485	476	481
	psi	680 to 720	719	715	710	702	690	697
Gas generator discharge pressure, absolute	N/cm^2	427 to 469	427	460	427	460	427	466
	psi	620 to 680	620	667	620	667	620	675
Turbopump speed	rpm	10 025 to 10 445	10 252	10 350	10 284	10 240	10 267	10 350
Vernier engine:								
Engine 1 thrust chamber pressure, absolute	N/cm^2	172 to 183	179	181	177	176	177	181
	psi	250 to 265	260	263	256	255	256	263
Engine 2 thrust chamber pressure, absolute	N/cm^2	172 to 183	174	180	174	179	171	181
	psi	250 to 265	252	261	252	259	248	263

[a]Values listed are just prior to sustainer and vernier engine cutoff.
[b]Not applicable.

TABLE VI-II. - CENTAUR MAIN ENGINE SYSTEM PERFORMANCE, AC-20 AND AC-19

Parameter	Units	Expected range	AC-20[a]				AC-19[a]			
			Main engine start + 90 seconds		Main engine cutoff		Main engine start + 90 seconds		Main engine cutoff	
			C-1	C-2	C-1	C-2	C-1	C-2	C-1	C-2
Fuel pump inlet total pressure, absolute	N/cm^2	16.2 to 24.1	19.0	19.8	16.3	16.5	20.7	21.4	17.3	17.4
	psi	23.5 to 33.9	27.5	28.7	23.6	24.0	30.0	31.0	25.0	25.3
Oxidizer pump inlet total pressure, absolute	N/cm^2	31.8 to 47.3	40.0	40.7	39.4	40.7	42.1	43.5	42.1	42.8
	psi	46.2 to 68.7	58.0	59.0	57.0	59.0	61.0	63.0	61.0	62.0
Oxidizer pump speed	rpm	11 865 to 12 507	12 300	12 400	12 375	12 352	12 018	12 430	11 888	12 280
Fuel venturi upstream pressure, absolute	N/cm^2	492 to 528	505	518	506	519	516	511	513	517
	psi	714 to 766	732	751	734	753	748	742	744	750
Fuel turbine inlet temperature	K	192 to 228	209	213	210	213	206	220	201	216
	^oR	345 to 411	377	383	378	383	371	397	362	388
Oxidizer injector differential pressure	N/cm^2	24.8 to 38.6	31.5	30.6	31.3	30.2	29.0	31.7	29.0	31.0
	psi	36 to 56	45.7	44.4	45.4	44.1	42.0	46.0	42.0	45.5
Thrust chamber pressure, absolute	N/cm^2	267 to 275	274	270	275	270	263	263	266	262
	psi	387 to 399	397	392	398	392	381	382	386	379
Thrust	kN	65.5 to 68.2	67.0	66.6	67.9	66.5	67.1	66.0	67.0	66.1
	lbf	14 700 to 15 300	15 060	14 994	15 246	14 961	15 086	14 821	15 026	14 862
Specific impulse	sec	439 minimum	442.8	442.6	442.8	442.9	442.5	441.3	442.7	441.8

[a]Values listed are for times at which the propellant utilization valves were nulled.

TABLE VI-III. - COMPARISON OF EXPECTED AND ACTUAL FLIGHT STEADY-STATE TURBINE INLET PRESSURES FOR CENTAUR BOOST PUMPS, AC-20 AND AC-19

Parameter	Units	AC-20		AC-19	
		Expected[a]	Actual	Expected[a]	Actual
Liquid-oxygen boost pump turbine inlet pressure, absolute	N/cm^2	65.9	66.2	68.2	67.9
	psi	95.6	96.1	99.0	98.5
Liquid-hydrogen boost pump turbine inlet pressure, absolute	N/cm^2	67.4	67.0	71.2	72.6
	psi	97.8	97.2	103.2	105.3

[a]Value obtained from prelaunch component acceptance test.

TABLE VI-IV. - COMPARISON OF EXPECTED AND ACTUAL FLIGHT STEADY-STATE TURBINE SPEEDS FOR CENTAUR BOOST PUMPS, AC-20 AND AC-19

Parameter	Units	AC-20		AC-19	
		Expected[a]	Actual	Expected[a]	Actual
Liquid-oxygen boost pump turbine speed	rpm	33 000	33 600	33 360	34 300
Liquid-hydrogen boost pump turbine speed	rpm	39 900	41 600	40 800	41 500

[a]Value obtained from prelaunch component acceptance test.

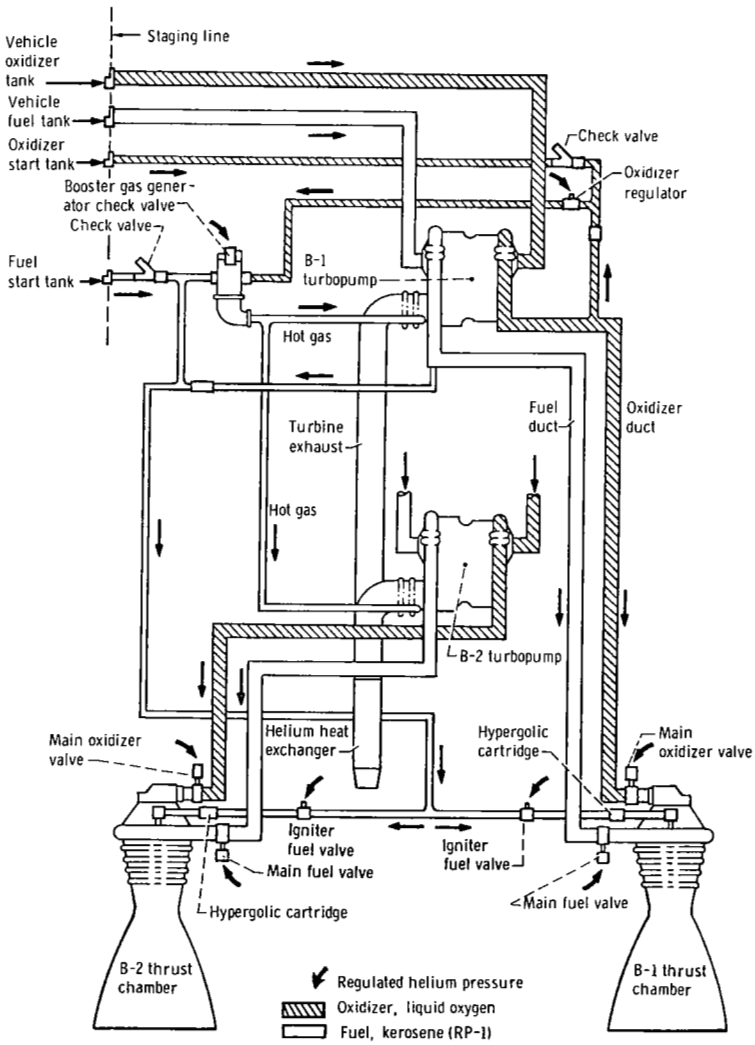

(a) Booster.

Figure VI-1. - Atlas propulsion system, AC-20 and AC-19.

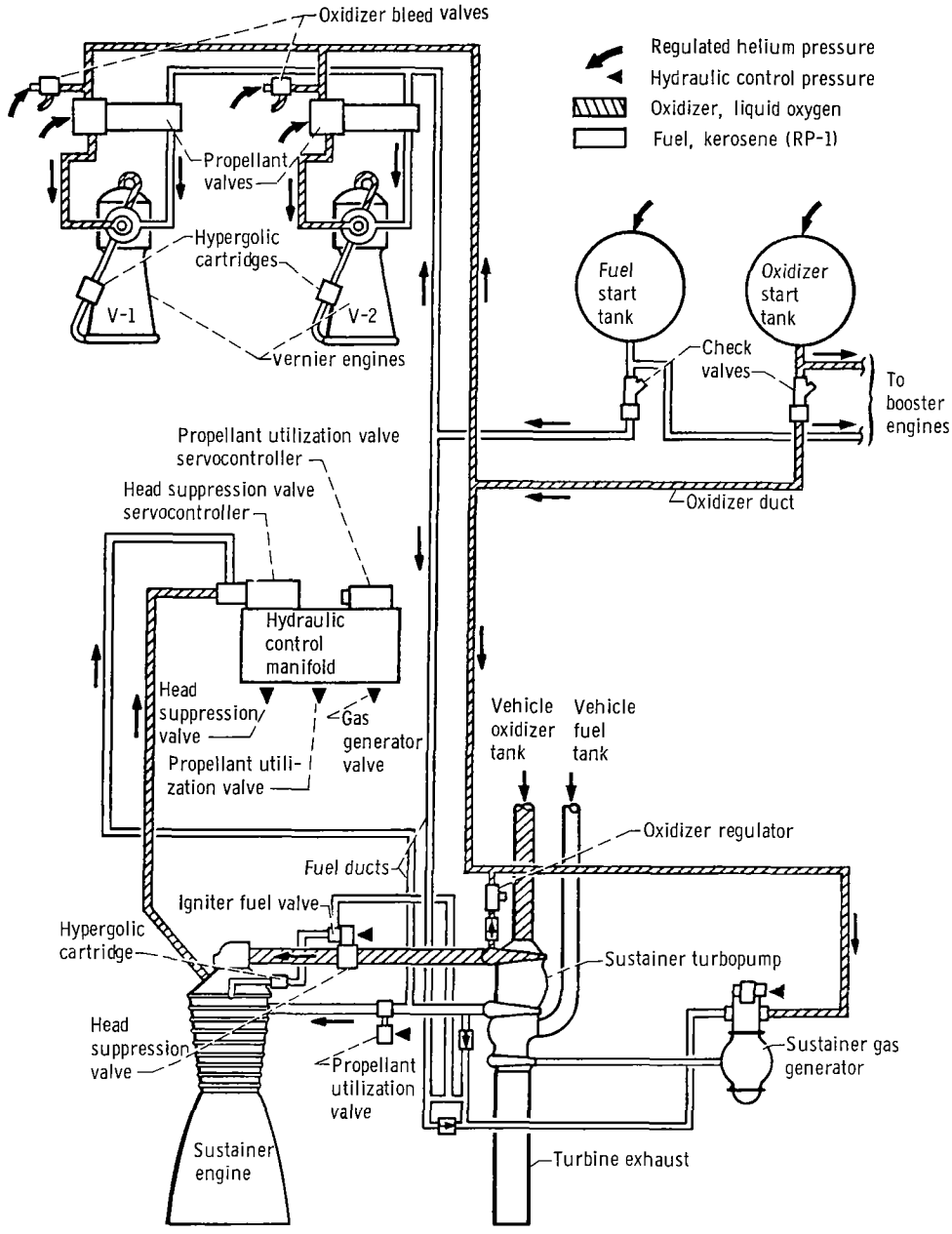

(b) Sustainer and vernier.

Figure VI-1. - Concluded.

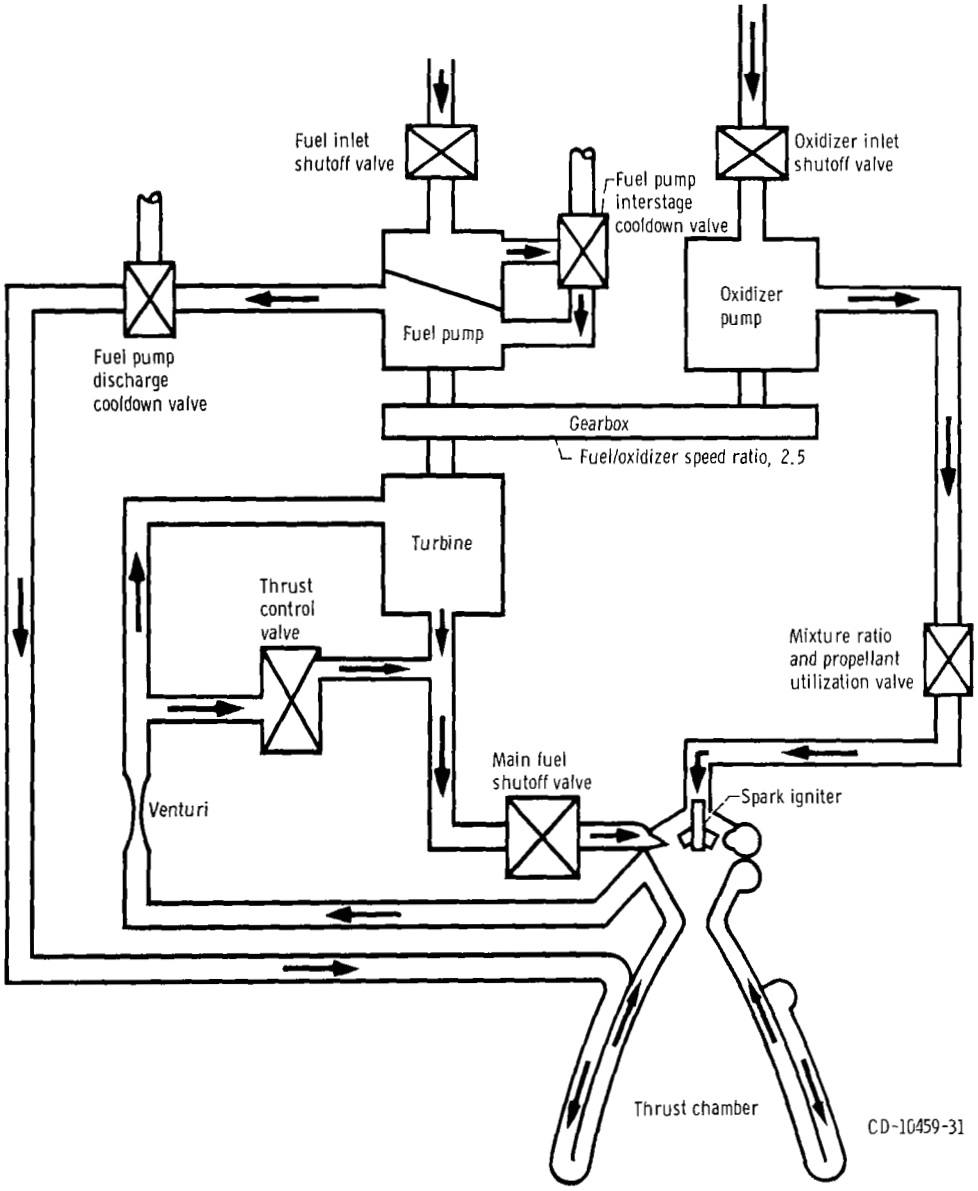

Figure VI-2. - Centaur main engine schematic drawing, AC-20 and AC-19.

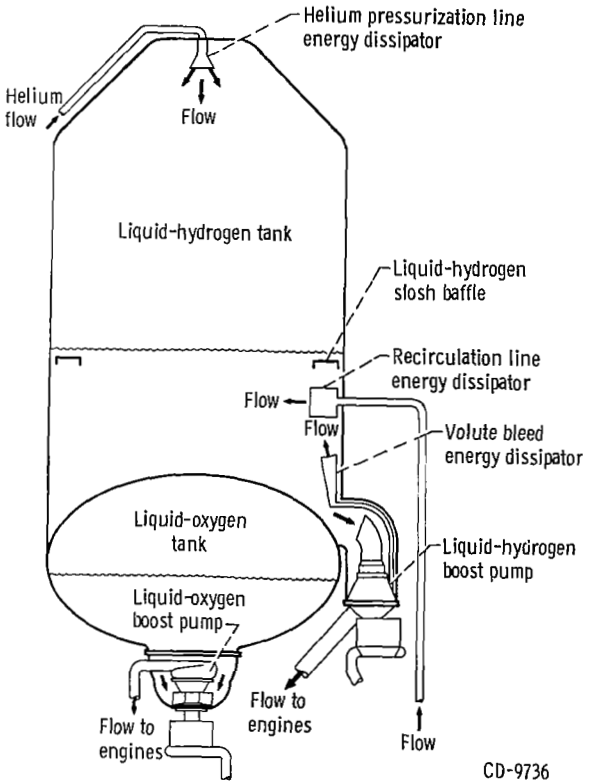

Figure IV-3. - Location of Centaur liquid-hydrogen and liquid-oxygen boost pumps, AC-20 and AC-19.

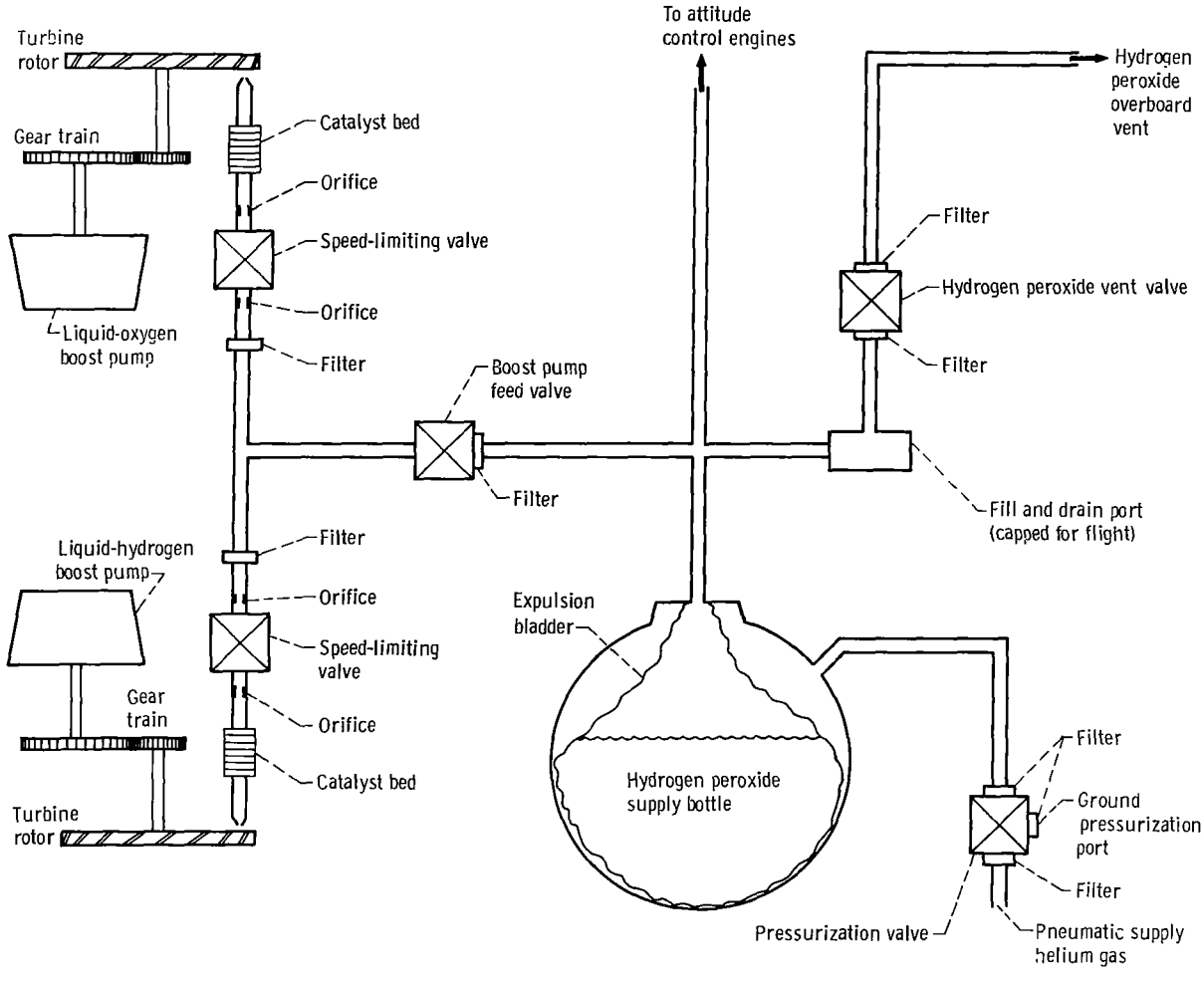

Figure VI-4. - Schematic drawing of Centaur boost pump hydrogen peroxide supply, AC-20 and AC-19.

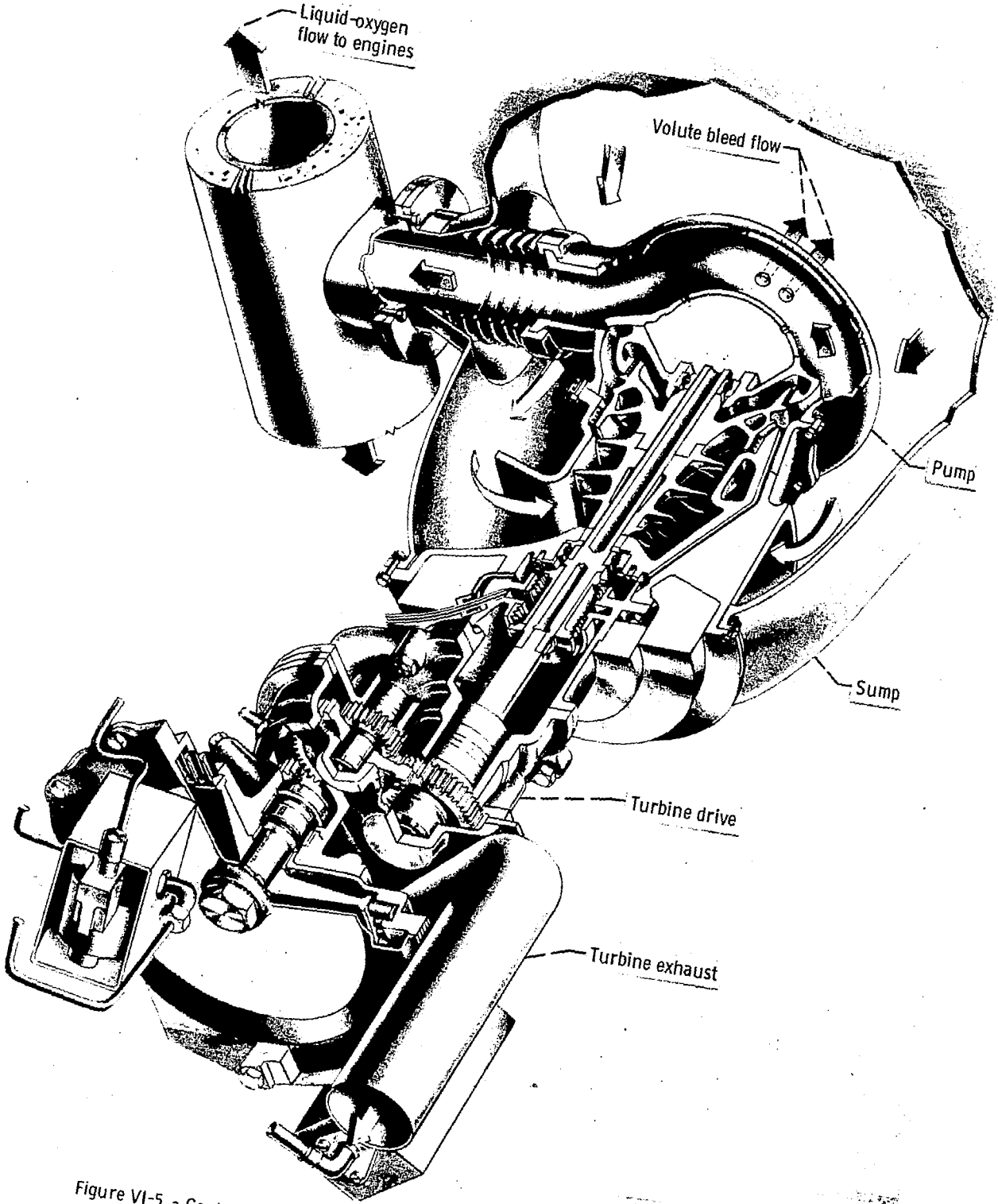

Figure VI-5. - Centaur liquid-oxygen boost pump and turbine cutaway, AC-20 and AC-19.

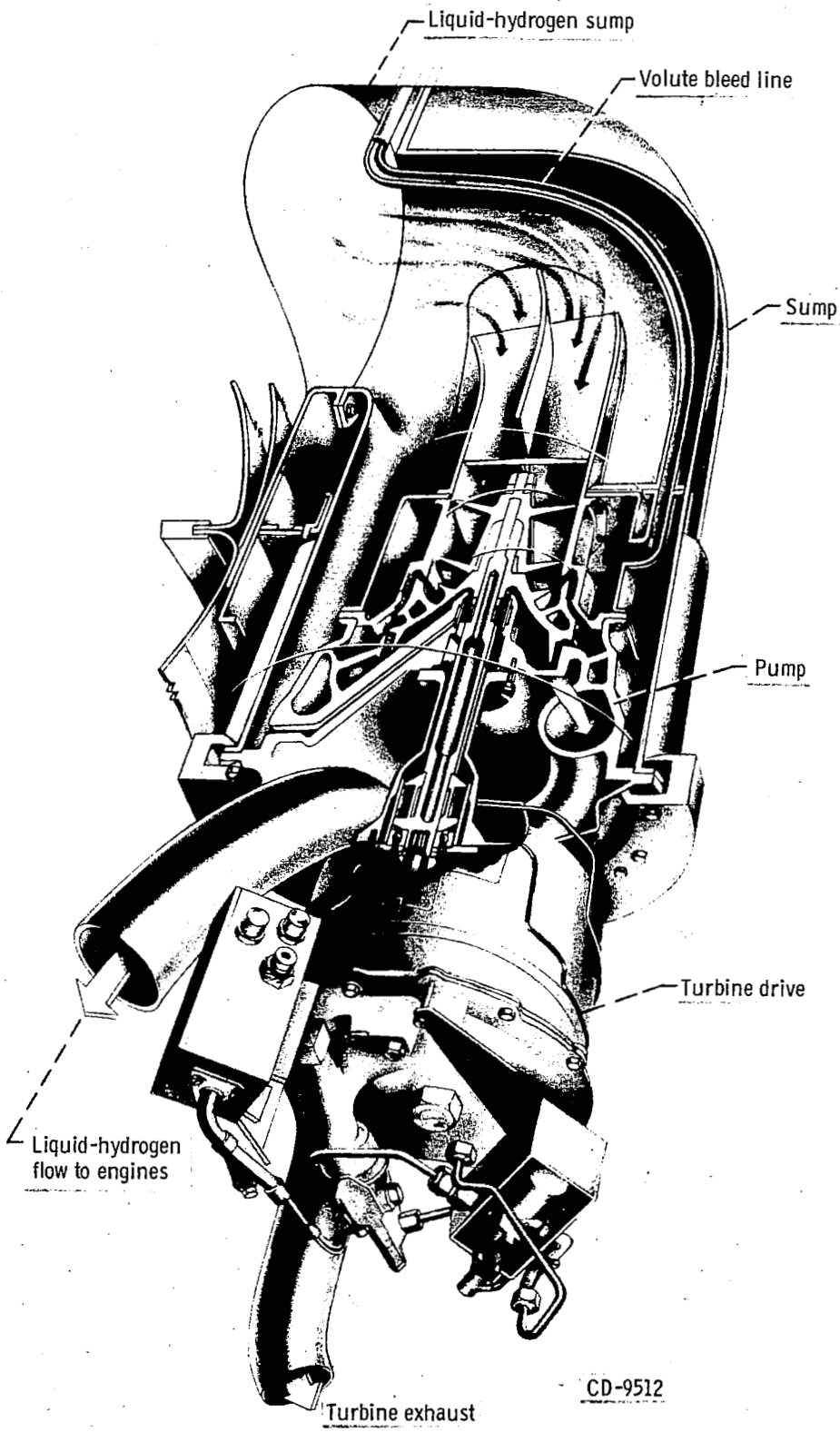

Figure VI-6. - Centaur liquid-hydrogen boost pump and turbine cutaway, AC-20 and AC-19.

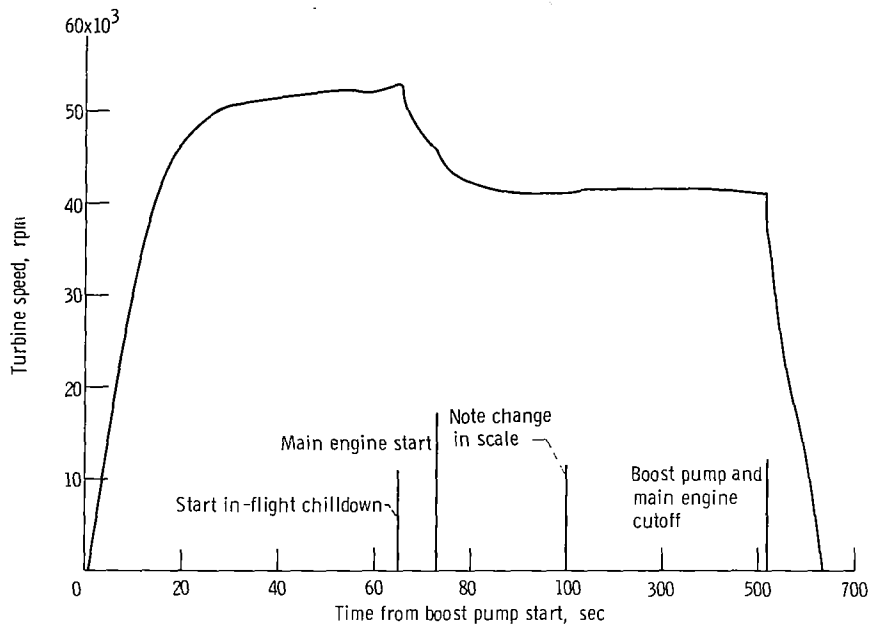

Figure VI-7. - Centaur liquid-hydrogen boost pump turbine speed, AC-20.

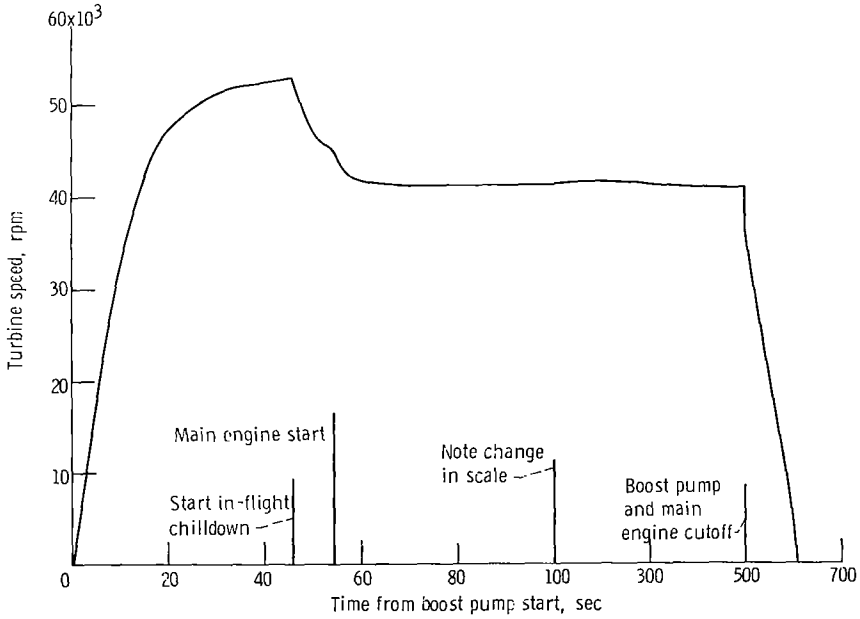

Figure VI-8. - Centaur liquid-hydrogen boost pump turbine speed, AC-19.

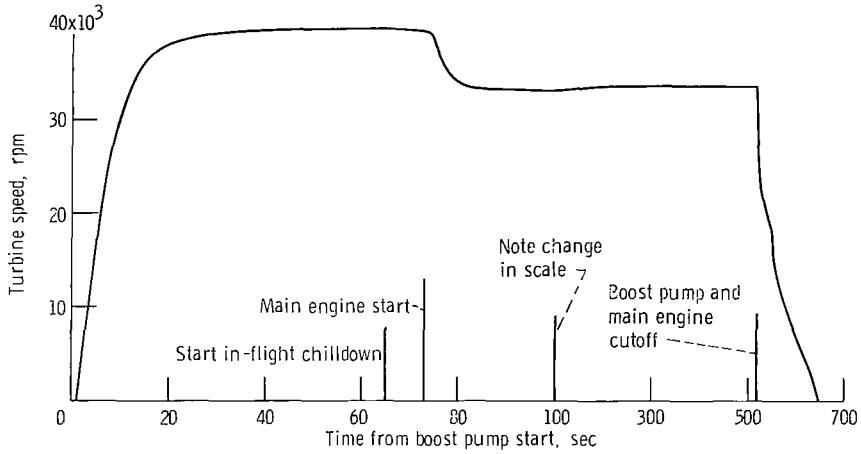

Figure VI-9. - Centaur liquid-oxygen boost pump turbine speed, AC-20.

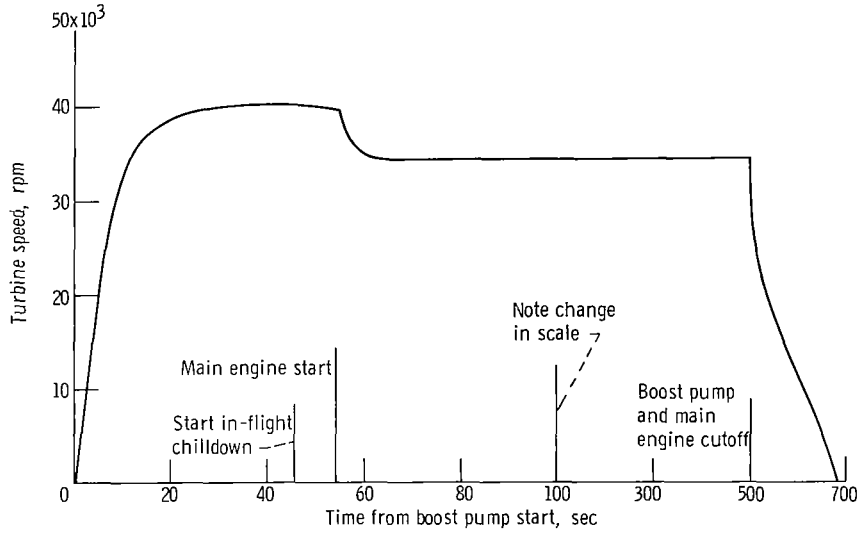

Figure VI-10. Centaur liquid-oxygen boost pump turbine speed, AC-19.

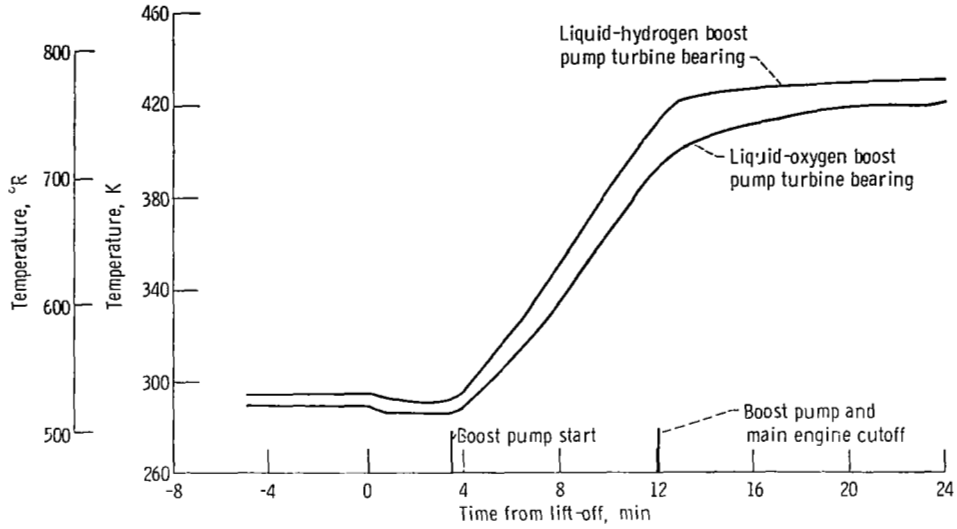

Figure VI-11. - Centaur boost pump turbine bearing temperatures, AC-20.

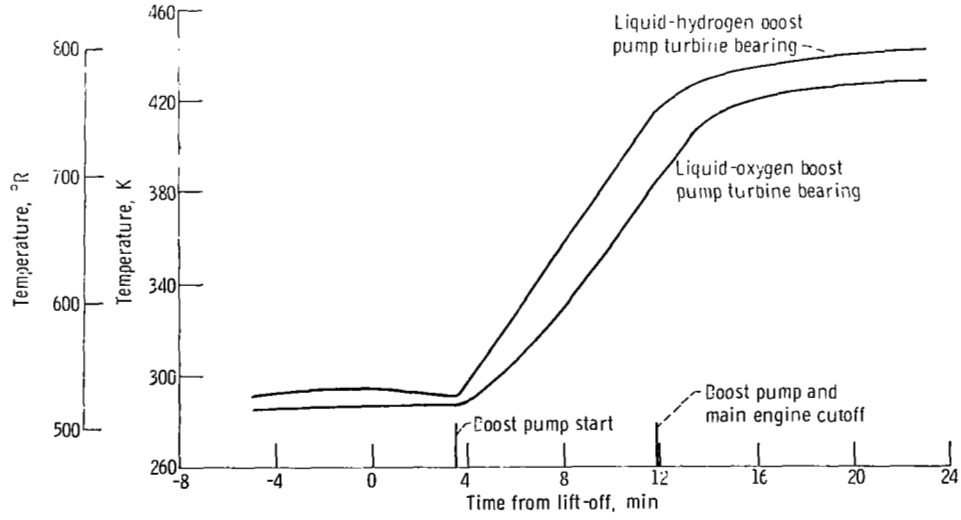

Figure VI-12. - Centaur boost pump turbine bearing temperatures, AC-19.

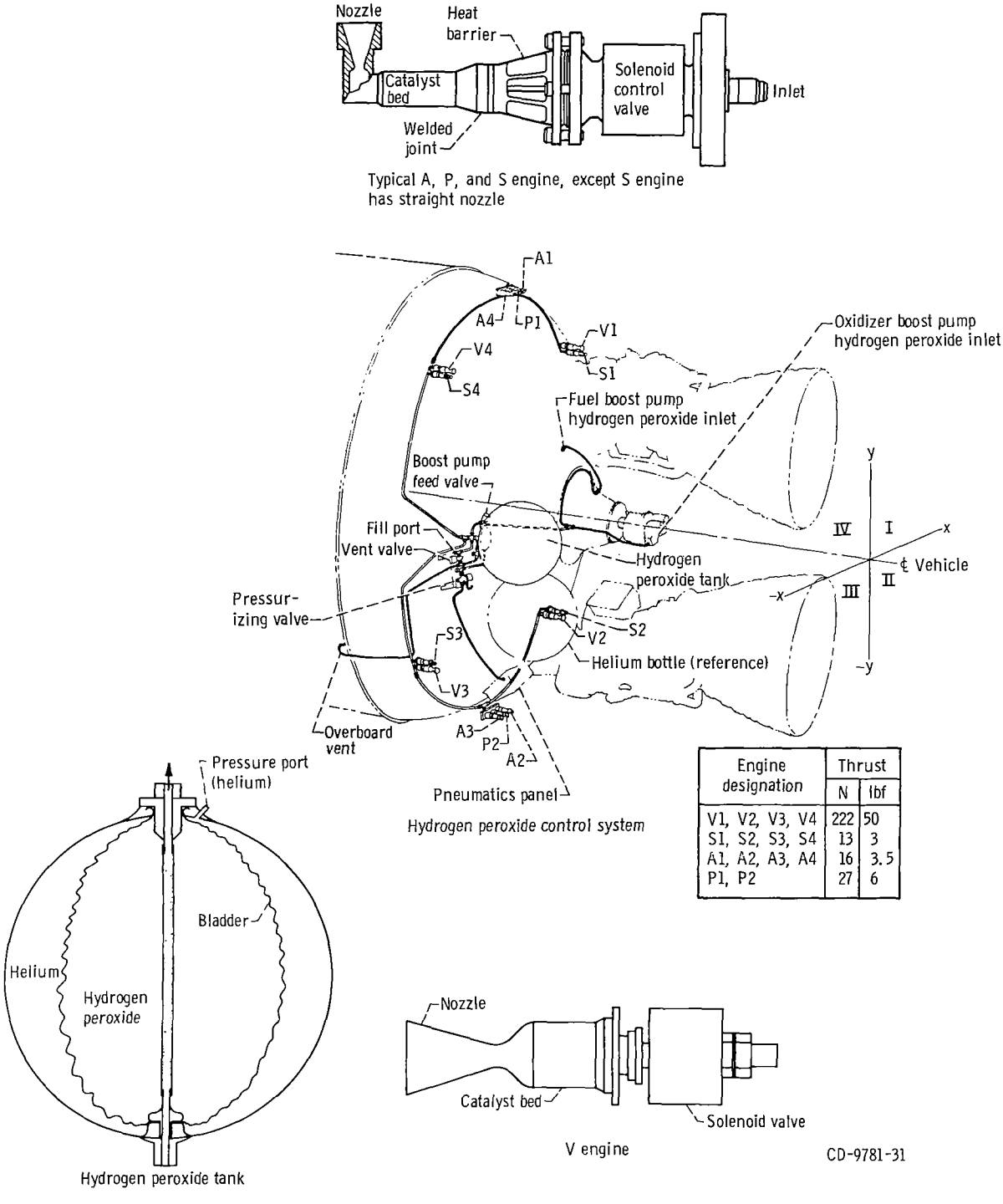

Figure VI-13. - Hydrogen peroxide system isometric, AC-20 and AC-19.

CP344T	Supply line between tee and liquid-oxygen boost pump
CP345T	Supply line between tee and liquid-hydrogen boost pump
CP346T	Supply line between bottle and boost pump feed valve
CP347T	Supply line between boost pump feed valve and tee
CP348T	Supply line between liquid-hydrogen speed-limiting valve and catalyst bed
CP349T	Supply line between liquid-oxygen speed-limiting valve and catalyst bed
CP351T	Supply line tee
CP93T	Hydrogen peroxide in bottle
CP369T	A1 engine chamber surface
CP370T	A2 engine chamber surface
CP373T	P1 engine chamber surface
CP690T	S1 engine chamber surface
CP692T	S3 engine chamber surface

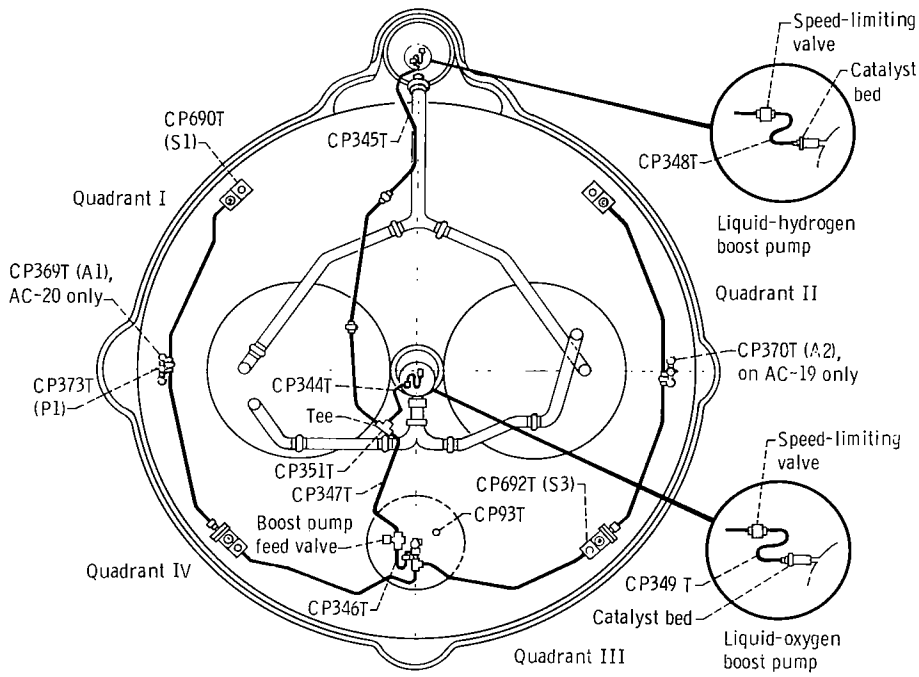

Figure VI-14. - Hydrogen peroxide system temperature instrumentation, AC-20 and AC-19. (All measurements common to both AC-20 and AC-19, except as noted; CP692T installed on V3 engine by error.)

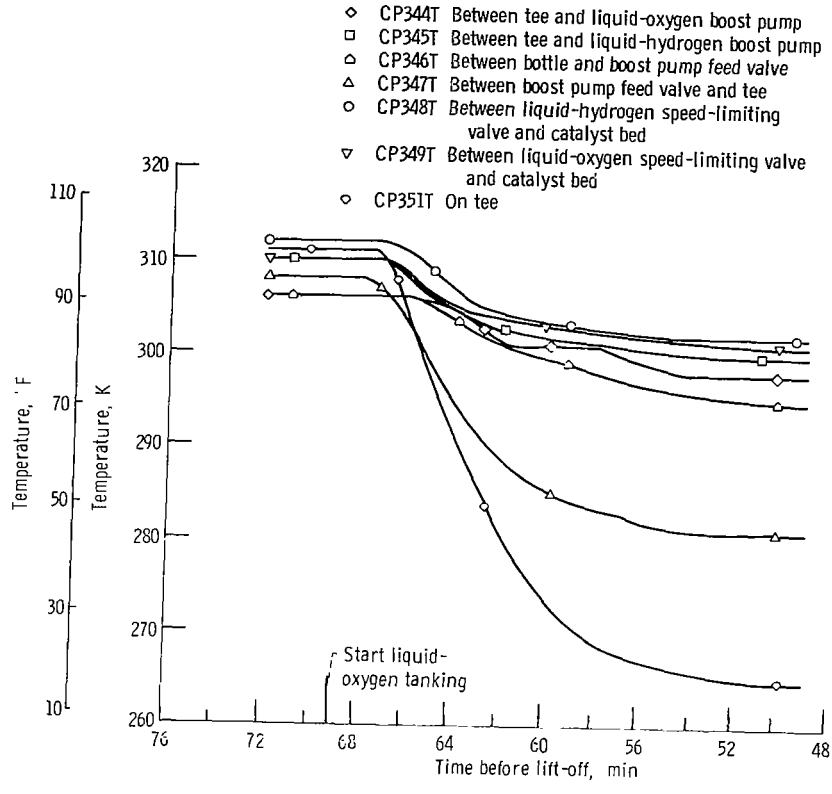

Figure VI-15. - Hydrogen peroxide system temperatures, AC-20.

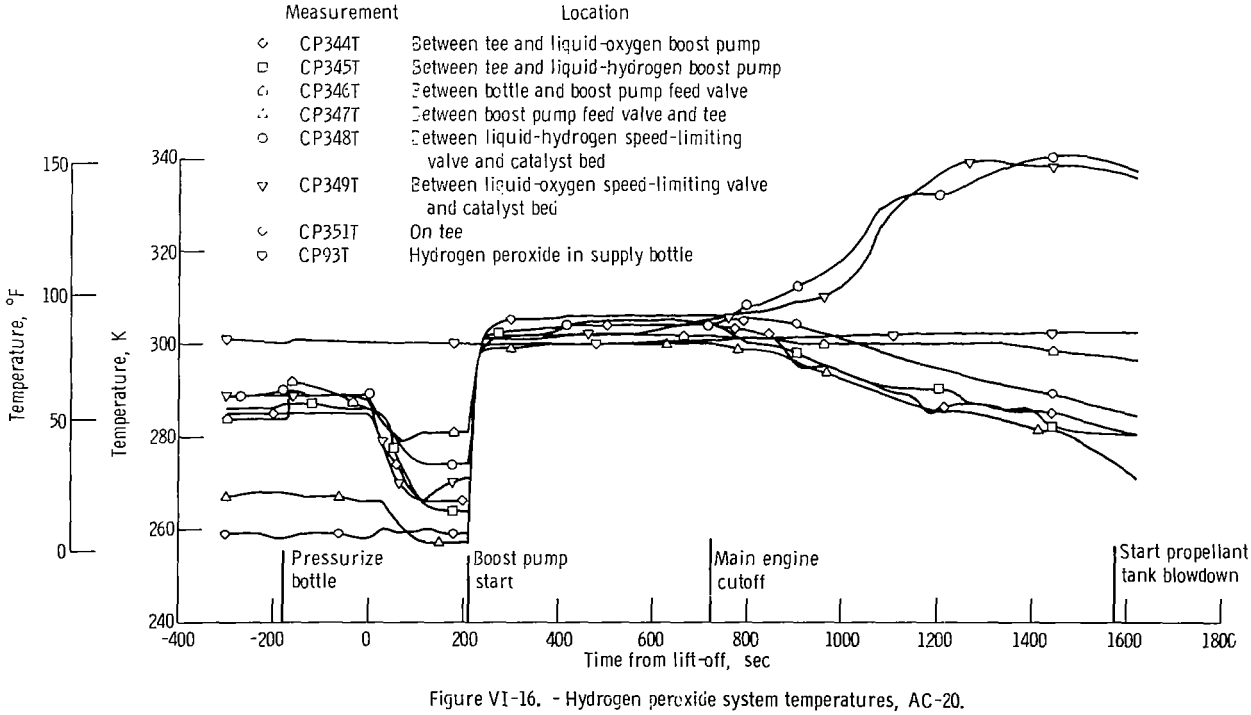

Figure VI-16. - Hydrogen peroxide system temperatures, AC-20.

PROPELLANT LOADING AND PROPELLANT UTILIZATION SYSTEMS

by Richard C. Kalo and Clifford H. Arth

Level-Indicating System for Propellant Loading

System description. - The Atlas propellant-level-indicating system (fig. VI-17) consists of a portable sight gage assembly for RP-1 fuel (kerosene) loading and platinum hot-wire-type sensors for oxidizer (liquid oxygen) loading.

The fuel (RP-1) loading levels are determined by visual observation of the sight gage assembly which is connected to the fuel probe by two temporary sense lines. After tanking, the fuel sight gage assembly and sense lines are removed and the connection points on the vehicle are secured for flight.

The liquid-oxygen loading levels are determined from liquid sensors located at discrete points in the oxidizer (liquid oxygen) tank. The sensing elements are the hot-wire type made with platinum wire (0.001 in. diam), which has a linear resistance-temperature coefficient. The sensors are supplied with a near-constant current of approximately 200 milliamperes; the voltage drop across a sensor reflects the resistance value of the sensor. When covered (immersed in a cryogenic fluid), it has a low resistance and low voltage drop. When uncovered, the wire has a higher resistance and therefore a high voltage drop. A control unit amplifies any change in voltage level and applies this signal to an electronic trigger circuit. When a sensor is wetted, a control relay is deenergized and a signal is sent to the propellant loading operator.

The Centaur propellant-level-indicating system (fig. VI-18) utilizes platinum hot-wire level sensors in both the liquid-oxygen and liquid-hydrogen tanks. These sensors are identical in operation to those used in the Atlas liquid-oxygen tank.

System performance. - Atlas and Centaur propellant loading was satisfactorily accomplished. The weight of the Atlas propellants tanked was calculated for both AC-20 and AC-19. These weights were calculated using a density of 800 kilograms per cubic meter (49 lbm/ft^3) for the fuel and a density of 1100 kilograms per cubic meter (69.29 lbm/ft^3) for the liquid oxygen. These calculated values are presented in the following table:

Propellant	Units	AC-20	AC-19
Fuel (RP-1)	kg	38 451	38 430
	lbm	84 548	84 413
Liquid oxygen	kg	85 205	85 112
	lbm	186 949	186 840

The weights of the Centaur propellant at lift-off were calculated using the data presented in table VI-V. These calculated values are presented in the following table:

Propellant	Units	AC-20	AC-19
Liquid hydrogen	kg	2 376	2 374
	lbm	5 246	5 242
Liquid oxygen	kg	11 570	11 548
	lbm	25 453	25 406

Atlas Propellant Utilization System

System description. - The Atlas propellant utilization system (fig. VI-19) consists of two mercury manometer assemblies, a computer-comparator, a hydraulically actuated propellant utilization fuel valve, sense lines, and associated electrical harnessing. The system is used to ensure nearly simultaneous depletion of the propellants and minimum propellant residuals at sustainer engine cutoff. This is accomplished by controlling the propellant mixture ratio (oxidizer flow rate/fuel flow rate) to the sustainer engine. During flight, the manometers sense propellant head pressures which are indicative of propellant mass. The mass ratio is then compared to a reference ratio (at lift-off the ratio is 2.27) in the computer-comparator. If needed, a correction signal is sent to the propellant utilization valve controlling the main fuel flow to the sustainer engine. The oxidizer flow is regulated by the head suppression valve. This valve senses propellant utilization valve movement and moves in a direction opposite to that of the propellant utilization valve. This opposite movement thus alters propellant mixture ratio to maintain constant propellant mass flow to the engine.

System performance. - The Atlas propellant utilization system operated satisfactorily for AC-20 and AC-19. The propellant utilization system valve angles are shown in figure VI-20 for AC-20 and in figure VI-21 for AC-19. The valve operates at the null position for the first 13 seconds of flight to prevent oscillations of the valve during lift-off.

During the flight of AC-20, the valve was in the fuel-rich position from T + 13 seconds to approximately T + 242 seconds, and then operated in the oxygen-rich position and reached the oxygen-rich stop by T + 245 seconds. The valve remained at the oxygen-rich stop until T + 255 seconds, and then operated alternately both in fuel- and oxygen-rich positions. After T + 265 seconds, the valve was commanded by the propellant utilization system to oxygen-rich stop to ensure liquid-oxygen depletion at sustainer engine cutoff.

During the flight of AC-19, the valve was in the fuel-rich position from T + 13 seconds until approximately T + 135 seconds. At this time the valve moved to the oxygen-

rich position and continued to the oxygen-rich stop. The valve reached the oxygen-rich stop at T + 144 seconds and remained on the stop for approximately 25 seconds. The valve then operated alternately in the oxygen- and fuel-rich conditions from T + 170 to T + 227 seconds, when it returned to the oxygen-rich stop to ensure liquid-oxygen depletion at sustainer engine cutoff.

The predicted and actual residual propellants above the sustainer engine pump inlets at sustainer engine cutoff for both AC-20 and AC-19 are presented in the following table. These residuals were calculated by using the time the head sensing port uncovers as a reference. Propellants consumed from the time the port uncovers to sustainer engine cutoff include the effect of flow-rate decay for a liquid-oxygen depletion.

Propellant	Units	AC-20		AC-19	
		Predicted	Actual	Predicted	Actual
Fuel (RP-1)	kg	128	78	127	87
	lbm	281	170	279	192
Liquid oxygen	kg	134	164	144	214
	lbm	294	361	317	469

Centaur Propellant Utilization System

System description. - The Centaur propellant utilization system (fig. VI-22) is used during flight to control the ratio of propellants consumed by the main engines and to provide minimum deviation from calculated weights of usable propellant residuals. The probes (sensors) of the propellant utilization system are also used during tanking to indicate propellant levels within the range of these probes. In flight, the mass of propellant in each tank is sensed by a capacitance probe and compared in a bridge balancing circuit. If the mass ratio of propellants in the tanks varies from the predetermined value (5:1 oxidizer to fuel), an error signal is sent to the proportional servopositioners which control the liquid-oxygen flow control valves (one on each engine). When the mass ratio is greater than 5:1, the liquid-oxygen flow is increased to return the ratio to 5:1. When the ratio is less than 5:1, the liquid-oxygen flow is decreased. The sensing probes do not extend to the top of the tanks, and therefore are not used for control until after the probes are uncovered at approximately 90 seconds after Centaur main engine start. For this 90 seconds, the liquid-oxygen flow control valves are maintained at approximately 5:1 propellant mixture ratio. The valves are also commanded to the null position at approximately a 5:1 propellant mixture ratio 27 seconds before Centaur main engine cutoff. This is done because the probes do not extend to the bottom of the tanks, and system control is

lost when the liquid level depletes below the bottom of the probe.

System performance. - The Centaur propellant utilization system operated satisfactorily for the flights of AC-20 and AC-19. The liquid-oxygen valve angles during flight are shown in figures VI-23 and VI-24 for AC-20 and AC-19.

During the AC-20 flight the liquid-oxygen probe was uncovered at main engine start plus 95.6 seconds. The liquid-hydrogen probe was uncovered 5 seconds later. The Centaur timer commanded the valves to begin controlling at main engine start plus 89.6 seconds. The valves then moved to the oxygen-rich stop and remained there for approximately 7.5 seconds. During this time, the system compensated for an excess of 20.2 kilograms (44.5 lbm) of oxygen.

During the AC-19 flight the liquid-oxygen probe was uncovered at main engine start plus 92.5 seconds. The liquid-hydrogen probe was uncovered 10 seconds later. The vehicle programmer commanded the valves to begin controlling at main engine start plus 89.6 seconds. The valves then moved to the oxygen-rich stop and remained there for approximately 8 seconds. During this time, the system compensated for an excess of 20.3 kilograms (44.6 lbm) of oxygen. The excess oxygen for both AC-20 and AC-19 resulted from

(1) Engine consumption rate error accumulated during the first 90 seconds

(2) Propellant loading tolerance

(3) System bias to ensure liquid-oxygen depletion first

The propellant residuals remaining at Centaur main engine cutoff were calculated using the times that the propellant level passed the bottom of the probes as a reference point. The actual and predicted residuals for AC-20 and AC-19 are presented in the following table:

	Units	AC-20		AC-19	
		Predicted	Actual	Predicted	Actual
Total propellant residual:					
Liquid hydrogen	kg	(a)	78	(a)	77
	lbm	(a)	173	(a)	169
Liquid oxygen	kg	(a)	250	(a)	247
	lbm	(a)	551	(a)	542
Usable propellants:					
Liquid hydrogen	kg	46	46	48	44
	lbm	100	101	105	97
Liquid oxygen	kg	193	219	192	215
	lbm	425	483	422	474
Time remaining to depletion:					
Liquid hydrogen	sec	(a)	9.0	(a)	8.35
Liquid oxygen	sec	(a)	8.6	(a)	8.40

[a]Not applicable.

TABLE VI-V. - CENTAUR PROPELLANT LOADING, AC-20 AND AC-19

Quantity or event	Units	AC-20		AC-19	
		Hydrogen	Oxygen	Hydrogen	Oxygen
Sensors required to be wet at T - 90 seconds	percent	99.8	-----	99.8	-----
Sensors required to be wet at T - 75 seconds	percent	------	100.2	------	100.2
Sensor location (vehicle station number)	-------	174.99	373.16	174.99	373.16
Tank volume at sensor[a]	m^3	35.6	12.9	35.6	12.9
	ft^3	1256.69	370.94	1256.69	370.94
Ullage volume at sensor	m^3	0.32	0.23	0.32	0.23
	ft^3	11.22	6.58	11.22	6.58
Liquid-hydrogen 99.8-percent sensor dry at-	sec	T - 49	-----	T - 60	-----
Liquid-oxygen 100.2-percent sensor dry at-	sec	------	T - 0	------	T - 0
Ullage pressure at time sensor goes dry	N/cm^2	15.7	20.8	15.3	21.8
	psia	22.7	30.2	22.3	31.7
Density at time sensor goes dry[b]	kg/m^3	66.96	1100	66.96	1099
	lb/ft^3	4.185	68.85	4.185	68.7
Weight in tank at sensor dry	kg	2382	11 570	2382	11 548
	lbm	5259	25 453	5259	25 406
Liquid-hydrogen boiloff to vent-valve close[c]	kg	6.0	-----	7.95	-----
	lbm	13.2	-----	17.49	-----
Liquid-oxygen boiloff to lift-off[c]	kg	------	0	------	0
	lbm	------	0	------	0
Ullage volume at lift-off	m^3	0.374	0.23	0.374	0.23
	ft^3	13.2	6.58	13.2	6.58
Weight at lift-off[d]	kg	2376	11 570	2374	11 548
	lbm	5246	25 453	5242	25 406

[a]Volumes include 0.05 m^3 (1.85 ft^3) liquid oxygen and 0.72 m^3 (2.53 ft^3) liquid hydrogen for lines from boost pumps to engine turbopump inlet valves.

[b]Liquid-hydrogen density taken from ref. 2; liquid-oxygen density taken from ref. 3.

[c]Boiloff rates determined from tanking test to be 0.15 kg/sec (0.33 lbm/sec) liquid hydrogen and 0.14 kg/sec (0.29 lbm/sec) liquid oxygen.

[d]Propellant loading accuracy: hydrogen, ±3.2 percent; and oxygen, ±1.5 percent.

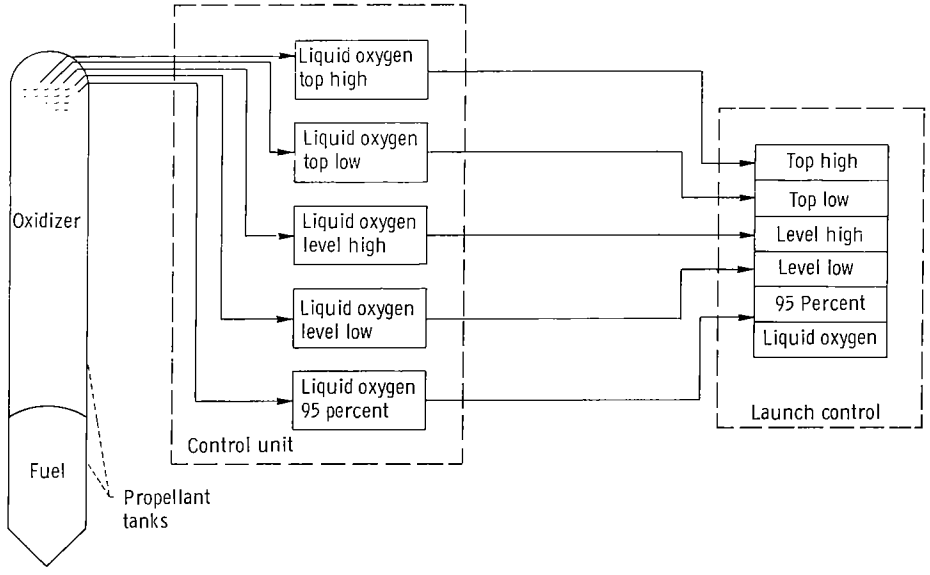

Figure VI-17. - Propellant-level-indicating system for liquid-oxygen loading - Atlas, AC-20 and AC-19. (Lights on launch control panel indicate if sensor is wet or dry. Percent levels indicate flight levels not total tank volume.)

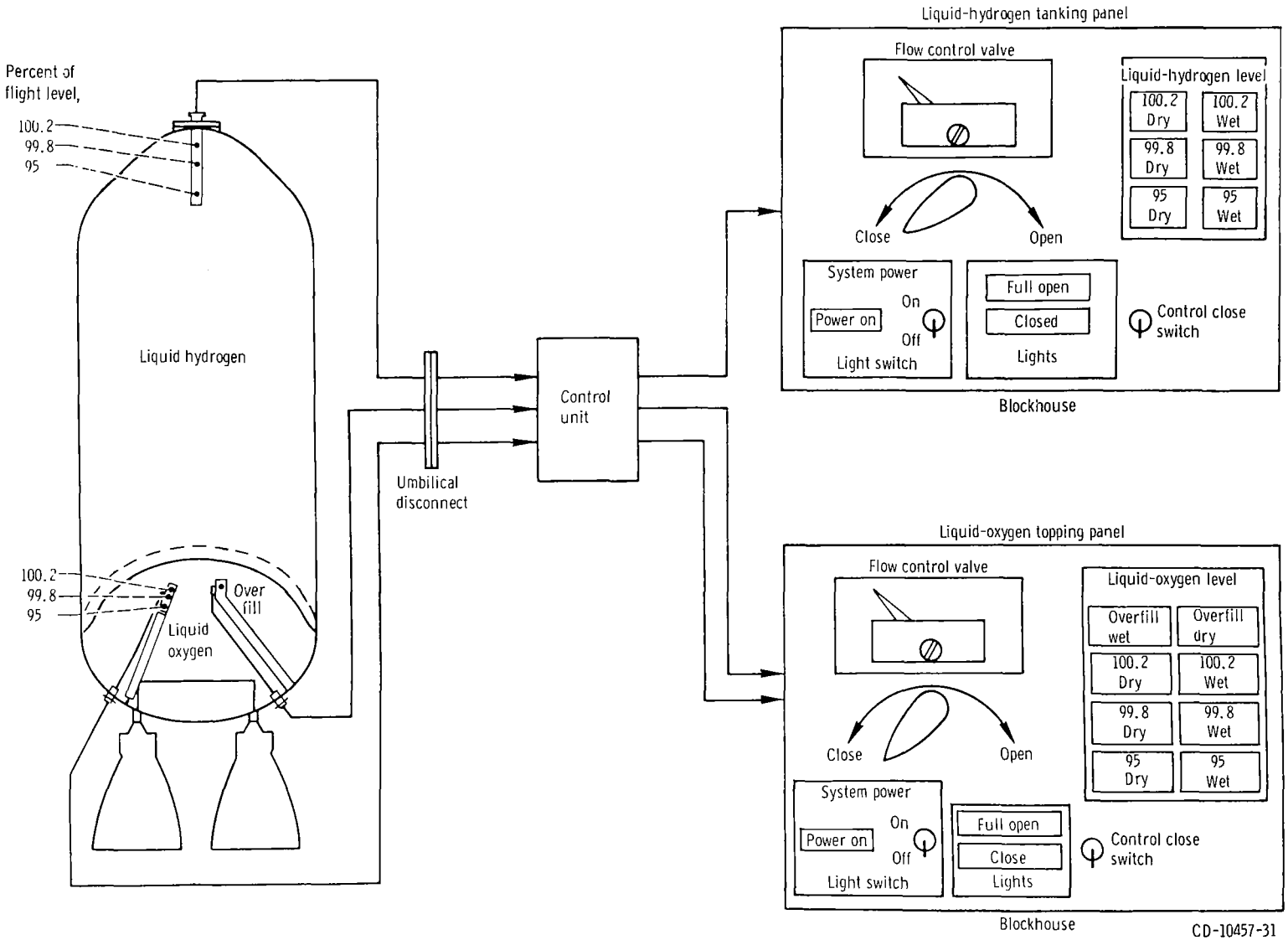

Figure VI-18. - Propellant-level-indicating system for Centaur propellant loading, AC-20 and AC-19.

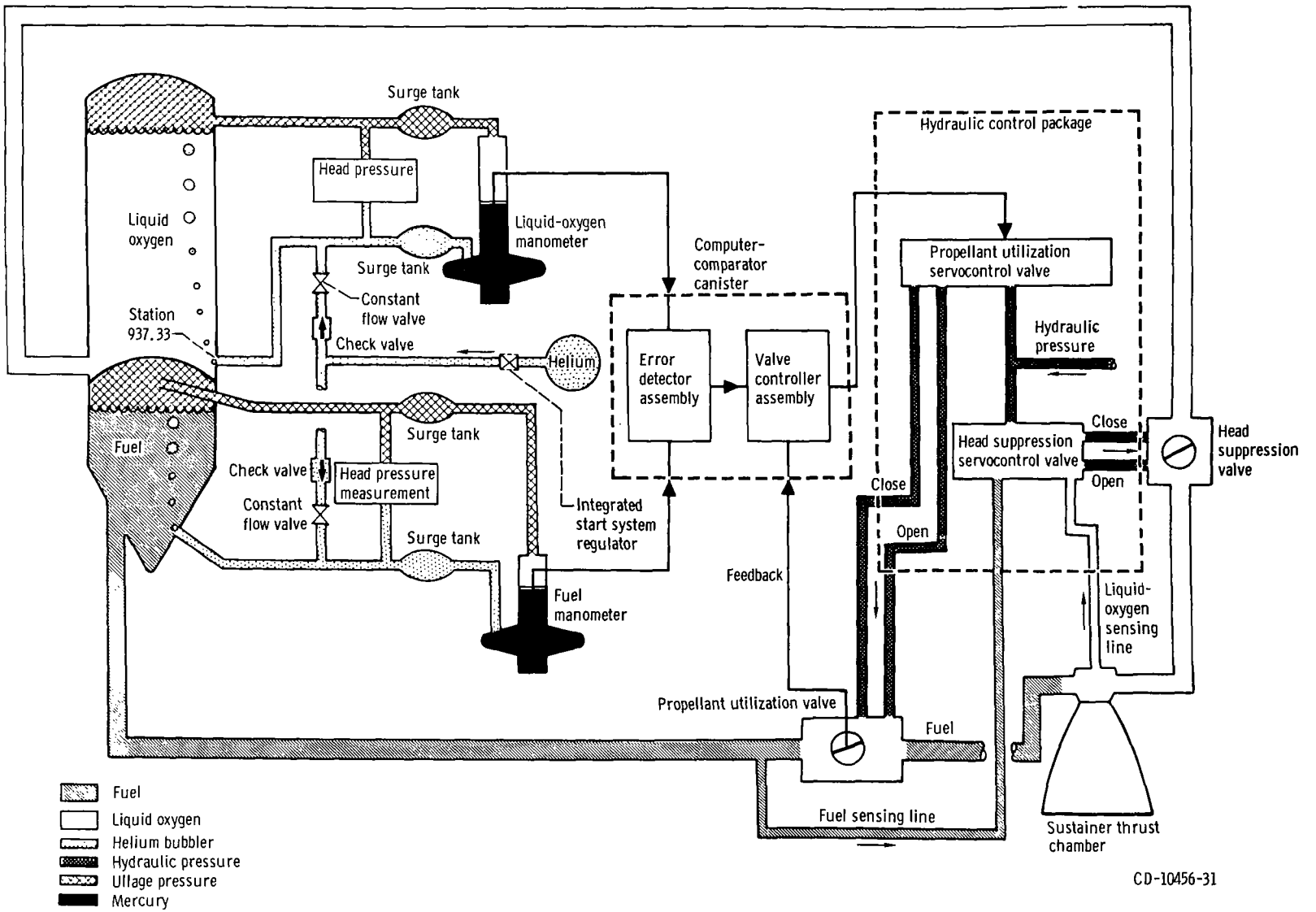

Figure VI-19. - Atlas propellant utilization system, AC-20 and AC-19.

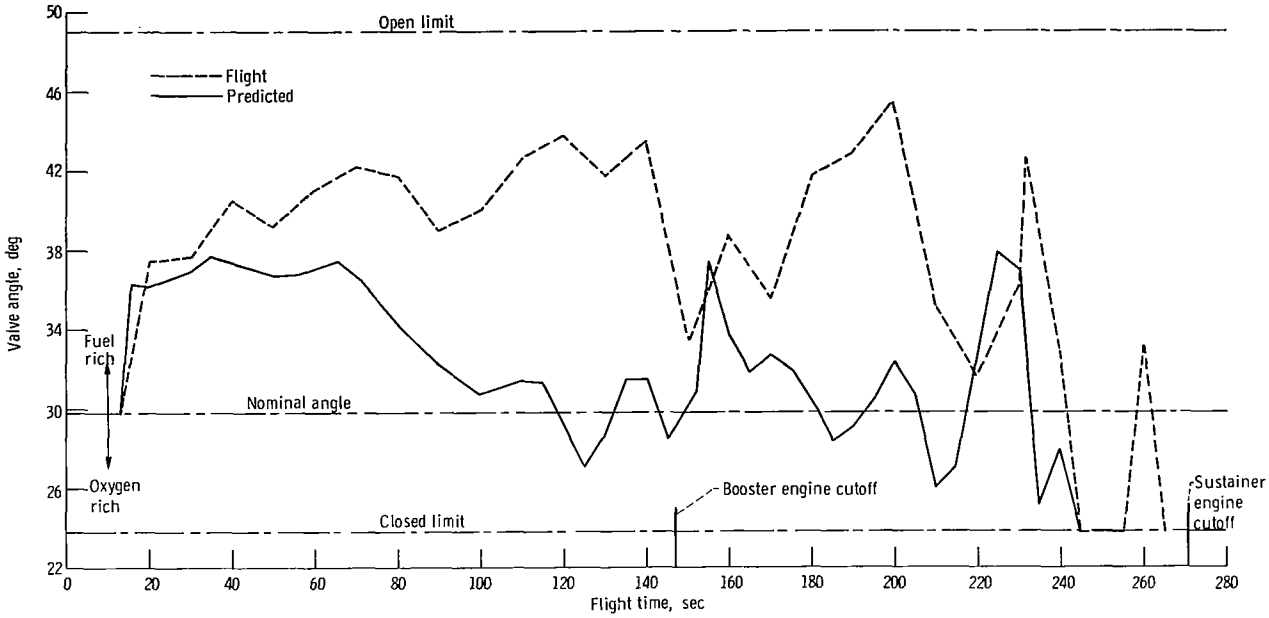

Figure VI-20. - Atlas propellant utilization valve angles, AC-20.

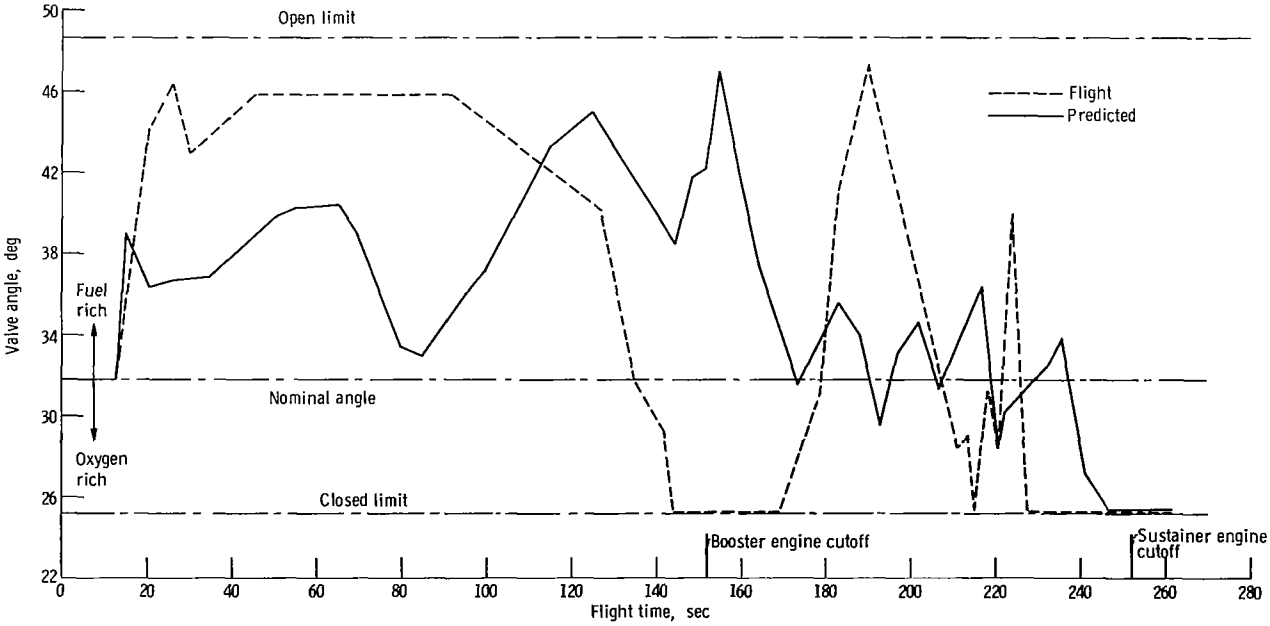

Figure VI-21. - Atlas propellant utilization valve angles, AC-19.

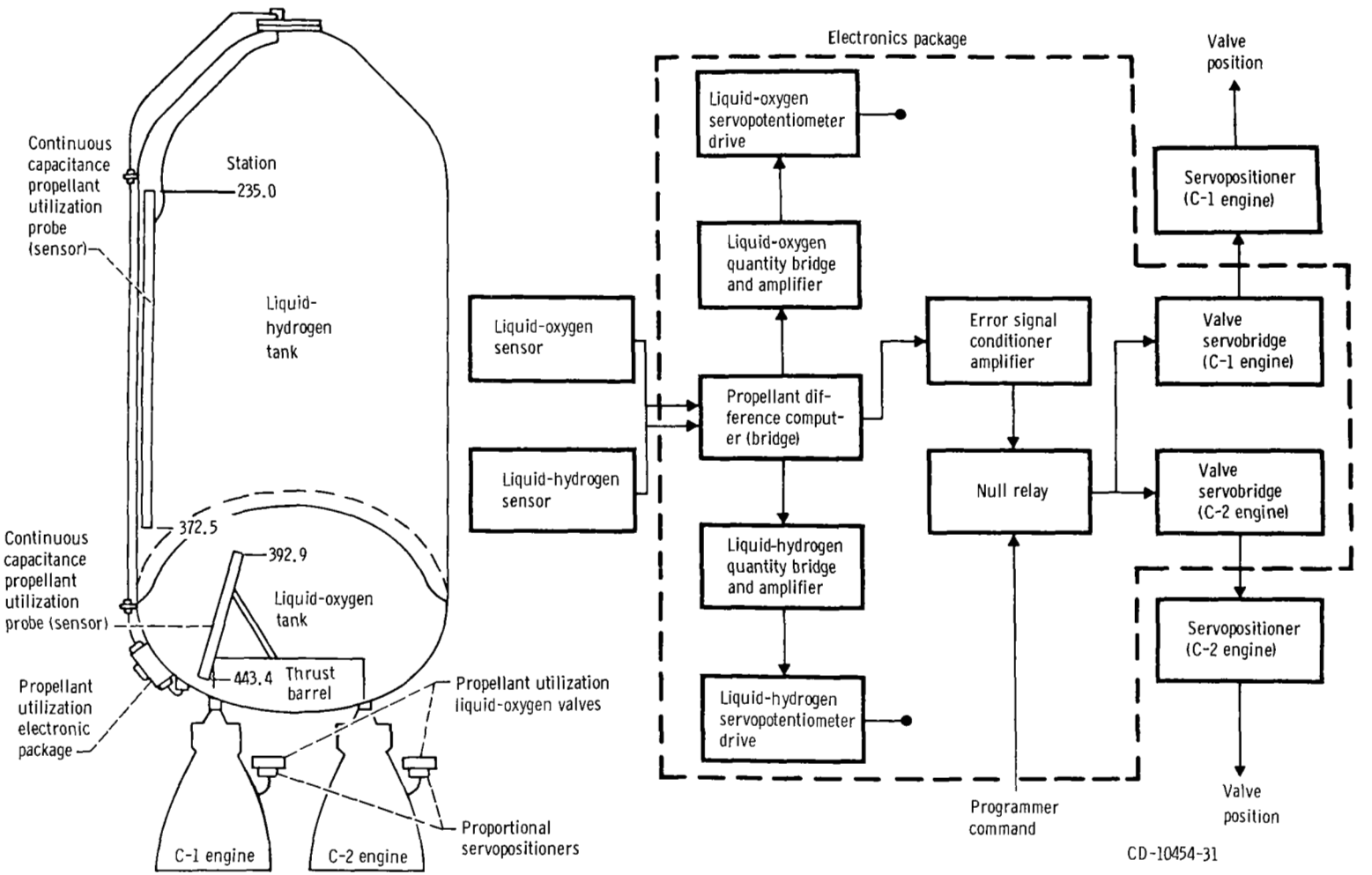

Figure VI-22. - Centaur propellant utilization system, AC-20 and AC-19.

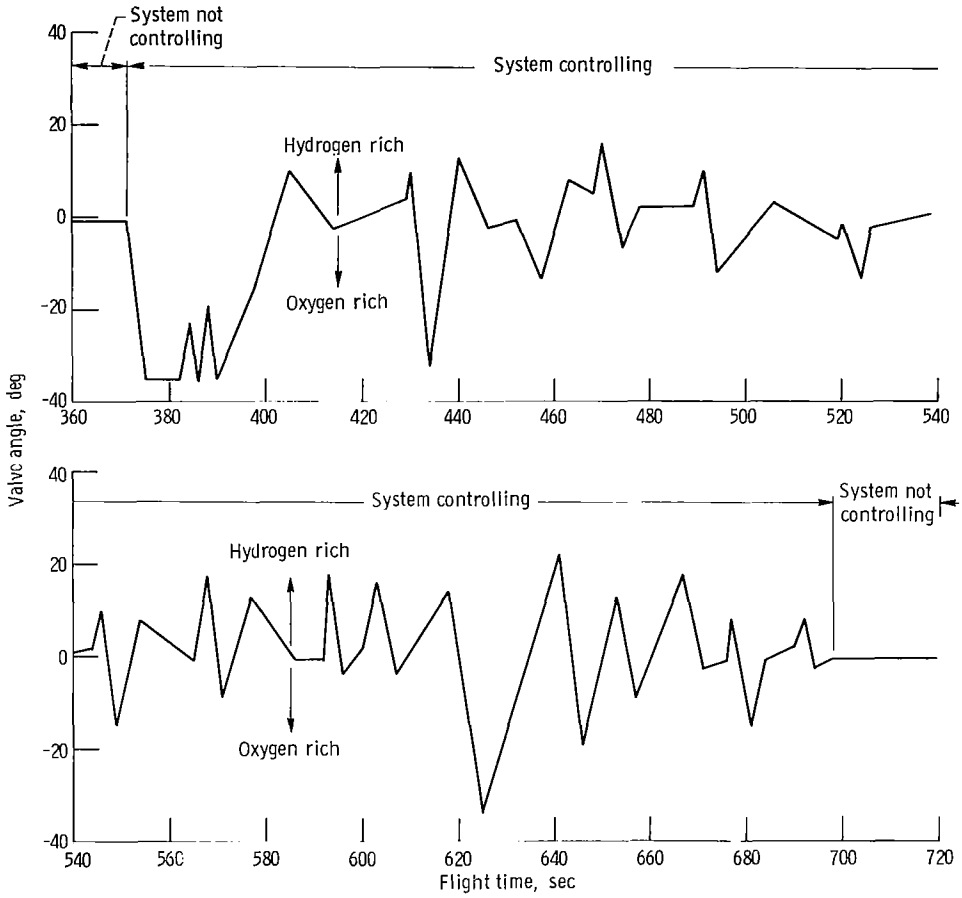

(a) For C-1 engine.

Figure VI-23. - Centaur propellant utilization valve angle, AC-20. Main engine start, 282.3 seconds; main engine cutoff, 725.5 seconds.

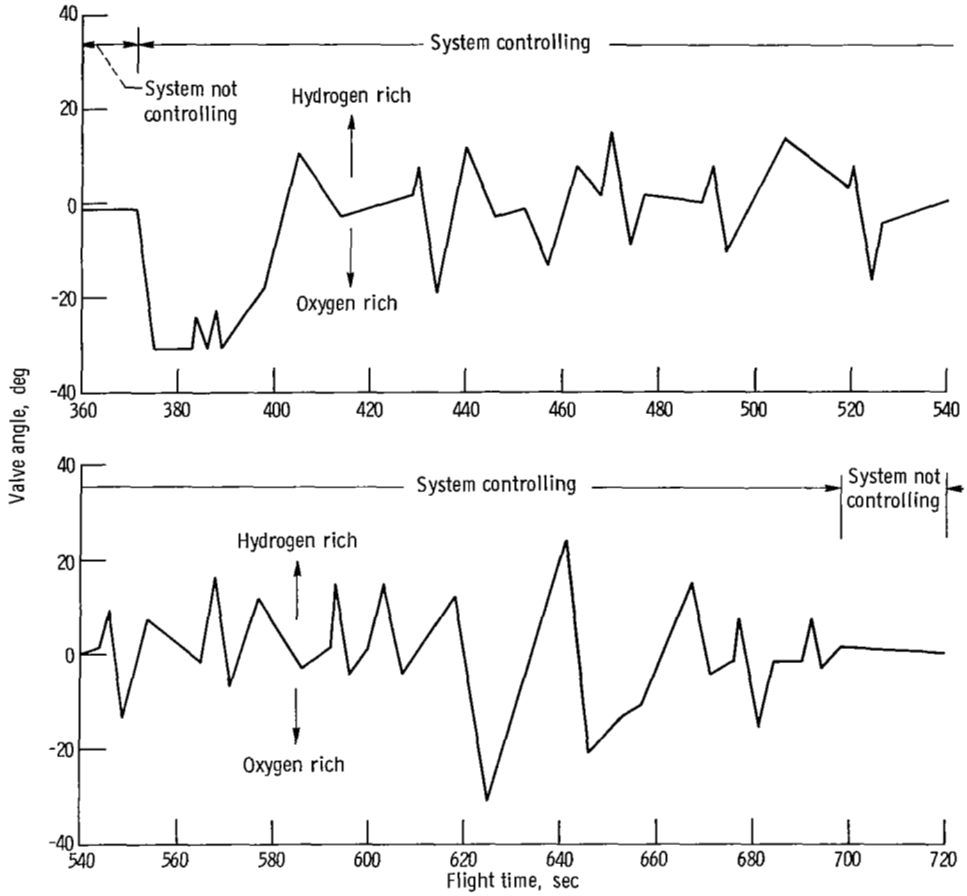

(b) For C-2 engine.

Figure 23. - Concluded.

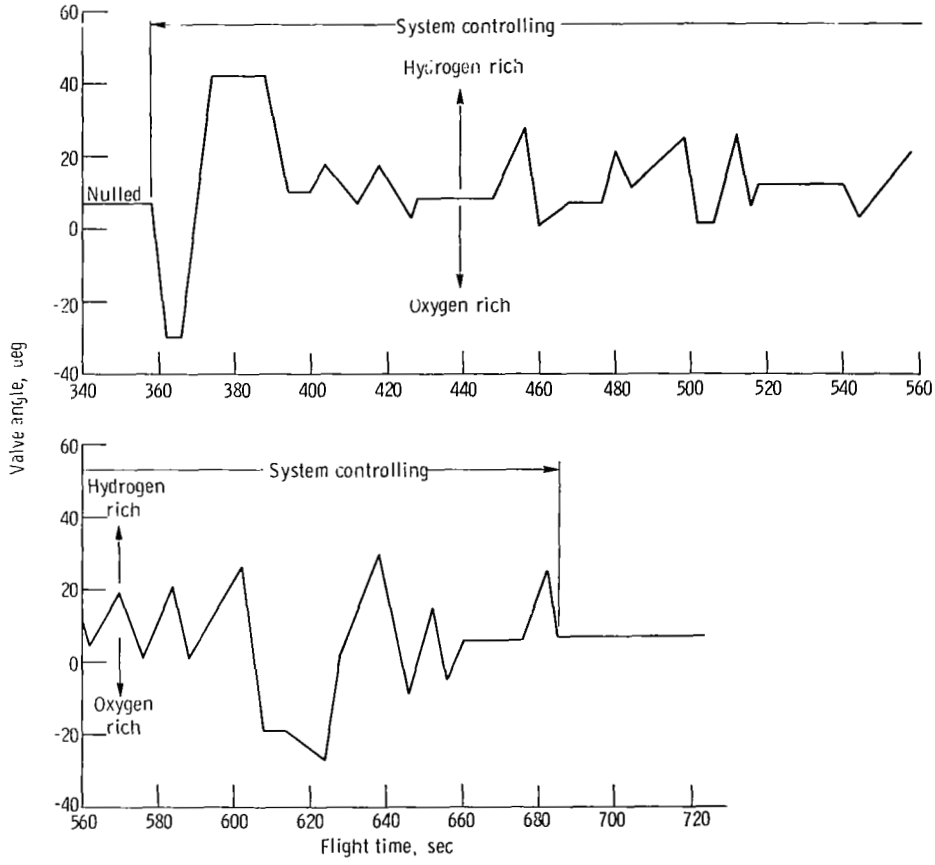

(a) For C-1 engine.

Figure VI-24. - Centaur propellant utilization valve angles, AC-19. Main engine cutoff, 712.2 seconds.

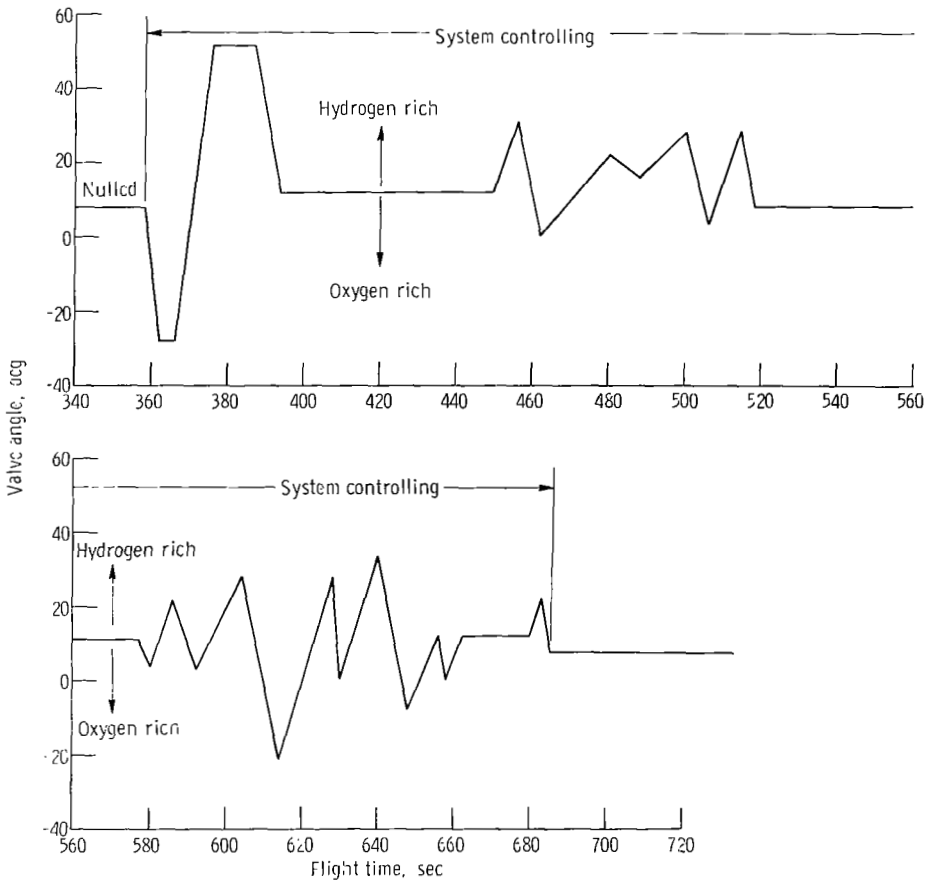

(b) For C-2 engine.

Figure 24. - Concluded.

PNEUMATICS SYSTEMS

by Eugene J. Fourney and Richard W. Heath

Atlas

System description. - The Atlas pneumatic system (fig. VI-25) supplied helium gas for tank pressurization and for various vehicle control functions. The system is comprised of three independent subsystems: propellant tank pressurization, engine control, and booster section jettison.

Propellant tank pressurization subsystem: This subsystem uses helium gas to maintain propellant tank pressures at required levels to support the pressure-stabilized tank structure, and to satisfy the inlet pressure requirements of the engine turbopumps. In addition, helium gas is supplied from the fuel tank pressurization line to pressurize the hydraulic reservoirs and turbopump lubricant storage tanks. The subsystem consists of eight shrouded helium storage bottles, a heat exchanger, and fuel and oxidizer tank pressure regulators and relief valves.

The eight shrouded helium storage bottles with a total capacity of 967 000 cubic centimeters (59 000 in.^{3}) are mounted in the jettisonable booster engine section. The bottle shrouds are filled with liquid nitrogen during prelaunch operations to chill the helium in order to provide a maximum storage capacity at about 2344 N/cm^2 (3400 psia). The liquid nitrogen drains from the shrouds at lift-off. During flight the cold helium passes through a heat exchanger located in the booster engine turbine exhaust duct and is heated before being supplied to the tank pressure regulators. The propellant tank pressurization subsystem pressurization control is switched from the ground to the airborne system at about T - 60 seconds. Airborne regulators are set to control fuel tank gage pressure between 44.1 and 46.2 N/cm^2 (64 and 67 psi) and the oxidizer tank pressure between 19.58 and 24.13 N/cm^2 (28.4 and 35.0 psi). From approximately T - 60 seconds to T + 20 seconds the liquid-oxygen regulator sense line is biased by a helium "bleed" flow into the liquid-oxygen tank regulator sensing line which senses ullage pressure at a lower level than the normal regulator setting. Depressing the liquid-oxygen tank pressure increases the differential pressure across the bulkhead between the propellant tanks to counteract the launch transient loads that act in a direction to cause bulkhead reversal. At T + 20 seconds the bias is removed by closing explosively actuated valves, and the ullage pressure in the liquid-oxygen tank increases to the normal regulator control range. The increased pressure then provides sufficient vehicle structural stiffness to withstand bending loads during the remainder of the ascent. Pneumatic regulation of tank pressure is terminated at booster staging. Thereafter, the fuel tank pressure decays slowly. The liquid-oxygen boiloff gases cause the oxidizer tank pressure to decay more slowly than the fuel tank pressure.

Engine controls subsystem: This subsystem supplies helium pressure for actuation of engine control valves, for pressurization of the engine start tanks, for purging booster engine turbopump seals, and for the reference pressure to the regulators which control oxidizer flow to the gas generator. Pressure control in the system is maintained through Atlas/Centaur separation. These pneumatic requirements are supplied from a single 76 000-cubic-centimeter (4650-in.^{3}) storage bottle pressurized to a gage pressure of about 2344 N/cm^2 (3400 psi) at lift-off.

Booster engine jettison subsystem: This subsystem supplies pressure for release of the pneumatic staging latches to separate the booster engine package. A command from the Atlas flight control system opens two explosively actuated valves to supply helium pressure to the 10 piston-operated staging latches. Helium for the system is supplied by a single 14 260-cubic-centimeter (870-in.^{3}) bottle charged to a gage pressure of about 2344 N/cm^2(3400 psi).

System performance. - The pneumatic system performance was satisfactory for both vehicles. All tank pressures were satisfactory and all control functions were performed properly. The pneumatic system performance data are presented in table VI-VI for AC-20 and for AC-19. The individual subsystem performance was as follows:

Propellant tank pressurization subsystem: Control of the propellant tank pressures was switched from the ground pressurization control unit (PCU) to the airborne regulators at approximately T - 60 seconds. Ullage pressures were properly controlled throughout both flights:

(1) AC-20 ullage pressures

(a) The fuel tank pressure regulator controlled at a gage pressure of about 44.9 N/cm^2 (65.0 psi) until termination of pneumatic control at booster staging. During the sustainer phase the fuel tank ullage pressure decreased normally and was 36.47 N/cm^2 (52.9 psi) at sustainer engine cutoff.

(b) The oxidizer tank ullage gage pressure was steady at 21.17 N/cm^2 (30.7 psi) after switching from the PCU to "pneumatics internal" at approximately T - 60 seconds. The pressure decreased to 20.34 N/cm^2 (29.5 psi) at engine start and continued to decrease slightly until T + 20 seconds. At T + 20 seconds the oxidizer ullage tank pressure was 19.86 N/cm^2 (28.8 psi). At this time the regulator sense line bias was terminated and the pneumatic regulator increased the liquid-oxygen tank ullage pressure to 22.34 N/cm^2 (32.4 psi). Four seconds was required for the ullage pressure to stabilize. The liquid-oxygen tank pressure remained within the required limits until termination of pneumatic regulation at booster engine staging. After booster engine staging the ullage pressure decreased from 22.55 N/cm^2 (32.7 psi) to 21.79 N/cm^2 (31.6 psi) at sustainer engine cutoff.

(2) AC-19 ullage pressures

(a) The fuel tank pressure regulator controlled at a gage pressure of about 44.9 N/cm^2 (65.0 psi) until termination of pneumatic control at booster staging. During the

sustainer phase the fuel tank ullage pressure decreased normally and was 35.18 N/cm^2 (51.03 psi) at sustainer engine cutoff.

(b) The oxidizer tank ullage pressure was steady at 20.48 N/cm^2 (29.7 psi) after switching from the PCU to pneumatics internal at approximately T - 60 seconds. The pressure decreased to 19.68 N/cm^2 (28.55 psi) at engine start and continued to decrease slightly until T + 20 seconds. At T + 20 seconds the oxidizer ullage tank pressure was 19.51 N/cm^2 (28.3 psi). At this time the regulator sense line bias was removed and the pneumatic regulator increased the liquid-oxygen tank ullage pressure to 22.06 N/cm^2 (32.0 psi). Four seconds was required for the ullage pressure to stabilize. The liquid-oxygen tank pressure remained within the required limits until termination of pneumatic regulation at booster engine staging. After booster engine staging the ullage pressure decreased from 23.19 N/cm^2 (33.53 psi) to 21.49 N/cm^2 (31.17 psi) at sustainer engine cutoff.

Engine control subsystem: On AC-20 and AC-19, the booster and sustainer engine control regulators provided the required helium pressure for engine control throughout these flights.

Booster section jettison subsystem: Subsystem performance was satisfactory on both flights. The pyrotechnically actuated valve was opened on command, allowing high-pressure helium to actuate the 10 booster staging latches.

Centaur

System description. - The Centaur pneumatic system (fig. VI-26) consists of five subsystems: propellant tank venting, propellant tank pressurization, propulsion pneumatics, helium purge pneumatics, and nose fairing pneumatics.

The structural stability of the propellant tanks is maintained throughout the flight by the propellant boiloff gas pressures. These pressures are controlled by a vent system on each propellant tank. Two pilot-controlled, pressure-actuated vent valves and ducting comprise the hydrogen tank vent system. The primary vent valve is fitted with a continuous-duty solenoid valve which, when energized, locks the vent valve and prevents operation. The secondary hydrogen vent valve does not have the control solenoids. The relief range of the secondary valve is above that of the primary valve, preventing overpressurization of the hydrogen tank when the primary vent valve is locked. The vented hydrogen gas is ducted overboard through a single vent. The oxygen tank vent system uses a single vent valve which is fitted with the control solenoid valve. The vented oxygen gas is ducted overboard through the interstage adapter. The duct, which remains with the Centaur after separation from the interstage adapter, is oriented to aline the venting thrust vector with the vehicle center of gravity.

The vent valves are commanded to the locked mode at specific times (1) to permit the hydrogen tank pressure to increase during the atmospheric ascent to satisfy the structural requirements of the pressure-stabilized tank, (2) to permit controlled pressure increases in the tanks to satisfy the boost pump pressure requirements, (3) to restrict oxygen venting during nonpowered flight to avoid vehicle disturbing torques, and (4) to restrict hydrogen venting to nonhazardous times. (A fire could conceivably occur during the early part of the atmospheric ascent if a plume of vented hydrogen washes back over the vehicle and if it is exposed to an ignition source. A similar hazard could occur at Atlas booster engine staging when residual oxygen envelops a large portion of the vehicle.)

The propellant tank pressurization subsystem supplies helium gas in controlled quantities for in-flight pressurization, in addition to that provided by the propellant boiloff gases. It consists of two normally closed solenoid valves and orifices, and a pressure switch assembly which senses oxygen tank pressure. The solenoid valves and orifices provide a metered flow of helium to both propellant tanks for step pressurization during the main engine start sequence, and to the oxygen tank at main engine cutoff. The pressure sensing switch controls the pressurization of the oxygen tank during the main engine start sequence.

The propulsion pneumatics subsystem supplies helium gas at regulated pressures for actuation of main engine control valves and pressurization of the hydrogen peroxide storage bottle. It consists of two pressure regulators, which are referenced to ambient pressure, and two relief valves. Pneumatic pressure supplied through the engine controls regulator is used for actuation of the engine inlet valves, the engine chilldown valves, and the main fuel shutoff valve. The second regulator, located downstream of the engine controls regulator, further reduces the pressure to provide expulsion pressurization for the hydrogen peroxide storage bottle. A relief valve downstream of each regulator prevents overpressurization.

A ground/airborne helium purge subsystem was used to prevent cryopumping and icing under the insulation panels and in propulsion system components. A common airborne distribution system was used for prelaunch purging from a ground helium source and postlaunch purging from an airborne helium storage bottle. This subsystem distributed helium gas for purging the cavity between the hydrogen tank and the insulation panels, the seal between the cylindrical section of the nose fairing and the forward bulkhead, the propellant feedlines, the boost pumps, the engine chilldown vent-ducts, the engine thrust chambers, and the hydraulic power packages. The umbilical charging connection for the airborne bottle could also be used to supply the purge from the ground source should an abort occur after ejection of the ground purge supply line.

The nose fairing pneumatic subsystem provided the required thrust for nose fairing jettisoning. It consisted of a nitrogen storage bottle and an explosive-actuated valve

with an integral thruster nozzle in each fairing half. Release of the gas through the nozzles provided the necessary thrust to propel the fairing halves away from each other and from the vehicle.

System performance. - The pneumatics systems performance of both vehicles was generally satisfactory. However, on AC-19, an anomaly occurred in the propulsion pneumatics subsystem. (This anomaly, which occurred in the engine controls regulator, is discussed in detail under propulsion pneumatics that follows.)

Propellant tank pressurization and venting: The ullage pressures in the hydrogen and oxygen tanks for AC-20 and AC-19 are shown in figures VI-27 and VI-28. The sequence of events for both vehicles was the same, but the timing of some of the events varied. At T - 8 seconds the primary hydrogen vent valve on each vehicle was locked, which subsequently resulted in an increase in the tank pressure. Each pressure increased to the relief setting of the secondary hydrogen vent valve which then began to regulate the tank pressure. The relief absolute pressure on AC-19 was 18.1 N/cm^2 (26.2 psi), and on AC-20 it was 18.2 N/cm^2 (26.5 psi). The tank pressure rise rate during this period was 2.50 N/cm^2/min (3.48 psi/min) on AC-19, and 2.44 N/cm^2/min (3.54 psi/min) on AC-20. At T + 90 seconds the primary hydrogen tank vent valves were enabled. The primary vent valves then reduced and regulated the tank pressures.

The primary hydrogen vent valve on each vehicle was again locked at the beginning of Atlas booster engine jettison and remained locked for approximately 8 seconds. Thereafter, the vent valves were enabled and allowed to regulate tank pressure. At Atlas sustainer engine cutoff the primary hydrogen vent valves were locked, and the tanks were pressurized with helium for 1 second as a part of the Centaur main engine start sequence. In each case, the pressure increased approximately 1 N/cm^2 (1.4 psi), and then decreased as the warm helium in the tank was cooled by the hydrogen gas.

The ullage pressure in each oxygen tank remained relatively constant for the first 30 seconds of flight until the increasing vehicle acceleration began to suppress the propellant boiling enough to cause the pressure to decrease. The pressure decreased in each flight until the oxygen vent valve reseated and venting ceased. The pressure then remained low on AC-20, but on AC-19 it varied between the operating limits of the vent valve until Atlas booster engine cutoff. At that time, on both flights, the sudden reduction in the acceleration caused an increase in the liquid-oxygen boiloff and a resulting pressure rise in the tanks. As thermal equilibrium was reestablished in the tanks, the pressures decreased to their original level.

Sixty-two seconds after Atlas booster engine cutoff the oxygen tank vent valve on each vehicle was locked, and the helium pressurization of the oxygen tank was initiated. The tank pressure increased to the upper limit of the pressurization switch, which terminated the pressurization. As the helium gas in AC-20 was cooled in the tank, the pressure decreased until the heat input, principally from the boost pump recirculation flow,

increased the boiloff and caused the pressure to increase again. On AC-19 the pressure decreased to the lower limit of the pressurization switch, which then caused additional helium to be injected into the tank. Following this second cycle, the heat input from the boost pump recirculation flow increased the boiloff and caused the pressure to increase before it reached the lower limit of the pressurization switch again. The pressure in the oxygen tanks of both vehicles continued to increase from the heat input until Centaur main engine first prestart. The pressure in each case then decreased gradually until Centaur main engine first start, when it decreased abruptly to the saturation pressure of the ullage gas.

The ullage pressures in both propellant tanks of the two vehicles decreased normally during the main engine firing. After main engine cutoff the primary hydrogen vent valves were enabled, while the oxygen vent valves remained locked.

At engine cutoff the oxygen tank was pressurized with helium for 30 seconds in order to preclude the possibility of the hydrogen tank pressure exceeding the oxygen tank pressure and reversing the intermediate bulkhead. During this period the tank pressure increased to 19.8 N/cm^2 (28.8 psia) on AC-20, and to 18.8 N/cm^2 (27.3 psia) on AC-19. On AC-20 the pressure continued to increase and reached a value of 20.0 N/cm^2 (29.1 psia) at T + 780 seconds. On AC-19 the pressure also continued to increase, reaching a value of 20.6 N/cm^2 (29.9 psia) at T + 1200 seconds. The hydrogen tank pressure on AC-20 and AC-19 began to increase after engine cutoff, reaching 10.6 N/cm^2 (15.4 psia) on AC-20 and 12.5 N/cm^2 (18.1 psia) on AC-19 by T + 1580 seconds. At this time retrothrust was initiated and the retrothrust propellant flow relieved the tank pressure. (See bottom part of figs. 27 and 28.)

During the early part of the retrothrust maneuver the hydrogen tank ullage pressure remained constant, indicating liquid outflow. The pressure then began to decrease, indicating either gaseous or two-phase outflow.

Propulsion pneumatics: The engine controls regulator and the hydrogen peroxide bottle pressure regulator maintained proper system pressure levels throughout the AC-20 flight. The AC-20 engine controls regulator output absolute pressure was 328 N/cm^2 (476 psi) at T - 0, while that of the hydrogen peroxide bottle pressure regulator was 218 N/cm^2 (316 psi). The corresponding values for AC-19 were 314 and 223 N/cm^2 (455 and 324 psi), respectively. After lift-off the AC-20 regulator output pressures decreased with a corresponding decrease in ambient pressure and remained relatively constant after the ambient pressure had decreased to zero. The same is true of the AC-19 hydrogen peroxide bottle pressure regulator. However, the AC-19 engine controls regulator output increased to an unexpectedly high level after about 14 minutes of flight. It increased to 347 N/cm^2 (504 psi) and then decreased to within the specified range, which is below 327 N/cm^2 (475 psi). This anomaly had no adverse effects on the flight. No reason can be determined for the high pressure output; all test data on the component indicated normal behavior.

Helium purge subsystem: The total helium purge flow rate to AC-19 at T - 10 seconds was 89 kilograms per hour (196 lbm/hr), and to AC-20 was 86 kilograms per hour (189 lbm/hr). The differential pressure across the insulation panels after hydrogen tanking was 0.08 N/cm^2 (0.12 psi) on AC-19 and 0.10 N/cm^2 (0.15 psi) on AC-20. The minimum allowable differential pressure required to prevent cryopumping and icing is 0.02 N/cm^2 (0.03 psi). At approximately T - 12 seconds the airborne purge system on each vehicle was activated, and at T - 4 seconds the ground purge was terminated. The supply of helium in each vehicle purge bottle lasted through most of the atmospheric ascent.

Nose fairing pneumatics: There was no airborne instrumentation for this system on either AC-20 or AC-19. However, jettisoning of the nose fairing on each flight indicated the system functioned properly each time.

TABLE VI-VI. - ATLAS PNEUMATIC SYSTEM PERFORMANCE, AC-20 AND AC-19

Parameter	Measurement number	Units	Design range	T - 10 sec		T - 0 sec		T + 20 sec		T + 24 sec		Booster engine cutoff		Sustainer and vernier engine cutoff	
				AC-20	AC-19	AC-20	AC-19	AC-20	AC-19	AC-20	AC-19	AC-20	AC-19	AC-20	AC-19
Oxidizer tank ullage pressure, gage	AF1P	N/cm^2 psi	(a) (b)	21.17 30.7	20.48 29.7	20.34 29.5	19.68 28.55	[c]19.86 [c]28.8	[c]19.51 [c]28.3	[d]22.34 [d]32.4	[d]22.06 [d]32.0	[e]22.55 [e]32.7	[e]23.19 [e]33.53	21.79 31.6	21.49 31.17
Fuel tank ullage pressure, gage	AF3P	N/cm^2 psi	44.13 to 46.19 64.0 to 67.0	45.71 66.3	45.02 65.3	45.02 65.3	45.02 65.3	44.68 64.8	44.68 64.8	44.68 64.8	44.68 64.8	[e]44.75 [e]64.9	[e]44.15 [e]64.03	36.47 52.9	35.18 51.03
Intermediate bulkhead differential pressure[f]	AF116P	N/cm^2 psi	0.345 (min.) 0.5 (min.)	14.06 20.4	14.06 20.0	14.06 20.0	14.06 20.0	12.07 17.5	11.72 17.0	8.96 13.0	8.96 13.0	15.86 23.0	17.37 25	14.48 21.0	14.55 21.1
Controls helium bottle pressure, absolute	AF291P	N/cm^2 psi	2344 (max.) 3400 (max.)	2199 3190	2344 3400	2124 3080	2324 3370	2075 3010	2220 3220	2075 3010	2220 3220	1834 2660	2034 2950	1640 2380	1944 2820
Booster helium bottle pressure, absolute	AF246P	N/cm^2 psi	2344 (max.) 3400 (max.)	2655 3270	2330 3380	2186 3170	2275 3300	1658 2405	1731 2510	1562 2265	1672 2425	527 765	534 775	----- -----	----- -----
Booster helium bottle temperature	AF247T	K ^oF	86.1 to 77.78 -305° to -320° (prior to engine start)	77.78 -320.0	80.2 -315.6	77.0 -321.4	80.2 -315.6	70.28 -333.5	74.06 -326.7	68.72 -336.3	71.72 -330.9	46.83 -375.7	49.56 -370.8	----- -----	----- -----

[a] 20.7 to 22.4 N/cm^2 (30.0 to 32.5 psig) prior to engine start.

[b] 22.06 to 24.13 N/cm^2 (32.0 to 35.0 psig) after T + 24 sec.

[c] Signal from programmer to fire programmed pressure conax valves.

[d] Liquid-oxygen tank pressure at termination of programmed pressure.

[e] Helium supply bottles jettisoned with booster engine at booster engine cutoff plus 3 sec.

[f] Lowest value for AC-20 was 8.55 N/cm^2 (12.4 psi) at T + 1 sec; lowest value for AC-19 was 8.96 N/cm^2 (13.0 psi) at T + 24 sec.

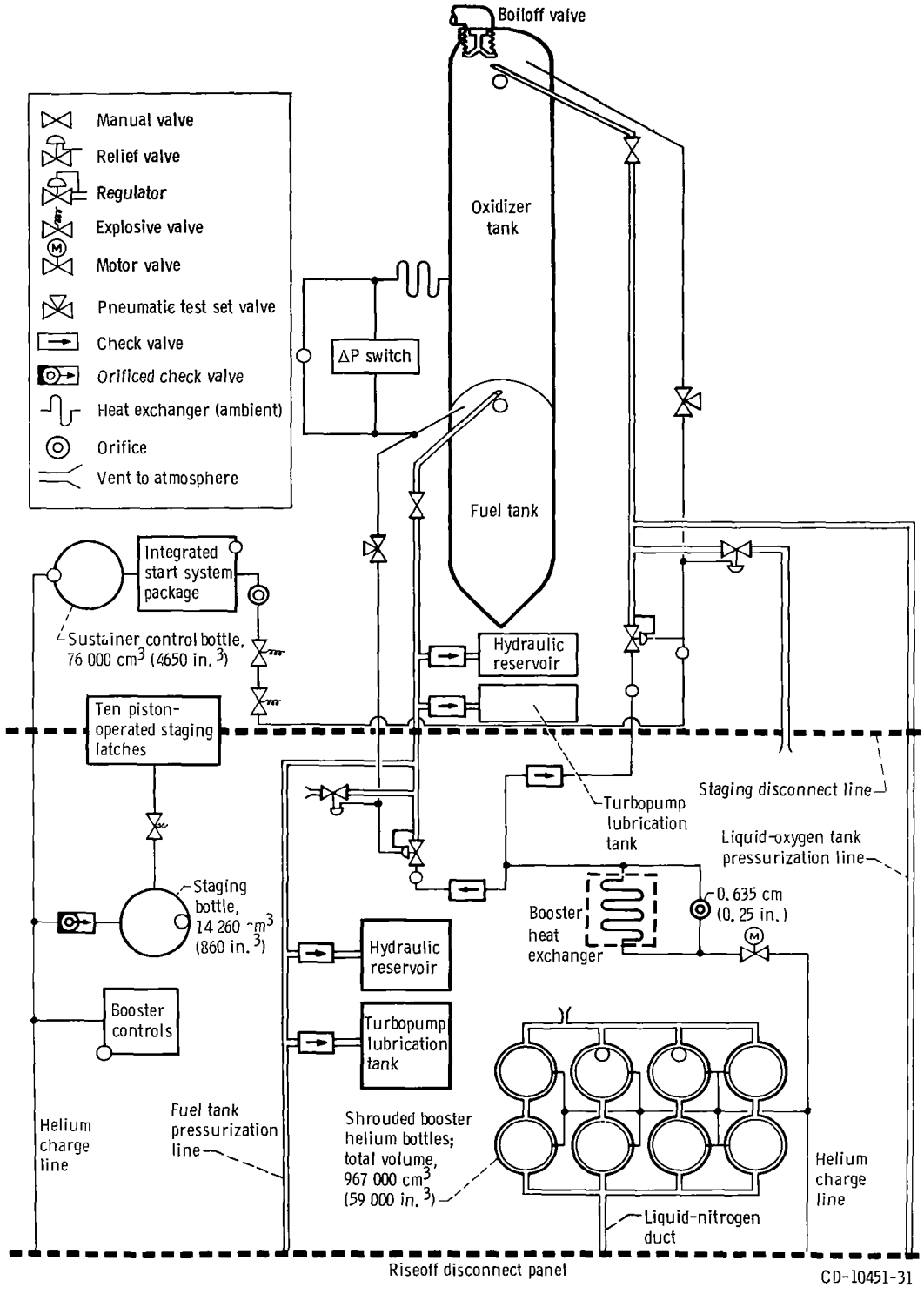

Figure VI-25. - Atlas vehicle pneumatic system, AC-20 and AC-19.

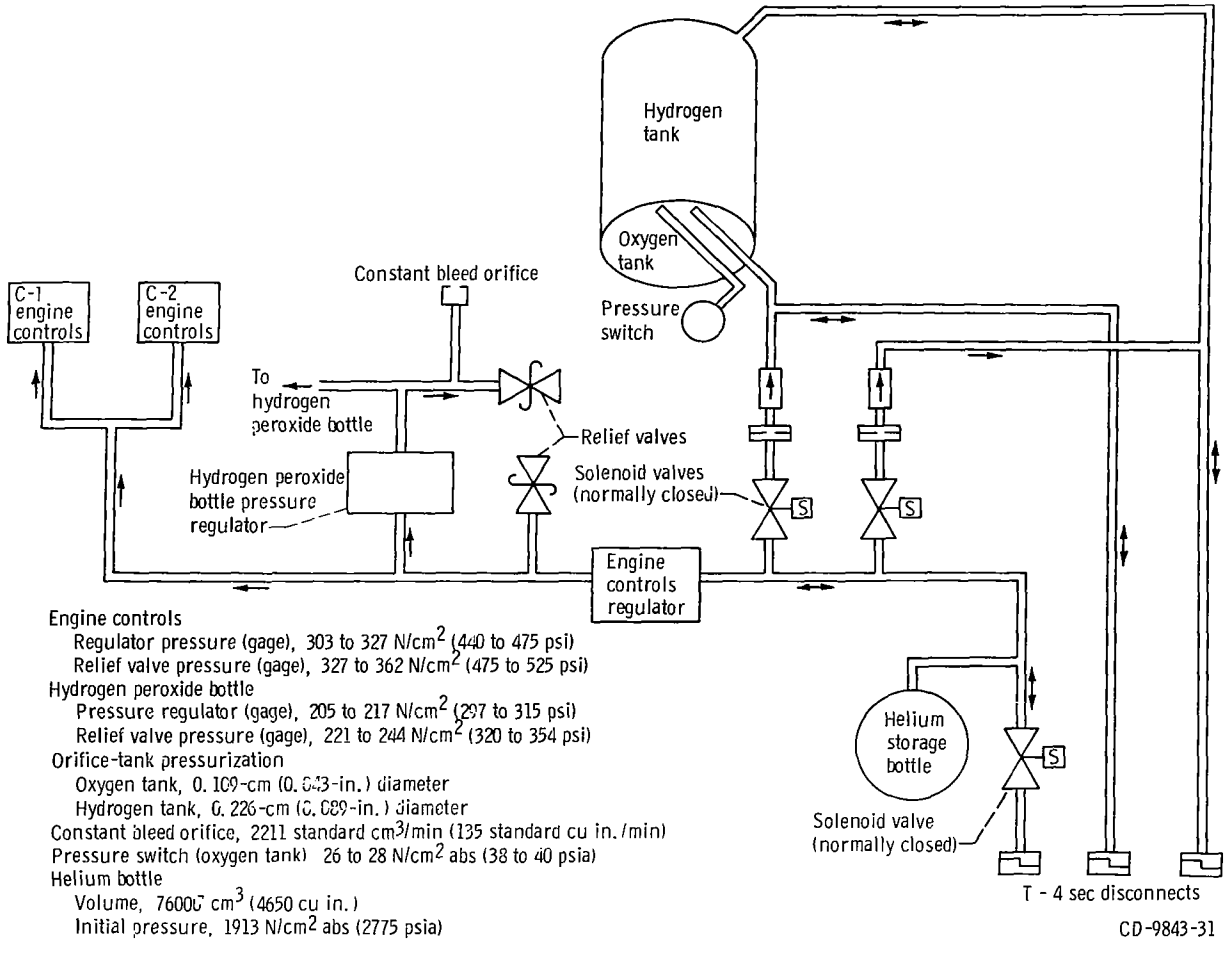

Engine controls
- Regulator pressure (gage), 303 to 327 N/cm^2 (440 to 475 psi)
- Relief valve pressure (gage), 327 to 362 N/cm^2 (475 to 525 psi)

Hydrogen peroxide bottle
- Pressure regulator (gage), 205 to 217 N/cm^2 (297 to 315 psi)
- Relief valve pressure (gage), 221 to 244 N/cm^2 (320 to 354 psi)

Orifice-tank pressurization
- Oxygen tank, 0.109-cm (0.043-in.) diameter
- Hydrogen tank, 0.226-cm (0.089-in.) diameter

Constant bleed orifice, 2211 standard cm^3/min (135 standard cu in./min)

Pressure switch (oxygen tank) 26 to 28 N/cm^2 abs (38 to 40 psia)

Helium bottle
- Volume, 76000 cm^3 (4650 cu in.)
- Initial pressure, 1913 N/cm^2 abs (2775 psia)

(a) Tank pressurization and propulsion pneumatics subsystems.

Figure VI-26. - Centaur pneumatic system, AC-20 and AC-19.

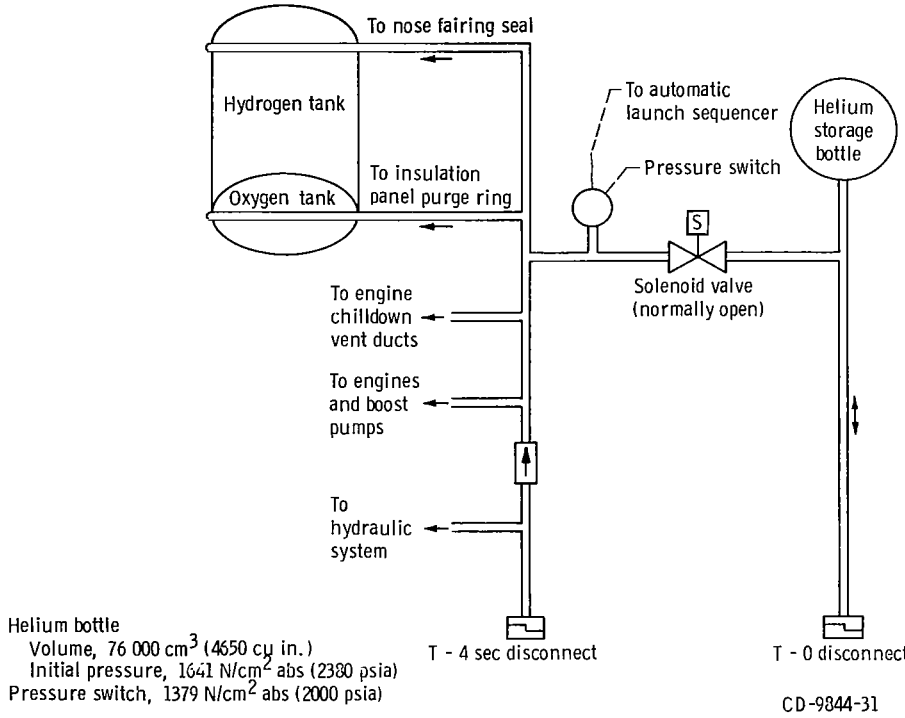

(b) Helium purge subsystem.

Figure VI-26. - Concluded.

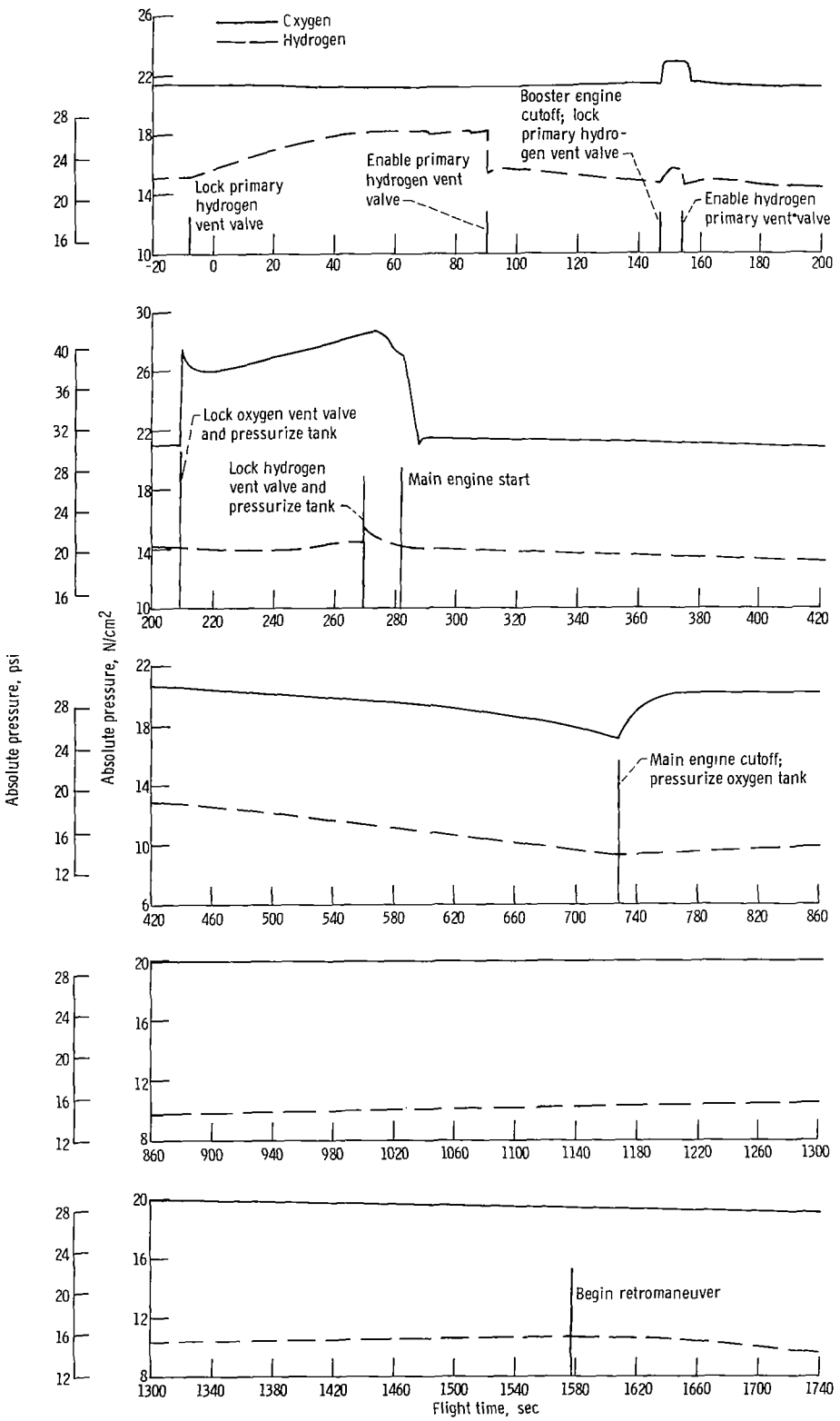

Figure VI-27. - Centaur tank pressure history, AC-20.

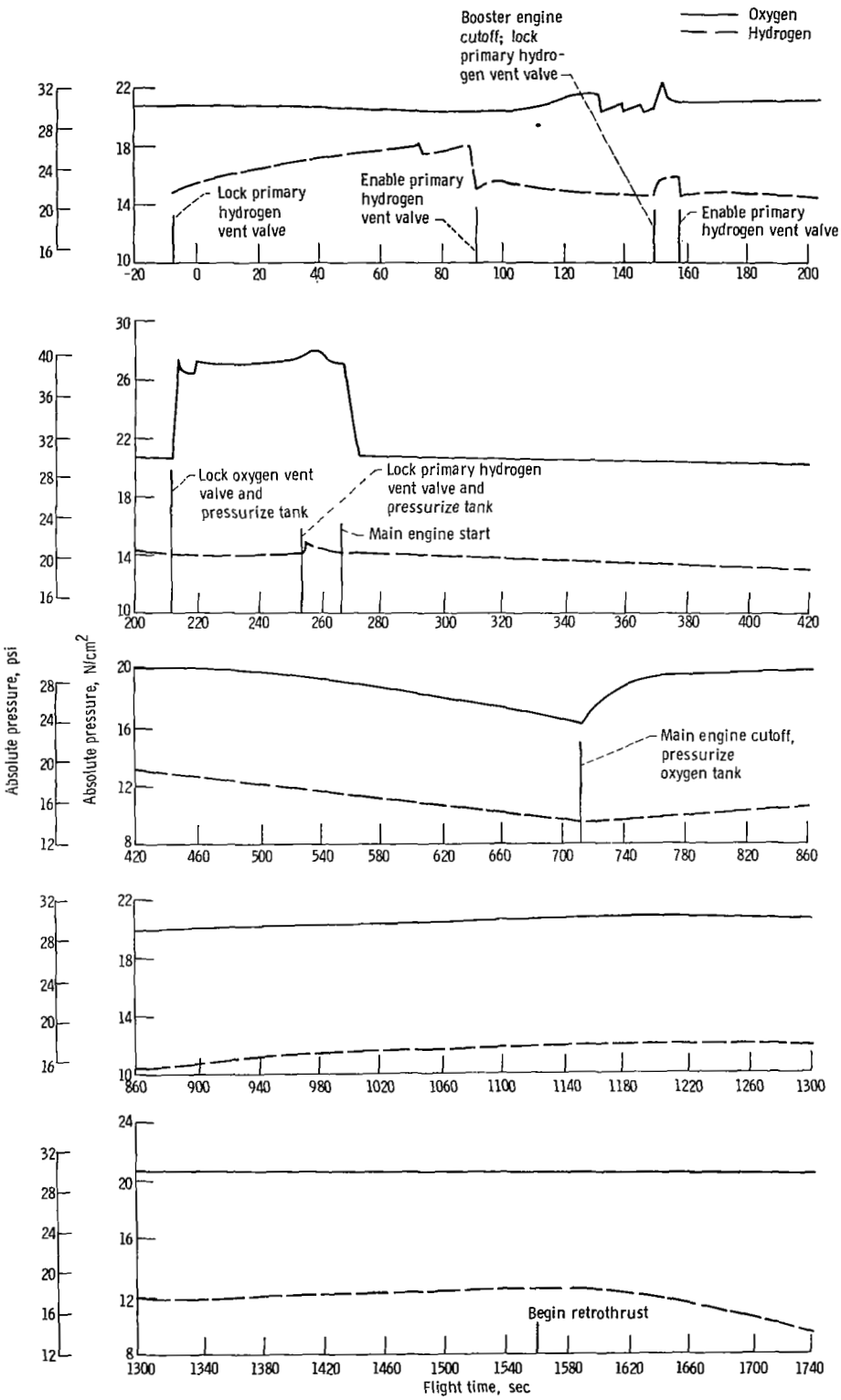

Figure VI-28. - Centaur tank pressure history, AC-19.

HYDRAULIC SYSTEMS

by Eugene J. Fourney

Atlas

System description. - Two hydraulic systems (figs. VI-29 and VI-30) are used on the Atlas vehicle to supply fluid power for operation of sustainer engine control valves and for thrust vector control of all engines. One system is used for the booster thrust chambers and the other for the sustainer and vernier engines.

The booster hydraulic system provides power solely for gimbaling the two booster thrust chambers. System pressure is supplied by a single, pressure-compensated, variable-displacement pump driven by the engine turbopump accessory drive. Additional components of the system includes four servocylinders, a high-pressure relief valve, an accumulator, and a reservoir. Engine gimbaling in response to flight control commands is accomplished by the servocylinders which provide separate pitch, yaw, and roll control during the booster engine phase of flight.

The sustainer stage uses a system similar to that of the booster, but in addition, provides hydraulic power for sustainer engine control valves and for gimbaling of the two vernier engines. Vehicle roll control is accomplished during the sustainer phase by differential gimbaling of the vernier engines.

System performance. - Hydraulic system pressure data for both vehicles was normal during flight. Pressures were stable throughout the boost flight phase. The transfer of fluid power from ground to airborne hydraulic systems was normal. Pump discharge absolute pressures increased from 1290 N/cm^2 (1980 psi) at T - 2 seconds to flight levels of 2100 N cm^2 (3150 psi) in less than 2 seconds. Starting transients produced a normal overshoot of about 10 percent in the pump discharge pressure. No return pressure transients were noted during either flight in the sustainer pump return system (measurement A4601P).

Flight data for AC-20 and AC-19 are presented in table VI-VII.

Centaur

System description. - Two separate but identical hydraulic systems, shown in figure VI-31, are used on the Centaur stage. Each system gimbals one engine for pitch, yaw, and roll control. Each system consists of two servocylinders and an engine-coupled power package containing high- and low-pressure pumps, reservoir, accumulator, pressure-intensifying bootstrap piston, and relief valves for pressure regulation. Hydraulic pressure and flow are provided by a constant-displacement vane-type pump

driven by the liquid-oxygen turbopump accessory drive shaft. An electrically powered recirculation pump is also used to provide low pressure for engine gimbaling requirements during prelaunch checkout, to aline the engines prior to main engine start, and for limited thrust vector control during the propellant tank discharge for the Centaur retrothrust operation. Maximum engine gimbal capability is $\pm 3^{o}$

System performance. - The hydraulic system properly performed all guidance and flight control commands throughout both flights. System pressures and temperatures for both flights were normal. System performance data for AC-20 and AC-19 are presented in table VI-VIII.

Hydraulic system operation was satisfactory for both vehicles. The C-1 and C-2 hydraulic recirculation pumps were commanded on by a Centaur timer discrete, at Centaur main engine start minus 11 seconds in order to "null" the C-1 and C-2 engines. After engine start the C-1 and C-2 main hydraulic pumps increased system pressure to normal flight levels.

TABLE VI-VII. - ATLAS HYDRAULIC SYSTEM PERFORMANCE, AC-20 AND AC-19

[All hydraulic system performance was normal.]

Parameter[a]	Measurement number	Units	After oil evacuation		Peak pressure prior to lift-off		Lift-off		Booster engine cutoff		Sustainer and vernier engine cutoff	
			AC-20	AC-19	AC-20	AC-19	AC-20	AC-19	AC-20	AC-19	AC-20	AC-19
Booster hydraulic pump discharge pressure	AH3P	N/cm^2	10.04	10.04	2348	2310	2206	2179	2195	2167	-----	-----
		psi	14.7	14.7	3405	3350	3200	3160	3185	3145	-----	-----
Booster hydraulic accumulator pressure	AH33P	N/cm^2	1365	1379	2344	2310	2179	2179	2167	2167	-----	-----
		psi	1980	2000	3400	3350	3160	3160	3145	3145	-----	-----
Booster hydraulic system return pressure	AH224P	N/cm^2	55.16	57.92	----	----	55.16	57.92	55.16	57.92	-----	57.92
		psi	80	84	----	----	80	84	80	84	-----	84
Sustainer/vernier hydraulic pump discharge pressure	AH130P	N/cm^2	10.04	10.04	2210	2210	2151	2140	2140	2130	2140	2103
		psi	14.7	14.7	3205	3205	3120	3105	3105	3090	3105	3050
Sustainer/vernier accumulator pressure	AH140P	N/cm^2	1365	1395	2216	2210	2151	2193	2140	2172	2140	2137
		psi	1980	2025	3215	3205	3120	3180	3105	3150	3105	3100
Sustainer/vernier system return pressure	AH601P	N/cm^2	52.78	57.92	----	----	52.78	57.92	52.78	57.92	52.78	57.92
		psi	78	84	----	----	78	84	78	84	78	84

[a]All pressures are absolute.

TABLE VI-VIII. - CENTAUR HYDRAULIC SYSTEM PERFORMANCE, AC-20 AND AC-19

Parameter	Measurement number	Units	Main engine start (MES)		MES + 10 sec		MES + 90 sec		Main engine cutoff	
			AC-20	AC-19	AC-20	AC-19	AC-20	AC-19	AC-20	AC-19
C-1 Power package pressure, absolute	CH1P	N/cm^2 psi	86.9 126	73.8 107	789.4 1145	755.0 1095	789.4 1145	755.0 1095	772.2 1120	748.1 1085
C-1 Manifold temperature	CH5T	K ^oF	285.45 53	285.45 53	288.65 60	292.05 66	309.25 97	309.25 97	349.15 169	349.15 169
C-2 Power package pressure, absolute	CH3P	N/cm^2 psi	77.9 113	78.6 114	779.1 1130	772.2 1120	779.1 1130	772.2 1120	768.8 1115	765.3 1110
C-2 Manifold temperature	CH6T	K ^oF	287.0 57	285.45 53	288.65 60	292.02 66	309.25 97	309.25 97	349.15 169	348.75 168

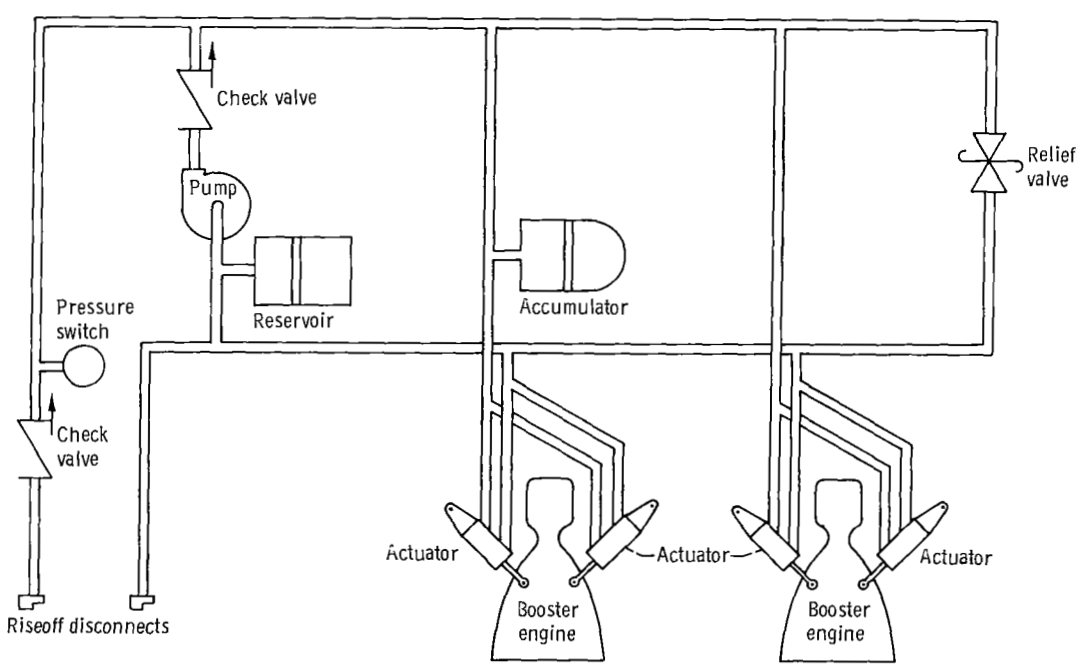

Figure VI-29. - Atlas booster hydraulic system, AC-20 and AC-19.

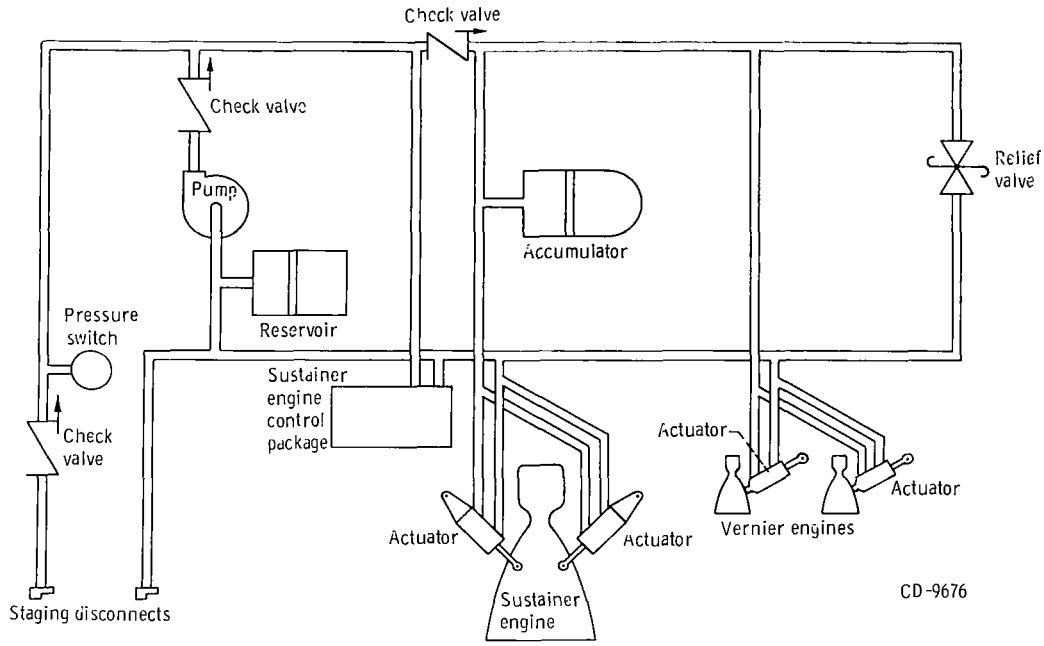

Figure VI-30. - Atlas sustainer hydraulic system, AC-20 and AC-19.

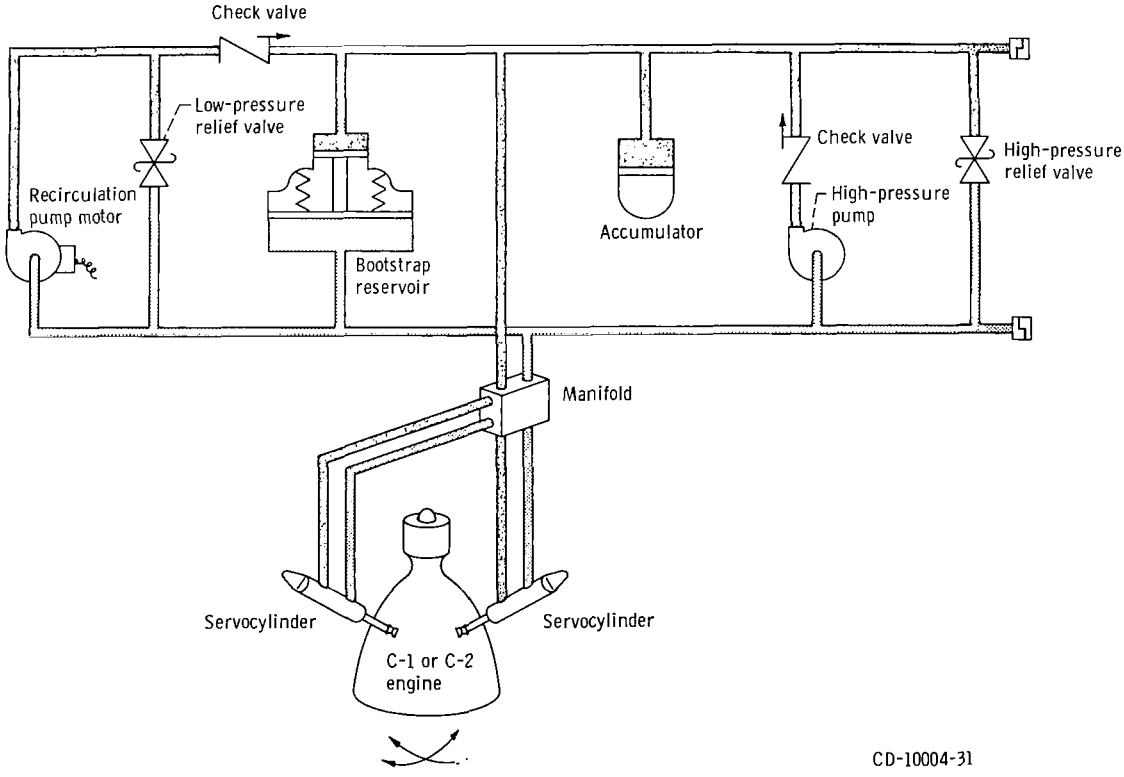

Figure VI-31. - Centaur hydraulic system, AC-20 and AC-19.

VEHICLE STRUCTURES

by Robert C. Edwards and Dana H. Benjamin

Atlas Structures

System description. - The primary Atlas vehicle structure is provided by the propellant tanks. These tanks are thin-walled, pressure-stabilized, monocoque sections of welded stainless-steel construction (see fig. VI-32). They require internal pressure in order to maintain structural stability. The tensile strength of the tank material determines the maximum allowable pressure in the propellant tanks.

The maximum allowable and minimum required tank pressures presented in figures VI-33 and VI-34 are computed using maximum design loads (as opposed to actual flight loads) with appropriate factors of safety. These required tank pressures are not constant because of varying aerodynamic loads, inertia loads, and ambient pressure during flight.

The Atlas vehicle is subjected to its highest design bending load between T + 40 and T + 110 seconds. The bending, inertia, and aerodynamic drag create compressive loads in the fuel and oxidizer tank skin. These loads are resisted by internal pressure to prevent buckling of the skin.

The maximum allowable differential pressure between the oxidizer and fuel tanks is limited by the strength of the Atlas intermediate bulkhead. The fuel tank pressure must always be greater than the oxidizer tank pressure to stabilize the intermediate bulkhead (prevent bulkhead reversal).

System performance. - The Atlas oxidizer and fuel tank ullage pressures did not approach the maximum allowable pressure during flight. The oxidizer and fuel tank ullage pressures were greater than the minimum required to resist the combined bending and axial design loads between T + 40 and T + 110 seconds (see figs. VI-33 and VI-34). The bulkhead differential pressure was within the maximum allowable and minimum required pressure limits for all periods of flight (see figs. VI-33 and VI-34).

The increase of longitudinal inertia force was as expected for AC-19. A maximum value of 5.68 g's was reached at booster engine cutoff. This value was within the specified limits of 5.59 to 5.81 g's. However, on the AC-20 flight the maximum longitudinal inertia force was only 5.35 g's due to a premature engine cutoff. This was caused by a malfunction of the booster engine cutoff backup accelerometer.

Centaur Structures

System description. - The primary Centaur vehicle structure is provided by the

propellant tanks. These tanks are thin-walled, pressure-stabilized, monocoque sections of welded stainless-steel construction (see fig. VI-35). They require internal pressure in order to maintain structural stability. The tensile strength of the tank material determines the maximum allowable pressure in the propellant tanks.

The tank locations and criteria which determine the maximum allowable and minimum required tank pressures during different phases of flight are described in figure VI-36. The maximum allowable and minimum required tank pressures presented in figures VI-37 and VI-38 are computed using maximum design loads (as opposed to actual flight loads) with appropriate factors of safety. The maximum allowable and minimum required tank pressures are not constant because of varying loads and varying ambient pressure during flight.

The oxidizer tank pressure most closely approaches the maximum allowable pressure at booster engine cutoff (T + 147.1 sec on AC-20 and T + 150.4 sec on AC-19) when the high inertia load causes maximum tension stresses on the aft bulkhead (see figs. VI-37 and VI-38). The minimum required oxidizer tank pressure for aft bulkhead stability is not pertinent because this required pressure is always less than the pressure required for intermediate bulkhead stability.

The strength of the fuel tank is governed by the capability of the conical section of the forward bulkhead to resist hoop stress. Thus, the differential pressure across the forward bulkhead determines the maximum allowable fuel tank pressure.

The margin between fuel tank ullage pressure and the minimum required pressure is least during the following events:

(1) Prior to launch, when the payload and nose fairing impose compression loads on the cylindrical skin at station 409.6 due to gravity and to ground winds

(2) During the launch phase from T + 0 to T + 10 seconds, when the payload and nose fairing impose compression loads on the cylindrical skin at station 409.6 due to longitudinal and lateral inertia and vibration

(3) From T + 40 to T + 110 seconds, when the Centaur is subjected to maximum design bending moments: The combined loads due to inertia, aerodynamic drag, and bending impose compression on the cylindrical skin at station 409.6.

(4) At nose fairing jettison, when the nose fairing exerts inboard radial loads at station 218.9

The maximum allowable differential pressure between the oxidizer and fuel tanks is limited by the strength of the Centaur intermediate bulkhead. The maximum design allowable differential pressure is 15.9 N/cm^2 (23.0 psi). The oxidizer tank pressure must always be greater than the combined fuel tank pressure and hydrostatic pressure of the liquid hydrogen; this is necessary to stabilize the intermediate bulkhead (prevent bulkhead reversal).

System performance. - The Centaur fuel and oxidizer tank ullage pressure profiles are compared with the design limits in figures VI-37 and VI-38.

The oxidizer tank pressure was less than the maximum allowable at booster engine cutoff and all other periods of flight. The oxidizer tank pressure was maintained above the minimum required for aft bulkhead stability during all periods of flight.

At no time during the flight did the fuel tank ullage pressure exceed the maximum allowable pressure. The fuel tank ullage pressure was safely above the minimum required pressure at all times.

The differential pressure across the Centaur intermediate bulkhead was less than the maximum allowable, 15.9 N/cm^2 (23.0 psi), for all periods of flight. The oxidizer tank pressure was always greater than the combined fuel tank ullage pressure and the hydrostatic pressure of the liquid hydrogen.

Vehicle Dynamic Loads

The Atlas-Centaur launch vehicle receives dynamic loading from three major sources: (1) external loads from aerodynamic and acoustic sources; (2) transients from engines starting and stopping and from the separation systems; and (3) loads due to dynamic coupling between major systems.

Research and development flights of the Atlas-Centaur launch vehicle have shown that these loads were within the structural limits established by ground test and model analysis. For operational flights such as AC-20 and AC-19, the number of dynamic flight measurements is limited by telemetry capacity. The instruments used and the parameters measured are tabulated below:

Instruments	Corresponding parameters
Low-frequency-range accelerometer	Vehicle longitudinal acceleration
Centaur pitch-rate gyro	Vehicle pitch-plane angular rate
Centaur yaw-rate gyro	Vehicle yaw-plane angular rate
Angle-of-attack sensor	Vehicle aerodynamic loads
High-frequency accelerometers	Local spacecraft vibration

Launch vehicle longitudinal vibrations measured on the Centaur forward bulkhead are presented in figure VI-39. The frequency and amplitude of the vibration data measured on AC-20 and AC-19 are shown in table VI-IX.

During launcher release, longitudinal vibrations were excited. The amplitude and frequency of these vibrations were similar to those observed on other flights. Atlas intermediate bulkhead pressure oscillations were the most significant effects produced by the launcher-induced longitudinal vibrations. For AC-20, the peak pressure oscillation computed from these vibrations was 4.1 N/cm^2 (5.9 psi). Since the minimum bulkhead

differential pressure measured for AC-20 at this time was 9.6 N/cm^2 (13.9 psi) (see fig. VI-34), the calculated minimum differential pressure across the bulkhead was 5.5 N/cm^2 (8.0 psi). A similar calculation was made for AC-19 and the minimum differential pressure across the bulkhead was found to be 5.9 N/cm^2 (8.6 psi). The minimum design allowable differential pressure across the bulkhead is 1.4 N/cm^2 (2.0 psi).

During Atlas flight between T + 80 and T + 82 seconds, intermittent longitudinal vibrations of 0.19 g, 12 hertz (AC-20 and AC-19) were observed on the Atlas fuel tank skin. These vibrations are believed to be caused by dynamic coupling between structure, engines, and propellant lines (commonly referred to as "POGO"). For a detailed discussion of this low-frequency longitudinal vibration see reference 1.

During the booster engine thrust decay, short-duration longitudinal vibrations of 0.7 g, 12 hertz (AC-20 and AC-19) were observed. The analytical models did not indicate significant structural loading due to these transients.

During the booster phase of flight the vehicle vibrates in the pitch plane and the yaw plane as an integral body at its natural frequencies. Previous analyses and tests have defined these natural frequencies, or modes, and the shapes which the vehicle assumes when the modes are excited. The rate gyros on the Centaur provide data for determining the deflection of these modes. The maximum first-mode deflection was seen in the pitch plane at T + 126 seconds for AC-20 and T + 127 seconds for AC-19 (figs. VI-40 and VI-41). The deflection was less than 6 percent of the allowable deflection. The maximum second-mode deflection was seen in the yaw plane at T + 32 seconds for AC-20 and T + 69 seconds for AC-19 (figs. VI-42 and VI-43). The yaw deflection was less than 19 percent of the allowable deflection.

Predicted angles of attack were based on upper-wind data obtained from a weather balloon released about 18 minutes after the time of launch for AC-20 and about 23 minutes after the time of launch for AC-19. Vehicle bending moments were calculated using predicted angles of attack, booster engine gimbal angle data, vehicle weights, and vehicle stiffnesses. These moments were added to axial load equivalent moments and to moments resulting from random dispersions. The most significant dispersions considered were uncertainties in launch vehicle performance and vehicle center-of-gravity offset. The total predicted bending moment (based upon wind data) was divided by the design bending moment allowable and added to the predicted axial load divided by the design axial load allowable to obtain the predicted structural capability ratio, as shown in figures VI-44 and VI-45. This ratio is expected to be greatest between T + 56 and T + 82 seconds due to high aerodynamic loads during this period. The maximum structural capability ratios predicted for this period were 0.875 for AC-20 and 0.801 for AC-19.

Transducers located on the nose fairing cap provided differential pressure measurements in the pitch plane and in the yaw plane. Total pressure was computed from a trajectory reconstruction. Angles of attack were computed from these data and are com-

pared with predicted angles of attack in figures VI-46 to VI-49. Since the actual angles of attack were within the expected dispersion values, it follows that the maximum predicted structural capability ratios of 0.875 (AC-20) and 0.801 (AC-19) were not exceeded.

Local shock and vibration were measured by three continuous piezoelectric high-frequency accelerometers located in the spacecraft area. Accelerometers were located near the forward flange of the forward payload adapter (Centaur station 136), on the forward end of the spacecraft bus structure (Centaur station 118), and at the spacecraft scan platform on the wide-angle television camera (Centaur station 144). These accelerometers, together with their amplifiers, had a frequency response of 2100 hertz, which (in all cases) exceeded the telemetry channel Inter-Range Instrumentation Group (IRIG) filter frequency. Therefore, the frequency range (for unattenuated data) was limited by the standard IRIG filter frequency for that channel. In addition to the three high-frequency accelerometers, there were six low-frequency accelerometers located on the payload adapter (Centaur station 159). These accelerometers were sensitive in the tangential and longitudinal directions.

A summary of the most significant shock and vibration levels measured by the three continuous high-frequency and six low-frequency accelerometers on AC-20 and AC-19 is shown in table VI-IX. The steady-state vibration levels were highest near lift-off, as expected. The maximum level of the shock loads (30 g's) on AC-20 and AC-19 occurred at insulation panel jettison and spacecraft separation. These shock loads were of short duration (about 0.025 sec) and did not provide significant loads. An analysis of the data indicates that the levels were well within spacecraft qualification levels.

TABLE VI-IX. - MAXIMUM SHOCK AND VIBRATION LEVELS OBSERVED AT MARK EVENTS, AC-20 AND AC-19

[Two of the high-frequency accelerometers exhibited periods of bias instability. This bias level instability was observed on AC-19 and on AC-20. The rms vibration was that averaged over a time period of approximately 1 sec.]

(a) AC-20 (Mariner VI mission)

Time of dynamic disturbance, sec after lift-off	Mark event	Accelerometer location (referenced to Centaur stations)								
		136	118	144	159					
		Axis or direction of sensitivity								
		Longitudinal						Tangential		
		Accelerometer system gain of 0 db limited to approximately-								
		2100 Hz			100 Hz			70 Hz		
		Standard telemetry channel cutoff filter frequency								
		790	790	1050	110	160	220	330	450	600
		Accelerometer range, g's								
		±30	±20		-3.0 to 9.0			±1.17	±1.19	
0	Launch:									
	Acceleration, g's	1.1 (rms)	0.3 (rms)	1.3 (rms)	0.60 (rms)	1.1 (rms)	1.2 (rms)	0.39 (rms)	0.48 (rms)	0.48 (rms)
		2.2	2.0	2.7	1.1	1.2	1.3	0.56	0.79	0.76
	Frequency, Hz	110	110	110	110	110	110	80 to 90	80 to 90	80 to 90
57	Transonic region:									
	Acceleration, g's	0.28 (rms)	0.41 (rms)	0.37 (rms)	0.16 (rms)	0.36 (rms)	0.40 (rms)	0.09 (rms)	0.11 (rms)	0.10 (rms)
		---	1.2	1.5	0.1	0.1	0.1	0.2	0.2	0.2
	Frequency, Hz	---	7.5	7.6	11	11	11	8	8	8
146.2	Booster engine cutoff:									
	Acceleration, g's	2	(a)	(a)	0.75	0.84	0.72	[b]0.33 / 0.33	0.12 / 0.25	0.12 / 0.24
	Frequency, Hz	13	(a)	(a)	12	12	12	[b]4.5 / 75	4.5 / 75	4.5 / 75
149.2	Booster jettison:									
	Acceleration, g's	(c)	(c)	(c)	(c)	(c)	(c)	0.33	0.43	0.38
	Frequency, Hz	(c)	(c)	(c)	(c)	(c)	(c)	5	4	4
191.4	Insulation panel jettison:									
	Acceleration, g's	29	10	5.1	2.4	1.4	2.2	0.38	0.48	0.62
	Frequency, Hz	500 to 600	400 to 500	110	>500	>500	>500	>500	>500	500
227.5	Nose fairing jettison:									
	Acceleration, g's	2.1	1.9	3.1	0.94	0.96	1.08	0.38	0.62	0.62
	Frequency, Hz	33	8	46	35	35	35	80	80	80
270.3	Sustainer engine cutoff:									
	Acceleration, g's	1.7	0.9	2.1	0.6	0.3	0.6	0.76	0.74	0.36
	Frequency, Hz	90	90	89	90	90	90	90	90	90
273.2	Atlas-Centaur separation:									
	Acceleration, g's	30	20	3.2	4.5	2.1	1.9	0.38	0.48	0.55
	Frequency, Hz	>600	>600	>600	>500	>500	>500	>500	>500	>500
281.9	Main engine start:									
	Acceleration, g's	(d)	0.7	1.4	0.2	0.15	0.15	0.23	0.21	0.2
	Frequency, Hz	(d)	40	40	40 to 50	40 to 50	40 to 50	40	80	80
724.6	Main engine cutoff:									
	Acceleration, g's	3.2	3.1	5.2	1.1	1.2	1.2	0.21	0.29	0.33
	Frequency, Hz	43	42	45	40	40	40	50	50	100
820.3	Spacecraft separation:									
	Acceleration, g's	(a)	19.7	4.3	0.79	0.90	1.2	0.27	0.21	0.20
	Frequency, Hz	(a)	>600	>500	>500	>500	>500	>500	>500	500

[a]Questionable data.

[b]Double entry indicates frequencies and amplitudes of two superimposed vibrations.

[c]Telemetry signal dropout.

[d]No detectable response.

TABLE VI-IX. - MAXIMUM SHOCK AND VIBRATION LEVELS OBSERVED AT MARK EVENTS, AC-20 AND AC-19

[Two of the high-frequency accelerometers exhibited periods of bias instability. This bias level instability was observed on AC-19 and on AC-20. The rms vibration was that averaged over a time period of approximately 1 sec.]

(a) AC-20 (Mariner VI mission)

Time of dynamic disturbance, sec after lift-off	Mark event	Accelerometer location (referenced to Centaur stations)								
		136	118	144	159					
		Axis or direction of sensitivity								
		Longitudinal						Tangential		
		Accelerometer system gain of 0 db limited to approximately-								
		2100 Hz			100 Hz			70 Hz		
		Standard telemetry channel cutoff filter frequency								
		790	790	1050	110	160	220	330	450	600
		Accelerometer range, g's								
		±30	±20		-3.0 to 9.0			±1.17	±1.19	
0	Launch:									
	Acceleration, g's	1.1 (rms) 2.2	0.3 (rms) 2.0	1.3 (rms) 2.7	0.60 (rms) 1.1	1.1 (rms) 1.2	1.2 (rms) 1.3	0.39 (rms) 0.56	0.48 (rms) 0.79	0.48 (rms) 0.76
	Frequency, Hz	110	110	110	110	110	110	80 to 90	80 to 90	80 to 90
57	Transonic region:									
	Acceleration, g's	0.28 (rms) ---------	0.41 (rms) 1.2	0.37 (rms) 1.5	0.16 (rms) 0.1	0.36 (rms) 0.1	0.40 (rms) 0.1	0.09 (rms) 0.2	0.11 (rms) 0.2	0.10 (rms) 0.2
	Frequency, Hz	---------	7.5	7.6	11	11	11	8	8	8
146.2	Booster engine cutoff:									
	Acceleration, g's	2	(a)	(a)	0.75	0.84	0.72	[b]0.33 | 0.33	0.12 | 0.25	0.12 | 0.24
	Frequency, Hz	13	(a)	(a)	12	12	12	[b]4.5 | 75	4.5 | 75	4.5 | 75
149.2	Booster jettison:									
	Acceleration, g's	(c)	(c)	(c)	(c)	(c)	(c)	0.33	0.43	0.38
	Frequency, Hz	(c)	(c)	(c)	(c)	(c)	(c)	5	4	4
191.4	Insulation panel jettison:									
	Acceleration, g's	29	10	5.1	2.4	1.4	2.2	0.38	0.48	0.62
	Frequency, Hz	500 to 600	400 to 500	110	>500	>500	>500	>500	>500	>500
227.5	Nose fairing jettison:									
	Acceleration, g's	2.1	1.9	3.1	0.94	0.96	1.08	0.38	0.62	0.62
	Frequency, Hz	33	8	46	35	35	35	80	80	80
270.3	Sustainer engine cutoff:									
	Acceleration, g's	1.7	0.9	2.1	0.6	0.3	0.6	0.76	0.74	0.36
	Frequency, Hz	90	90	89	90	90	90	90	90	90
273.2	Atlas-Centaur separation:									
	Acceleration, g's	30	20	3.2	4.5	2.1	1.9	0.38	0.48	0.55
	Frequency, Hz	>600	>600	>600	>500	>500	>500	>500	>500	>500
281.9	Main engine start:									
	Acceleration, g's	(d)	0.7	1.4	0.2	0.15	0.15	0.23	0.21	0.2
	Frequency, Hz	(d)	40	40	40 to 50	40 to 50	40 to 50	40	80	80
724.6	Main engine cutoff:									
	Acceleration, g's	3.2	3.1	5.2	1.1	1.2	1.2	0.21	0.29	0.33
	Frequency, Hz	43	42	45	40	40	40	50	50	100
820.3	Spacecraft separation:									
	Acceleration, g's	(a)	19.7	4.3	0.79	0.90	1.2	0.27	0.21	0.20
	Frequency, Hz	(a)	>600	>500	>500	>500	>500	>500	>500	>500

[a]Questionable data.

[b]Double entry indicates frequencies and amplitudes of two superimposed vibrations.

[c]Telemetry signal dropout.

[d]No detectable response.

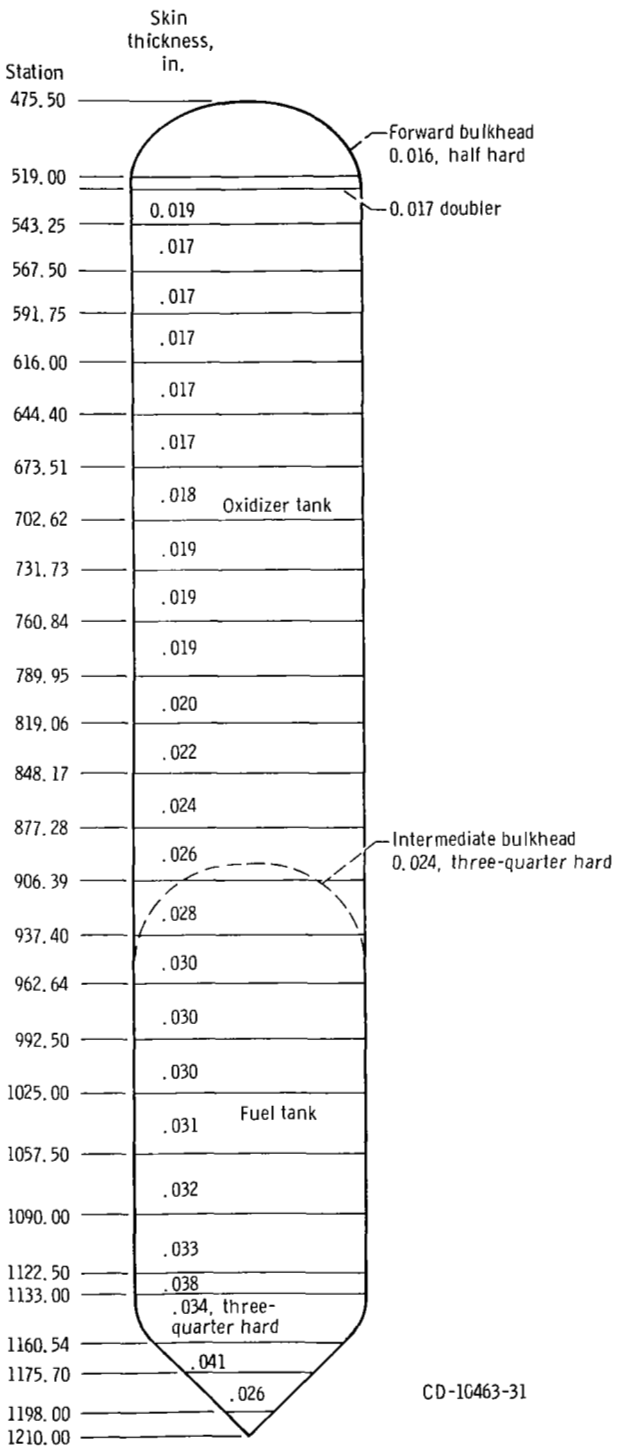

Figure VI-32. - Atlas propellant tanks, AC-20 and AC-19.

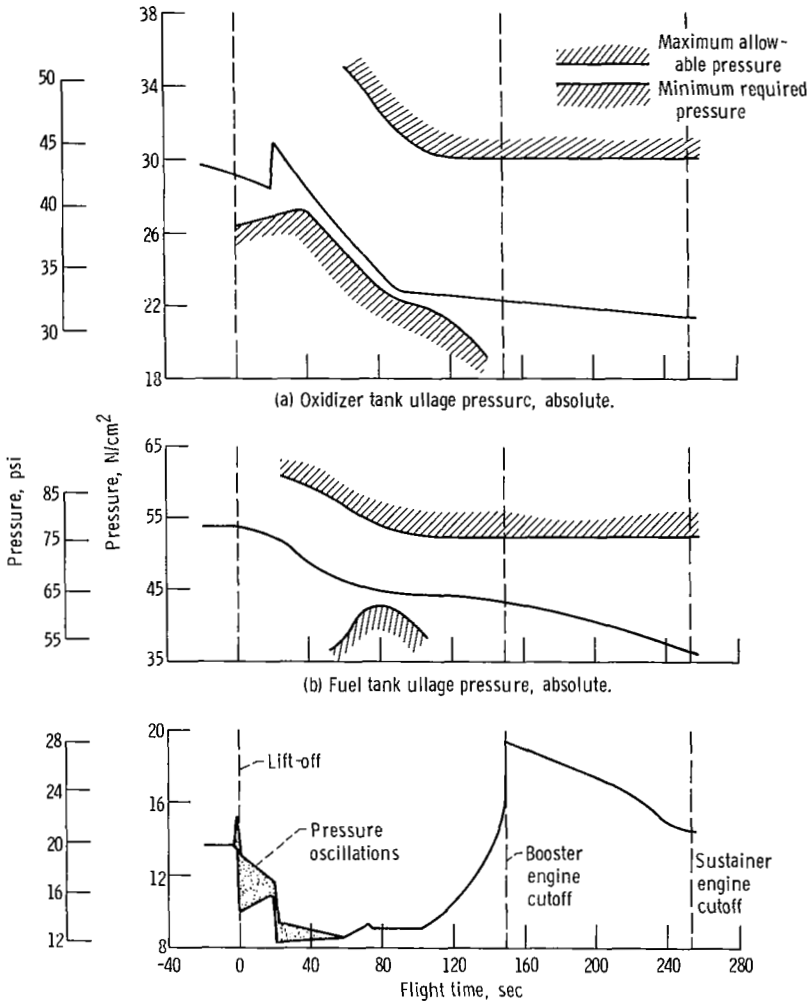

(a) Oxidizer tank ullage pressure, absolute.

(b) Fuel tank ullage pressure, absolute.

(c) Intermediate bulkhead differential pressure; maximum allowable during flight, 42 N/cm^2; minimum required during flight, 1.4 N/cm^2.

Figure VI-33. - Atlas fuel and oxidizer pressures, AC-19.

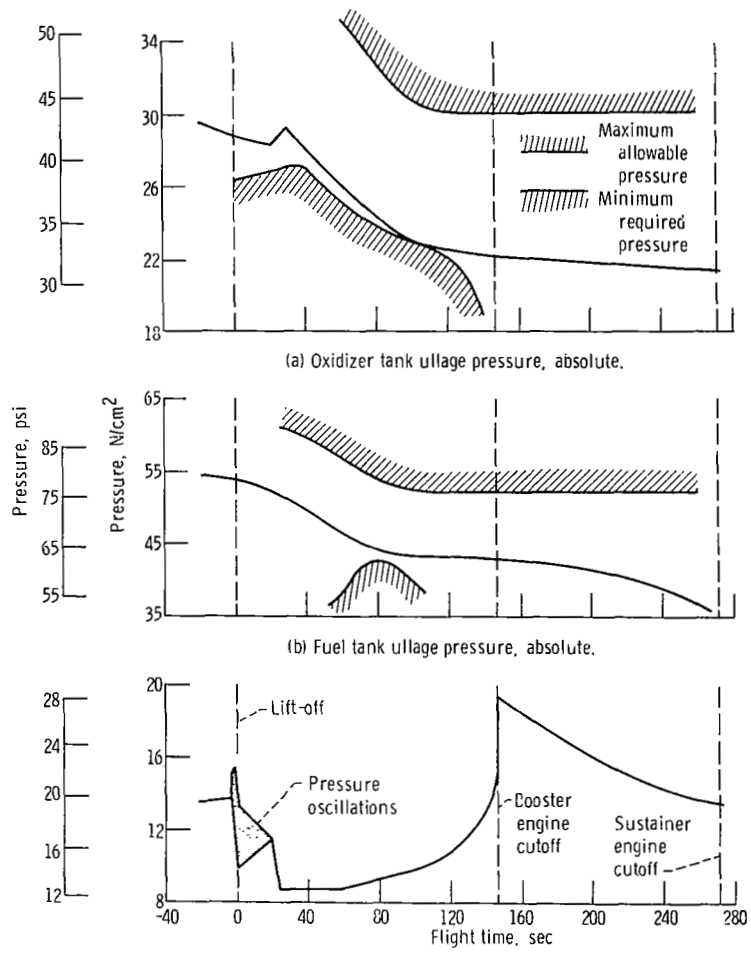

(a) Oxidizer tank ullage pressure, absolute.

(b) Fuel tank ullage pressure, absolute.

(c) Intermediate bulkhead differential pressure; maximum allowable during flight, 42 N/cm^2; minimum required during flight, 1.4 N/cm^2.

Figure VI-34. - Atlas fuel and oxidizer tank pressures, AC-20.

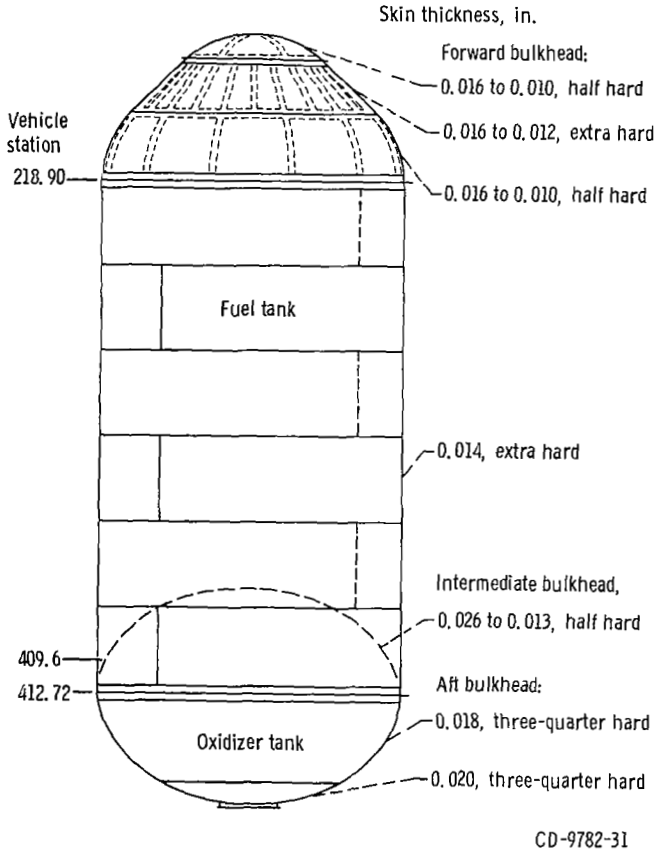

Figure VI-35. - Centaur propellant tanks, AC-20 and AC-19.
(All material 301 stainless steel, of hardness indicated.)

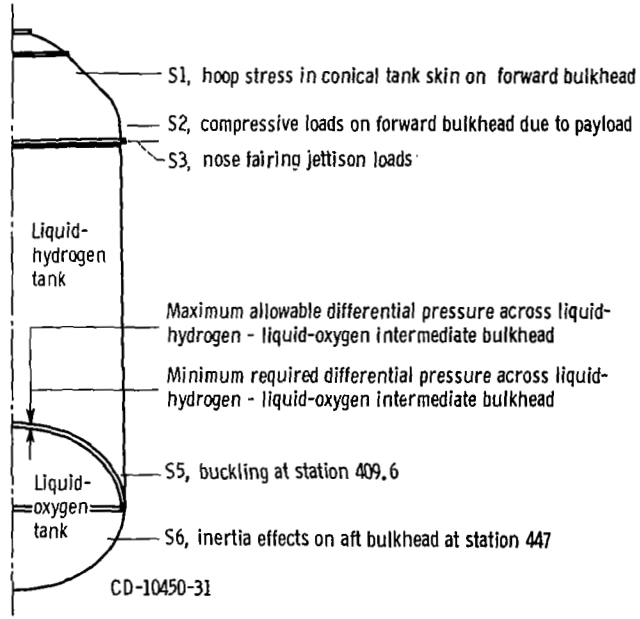

Figure VI-36. - Tank locations and criteria which determine allowable pressures, AC-20 and AC-19.

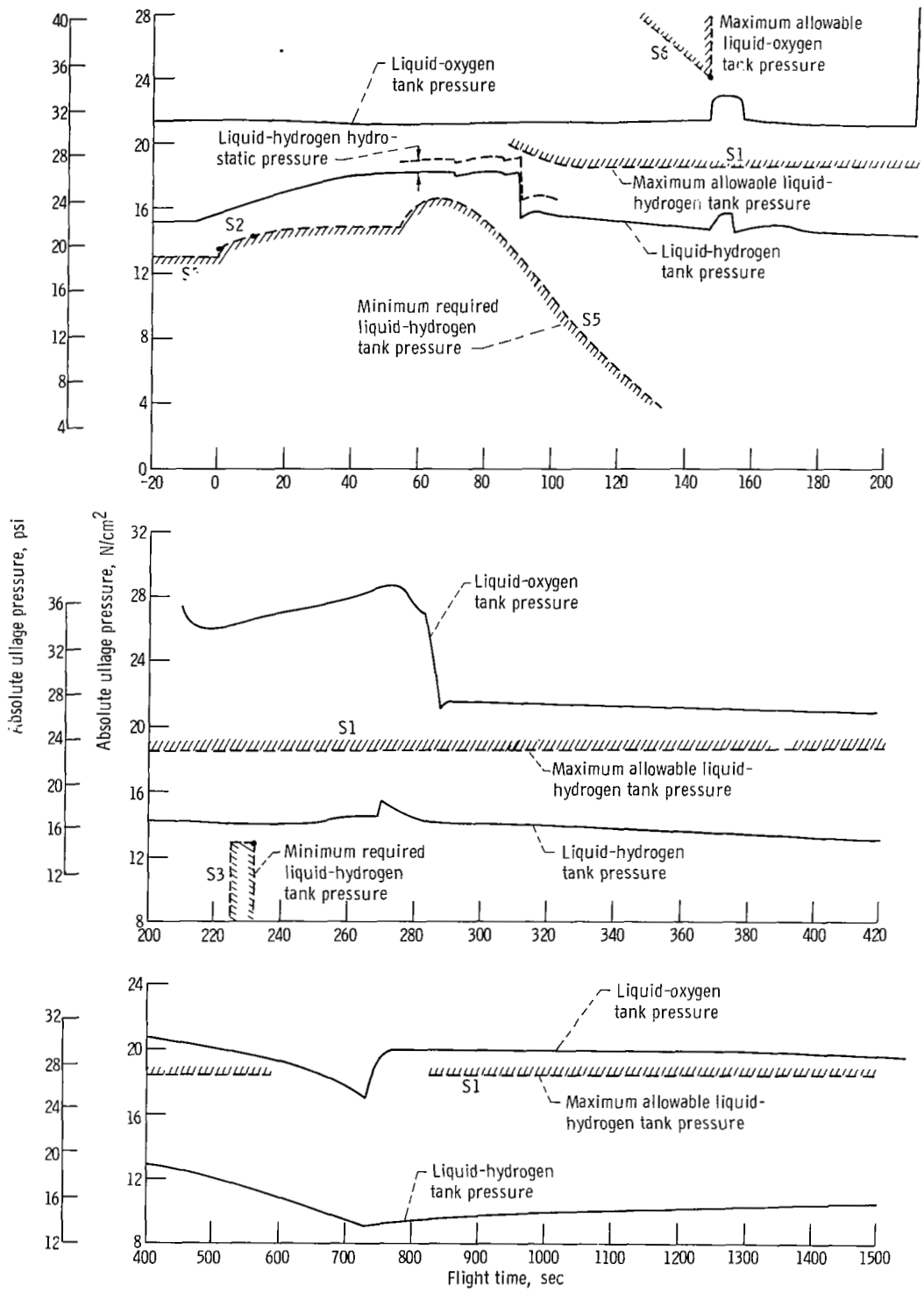

Figure VI-37. - Centaur fuel and oxidizer tank pressure, AC-20. S1, S2, etc. indicate tank structure areas which determine the allowable tank pressure (see fig. VI-36).

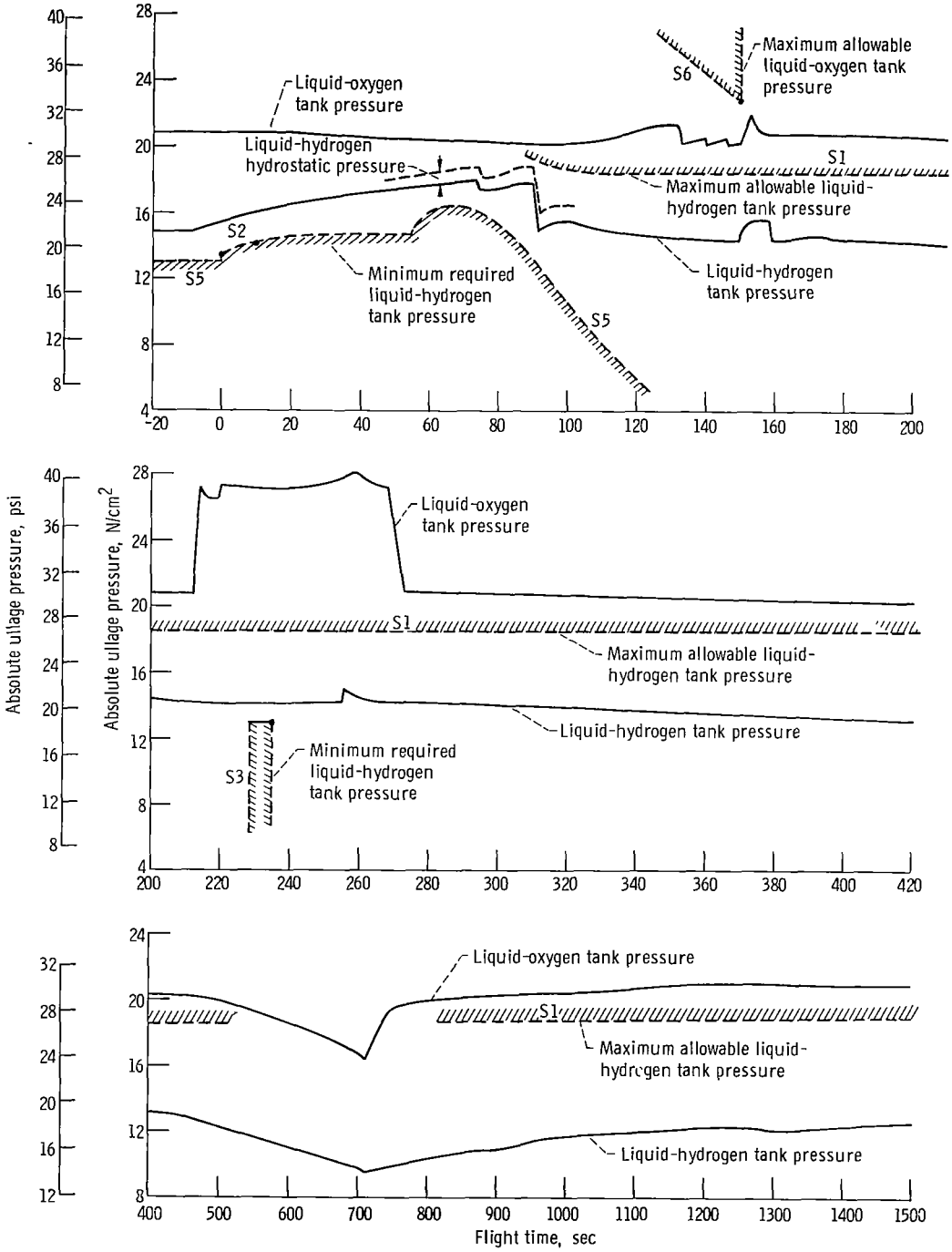

Figure VI-38. - Centaur fuel and oxidizer tank pressure, AC-19. S1, S2, etc. indicate tank structure areas which determine the allowable tank pressure (see fig. VI-36).

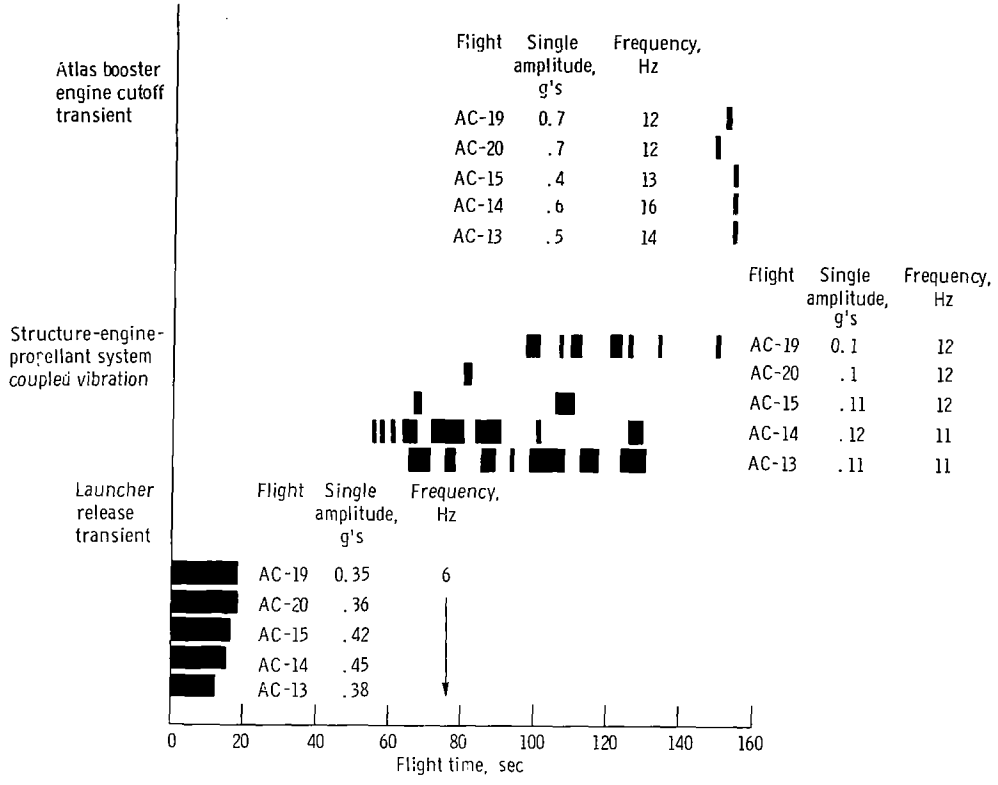

Figure VI-39. - Longitudinal vibrations for Atlas-Centaur flights.

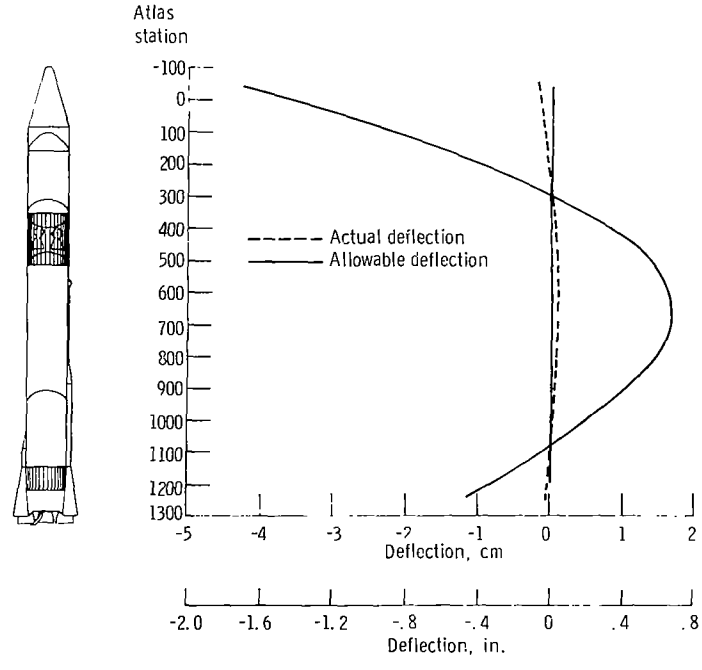

Figure VI-40. - Maximum pitch plane first-bending-mode amplitudes at T + 126 seconds, AC-20.

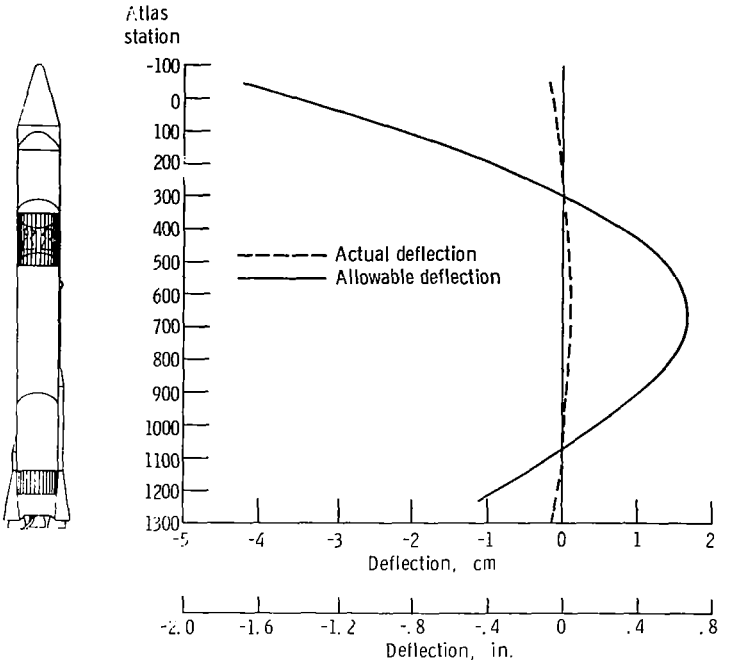

Figure VI-41. - Maximum pitch plane first-bending-mode amplitudes at T + 127 seconds, AC-19.

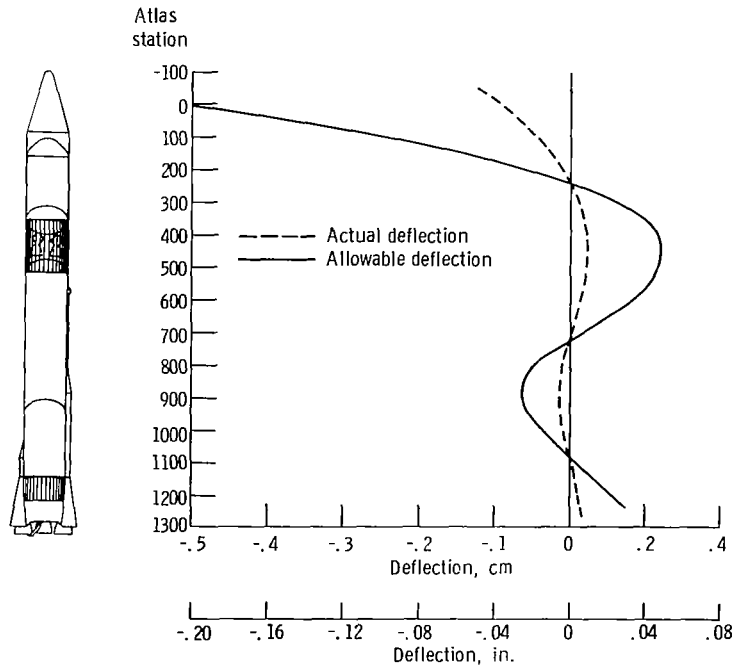

Figure VI-42. - Maximum yaw plane second-bending-mode amplitudes at T + 32 seconds, AC-20.

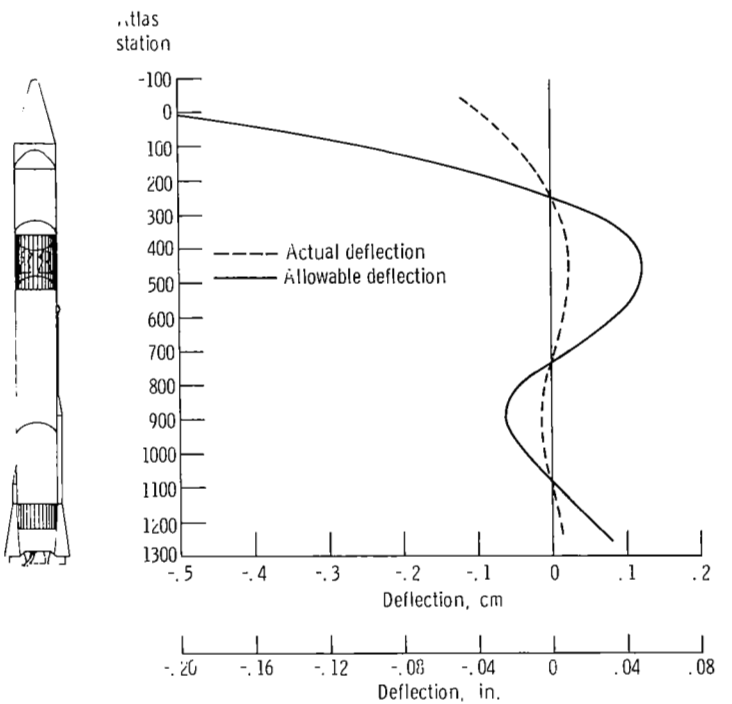

Figure VI-43. - Maximum yaw plane second-bending-mode amplitudes at T + 69 seconds, AC-19.

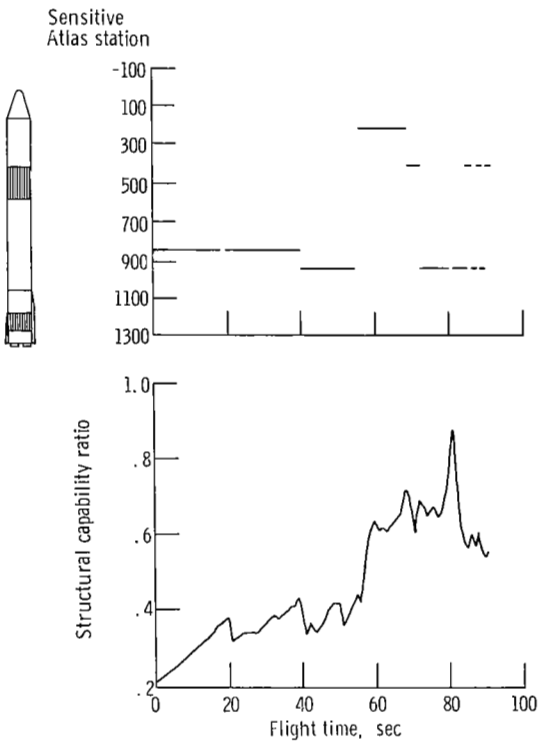

Figure VI-44. - Maximum predicted structural capability ratio (total equivalent predicted bending moment/bending moment allowable) and sensitive station, AC-20. (Based upon T + 0 weather balloon.)

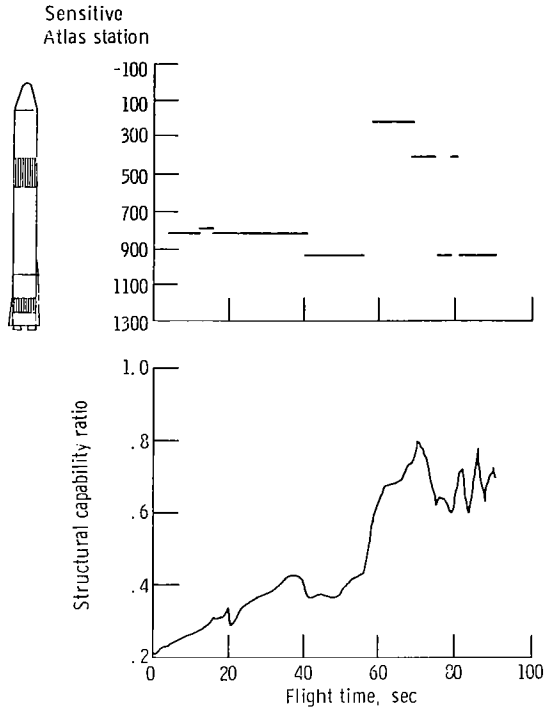

Figure VI-45. - Maximum predicted structural capability ratio (total equivalent predicted bending moment/bending moment allowable) and sensitive station, AC-19. (Based upon T + 0 weather balloon.)

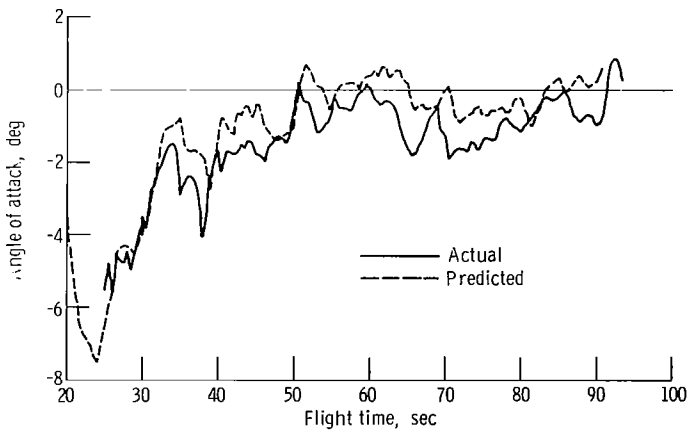

Figure VI-46. - Predicted and actual pitch angles of attack, AC-20. (Based upon T + 0 weather balloon.)

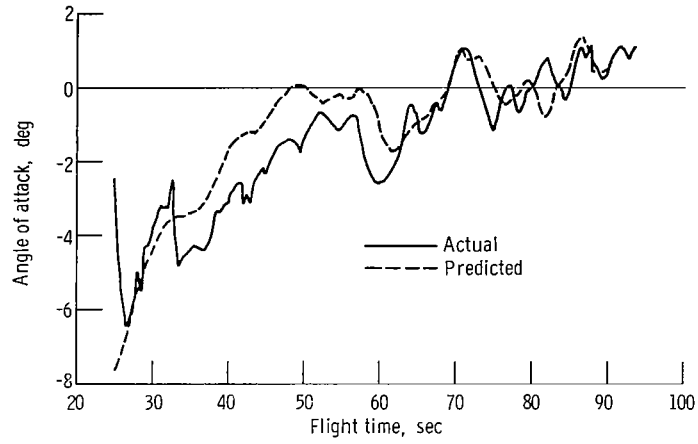

Figure VI-47. - Predicted and actual pitch angles of attack, AC-19. (Based upon T + 0 weather balloon.)

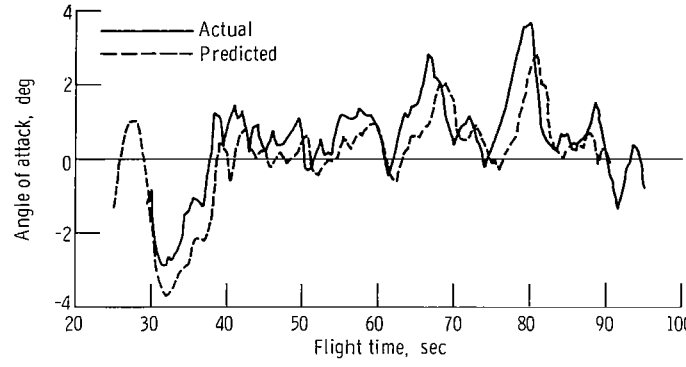

Figure VI-48. - Predicted and actual yaw angles of attack, AC-20. (Based upon T + 0 weather balloon.)

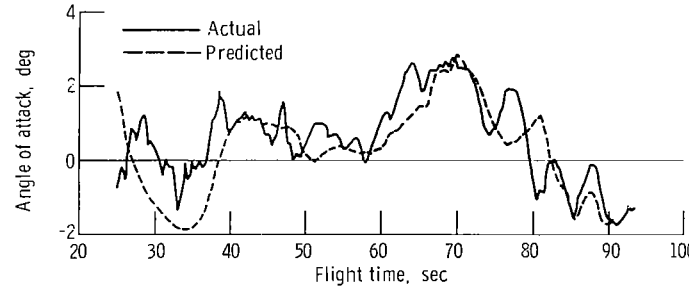

Figure VI-49. - Predicted and actual yaw angles of attack, AC-19. (Based upon T + 0 weather balloon.)

SEPARATION SYSTEMS

by Charles W. Eastwood and William M. Prati

Stage Separation

System description. - The Atlas-Centaur vehicle requires systems for Atlas booster engine section separation, Atlas/Centaur separation, and Centaur/spacecraft separation.

The Atlas booster engine stage separation system consists of 10 helium-gas-operated latch mechanisms. These latches, as shown in figures VI-50 and VI-51, are located circumferentially around the Atlas aft bulkhead thrust ring at station 1133. An explosive valve supplies helium at a gage pressure of 2068 N/cm^2 (3000 psi) to the distribution manifold. The actuation of the latch mechanism results in the disengagement of the booster engine from the Atlas vehicle. Two jettison tracks (fig. VI-52) attached to the thrust ring are used to guide the booster engine section as it separates from the Atlas.

Atlas-Centaur staging systems, as shown in figure VI-53, consist of a flexible linear shaped charge mounted circumferentially which severs the forward end of the interstage adapter at Centaur station 413; separation force is provided by eight retrorockets mounted near the aft end of the Atlas.

The Mariner spacecraft is separated from Centaur by release of a two-segment V-band that clamps the spacecraft to the forward payload adapter. Release of the segmented band is accomplished by the actuation of two pyrotechnically operated latches. Separation force is provided by four mechanical spring assemblies mounted on the flange of the forward payload adapter.

System performance. - Atlas booster engine section staging occurred 3 seconds after booster engine cutoff for both flights. Staging was verified by data from the B-1 booster thrust chamber pitch actuator position instrumentation and from the vehicle axial (fine) accelerometer. The following table summarizes booster engine cutoff and booster engine section staging event times:

Flight	Booster engine cutoff, sec	Booster engine section staging, sec
AC-20	T + 147.1	T + 150.1
AC-19	T + 150.4	T + 153.5

Atlas/Centaur staging was successful on both flights. Vehicle staging was commanded and firing of the flexible linear shaped charge severed the interstage adapter at station 413. The eight retrorockets, mounted around the aft end of the Atlas, fired 0.1 second later to decelerate the Atlas and provide separation from the Centaur. Accelerometer and other data indicated that all eight retrorockets functioned as expected for both flights. Figures VI-54 and VI-55 show the separation distance as a function of time between the Atlas and the Centaur vehicle for both flights. These figures also indicate clearance losses due to pitch and yaw motions of Atlas during separation for both flights.

The following table summarizes shaped charge firing times, retrorocket firing times, and the resulting pitch and yaw motions as the Atlas cleared the aft end of the Centaur engines:

Flight event	Units	AC-20	AC-19
Shaped charge firing time	sec	T + 272.8	T + 256.9
Retrorocket firing time	sec	T + 272.9	T + 257.0
Pitch clearance, nominal	cm	27.9	27.9
	in.	11	11
Pitch clearance loss	cm	2.7	3.8
	in.	1.1	1.5
Pitch clearance, actual	cm	25.2	24.1
	in.	9.9	9.5
Yaw clearance, nominal	cm	79	79
	in.	31	31
Yaw clearance loss	cm	6.4	7.1
	in.	2.5	2.8
Yaw clearance, actual	cm	72.6	71.9
	in.	28.5	28.2

The spacecraft was successfully separated from the Centaur vehicle on each flight. Spacecraft separation for AC-20 occurred at T + 820.6 seconds and for AC-19 at T + 807.4 seconds. Vehicle rates prior to and immediately after the spacecraft separation event were normal for both flights (see section GUIDANCE AND FLIGHT CONTROL SYSTEMS).

Jettisonable Structures

System description. - The Atlas-Centaur vehicle jettisonable structure consists of hydrogen tank insulation panels, a nose fairing, and related separation systems.

The hydrogen tank insulation is made up of four polyurethane foam-filled fiber-glass honeycomb panels bolted together along the longitudinal axis to form a cylindrical cover around the Centaur tank. The panels are bolted at their aft end to a support on the Centaur vehicle (fig. VI-56). At the forward end a circumferential Tedlar-and-fiber-glass-laminated cloth forms a seal between the panels and the base of the nose fairing at station 219 (fig. VI-57). Separation of the four insulation panels is accomplished by firing the flexible linear shaped charges located at the forward, aft, and longitudinal seams. The shaped charge at the insulation panel forward seal simultaneously severs the aft attachment of the nose fairing preparatory to fairing jettison at a later time in flight. Immediately following shaped-charge firing, the panels rotate about hinge points at their aft end (fig. VI-58) due to the preload hoop tension, the center-of-gravity offset, and the in-flight residual purge pressure. The panels jettison free of the Centaur vehicle after approximately 45° of panel rotation on the hinge pins.

The nose fairing is a fiber-glass skin and honeycomb structure. It consists of a cylindrical section approximately 1.83 meters (6 ft) long bolted to a conical section which is approximately 4.87 meters (16 ft) long. It is assembled in two jettisonable halves with the split line along the X-X axis, as shown in figure VI-59. A subliming agent is applied to the external surface of the fairing to limit the structure temperature during the aerodynamic heating phase of flight.

In addition to the flexible linear shaped charge which severs the aft attachment, the nose fairing separation system consists of latches and thrusters. The eight pyrotechnically operated pin puller latches release the fairing halves along the split line as shown in figure VI-59. Separation force is provided by two nitrogen gas thrusters located at the forward end of the nose cone, one in each fairing half. Each fairing half is hinged at a single point on the Centaur hydrogen tank at station 219 on the Y-Y axis (fig. VI-59).

System performance. - Flight data indicated that the insulation panels were jettisoned satisfactorily on the AC-20 and AC-19 flights. The insulation panel jettison sequence was initiated by a command signal issued from the Atlas programmer. Following

issuance of the command, the linear shaped charge fired to sever the panel attachments. Shaped-charge firing times were determined from accelerometers mounted on the payload aft adapter. The firing event times were at T + 191.7 seconds for AC-20 and T + 195.1 seconds for AC-19.

When the panels rotated through 35°, the breakwire transducers functioned and provided event time data. These transducers were attached to one hinge arm of each panel, as shown in figure VI-60. Since the breakwire data were monitored on commutated channels, the panel 35° position event times in the following table are mean times:

Insulation panel location, quadrant	Instrumented hinge arm location, quadrant	Insulation panel 35° rotation position event mean time, T + sec	
		AC-20	AC-19
I-II	1	192.25	195.54
II-III	3	192.33	195.64
III-IV	3	192.31	195.58
IV-I	1	192.24	195.60

The rotational velocity of each panel, assuming first motion at shaped charge firing, was determined from the mean time of the 35° position. Panel velocities from both flights are compared in the following table:

Panel location, quadrant	Average rotation velocities from shaped-charge firing to mean time of 35° position, deg/sec	
	AC-20	AC-19
I-II	69.9	84.2
II-III	59.6	68.8
III-IV	62.3	76.5
IV-I	71.3	73.5

The rotational rate for each panel on AC-20 was lower than the comparable value for AC-19. The slower rates are attributed to the lower axial acceleration of the AC-20 vehicle at panel jettison. However, the rates were well above the minimum limit of 40 degrees per second.

For both AC-20 and AC- 19 flights, the vehicle rates and dynamics at the event time indicated a completely satisfactory insulation panel jettison sequence.

The AC-20 and AC-19 nose fairings were successful jettisoned. Nose fairing jettison was initiated by a command from the Atlas programmer and the eight pyrotechnically operated pin pullers then unlatched the nose fairing split line. Approximately 0. 5 second later the two nitrogen thrusters operated, causing the fairing halves to begin rotating about their hinge points. Nose fairing latch actuation and initiation of the thruster operation were determined from accelerometer data. Rotation of each fairing half was sensed by disconnect pins in the electrical connectors which separated after approximately 3^{o} of fairing rotation. The following table summarizes significant nose fairing separation event times for both flights:

Event	Nose fairing jettison event time, T + sec	
	AC-20	AC-19
Split line latch actuation	227. 967	231. 424
Nitrogen thruster actuation	228. 464	231. 924
3^{o} rotation position (each fairing half)	[a]227. 62 to 228. 59	[a]231. 37 to 232. 42

[a]Data from commutated channel.

During fairing jettison the payload compartment pressure remained at zero with no pressure surge occurring at thruster bottle discharge.

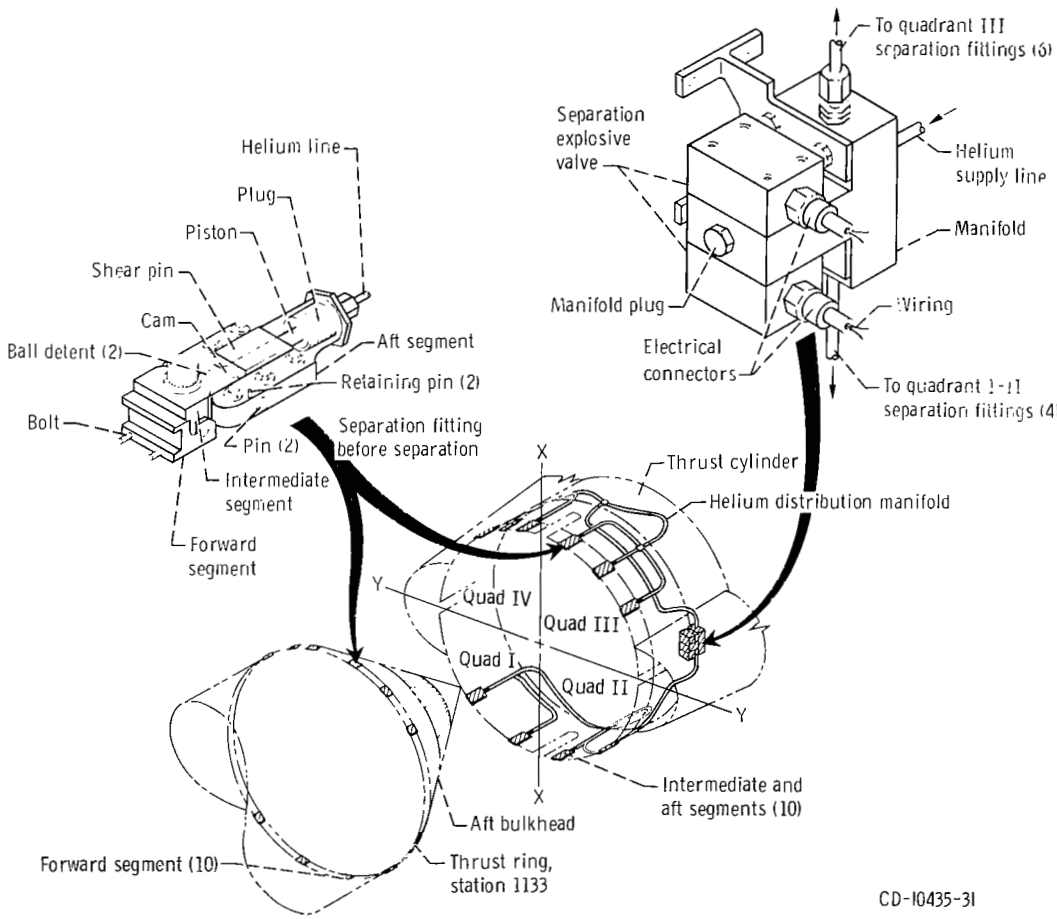

Figure VI-50. - Atlas booster engine section separation system details, AC-20 and AC-19.

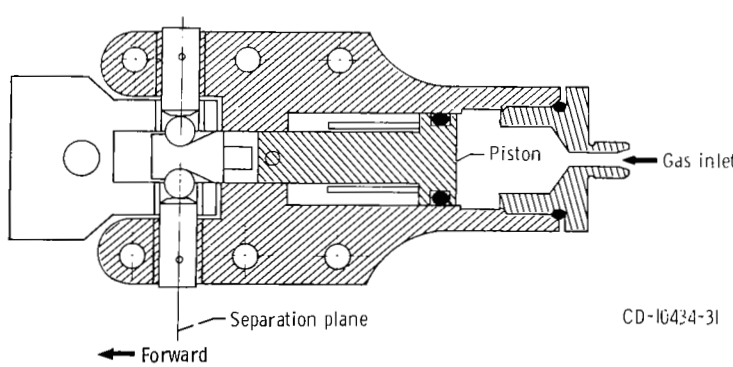

Figure VI-51. - Atlas booster engine section separation fitting, AC-20 and AC-19.

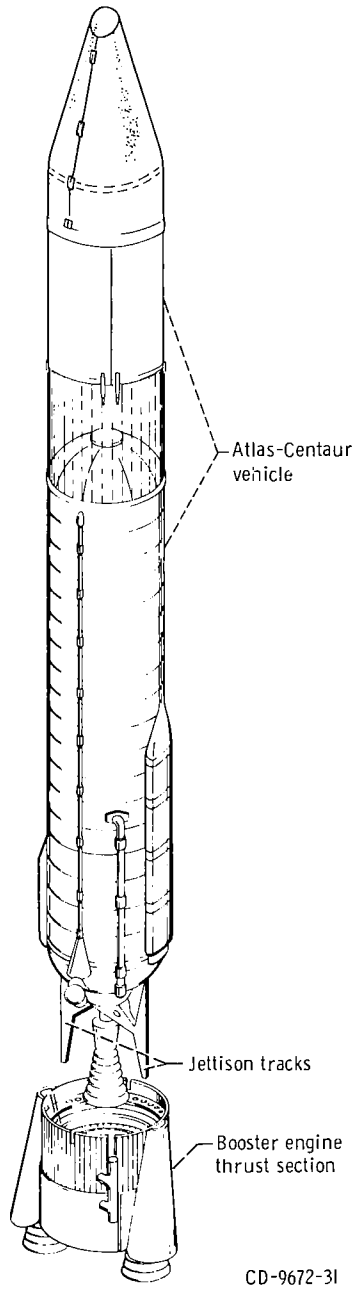

Figure VI-52. - Atlas booster engine section staging system, AC-20 and AC-19.

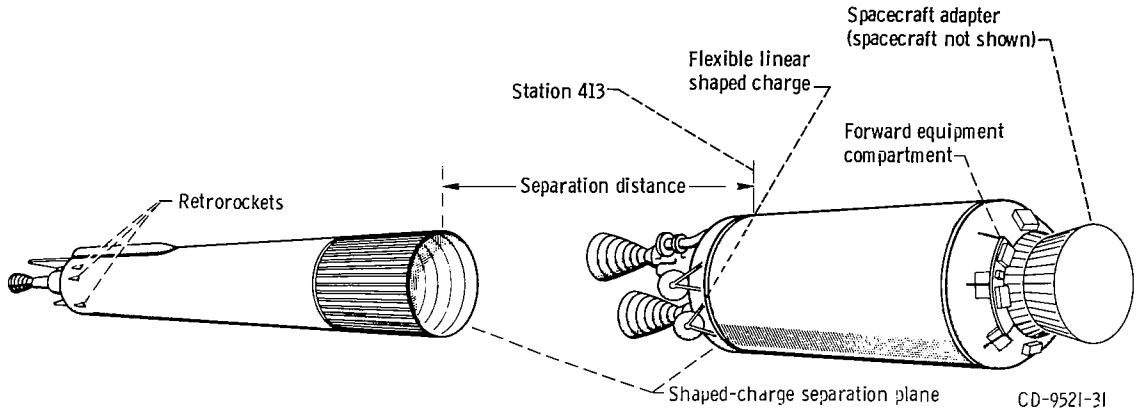

Figure VI-53. - Atlas-Centaur separation system, AC-20 and AC-19.

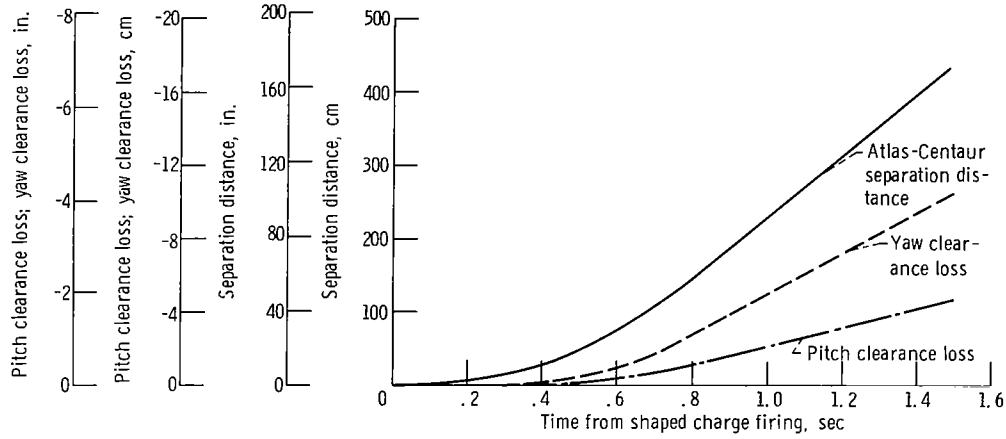

Figure VI-54. - Atlas-Centaur separation distances and clearance losses, AC-20. All clearance losses referenced to forward end of interstage adapter.

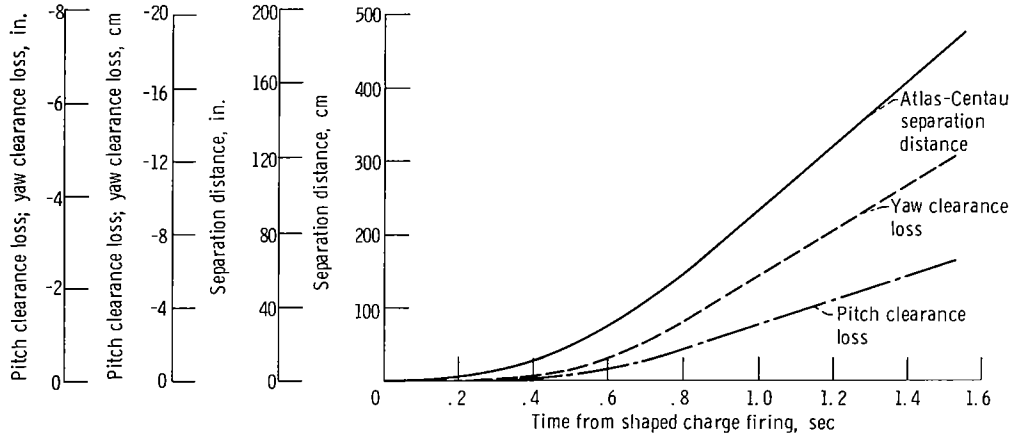

Figure VI-55. - Atlas-Centaur separation distances and clearance losses, AC-19. All clearance losses referenced to forward end of interstage adapter.

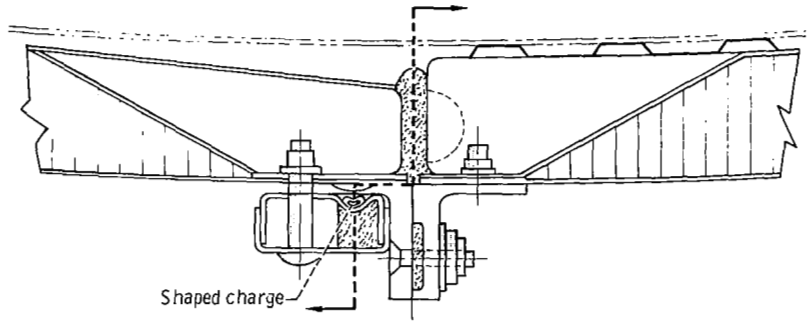

Section B-B. Longitudinal joint

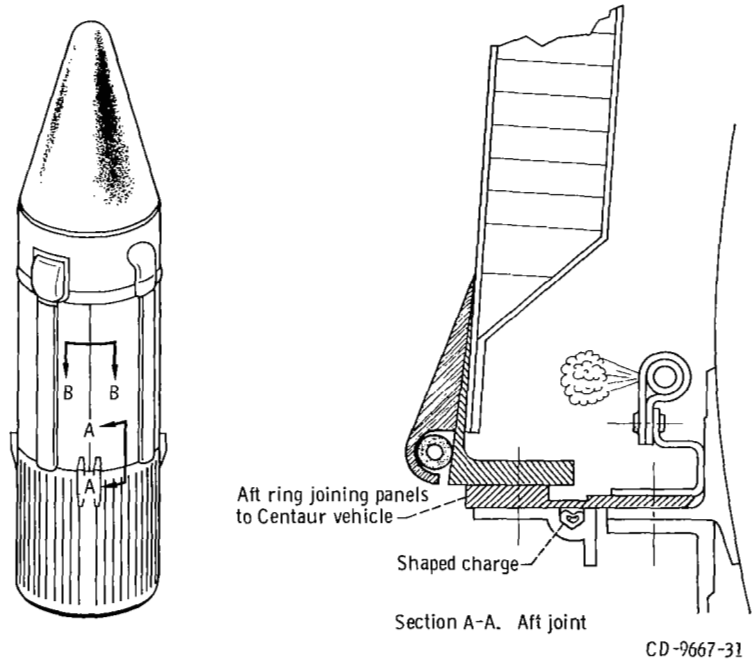

Figure VI-56. - Hydrogen tank insulation panels and separation system, AC-20 and AC-19.

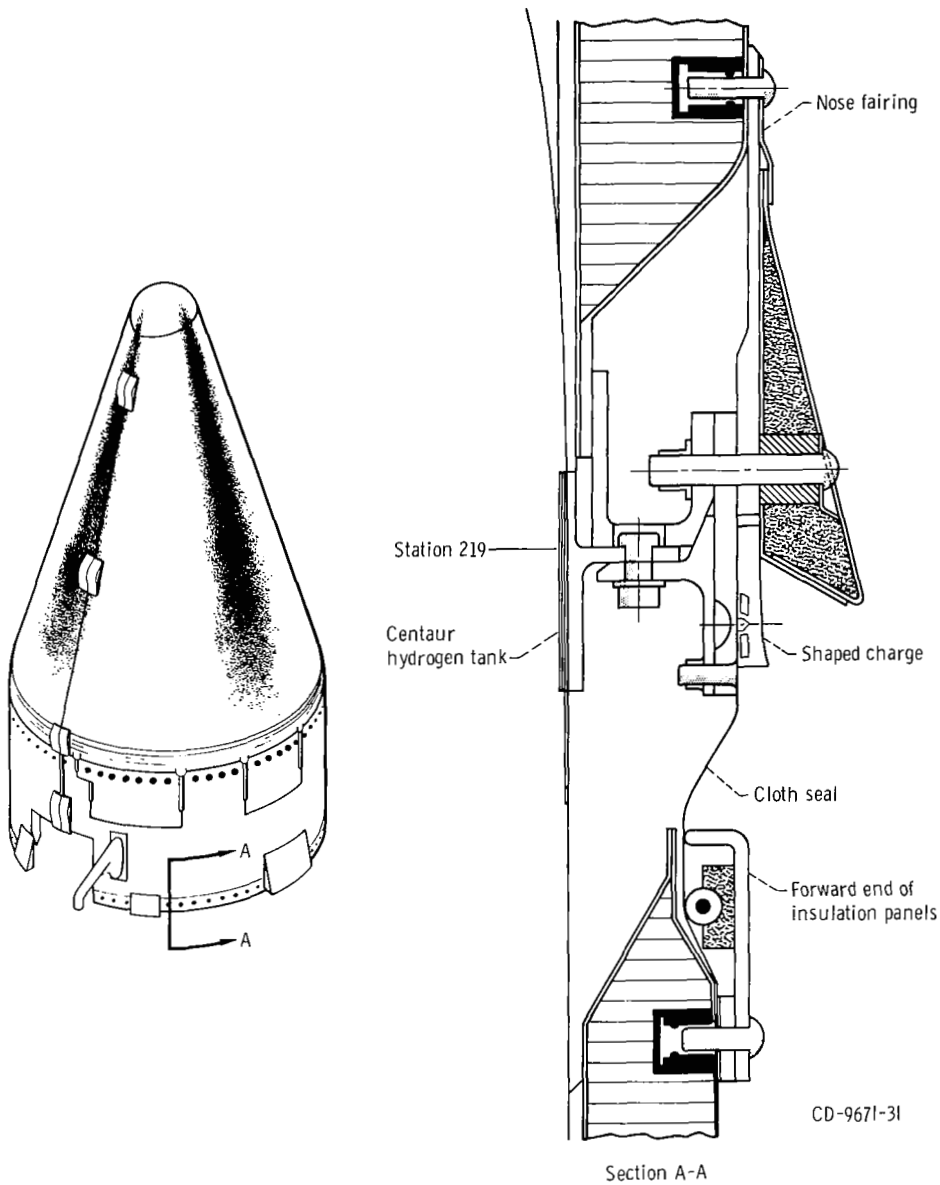

Figure VI-57. - Nose fairing aft separation system, AC-20 and AC-19.

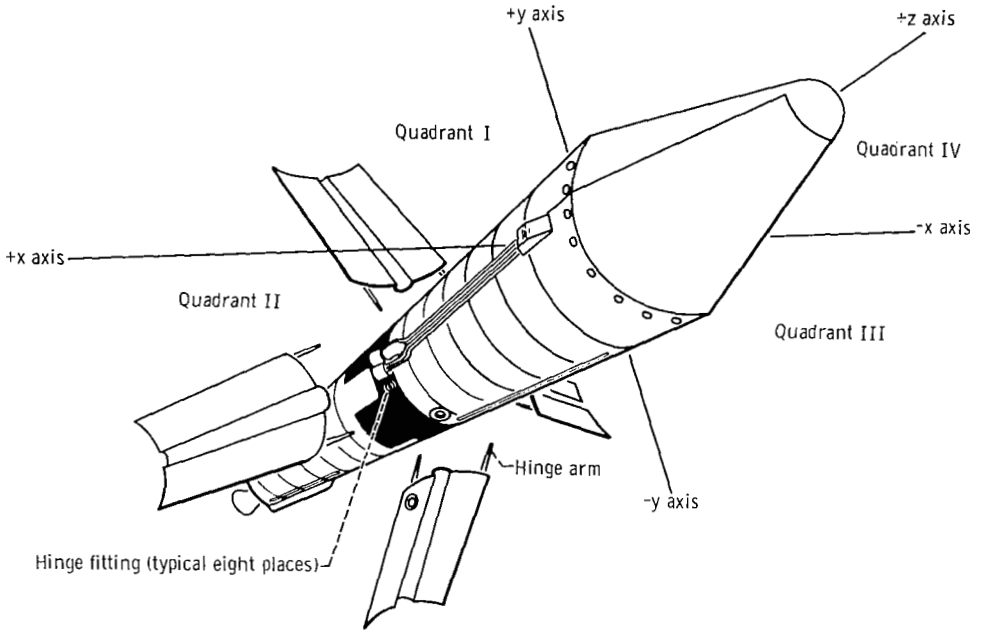

Figure VI-58. - Hydrogen tank insulation panel jettison system, AC-20 and AC-19.

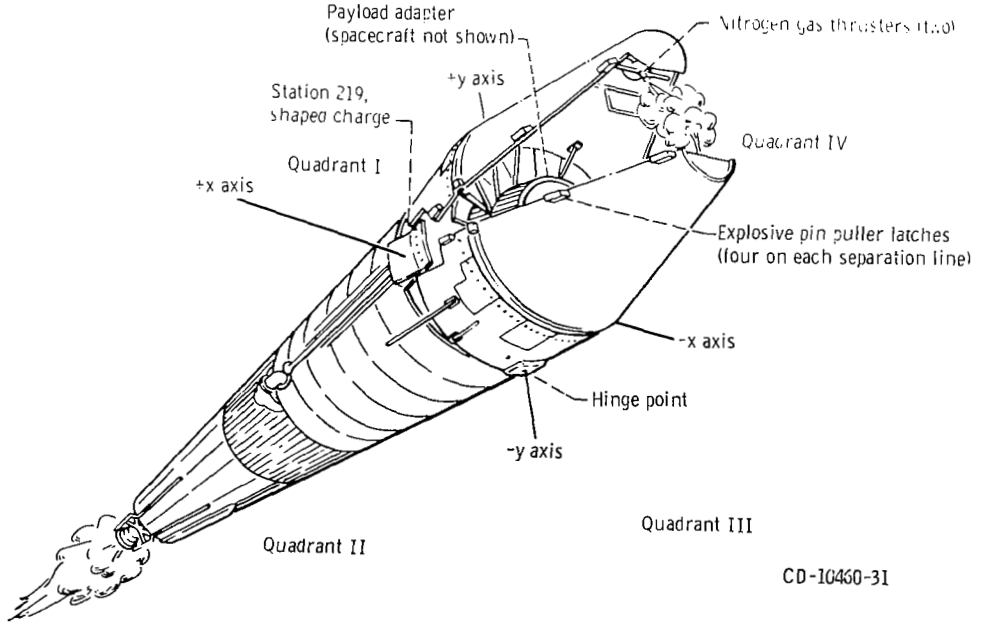

Figure VI-59. - Nose fairing jettison system, AC-20 and AC-19.

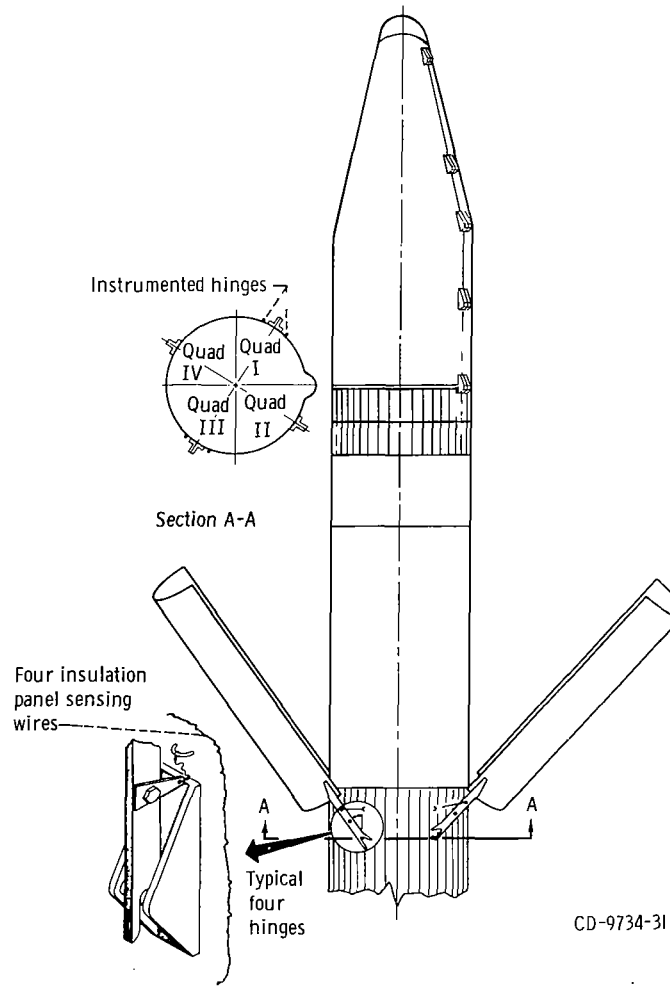

Figure VI-60. - Insulation and breakwire locations, AC-20 and AC-19.

ELECTRICAL SYSTEMS

by John B. Nechvatal and John M. Bulloch

Power Sources and Distribution

System description - Atlas. - The Atlas electrical system (fig. VI-61) consists of a power changeover switch, a main battery, and a three-phase 400-hertz rotary inverter. It also includes (not shown) two independent range safety command (vehicle destruct) batteries and a telemetry battery.

System performance - Atlas. - On AC-20 and AC-19 the transfer of the Atlas electrical load from external to internal power was accomplished by the main power changeover switch at T - 2 minutes. Performance of the Atlas electrical system was normal throughout each flight. Voltages and current levels furnished to the dependent systems were within specification limits.

On both vehicles the Atlas main battery supplied the requirements of the user systems at normal levels (25 to 30 V). The telemetry battery and the two range safety command batteries also provided normal levels throughout Atlas flight. The voltages at lift-off are shown in table VI-X. Although voltages were not monitored during flight, telemetered information on pyrotechnic systems, range safety receiver operation, booster and sustainer cutoffs, etc., indicated that all systems performed as planned. No deviations were observed in the electric power system performance.

On AC-20 and AC-19 the Atlas rotary inverter supplied 400-hertz power within specified voltages and frequency limits. Phase voltages monitored throughout each flight remained almost steady with a decrease in voltage of less than 1/2 volt in the time from lift-off to Atlas/Centaur separation. On both flights the frequency of the inverter drifted slightly upward from the value at lift-off (see table VI-XI). The gradual rise in frequency is typical of the Atlas inverter. The required frequency difference of 1.3 to 3.7 hertz between the Atlas and Centaur inverter frequencies was properly maintained on both vehicles. Operation in this range prohibits the possibility of generating undesirable beat frequencies within the flight control system, thereby precluding the chance of resonant excitation of propellant slosh modes or natural frequencies of the vehicle structure.

System description - Centaur. - The Centaur electric power system (fig. VI-62) consists of a power changeover switch, a main battery, two independent range safety command (vehicle destruct) batteries, two pyrotechnic system batteries, and a solid-state inverter supplying 400-hertz current to the guidance, flight control, and propellant utilization systems.

System performance - Centaur. - Performance of the Centaur electrical system was satisfactory throughout each flight. Transfer of the Centaur electrical load from external

power to the internal battery was accomplished at T - 4 minutes by the power changeover switch in 250 milliseconds (specification value, 2.00 sec max.). The maximum voltage excursion at power transfer was 0.5 volt, which is considered negligible.

The Centaur electric system voltages and currents measured at lift-off were normal and satisfactorily supplied power to all loads throughout the AC-20 and AC-19 flights (see table VI-X).

The main battery load profile was normal for each flight and compared closely with values recorded during preflight tests. Main battery current values observed at significant events are presented in table VI-XII.

The Centaur solid-state inverter, powered by the main battery, supplied stable 400-hertz power for the guidance, flight control, and propellant utilization systems. Telemetered voltage levels were normal and compared closely with values obtained during preflight testing. Voltage levels increased slightly during flight, a characteristic of the Centaur inverter. Table VI-XI summarizes the inverter performance in flight for both flights.

Proper operation of the pyrotechnic subsystem for AC-20 and AC-19 was verified by the successful jettison of the insulation panels and nose fairing.

Performance of the range safety command (vehicle destruct) subsystem batteries was satisfactory, as verified by telemetered data of the two receivers during each launch and each flight.

Short-duration current demands were noted on the recorded battery current profile. These current pulses were caused by the spacecraft separation squib bridgewires shorting to ground following squib firing. Bridgewires may short after squib firing; therefore, thermal relays are so designed to remove the short-circuit loads in approximately 150 to 200 milliseconds, depending on the current demand. Figures VI-63 and VI-64 show the current demands and the removal of these loads by the thermal relays. Figure VI-65 is the schematic diagram of the pyrotechnic circuits used for AC-20 and AC-19.

Tracking System

System description. - A C-band radar subsystem with associated ground stations provides position and velocity data to the range safety tracking system. These data are also used for guidance and flight trajectory data analysis. The airborne equipment includes a lightweight transponder, a circulator (to channelize receiving and sending signals), a power divider, and two antennas located on opposite sides of the propellant tank. The ground and ship stations use standard radar equipment and are located as shown in figures VI-66 and VI-67 for AC-20 and AC-19, respectively. A block diagram of the

AC-20 and AC-19 C-band systems is shown in figure VI-68. The locations of the C-band antennas are shown in figure VI-69.

System performance. - AC-20 C-band radar coverage was obtained until T + 5425 seconds, as shown in figure VI-70. Cape Kennedy, Merritt Island, Grand Bahama Island, Bermuda, and Antigua provided coverage during Atlas-Centaur powered flight. Bermuda, Antigua, Ascension, and Pretoria provided data for near-real-time orbit calculation. Ascension and Pretoria tracking data were prime in determining the postdeflection orbit. Antigua reported two periods of beacon frequency shifts of +3 megacycles; however, these shifts did not interfere with the tracking system performance. Antigua, Twin Falls (ship), and Grand Turk recorded a 15-decibel decrease in signal strength at T + 903 seconds. Grand Turk lost track at T + 904 seconds. Antigua and the Twin Falls recorded an increase of 15 decibels at T + 917 seconds and a decrease of 15 decibels at T + 967 seconds. The Antigua and Twin Falls tracking data quality was poor between T + 903 and T + 917 seconds and after T + 967 seconds.

AC-19 C-band radar coverage was obtained up to T + 5513 seconds, as shown in figure VI-71. Cape Kennedy, Merritt Island, Patrick Air Force Base, Grand Bahama Island, Bermuda, Antigua, Ascension, and Pretoria radar provided data for near-real-time orbit calculations. Pretoria provided excellent tracking data and was prime in the computation of the postdeflection orbit. The ground station at Ascension experienced problems with the ground equipment for the FPQ-6 radar and with low signal strength for the FPQ-16 radar. Grand Turk, Bermuda, and Antigua experienced a 15-decibel reduction in signal strength at T + 759 seconds, which resulted in low-quality tracking data.

Range Safety Command System

System description. - The Atlas and Centaur stages each contain independent vehicle destruct systems. These systems were designed to function simultaneously upon command from the ground stations. Each system included redundant receivers, power control units, destructor, antennas, and batteries. The batteries for these systems operate independently of the main vehicle power system. The location of the Centaur range safety antennas is shown in figure VI-69. Block diagrams of the Atlas and Centaur range safety command systems are shown in figures VI-72 and VI-73, respectively.

The Atlas and Centaur vehicle destruct system has the capability of shutting down the engines only or shutting down the engines and destroying the vehicle if it had left the safe flight corridor. The destruct system consists of an explosive charge which ruptures the propellant tanks and allows the liquid propellants of the Atlas and Centaur stages to disperse.

System performance. - The Atlas and Centaur range safety command systems were

prepared to execute destruct commands throughout the flight. The command from the Antigua ground station to disable the Centaur range safety command system shortly after Centaur main engine cutoff was properly received and executed. Figures VI-74 and VI-75 depict ground transmitter coverage to support the vehicle destruct systems for AC-20 and AC-19, respectively.

Signal strength at the Atlas and Centaur range safety command receivers was satisfactory throughout the AC-20 and AC-19 flights, as indicated by telemetry measurements.

Instrumentation and Telemetry

System description - Atlas. - The Atlas telemetry system (fig. VI-76) consists of a radiofrequency telemetery package, two antennas, a telemetry battery and transducers. It is a pulse amplitude modulation/frequency modulation/frequency modulation (PAM/FM/FM) telemetry system and operates at a carrier frequency of 229.0 megahertz. The PAM technique used on all Atlas-Centaur commutated (sampled) channels makes possible a larger number of measurements on one subcarrier channel. This increases the data handling capability of the telemetry system. The FM/FM technique uses analog values from transducers to frequency modulate the subcarrier oscillators which, in turn, frequency modulate the main carrier (radiofrequency link).

System performance - Atlas. - The telemetry coverage for the Atlas portion of the flight (see figs. VI-77 and VI-78 for AC-20 and AC-19, respectively) extended well beyond Atlas/Centaur separation and met all telemetry coverage requirements. Station locations for AC-20 and AC-19 are shown in figures VI-66 and VI-67, respectively.

The 106 Atlas operational measurements (table VI-XIII) made on AC-20 all provided useful data, except that the following three measurements showed unexpected outputs:

(1) The angle-of-attack calibration measurement (CA475P) failed to provide valid data between T + 60 and T + 106 seconds, the period of maximum interest. Data during this period were characterized by steep slope changes and spurious level fluctuations. The cause of the unsatisfactory data period has not been determined.

(2) The sustainer fuel pump discharge pressure measurement (AP330P) failed at T + 16 seconds. This failure was characteristic of a frozen transducer sensing line.

(3) The sustainer fuel pump inlet pressure measurement (AP55P) failed at T + 255 seconds. This failure was characteristic of a frozen transducer sensing line.

The 106 Atlas operational measurements (table VI-XIII) made on AC-19 all provided useful data, except that the following two measurements showed unexpected outputs:

(1) The nose cap angle-of-attack calibration measurement (CA475P) indicated a 20- to 30-percent data level attenuation throughout the flight.

(2) The sustainer pitch position measurement (AS275D) exhibited an approximately 7-percent information bandwidth (IBW) step decrease in the bias level at lift-off. The cause of this shift is unknown, but is believed to be slippage of the gimbal block shaft within the clamping arrangement between the transducer and the gimbal shaft. No data were lost because of this shift.

System description - Centaur. - The Centaur telemetry system (fig. VI-79) consists of two radiofrequency telemeter packages, one antenna (fig. VI-69), and transducers. It is a PAM/FM/FM system which operates at frequencies of 225.7 and 259.7 megahertz for radiofrequency telemetry package 1 (RF1) and radiofrequency telemetry package 2 (RF2), respectively. Telemetry package RF1 was used for vehicle operational measurements; and RF2 was installed in order to define (1) payload adapter vibration, (2) spacecraft vibration environment, (3) spacecraft compartment environment, and (4) spacecraft separation initiation.

System performance - Centaur. - The telemetry coverage for AC-20 was satisfactory (see fig. VI-80). The station locations for AC-20 are shown in figure VI-66. The ground station at Bermuda did not record RF1 because of an interferring signal from the Bermuda radar. Varying signal strengths were experienced at the Bermuda, Antigua, and Ascension stations, as well as by the Twin Falls tracking ship. However, the only data degraded was that received at Ascension and by the Twin Falls.

Of the total of 156 measurements (table VI-XIV) that were made on AC-20, the following four measurements showed unexpected outputs:

(1) The high-frequency accelerometers 2 (CY125O) and 3 (CY126O) located on the spacecraft exhibited low-frequency trapezoidal wave shapes not representative of data at lift-off and at booster engine cutoff. A review of ground test data by the spacecraft manufacturer indicated that similar data characteristics occurred during vibration testing of the proof-test vehicle. Valid data were obtained during the entire flight at frequencies of over 100 hertz.

(2) The Centaur C-1 engine fuel pump temperature measurement (CP122T) exhibited a slow response to change in temperature. The cause of this anomaly is unknown.

(3) The propellant retention engine (S3 engine) chamber surface temperature measurement (CP692T) was erroneously installed on the propellant settling engine (V engine) chamber.

The telemetry coverage for AC-19 was satisfactory (see fig. VI-81). The station locations for AC-19 are shown in figure VI-69. Antigua ground station signal strength was satisfactory until approximately T + 1090 seconds. At this time the signal began to vary rapidly and the data were degraded thereafter. Ascension and the Twin Falls stations reported similar conditions that began at T + 881 and T + 992, respectively.

Of the 156 measurements (table VI-XIV) made on AC-19, the following four measurements showed unexpected outputs:

(1) The Centaur C-2 engine chamber jacket temperature measurement (CP98T) indicated unrealistic values and erratic behavior during Centaur main engine firing and after main engine cutoff. The exact cause of these characteristics is unknown; however, it is believed the transducer lost surface contact with the thrust chamber jacket and was actually measuring the temperature just above the surface rather than on the surface. No valid data were obtained from this measurement during the period of interest.

(2) The high-frequency accelerometers 2 and 3 located on the spacecraft exhibited identical low-frequency trapezoidal wave shapes not representative of data at lift-off and at booster engine cutoff. Similar shifts were observed on the AC-20 flight, as previously discussed.

(3) The Centaur C-2 engine fuel pump temperature measurement (CP123T) exhibited a slow response to temperature changes. The cause of this anomaly is unknown.

(4) The Centaur C-1 engine thrust chamber jacket temperature measurement (CP63T) exhibited a slow response to temperature changes. The cause of the erroneous data is caused by poor bonding of the instrument to the thrust chamber jacket. A better bonding material will be used on future vehicles.

(5) The propellant retention engine (S3 engine) chamber surface temperature measurement (CP692T) was erroneously installed on the propellant settling engine (V engine) chamber.

TABLE VI-X. - ELECTRICAL DATA AT LIFT-OFF, AC-20 AND AC-19

(a) Atlas

Component	AC-20	AC-19
Main battery, V	27.35	27.30
Telemetry battery, V	28.60	28.30
Range safety command battery 1, V	29.50	29.20
Range safety command battery 2, V	29.70	29.20

(b) Centaur

Main battery, A	43.20	43.50
Main battery, V	28.20	28.27
Range safety command battery 1, V	32.60	32.40
Range safety command battery 2, V	32.60	32.40
Pyrotechnic battery 1, V	35.10	34.95
Pyrotechnic battery 2, V	35.08	35.00

TABLE VI-XI. - INVERTER PERFORMANCE,

AC-20 AND AC-19

(a) Atlas

Measurement	AC-20		AC-19	
	At lift-off	Drift from lift-off value during programmed flight, Δ	At lift-off	Drift from lift-off value during programmed flight, Δ
Phase A, V	114.5	-0.4	115.3	-0.4
Phase B, V	116.2	-0.3	115.8	-0.5
Phase C, V	116.2	-0.4	116.1	-0.5
Frequency, Hz	401.9	+0.9	402.0	+0.6

(b) Centaur

Phase A, V	116.0	+0.2	115.8	+0.5
Phase B, V	116.1	+0.2	115.2	+0.4
Phase C, V	114.9	+0.3	115.0	-0.4
Frequency, Hz	400.0	0.0	400.0	0.0
Temperature:				
K	303	+22.5	303.2	+19.8
^{o}F	86.0	+40.5	86.2	+35.8

TABLE VI-XII. - CENTAUR MAIN BATTERY CURRENT PROFILE,

AC-20 AND AC-19

Event	Current, A	
	AC-20	AC-19
Preload	13.5	13.5
Changeover, external power to battery	42.5	43.0
Lock liquid-hydrogen vent valve	44.0	44.5
Eject Centaur umbilicals	43.2	43.5
Lift-off (T - 0)	43.2	43.5
Unlock liquid-hydrogen vent valve	41.5	42.0
Lock liquid-hydrogen vent valve	43.0	43.8
Unlock liquid-hydrogen vent valve	41.5	42.0
Start boost pumps, lock liquid-oxygen vent valve, and pressurize liquid-oxygen tank	45.5	45.5
End liquid-oxygen tank pressurization	44.5	44.8
Lock liquid-hydrogen vent valve, start timer and pressurize liquid-hydrogen tank	47.0	48.0
Hydraulic circulating pumps on	52.3	53.0
Liquid-hydrogen tank pressurization off	51.5	52.0
Engine prestart valves on	54.0	55.0
Main engine start valve on, igniters on, and liquid-oxygen tank pressurization off	60.3	61.0
Hydraulic circulating pumps off and igniters off	51.2	51.8
Unnull propellant utilization system	51.0/51.5	51.2/51.8
Stop timer	51.0/51.5	51.0/51.5
Null propellant utilization system	51.2/50.0	51.2/50
Main engine start valves and prestart valves off, start timer, boost pumps off, and pressurize liquid-oxygen tank	45.0	45.0
Liquid-oxygen tank pressurization off	43.5	44.0
Spacecraft separation (see figs. VI-63 and VI-64)	65/50/60	68/46/56
Steady-state current following separation	43.5	44.0
Squib short to ground - not programmed (see fig. VI-64)	---------	56.0
Steady-state current after removal of short	---------	44.0
Vernier engines to half on	46.0	46.0
Vernier engines off	43.5	44.0
Hydraulic circulating pumps and prestart valves on	51.0	51.0
Stop timer	50.8/51.3	51.5
Steady-state current to battery depletion	51.0	51.0

TABLE VI-XIII. - ATLAS MEASUREMENT SUMMARY, AC-20 AND AC-19

System	Measurement type									
	Acceleration	Rotation rate	Displacement	Pressure	Frequency	Rate	Temperature	Voltage	Discretes	Totals
Airframe				3			2		4	9
Range safety								3	1	4
Electrical					1			4		5
Pneumatics				7			1			8
Hydraulics				6						6
Dynamics	1								2	3
Propulsion		3	3	18			6		6	36
Flight control			11			3		4	13	31
Propellants	1			2				1		4
Totals	2	3	14	36	1	3	9	12	26	106

TABLE VI-XIV. - CENTAUR MEASUREMENT SUMMARY, AC-20 AND AC-19

System	Measurement type												
	Acceleration	Rotation rate	Current	Displacement	Vibration	Pressure	Frequency	Rate	Temperature	Digital	Voltage	Discretes	Totals
Airframe	6			1					2			3	12
Range safety											2	3	5
Electrical			1				1		1		4		7
Pneumatics						5			3			2	10
Hydraulics						2			2				4
Guidance									1	1	16		18
Propulsion		4				12			28			10	54
Flight control								3			4	29	36
Propellant				2							2		4
Spacecraft					3	1	1		1				6
Totals	6	4	1	3	3	20	2	3	38	1	28	47	156

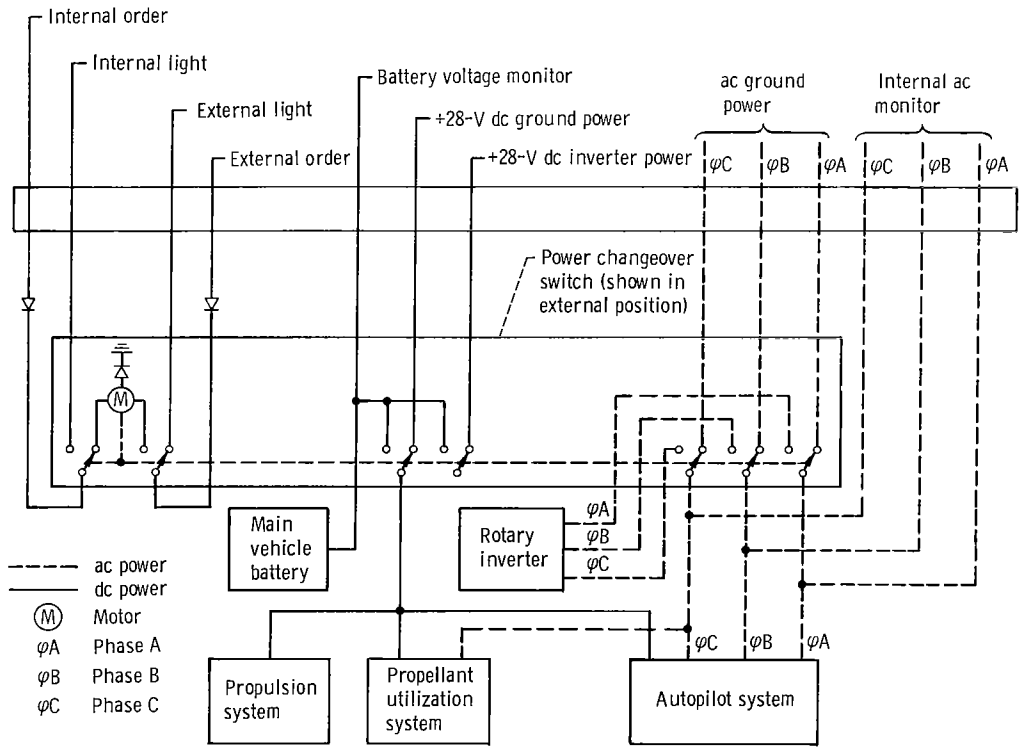

Figure VI-61. - Block diagram of Atlas electrical system, AC-20 and AC-19.

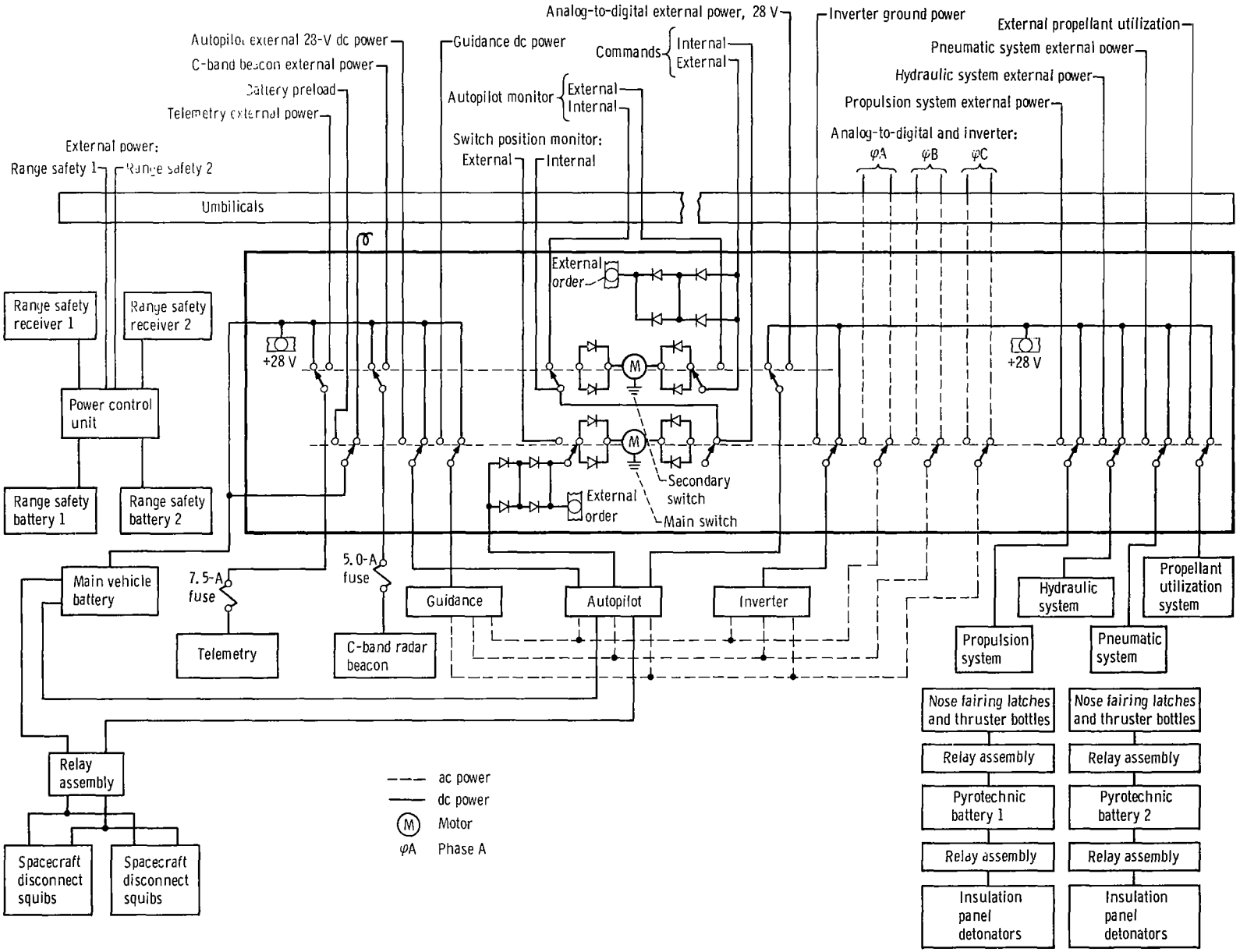

Figure VI-62. - Block diagram of Centaur electrical system, AC-20 and AC-19.

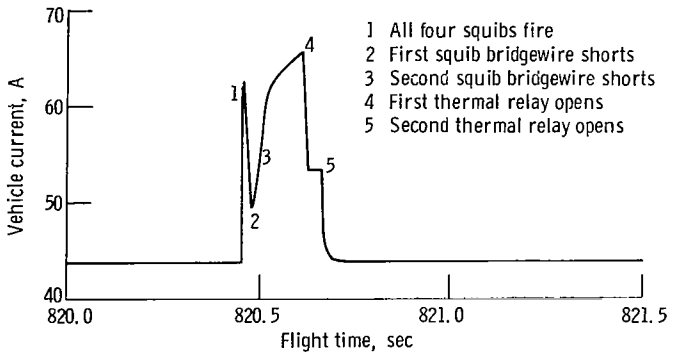

Figure VI-63. - Spacecraft squib firing current, AC-20.

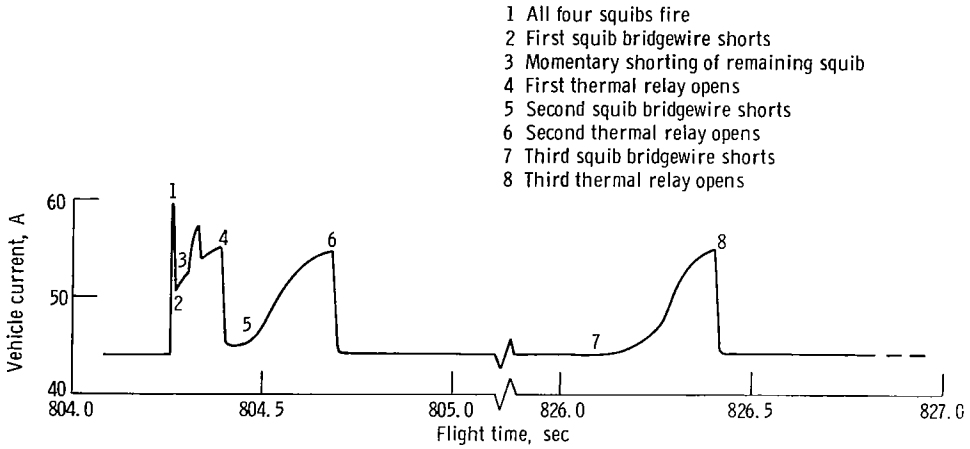

Figure VI-64. - Spacecraft squib firing current, AC-19.

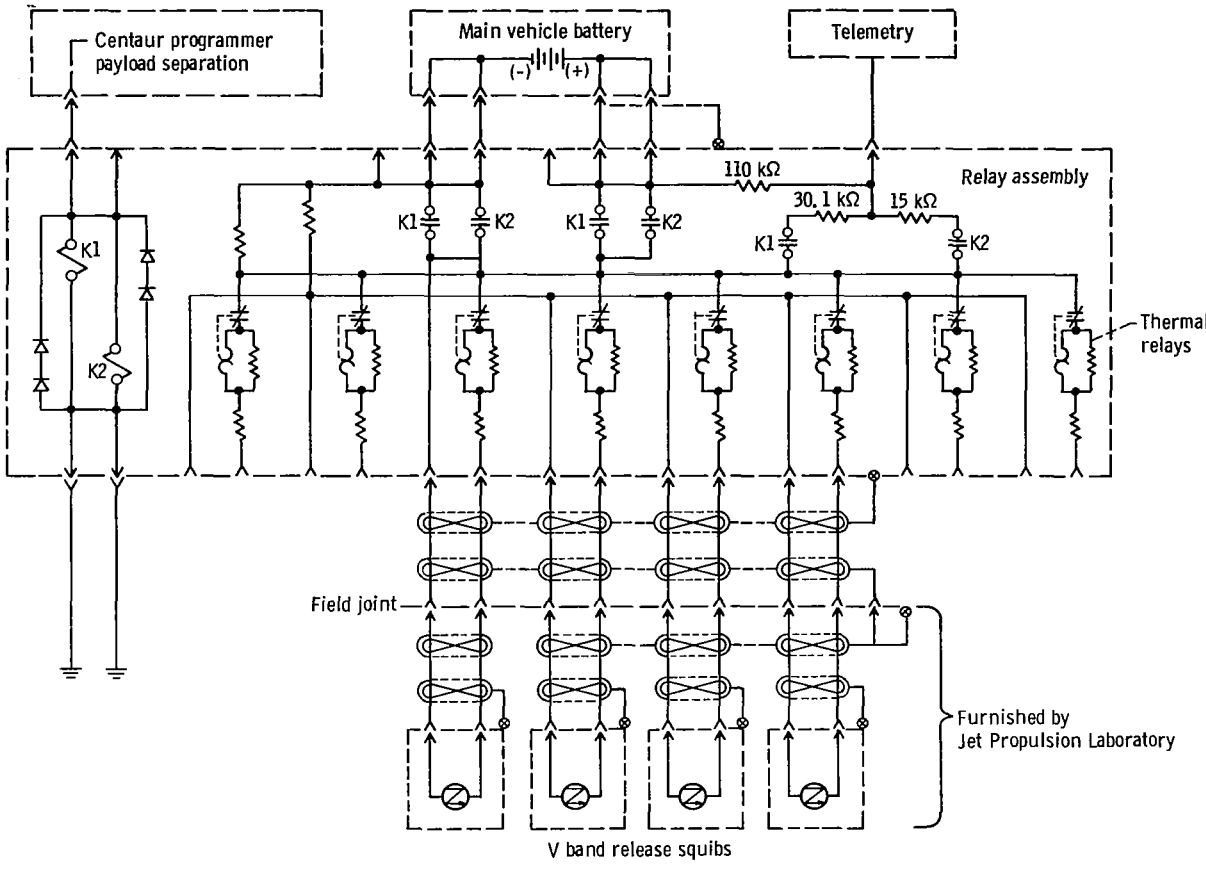

Figure VI-65. - Spacecraft pyrotechnic separation system, AC-20 and AC-19.

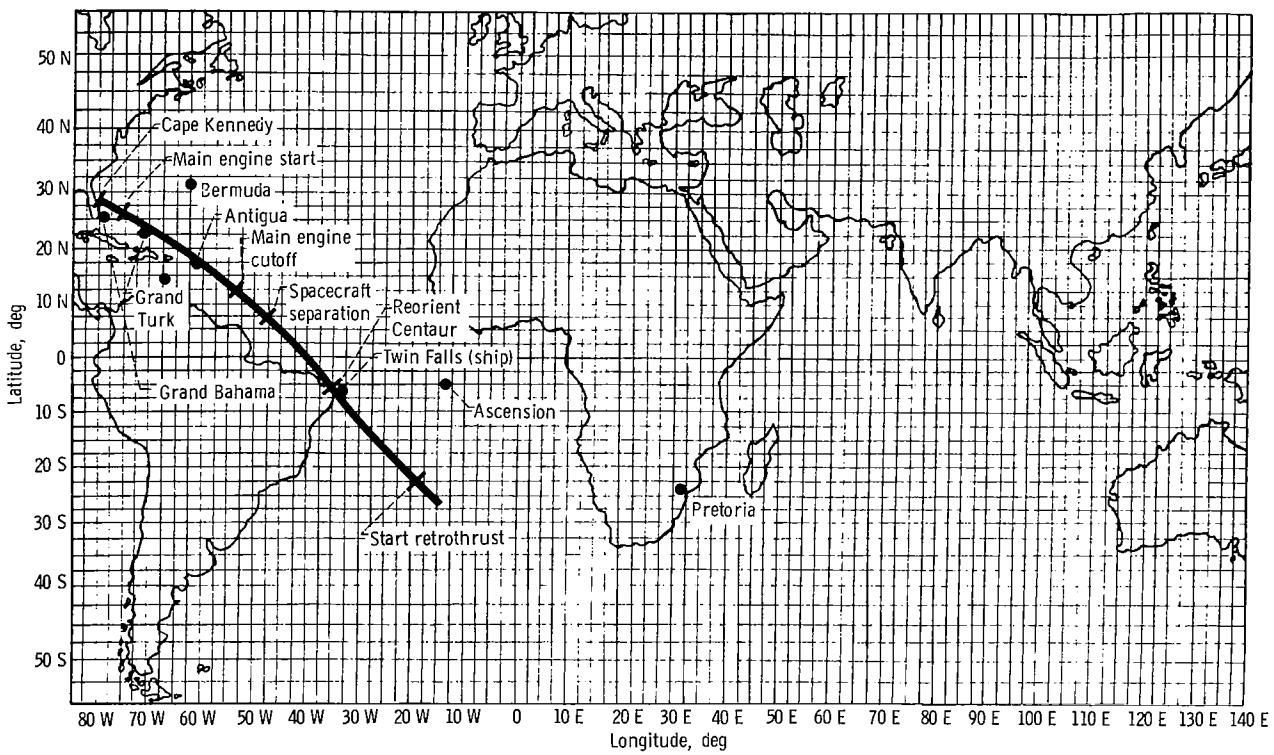

Figure VI-66. - Tracking station location and vehicle trajectory, Earth track, AC-20.

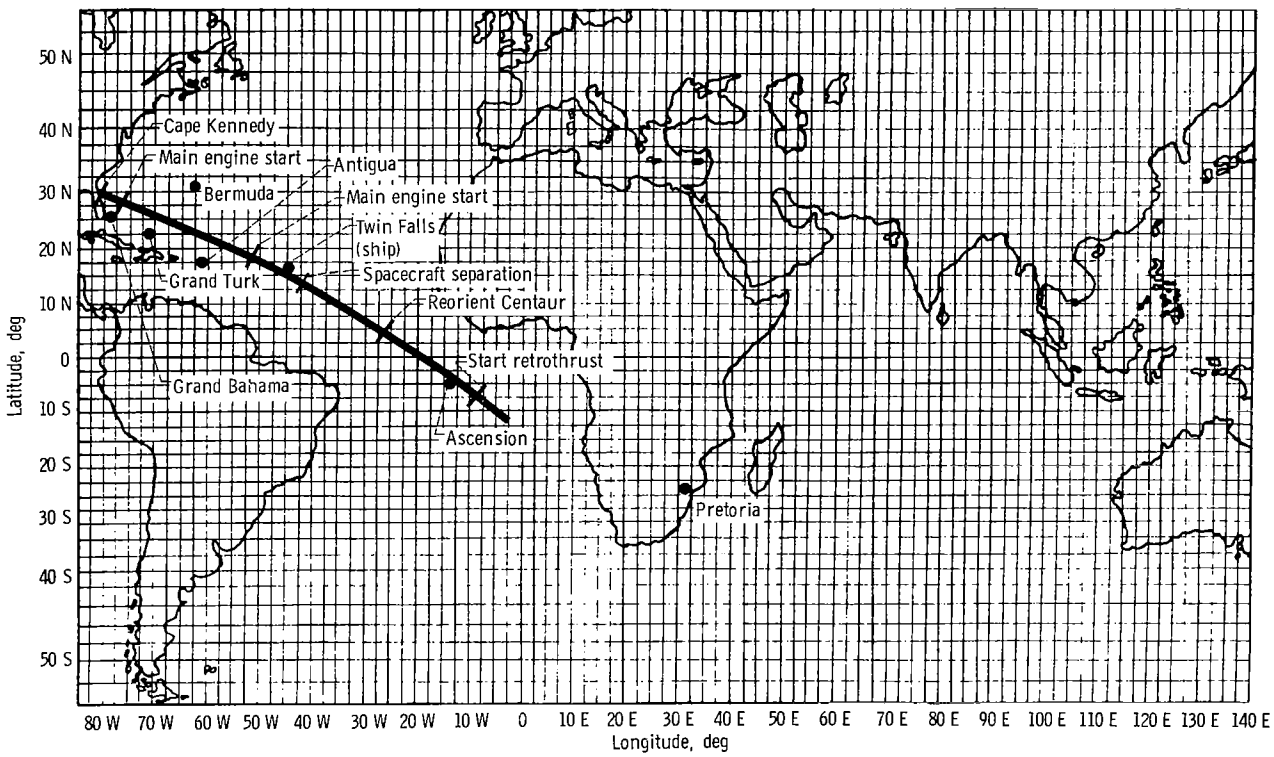

Figure VI-67. - Tracking station location and vehicle trajectory, Earth track, AC-19.

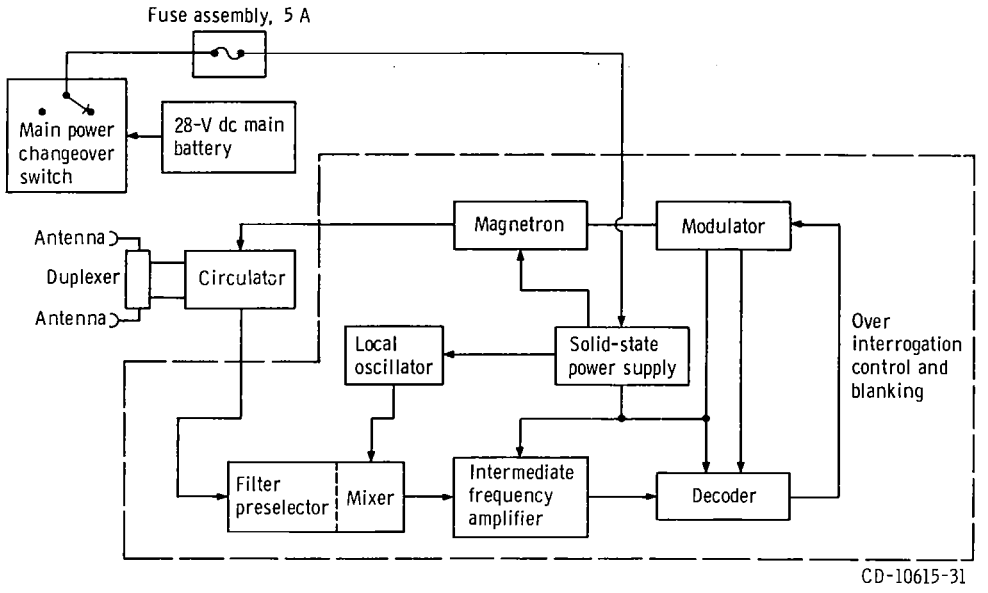

Figure VI-68. - Centaur C-band beacon subsystem, AC-20 and AC-19.

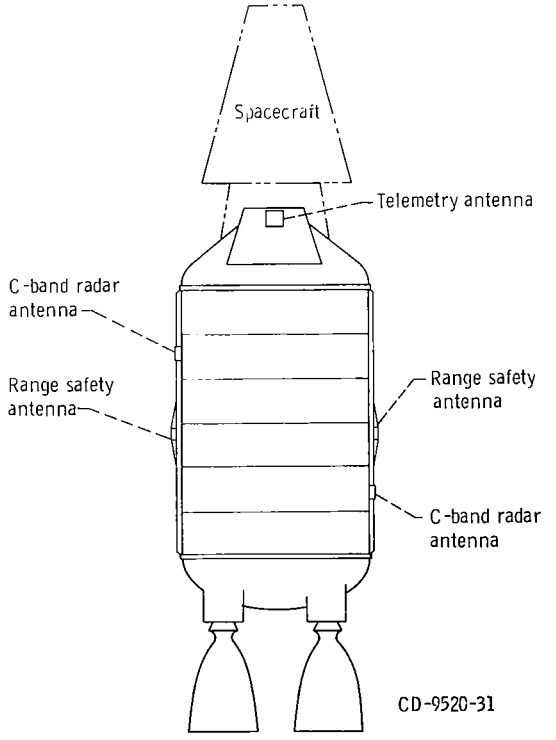

Figure VI-69. - Locations of Centaur antennas, AC-20 and AC-19.

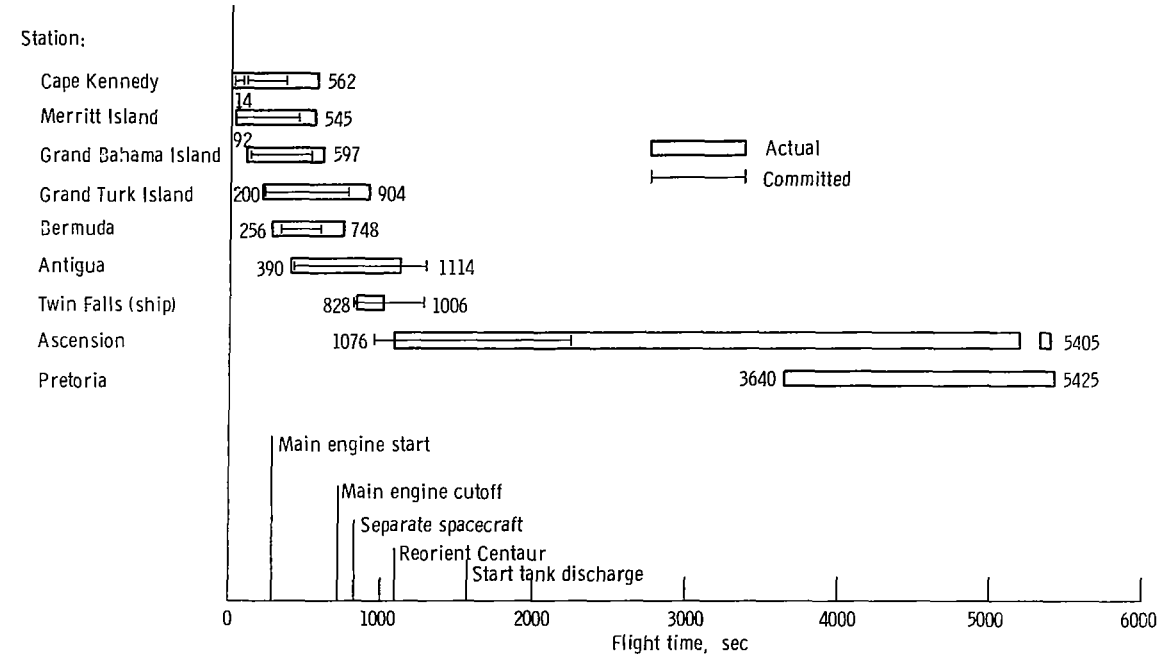

Figure VI-70. - C-band radar coverage, AC-20. Coverage shown is for autobeacon track only.

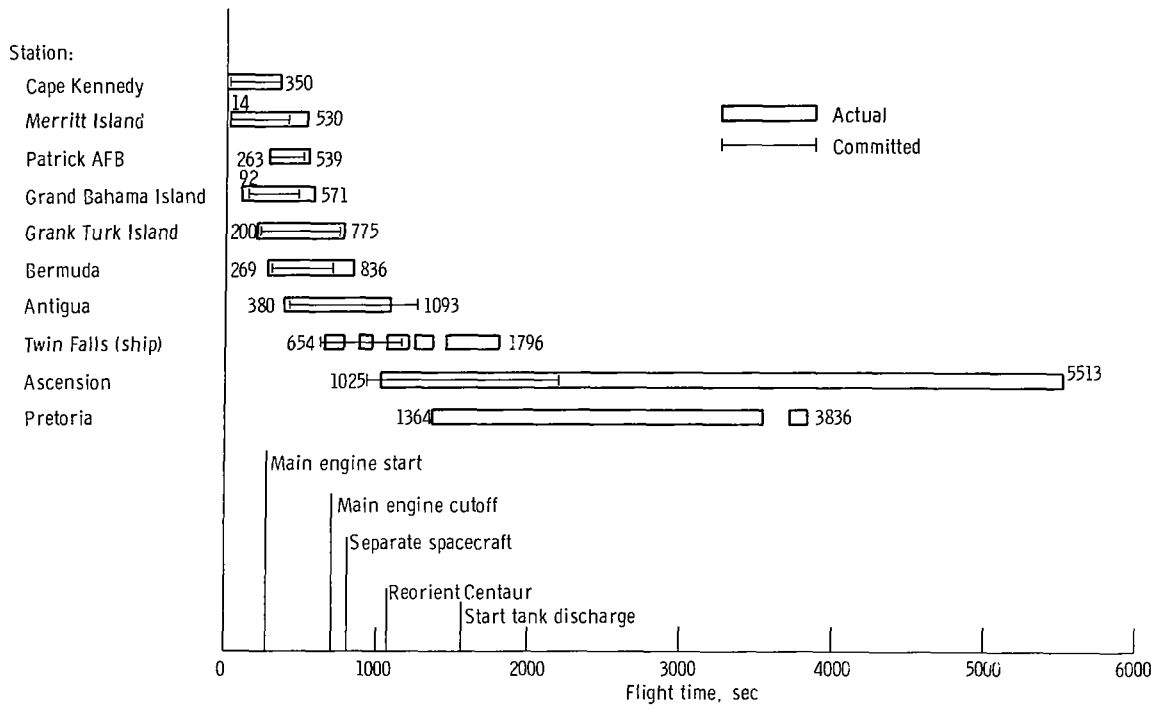

Figure VI-71. - C-band radar coverage, AC-19. Coverage shown is for autobeacon track only; many intermittent dropouts at Ascension due to ground equipment problems for the FPQ-6 radar and low signal strength for the FPQ-16 radar.

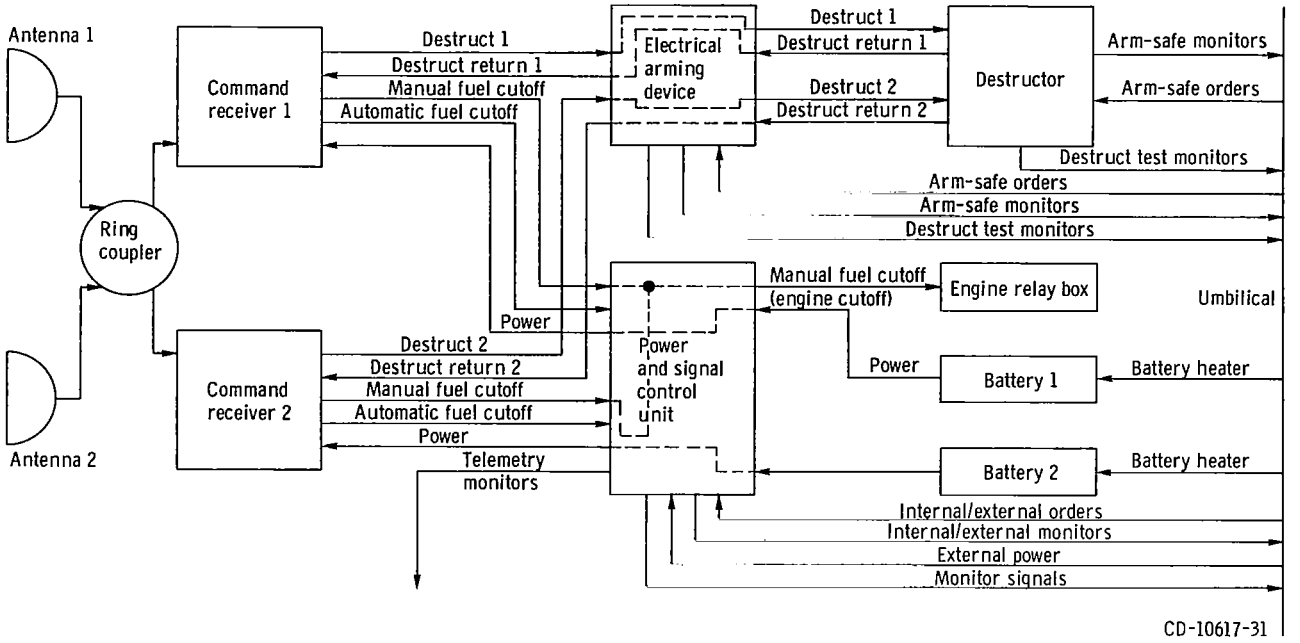

Figure VI-72. - Atlas vehicle destruct subsystem block diagram, AC-20 and AC-19.

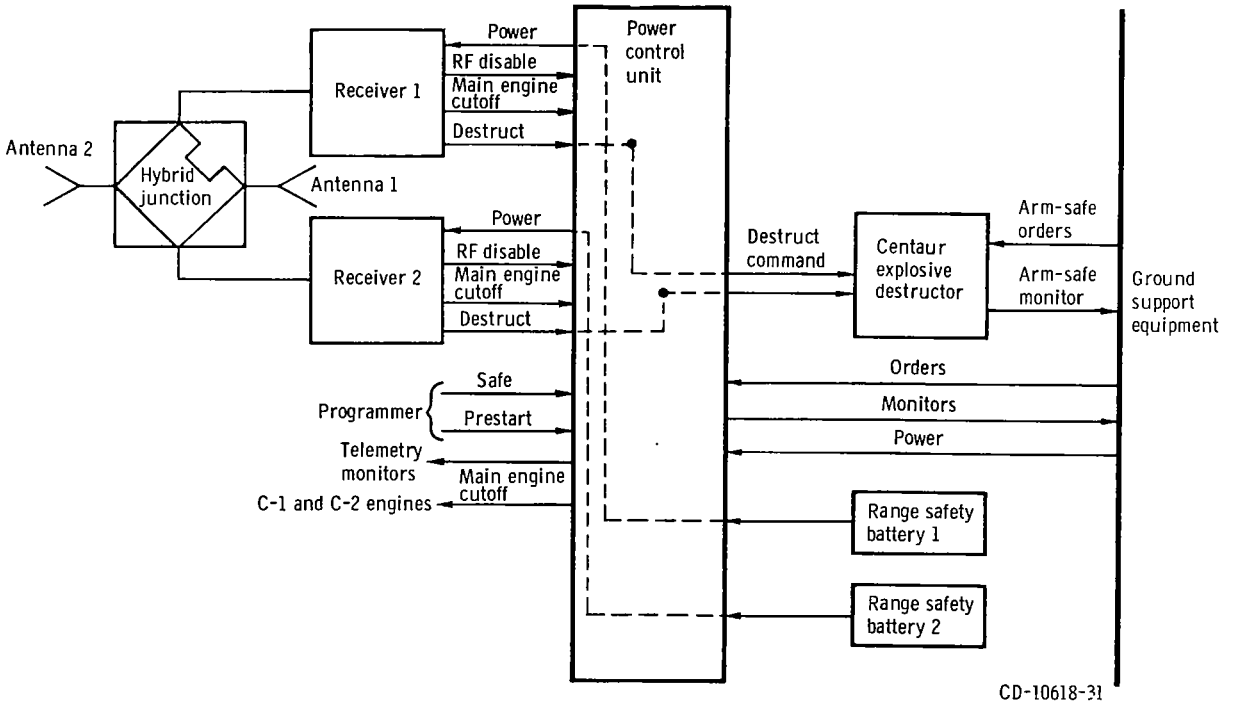

Figure VI-73. - Centaur vehicle destruct subsystem block diagram, AC-20 and AC-19.

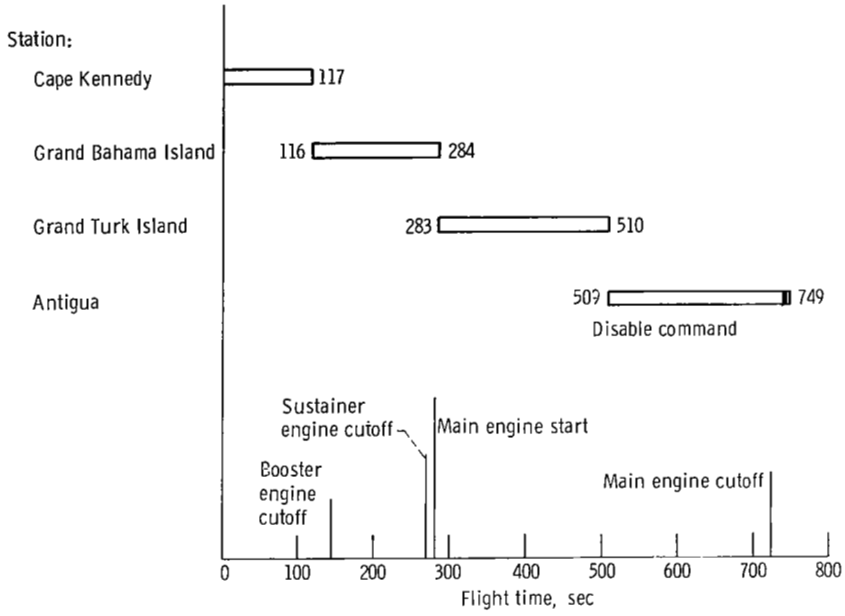

Figure VI-74. - Range safety command system transmitter coverage, AC-20.

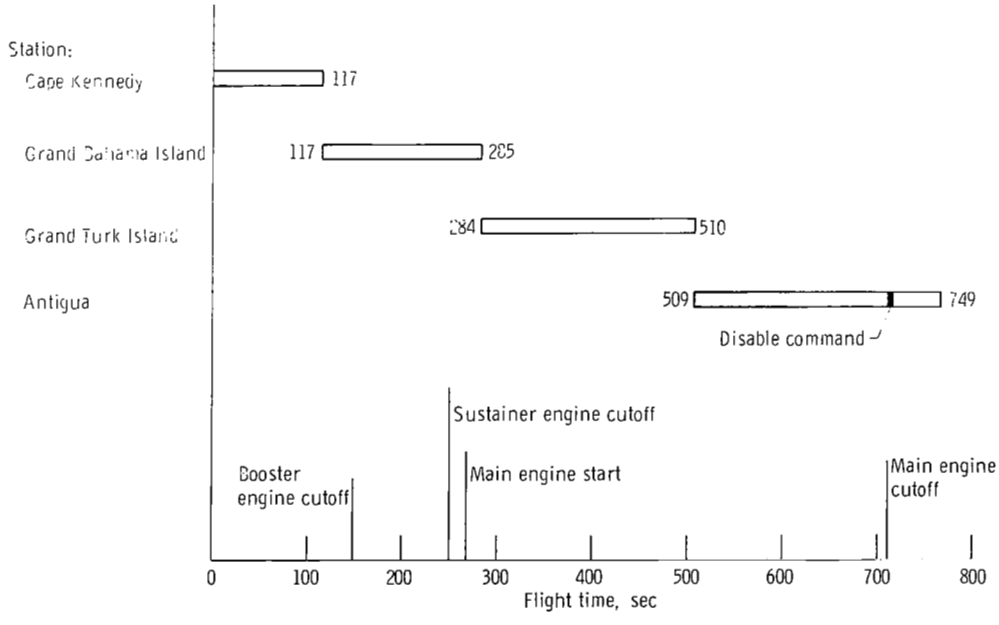

Figure VI-75. - Range safety command system transmitter coverage, AC-19.

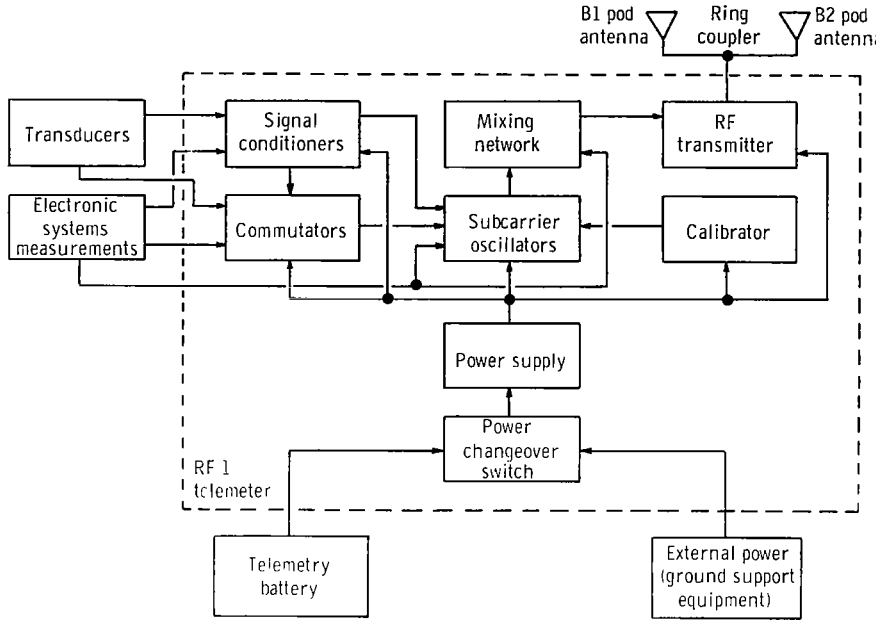

Figure VI-76. - Atlas telemetry system block diagram, AC-20 and AC-19.

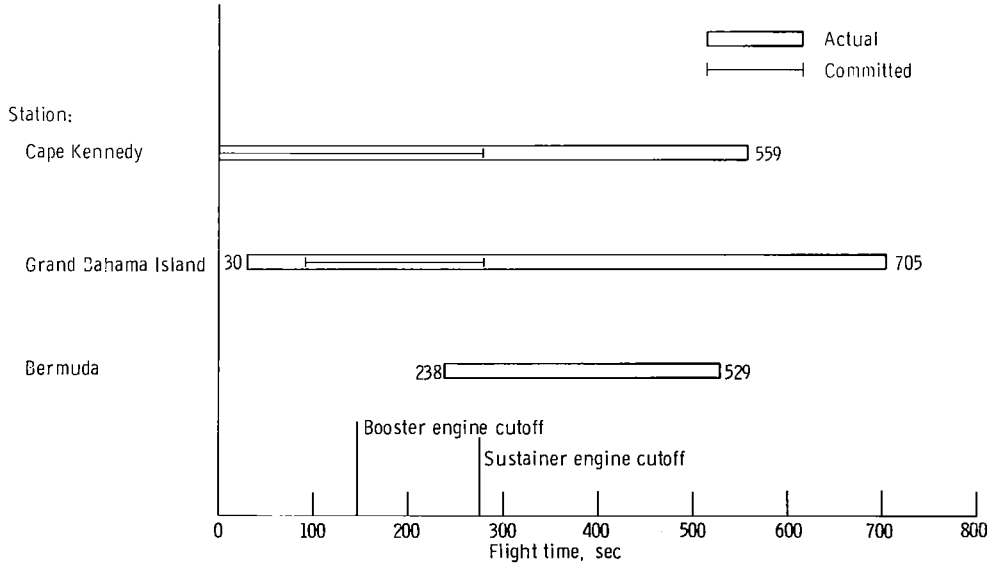

Figure VI-77. - Atlas telemetry coverage, AC-20.

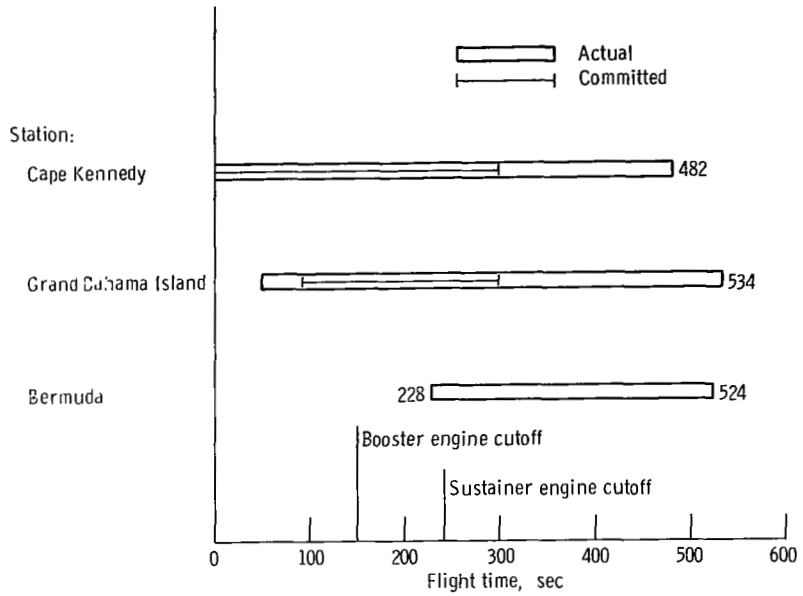

Figure VI-78. - Atlas telemetry coverage, AC-19.

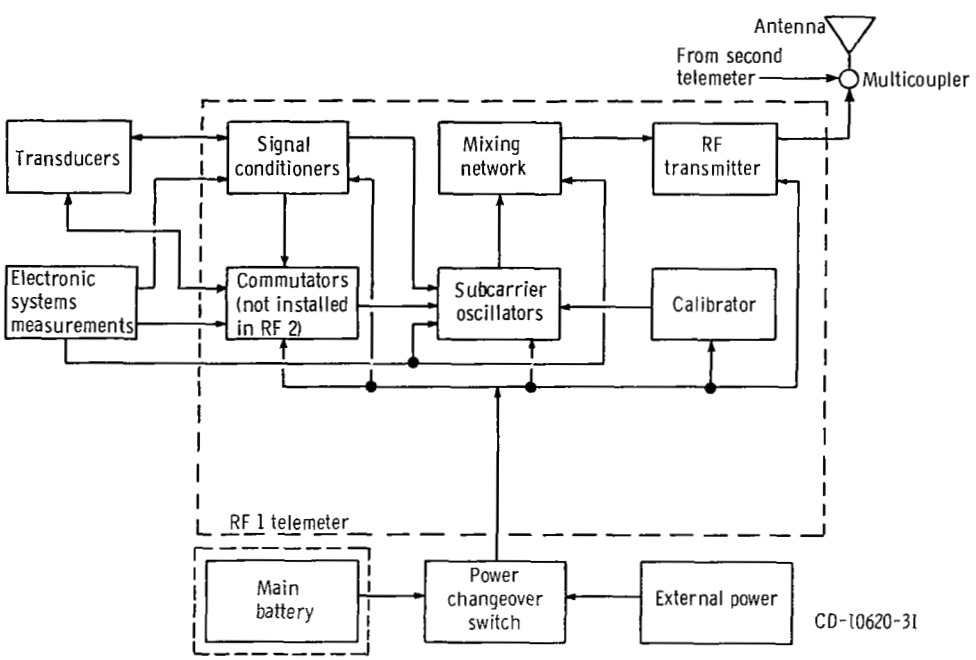

Figure VI-79. - Centaur telemetry system, typical both telemeters, AC-20 and AC-19.

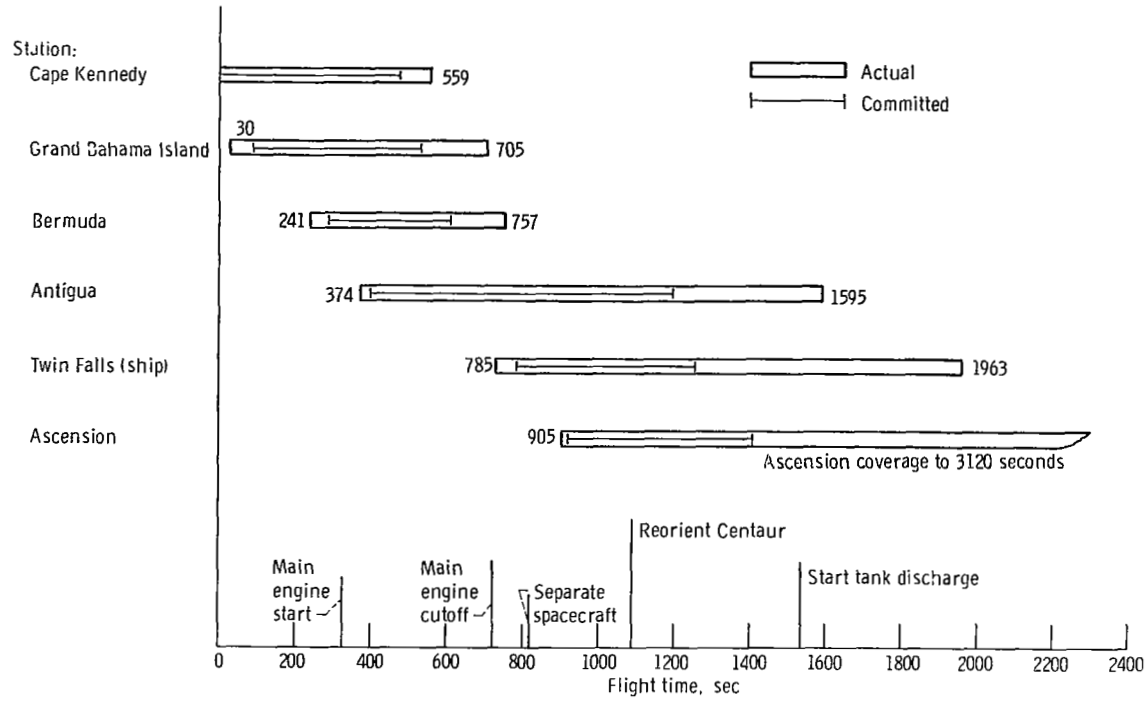

Figure VI-80. - Centaur telemetry coverage, AC-20.

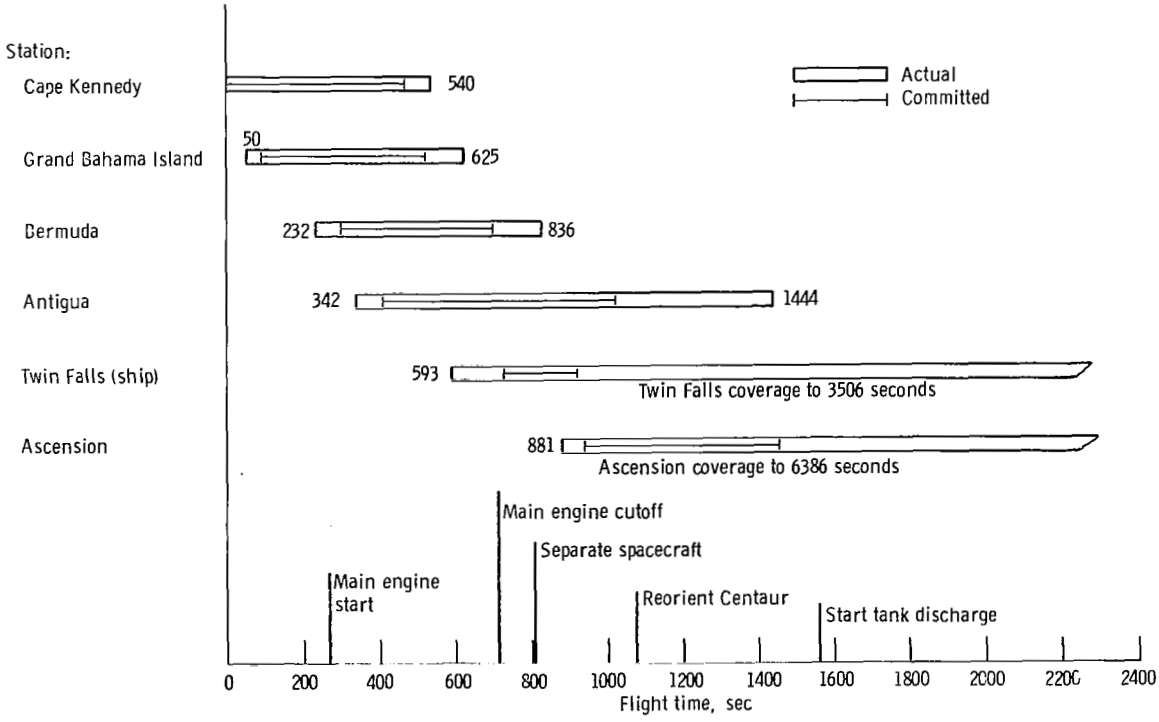

Figure VI-81. - Centaur telemetry coverage, AC-19.

GUIDANCE AND FLIGHT CONTROL SYSTEMS

by Larry Feagan, Corrine Rawlin, and Edmund Ziemba

The objectives of the guidance and flight control systems are to guide the launch vehicle to the orbit injection point and establish the vehicle velocity necessary to place the Mariner spacecraft in a Mars transfer orbit. To accomplish these objectives the flight control system provides vehicle stabilization and control while the guidance system steers the vehicle along the flightpath. The systems (guidance and flight control) also provide the sequence flight events of the launch vehicle. These functions are performed at specified time periods from vehicle lift-off through completion of the Centaur retromaneuver after spacecraft separation. An inertial guidance system is installed on the Centaur stage. Separate flight control systems are installed on the Atlas and Centaur stages. The guidance system, operating with the flight control systems, provides the capability to stabilize the vehicle and to compensate for trajectory dispersions resulting from thrust misalinement, winds, and vehicle performance variations.

Three modes of operation are used for stabilization, control, and guidance of the launch vehicle. These modes are "rate stabilization only," "rate stabilization and attitude control," and "rate stabilization and guidance control." Block diagrams of the three modes are shown in figure VI-82. The flight times during which a particular mode is used are shown in figure VI-83. Figure VI-83 also shows the modes of operation of the Centaur hydrogen peroxide attitude control system, which are discussed in this section.

The Atlas flight control system controls the Atlas-Centaur vehicle by gimbaling the Atlas booster, sustainer, and vernier engines to provide thrust vector control. The Centaur flight control system controls the Centaur by gimbaling the main engines to provide thrust vector control while the main engines are firing, or by commanding various combinations of the hydrogen peroxide attitude control engines on or off during coast periods, when the main engines are not firing.

The rate-stabilization-only mode stabilizes the roll axis of the Centaur stage continuously after Atlas/Centaur separation. This mode is also used to stabilize the pitch and yaw axes of the Centaur stage for 15.5 seconds following Atlas/Centaur separation. In this mode, output signals from rate gyros are used to control the vehicle. The output signal of each rate gyro is proportional to the angular rate of rotation of the vehicle about the input axis of the gyro. The vehicle angular rates are minimized by the flight control system to stabilize the vehicle. Rate stabilization is also combined with position (attitude) information in the other two modes of operation.

The rate-stabilization-and-attitude-control mode is used for pitch, yaw, and roll control during the Atlas booster phase of flight and for roll control only during the Atlas sustainer phase. This mode is termed "attitude control" since the displacement gyros

(one each for the pitch, yaw, and roll axes) provide a reference attitude to which the vehicle is to be alined. However, if the actual flightpath differs from the desired flightpath, there is no way of determining the difference and correcting the flightpath. The reference attitude is programmed to change during booster phase. These changes in reference attitude cause the vehicle to roll to the programmed flight azimuth angle and to pitch downward. Vehicle stabilization is accomplished in the same manner as in the rate-stabilization-only mode. The rate stabilization signals are algebraically summed with the attitude reference signals. The resultant signals are used to control and stabilize the vehicle.

The rate-stabilization-and-guidance-control mode is used for the pitch and yaw axes during Atlas sustainer phase, during Centaur main engine firing, and during the coast period following main engine cutoff. In this mode, the guidance system provides the attitude and direction reference. If the resultant flightpath, as measured by the guidance system, is not the desired flightpath, the guidance system issues steering signals to direct the vehicle to the desired flightpath. Vehicle stabilization is accomplished in the same manner as in the rate-stabilization-only mode. The pitch and yaw rate stabilization signals are algebraically summed with the appropriate pitch and yaw steering signals from the guidance system. The resultant signals are used to control and stabilize the vehicle.

Figure VI-84 is a simplified diagram of the interface between the guidance system and the flight control system.

Guidance System

System description. - The Centaur guidance system performs the following functions:

(1) Measures vehicle acceleration in fixed inertial coordinates

(2) Computes the value of actual vehicle velocity and position, and computes the vehicle flightpath to attain the trajectory injection point

(3) Compares the actual position to the desired flightpath and issues steering signals

(4) Issues discrete commands

The Centaur guidance system is an inertial system which becomes completely independent of ground control approximately 10 seconds before lift-off of the vehicle. The guidance system consists of five separate units. Three of the units form an inertial measurement group. A simplified block diagram of the guidance system is shown in figure VI-85.

Inertial measurement group: Vehicle acceleration is measured by

(1) The inertial platform unit, which contains the platform assembly, gyros, and accelerometers

(2) The pulse rebalance, gyro torquer, and power supply unit, which contains the electronics associated with the accelerometers

(3) The platform electronics unit, which contains the electronics associated with the gyros

The platform assembly uses four gimbals which provide a three-axis coordinate system. The use of four gimbals, instead of three, allows complete rotation of all three vehicle axes about the platform without gimbal lock. Gimbal lock is a condition in which two axes coincide, causing loss of one degree of freedom. A gimbal diagram is shown in figure VI-86. The azimuth gimbal is isolated from movements of the vehicle airframe by the other three gimbals. The inertial components (three gyros and three accelerometers) are mounted on the azimuth or inner gimbal. A gyro and an accelerometer are mounted as a pair with their sensing axes parallel. The gyro and accelerometer pairs are also alined on three mutually perpendicular (orthogonal) axes corresponding to the three axes of the platform.

The three gyros are identical and are of the single-degree-of-freedom, floated-gimbal, rate-integrating type. Each gyro monitors one of the three axes of the platform. These gyros are elements of control loops the sole purpose of which is to maintain each axis fixed in inertial space. The output signal of each gyro is connected to a servoamplifier whose output controls a direct-drive torque motor which moves a gimbal of the platform assembly. The orientation of the azimuth gimbal is fixed in inertial space and the outer roll gimbal is attached to the vehicle. The angles between the gimbals provide a means for transforming steering signals from inertial coordinates to vehicle coordinates. The transformation is accomplished by electromechanical resolvers, mounted between gimbals, to produce analog electrical signals proportional to the sine and cosine functions of the gimbal angles. These electrical signals are used for an analog solution of the mathematical equations for coordinate transformation by interconnecting the resolvers in a multiple resolver chain.

The three accelerometers are identical and are of the single-axis, viscous-damped, hinged-pendulum type. The accelerometer associated with each axis measures the change in vehicle velocity along that axis by responding to acceleration. Acceleration of the vehicle causes the pendulum to move off center. The associated electronics then produce precise current pulses to re-center the pendulum. These rebalance pulses are either positive or negative depending on an increase or decrease in vehicle velocity. These pulses, representing changes in velocity (incremental velocity), are then routed to the navigation computer for computation of vehicle velocity.

Proper flight operation requires alinement and calibration of the inertial measuring unit during launch countdown. The azimuth of the platform, to which the desired flight trajectory is referenced is alined by ground-based optical equipment. The platform is alined perpendicular to the local vertical by using the two accelerometers in the hori-

zontal plane. Each gyro is calibrated to determine its characteristic constant torque drift rate and mass unbalance along the input axis. The scale factor and zero bias offset of each accelerometer are determined. These prelaunch-determined calibration constants and scale factors are stored in the navigation computer for use during flight.

Navigation computer unit: The navigation computer unit is a serial, binary, digital machine with a magnetic drum memory. The memory drum has a capacity of 2816 words (25 bits per word) of permanent storage, 256 words of temporary storage, and six special-purpose tracks. Permanent storage is prerecorded and cannot be altered by the computer. The temporary storage is the working storage of the computer.

Incremental velocity pulses from the accelerometers are the information inputs to the navigation computer. The operation of the navigation computer is controlled by the prerecorded program. This program directs the computer to use the prelaunch equations, navigation equations, and guidance equations.

The prelaunch equations establish the initial conditions for the navigation and guidance equations. Initial conditions include (1) a reference trajectory, (2) launch-site values of geographical position, and (3) initial values of navigation and guidance functions. Based on these initial conditions the guidance system starts flight operation approximately 10 seconds before lift-off.

The navigation equations are used to compute vehicle velocity and actual position. Velocity is determined by algebraically summing the incremental velocity pulses from the accelerometers. An integration is then performed on the computed velocity to determine actual position. Corrections for the prelaunch-determined gyro and accelerometer constants are also made during the velocity and position computation to improve the navigation accuracy. For example, the velocity data derived from the accelerometer measurements are adjusted to compensate for the accelerometer scale factors and zero offset biases measured during the launch countdown. The direction of the velocity vector is also adjusted to compensate for the gyro constant torque drift rates measured during the launch countdown.

The guidance equations continually compare actual position and velocity with the position and velocity desired at the time of injection. Based upon this position comparison, steering signals are generated to guide the vehicle along an optimized flightpath to obtain the desired injection conditions. The guidance equations are used to generate four discrete commands: (1) booster engine cutoff, (2) sustainer engine cutoff backup, (3) Centaur main engine cutoff, and (4) "null" the propellant utilization system. The booster engine cutoff command and the sustainer engine cutoff backup commands are issued when the measured vehicle acceleration equals predetermined values. The Centaur main engine cutoff command is issued when the extrapolated vehicle orbital angular momentum equals that required for injection into orbit. The command to null the propellant utilization system is issued 15 seconds before the Centaur main engine cutoff command.

During the booster phase of flight, the navigation computer supplies pitch and yaw signals for steering the Atlas stage. From a series of predetermined programs, one pitch program and one yaw program are selected based on trajectory requirements and prelaunch upper-air wind soudings. The selected programs are entered and stored in the computer during launch countdown. The programs consist of pitch and yaw turning rates for specified time intervals from T + 15 seconds until booster engine cutoff. These programs permit changes to be made in the flight reference trajectory during countdown to reduce anticipated aerodynamic heating and structural loading conditions on the vehicle.

Signal conditioner unit: The signal conditioner unit is the link between the guidance system and the vehicle telemetry system. This unit modifies and scales guidance system parameters to match the input range of the telemetry system.

System performance. - The performance of the Centaur guidance system was satisfactory as indicated by the following orbital parameters which were determined by ground-based tracking of the spacecraft:

Orbital parameter	Units	AC-20		AC-19	
		Actual trajectory	Simulated trajectory	Actual trajectory	Simulated trajectory
Midcourse correction requirement[a]:					
Miss only	m/sec	0.9	0.8	1.9	0.5
	ft/sec	3.0	2.7	6.1	1.7
Miss plus time of flight	m/sec	2.18	0.9	2.01	0.7
	ft/sec	7.2	3.1	6.6	2.4
Inclination at injection	deg	43.36	43.37	31.01	30.98
Eccentricity at injection	--------	1.1815	1.1815	1.27489	1.2478
Energy at injection	km^2/sec^2	11.191	11.185	16.881	16.881
	ft^2/sec^2	1.2046×10^8	1.2039×10^8	1.8170×10^8	1.8170×10^8
Arrival time (Gmt)	--------	4:32 July 31, 1969	4:56.8 July 31, 1969	4:46.7 Aug. 5, 1969	4:39.9 Aug. 5, 1969

[a]The midcourse corrections required are given for both miss only and miss plus time of flight. They are calculated at 10 days out and would be required to hit the preflight launch vehicle target. This target is biased away from the final spacecraft target. Actual midcourse corrections performed by the spacecraft are presented in section V.

Discrete commands: All discrete commands were issued properly. Table VI-XV lists the discretes, the criteria for the issuance of the discretes, and the computed values at the time the discretes were issued. Actual and predicted times from lift-off are also shown for reference only.

Guidance steering loop: The pitch and yaw steering signals issued by the guidance system are proportional to the components of the steering vector (desired vehicle point-

ing vector) along the vehicle pitch and yaw axes. In this section of the report, the steering signals have been converted into the approximate angular attitude errors between the steering vector and the vehicle roll axes (vehicle pointing vector) in the pitch and yaw planes. During the sustainer phase of flight and during Centaur main engine firing, the attitude errors were negligible, for both flights, except at times when steering was disabled or when a sudden change in the steering vector occurred.

Attitude errors at guidance steering activation are tabulated below:

Event	Units	AC-20		AC-19	
		Pitch	Yaw	Pitch	Yaw
Sustainer enable	deg	7.8 nose up	2.7 nose left	11.6 nose up	1.0 nose right
Centaur enable	deg	6.5 nose up	7.8 nose left	2.0 nose up	2.0 nose right

After MECO a launch-time-dependent spacecraft separation attitude vector is generated by the airborne computer. This maneuver is followed by spacecraft separation, and then the final retrovector is generated and the vehicle is reoriented to this attitude. This sequence of events for both vehicles is tabulated below:

Orient to-	Flight	Time, T + sec		Attitude - direction
		Began	Completed	
Spacecraft separation vector	AC-20	728	801	88^{o} pitch plane
	AC-19	715	788	87^{o} pitch plane
Centaur reorient vector	AC-20	1091.2	1151	74^{o} plus in pitch and minus in yaw
	AC-19	1078.8	1156	70^{o} plus in pitch and minus in yaw

Gyro control and accelerometer loops: The accelerometer loops operated satisfactorily. The accelerometer pendulum offsets from null remained within a band of approximately 2 arc-seconds throughout the AC-19 and AC-20 flights. The gimbal control loops operated satisfactorily and the inertial platform of each system remained stable during the AC-20 and AC-19 flights. The maximum gimbal displacement errors, as well as the angle and time of fourth gimbal uncaging, are tabulated below:

Gimbal	AC-20	AC-19
	Displacement time, arc-sec	
1	+13 -10	+10 -10
2	+8 -8	+8 -5
2	+18 -12	+12 -9
4	+335 -335	+335 -352
Uncaging gimbal 4: Time, T + sec Angle, deg	 51.7 20	 51.5 20

Other measurements: All the guidance system signals and measurements which were monitored during the flight were normal and indicated satisfactory operation of the guidance system. On AC-20 the skin temperature of a similar package was 288 K (58.2° F) at lift-off and had decreased to 287 K (56° F) by T + 2200 seconds. On AC-19 the skin temperature of the pulse rebalance electronics was 302 K (84.6° F) at lift-off and decreased to 297 K (75° F) by T + 2200 seconds.

Flight Control Systems

System description - Atlas. - The Atlas flight control system provides the primary functions required for vehicle stabilization, control, sequencing, and execution of guidance steering signals; and consists of the following major units:

(1) The displacement gyro unit, which contains three single-degree-of-freedom, floated, rate-integrating gyros and associated electronic circuitry for gain selection and signal amplification: These gyros are mounted to the vehicle airframe in an orthogonal triad configuration alining the input axis of a gyro to its respective vehicle axis of pitch, yaw, or roll. Each gyro provides an electrical output signal proportional to the integral of the time rate of change of angular displacement from the gyro reference axis.

(2) The rate gyro unit, which contains three single-degree-of-freedom, floated rate gyros and associated electronic circuitry: These gyros are mounted in the same manner as the displacement gyro unit. Each gyro provides an electrical output signal proportional to the angular rate of rotation of the vehicle about the gyro input (reference) axis.

(3) The servoamplifier unit, which contains electronic circuitry to amplify, filter, integrate, and algebraically sum combined position and rate signals with engine position feedback signals: The electrical outputs of this unit direct the hydraulic actuators which gimbal the engines to provide thrust vector control.

(4) The programmer unit, which contains an electronic timer, arm-safe switch, high-, low-, and medium-power electronic switches, and circuitry to set the roll program from launch ground equipment: The programmer issues discrete commands to other units of the Atlas flight control system, to Atlas propulsion and pneumatic systems, to vehicle separation systems, and to the Centaur flight control system.

System performance - Atlas. - The Atlas flight control system performed satisfactorily for the AC-20 and AC-19 flights, except for early actuation of the booster staging backup accelerometer on AC-20, which caused booster engine cutoff to be about 4.9 seconds earlier than expected. The vehicle dynamic responses resulting from each flight event were evaluated in terms of amplitude, frequency, and duration as observed on rate gyro data (see table VI-XVI). In this table, the control capability is the ratio of engine gimbal angle used to the available total engine gimbal angle, in percent. The control capability value includes that necessary for correction of the vehicle transient disturbances and for steady-state requirements. In the remainder of this section, all numbers indicative of performance are the maximum values observed on the AC-20 and AC-19 flights.

The programmer was started at approximately T + 1 second by the 1.1-meter-(42-in.) rise disconnect. At this time the flight control system began to issue signals to gimbal the engines for vehicle control. An unusually high roll transient was experienced on AC-19. The peak-to-peak roll rate reached 7.62 degrees per second by T + 1 second and was damped within 1.0 second. The cause of the size of this transient is unknown.

The roll program was initiated at T + 2 seconds to roll the vehicles to the desired flight azimuths. The roll rate, which depended upon the launch pad and flight azimuth orientations, continued for approximately 13 seconds. The pitch program was initiated

at T + 15 seconds. The subsequent pitch rates varied for each flight due to the pitch programs which were selected in accordance with flight trajectory and launch day upper-wind data. Rate gyro data indicated that the periods of maximum aerodynamic loading for the two flights were generally from T + 75 to T + 95 seconds. During these periods a maximum of 40 percent (AC-20) of the control capability was required to overcome both steady-state and transient loading.

The Atlas booster engine was cut off at T + 150.4 seconds on AC-19. On AC-20 a malfunction of the Atlas staging accelerometer, which provides backup staging commands to the flight control programmer, caused initiation of the 28-volt signal at T + 144 seconds. The staging sequence did not start until T + 147.1 seconds, when the programmer booster engine cutoff (BECO) logic was enabled. At T + 147.1 booster engine cutoff occurred; this was 4.9 seconds premature. The rates imparted to either of the vehicles by the BECO transient required a maximum of 16 percent (AC-20) of the sustainer engine gimbal capability. The Atlas booster engine section was jettisoned about 3 seconds after booster engine cutoff. The maximum angular rate imparted by this disturbance was 4.49 degrees per second (AC-19) in the yaw plane.

During the Atlas booster phase of the flights, the Atlas flight control system provided the vehicle attitude reference. At approximately BECO + 8 seconds the Centaur guidance system provided the attitude reference. The transfer of attitude reference from Atlas to Centaur required a maximum of 28 percent of the total control capability (AC-20). The maximum vehicle rate transient during this change was a pitch rate of 3.16 degrees per second, peak-to-peak, with a duration of 12 seconds.

The observed vehicle rate transients resulting from insulation panel jettison and nose fairing jettison events were damped within 2 seconds and required 8 percent of the control capability. Only small transients were observed at sustainer engine cutoff. Atlas/Centaur separation was smooth, with resulting transient rates of less than 1.1 degrees per second.

System description - Centaur. - The Centaur flight control system provides the primary means for vehicle stabilization and control, execution of guidance steering signals, and timed switching sequences for programmed flight events. The Centaur flight control system (fig. VI-87) consists of the following major units:

(1) The rate gyro unit, which contains three single-degree-of-freedom, floated rate gyros with associated electronics for signal amplification gain selection and conditioning of guidance steering signals: These gyros are mounted to the vehicle in an orthoginal triad configuration alining the input axis of each gyro to its respective vehicle axis of pitch, yaw, or roll. Each gyro provides an electrical output signal proportional to the angular rate of rotation of the vehicle about the gyro input (reference) axis.

(2) The servoamplifier unit, which contains electronics to amplify, filter, integrate, and algebraically sum combined position and rate signals with engine position feedback

signals: The electrical outputs of this unit issue signals to the hydraulic actuators which control the gimbaling of the engines. In addition, this unit contains the logic and threshold circuitry controlling the engines of the hydrogen peroxide attitude control system.

(3) The electromechanical sequence timer unit, which contains a 400-hertz synchronous motor to provide the time reference and actuate switches at program times.

(4) The auxiliary electronics unit which contains logic, relay switches, transistor switches, power supplies, control circuitry for the electromechanical timer, circuitry for conditioning computer-generated discretes, and an arm-safe switch: The arm-safe switch electrically isolates valves and pyrotechnic devices from the control switches. The combination of the electromechanical timer units and the auxiliary electronics unit issues discretes to other units of the Centaur flight control system, and to the propulsion, pneumatic, hydraulic, separation, propellant utilization, telemetry, spacecraft, electrical, and Atlas flight control systems.

Vehicle steering during Centaur powered flight is by thrust vector control through gimbaling of the two main engines. There are two actuators for each engine to provide pitch, yaw, and roll control. Pitch control is accomplished by moving both engines together in the pitch plane. Yaw control is accomplished by moving both engines together in the yaw plane, and roll control is accomplished by moving the engines differentially in the yaw plane. Thus, the yaw actuator responds to an algebraically summed yaw-roll command. By controlling the direction of thrust of the main engines, the flight control system maintains the flight of the vehicle on a trajectory directed by the guidance system. After main engine cutoff, control of the vehicle is maintained by the flight control system through selective firing of hydrogen peroxide engines. A more complete description of the engines and the propellant supply for the attitude control system is presented in the section PROPULSION SYSTEMS.

The logic circuitry, which commands the 14 hydrogen peroxide engines either on or off, is contained in the servoamplifier unit of the flight control system. Figure VI-88 shows the alphanumeric designations of the engines and their locations on the aft end of the vehicle. Algebraically summed position and rate signals are the inputs to the logic circuitry. The logic circuitry provides five modes of operation designated "all off," "separate on," "A and P separate on," "V half on," and "S half on." These modes of operation are used during different periods of the flight and are controlled by the sequence timer unit. A summary of the modes of operation is presented in table VI-XVII. In this table "threshold" designates the vehicle rate in degrees per second that has to be exceeded before the engines are commanded "on."

System performance - Centaur. - The Centaur flight control system performances were satisfactory for AC-20 and AC-19. Vehicle stabilization and control were maintained throughout the flights. All events sequenced by the timer were executed at the re-

quired times. (Refer to fig. VI-83 for the time periods of guidance and flight control and attitude control system modes of operation.) Except where otherwise noted, all numbers indicative of performance are the maximum values observed on the AC-20 and AC-19 flights. Vehicle dynamic responses for selected flight events are tabulated in table VI-XVI. The following evaluation of system performance is presented in the order of time-sequenced portions of the flight.

Sustainer engine cutoff to Centaur main engine cutoff: The Centaur timer was started at Atlas sustainer engine cutoff by commands from the Atlas programmer. Appropriate commands were issued to separate the Centaur stage from the Atlas stage and to initiate the Centaur main engine prestart sequence. There were no significant vehicle transients during Atlas/Centaur separation for the AC-20 and AC-19 flights. Vehicle control was maintained during the period between sustainer engine cutoff and main engine start by gimbaling the main engines; at this time the Centaur main engines were discharging boost pump turbine exhaust products and chilldown flow. The maximum angular rate due to main engine start transients was a pitch rate of 6.79 degrees per second (AC-19), peak-to-peak, indicating a large differential impulse. When guidance steering was enabled, 4 seconds after main engine start, the maximum steering command for the two flights was 3.76 degrees per second in pitch (AC-20). Vehicle transients resulting from guidance steering enable and main engine start disturbances were damped out within 8 seconds on both flights. Vehicle steady-state angular rates during the periods of closed-loop control were less than 1.3 degrees per second. The maximum angular rate imparted to the vehicles at main engine cutoff was measured in pitch and was 5.88 degrees per second (AC-19), peak-to-peak.

Centaur main engine cutoff through retrothrust: The hydrogen peroxide attitude control system was activated at the time of Centaur engine cutoff in the A and P separate-on mode (see table VI-XVII). Angular rates imparted to the vehicles resulting from differences in the shutdown characteristics of the two Centaur main engines were reduced to acceptable control levels in 1.5 seconds. During the time from main engine cutoff (MECO) to spacecraft separation, the vehicle alined to the separation vector. Rates of the vehicles just prior to spacecraft separation were less than 0.1 degree per second, well within spacecraft requirements. Spacecraft separation occurred approximately 95 seconds after MECO. On AC-19, roll control thrusting occurred at approximately 0.1 second before the separation event; this thrusting had a negligible effect upon separation dynamics. No pitch and yaw control thrusting occurred. On AC-20 and AC-19, the Centaur angular rates following spacecraft separation were less than 0.60 degree per second. For about the next 270 seconds, the Centaurs had no scheduled events and maintained attitude with A and P separate-on mode. Following this period, the retromaneuver sequence was initiated. After the vehicles turned approximately 74°, the V half-on mode was initiated. The V engines provided 445 newtons (100 lbf) of thrust for 40 seconds.

These maneuvers increased the lateral separations between Centaur and the spacecrafts and minimized impingement of the residual propellants on the spacecrafts during the subsequent periods of retrothrust. The S half-on mode was then employed for 350 seconds to continue increasing the separation distance while using less hydrogen peroxide and maintaining attitude control. This period is followed by the concurrent switch to the separate-on mode of control and the initiation of retrothrust. As expected, vehicle disturbance torques increased as a result of propellant discharge but were well within control limits.

TABLE VI-XV. - DISCRETE COMMANDS, AC-20 AND AC-19

Discrete command	Criteria for discrete to be issued	Discrete issued at this computed value		Actual time, T + sec		Predicted time, T + sec	
		AC-20	AC-19	AC-20	AC-19	AC-20	AC-19
Booster engine cutoff	When square of vehicle thrust acceleration is greater than 27.53 g's $(5.25\ g's)^2$	(a)	28.15 g's $(5.31\ g's)^2$	(a)	150.4	152.0	152.5
Sustainer engine cutoff backup	When the square of vehicle thrust acceleration is less than $(0.54\ g)^2$	----	$(0.32\ g)^2$	276.2	259.0	248	248
Null propellant utilization system	A maximum of 33 seconds prior to main engine cutoff discrete	28.2	26.9	697.3	685.3	681	681
Main engine cutoff	Computer-calculated time	----	---------	725.5	712.2	699.6	701.5

[a]The L3 discrete was not generated by guidance because booster engine cutoff had been prematurely issued by a faulty backup accelerometer on the first stage.

TABLE VI-XVI. - VEHICLE DYNAMIC RESPONSE FLIGHT DISTURBANCES, AC-20 AND AC-19

Event	Time,[a] T + sec		Measurement	Rate gyro peak-to-peak amplitude, deg/sec		Transient frequency, Hz		Transient duration, sec		Required control capability, percent	
	AC-20	AC-19		AC-20	AC-19	AC-20	AC-19	AC-20	AC-19	AC-20	AC-19
Lift-off	0	0	Pitch	6.48	1.10	0.77	~40	3	----	(b)	(b)
			Yaw	1.05	1.12	.56	~30	3	----	(b)	(b)
			Roll	3.04	.74	.56	~40	.2	----	(b)	(b)
1.1 Meter (42-in.) rise	1	1	Pitch	1.76	1.84	6.3	10	2	2	24	18
			Yaw	.88	.37	5.9	35	2	2	4	4
			Roll	.72	7.62	5.0	3.3	.2	1	4	4
Region of maximum aerodynamic pressure (75-95)	92	87	Pitch	1.58	1.56	0.22	Mixed	8	20-sec period	32	34
	91	86.5	Yaw	1.93	1.68	.27	Mixed	9		40	20
	91	86.5	Roll	1.79	1.68	.25	Mixed	9		40	20
Booster engine cutoff	146.2	150.6	Pitch	1.93	3.67	50	10	3.0	3	16	4
			Yaw	1.93	1.68	50	12.5	3.0	3	16	4
			Roll	2.06	2.42	.63	1.25	2.5	1.9	16	4
Booster engine section jettison	149.1	153.5	Pitch (Low frequency)	7.17	1.47	7.7	6.76	4	2	(c)	(c)
			Yaw (Low frequency)	1.93	4.49	.5	6.76	3	(d)	(c)	(c)
			Roll (Low frequency)	1.07		1.25		4	----	(c)	(c)
			Pitch (High frequency)	7.18	----	30	-----	0.5	----	(c)	(c)
			Yaw (High frequency)	5.97	----	30	-----	.5	----	(c)	(c)
			Roll (High frequency)	7.35	3.42	50	30	.5	0.2	(c)	(c)
Admit guidance	154.1	158.6	Pitch	3.16	3.00	0.09	0.09	12	16	24	8
			Yaw	1.58/2.98	1.31	6.25/0.25	.17	7.9	8	28	10
			Roll	1.07	.65	.83	1.25	5	6	8	6
Insulation panel jettison	190.7	195.2	Pitch	3.14	3.45	30	40	1.2	0.5	4	4
			Yaw	2.02	2.34	40	35	.7	.5	8	4
			Roll	1.43	1.12/1.5	40	30/6.7	.9	.7	8	6
Nose fairing jettison	227.5	231.9	Pitch	5.16	0.53	35	35	1.7	1.1	4	2
			Yaw	2.72	1.77	35	40	1.0	.7	8	2
			Roll	3.22	2.13	35	40	1.5	.3	4	4
Sustainer engine cutoff	253.9	253.9	Pitch	1.22	2.02	40	40	2.2	2	---	---
			Yaw	.74	.84	40	40	2.2	(e)	---	---
			Roll	.84	.84	25 and 40	40	1.7	2	---	---
Atlas/Centaur separation	256.9	256.9	Pitch	1.31	1.1	40	40	0.2	0.7	---	---
			Yaw	.55	.84	40	35	.2	(e)	---	---
			Roll	.65	.37	40	40	.2	(e)	---	---
Main engine start	282.5	267.5	Pitch (High frequency)	1.57	----	40	-----	3	----	32	---
			Yaw (High frequency)	1.05	0.75	30	30	3	0.3	32	12
			Roll (High frequency)	.89	----	40	-----	3	----	32	---
			Pitch (Low frequency)	4.38	6.79	0.5	0.5	2.2	(d)	32	56
			Yaw (Low frequency)	.88	----	.67	-----	3	----	32	---
			Roll (Low frequency)	4.30	3.16	.45	.67	3	(d)	32	12
Admit guidance	286.5	271.5	Pitch	3.76	3.67	0.21	0.24	8	6	20	36
			Yaw	3.08	1.31	.24	.22	8	6	24	8
			Roll	.54	1.21	1.25	.67	3	5	24	8
Main engine cutoff	724.6	712.3	Pitch	5.77	5.88	30	40	1.5	1.3	16	(f)
			Yaw	4.56	5.24	30	40	1.0	.5	16	(f)
			Roll	3.94	2.23	35	40	1.2	.2	16	(f)
			Roll	90	1.86	1	.67	1.2	1.5	16	(f)

[a] Time of transient as indicated on rate gyro data.
[b] Flight control system not active.
[c] Sustainer engine control inactive during booster engine section jettison.
[d] Until "admit guidance."
[e] Too small to measure.
[f] Engine gimbal data not yet recorded.

TABLE VI-XVII. - DESCRIPTION OF ATTITUDE CONTROL SYSTEM MODES OF OPERATION, AC-20 AND AC-19

[A engines, 16.6 N (3.5 lbf) thrust; P engines, 26.7 N (6.0 lbf) thrust; S engines, 13.3 N (3.0 lbf) thrust; V engines, 222.4 N (50 lbf) thrust.]

Mode	Flight period	Description
All off	Powered phase	This mode inhibits the operation of all attitude control engines.
Separate on	Main engine cutoff (MECO) plus 850 seconds until end of flight	When in the separate-on mode a maximum of two V and two A engines and one P engine fire. These engines fire only when appropriate error signals surpass their respective thresholds. A engines: when a 0.2-deg/sec threshold is exceeded, suitable A engines fire to control in yaw and roll. A_1A_4 and A_2A_3 combinations are inhibited. P engines: when 0.2-deg/sec threshold is exceeded, suitable P engine fires to control in pitch. P_1P_2 combination is inhibited. S engines: off V engines: when 0.3-deg/sec threshold is exceeded, suitable V engines fire (as a backup for higher rates). V_1V_3 and V_2V_4 combinations are inhibited.
A and P separate on	MECO until MECO + 460 seconds	This mode is the same as separate-on mode, except V engines are inhibited.
V half on	MECO + 460 seconds until MECO + 500 seconds	In this mode the engines perform as follows: A engines: when 0.2-deg/sec threshold is exceeded, suitable A engines fire to control in roll only. P engines: off S engines: off V engines: when there are no error signals, V_2V_4 combination fires continuously. This continuous firing provides increased lateral separation.
S half on	MECO + 500 seconds until MECO + 850 seconds	In this mode the engines perform as follows: A engines: when 0.2-deg/sec threshold is exceeded, suitable A engines fire to control in roll only. P engines: off S engines: when there are no error signals, S_2S_4 combination fires continuously. When 0.2-deg/sec threshold is exceeded, a minimum of two and a maximum of three S engines fire to control in pitch and yaw. V engines: when 0.3-deg/sec threshold is exceeded, a minimum of one and a maximum of two V engines fire to control in pitch and yaw. When a V engine fires, the corresponding S engine is commanded off.

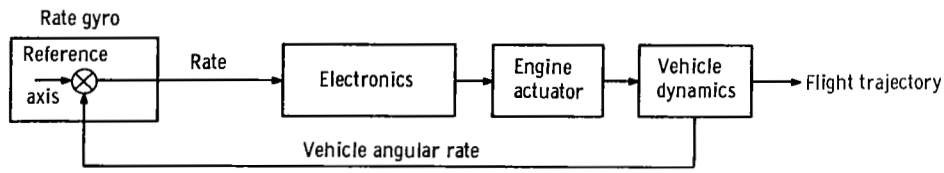

(a) Rate-stabilization-only mode.

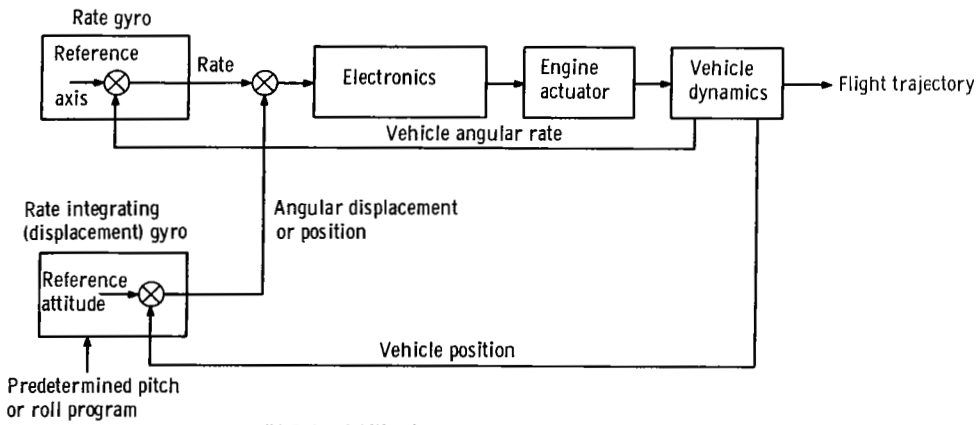

(b) Rate-stabilization-and-attitude-control mode.

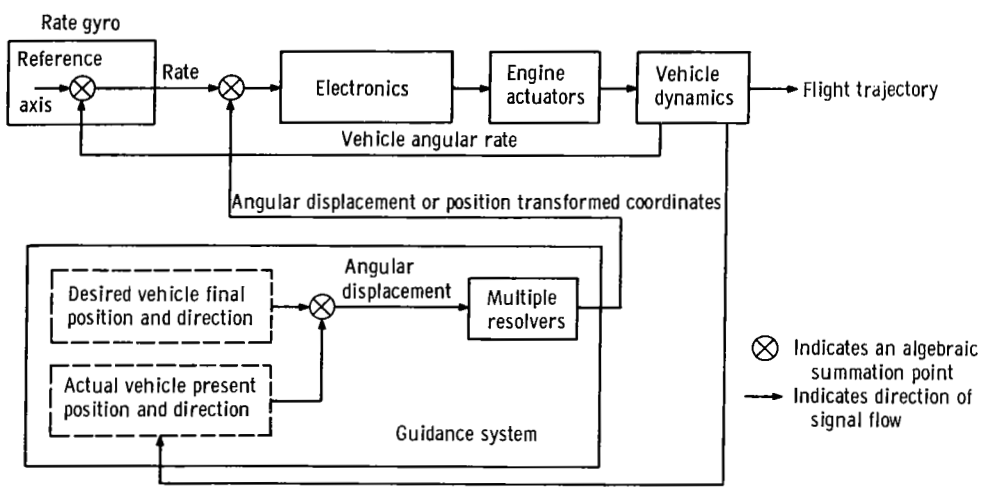

(c) Rate-stabilization-and-guidance-control mode.

CD-10611-31

Figure VI-82. - Guidance and flight control modes of operation, AC-20 and AC-19.

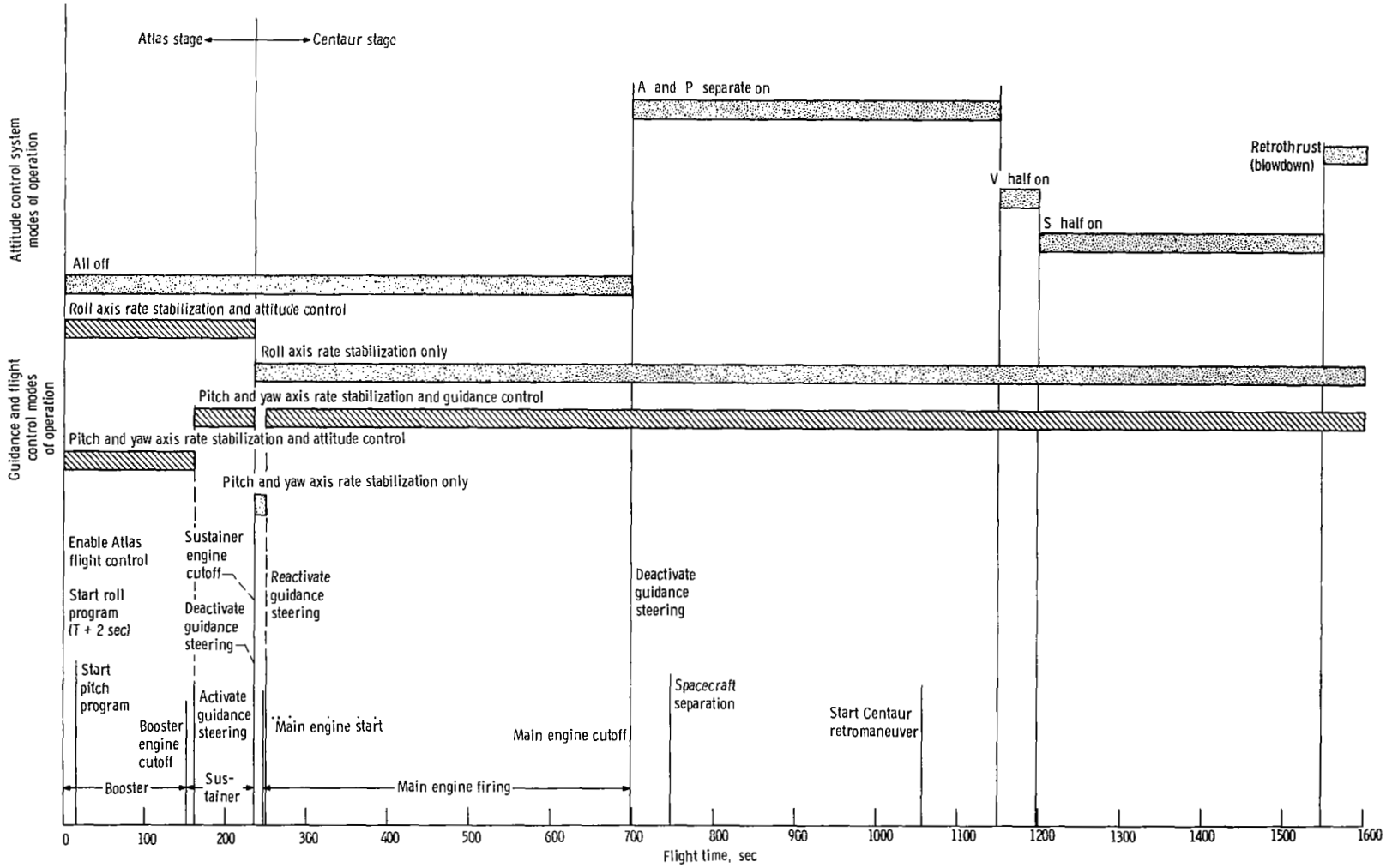

Figure VI-83. - Time periods of guidance and flight control modes and attitude control system modes of operation, AC-20 and AC-19. (There is no rate control during a 3.5-second period following sustainer engine cutoff because the engines are not developing thrust.)

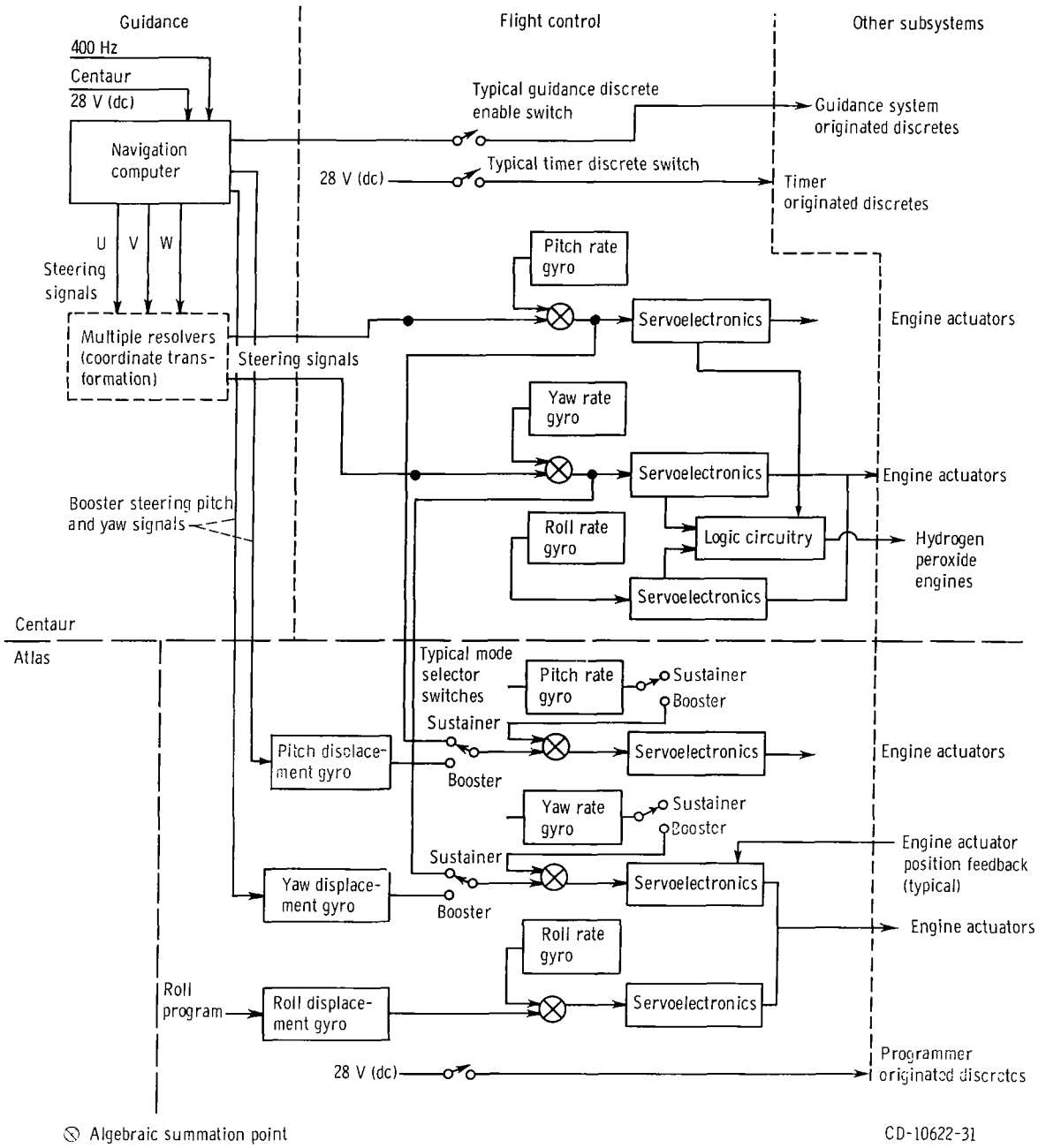

Figure VI-84. - Simplified guidance and flight control systems interface, AC-20 and AC-19.

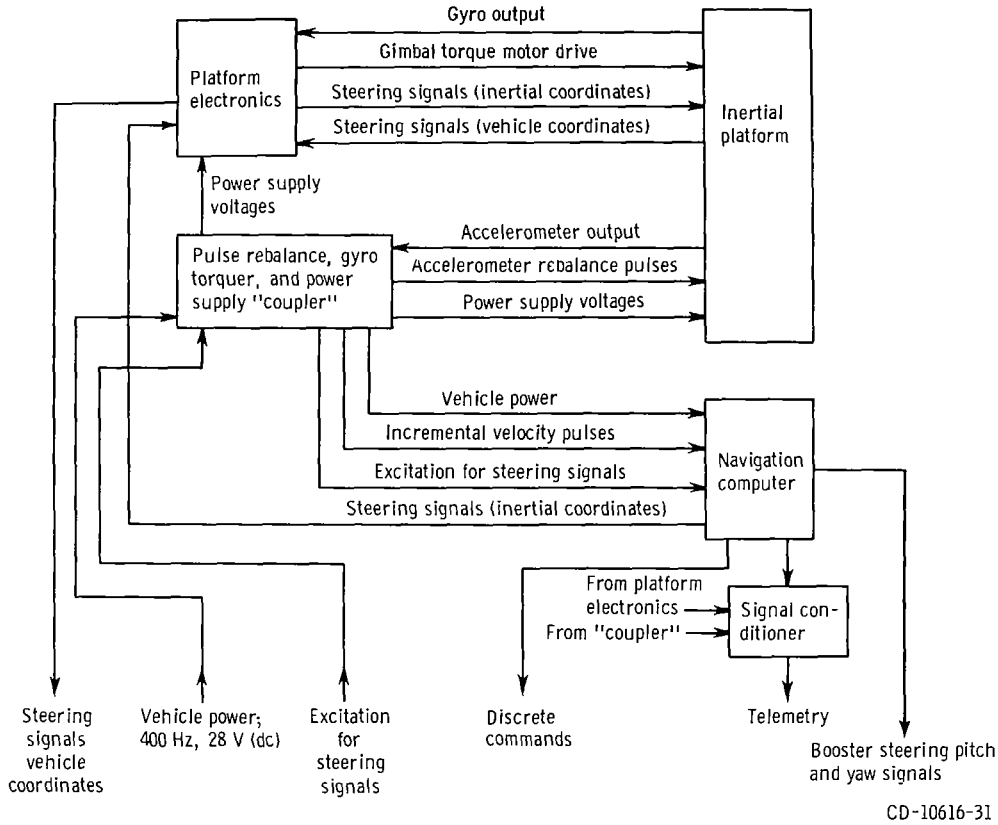

Figure VI-85. - Simplified block diagram of Centaur guidance system, AC-20 and AC-19.

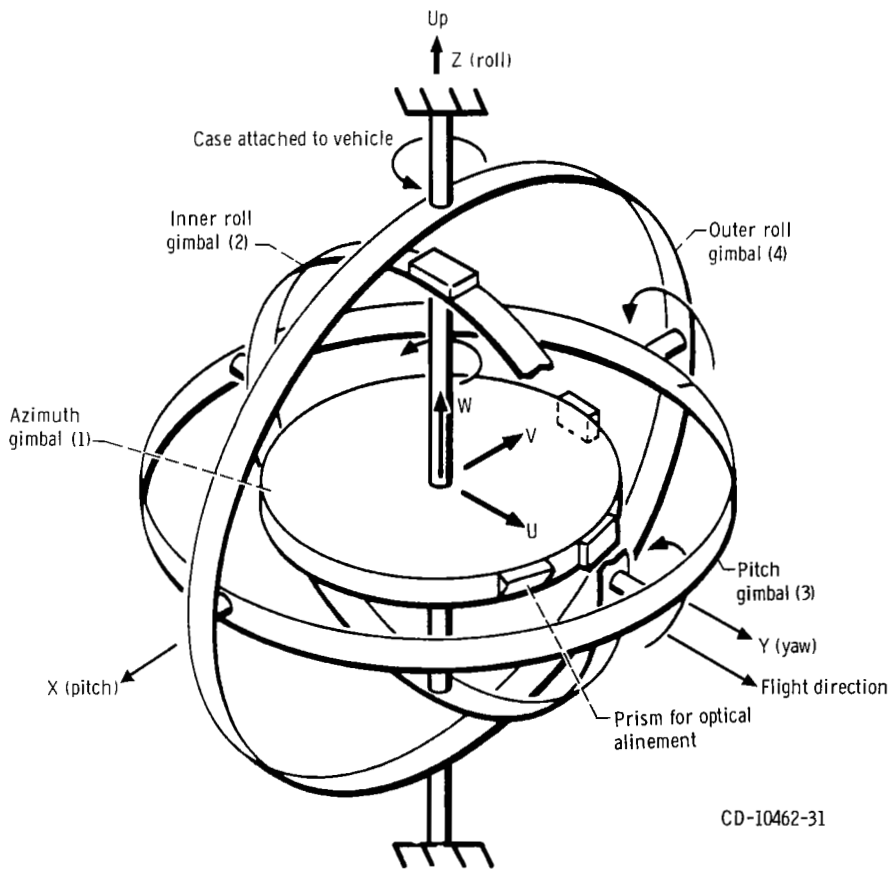

Figure VI-86. - Gimbal diagram, AC-20 and AC-19. Launch orientation: inertial platform coordinates, U, V, and W; vehicle coordinates, X, Y, and Z.

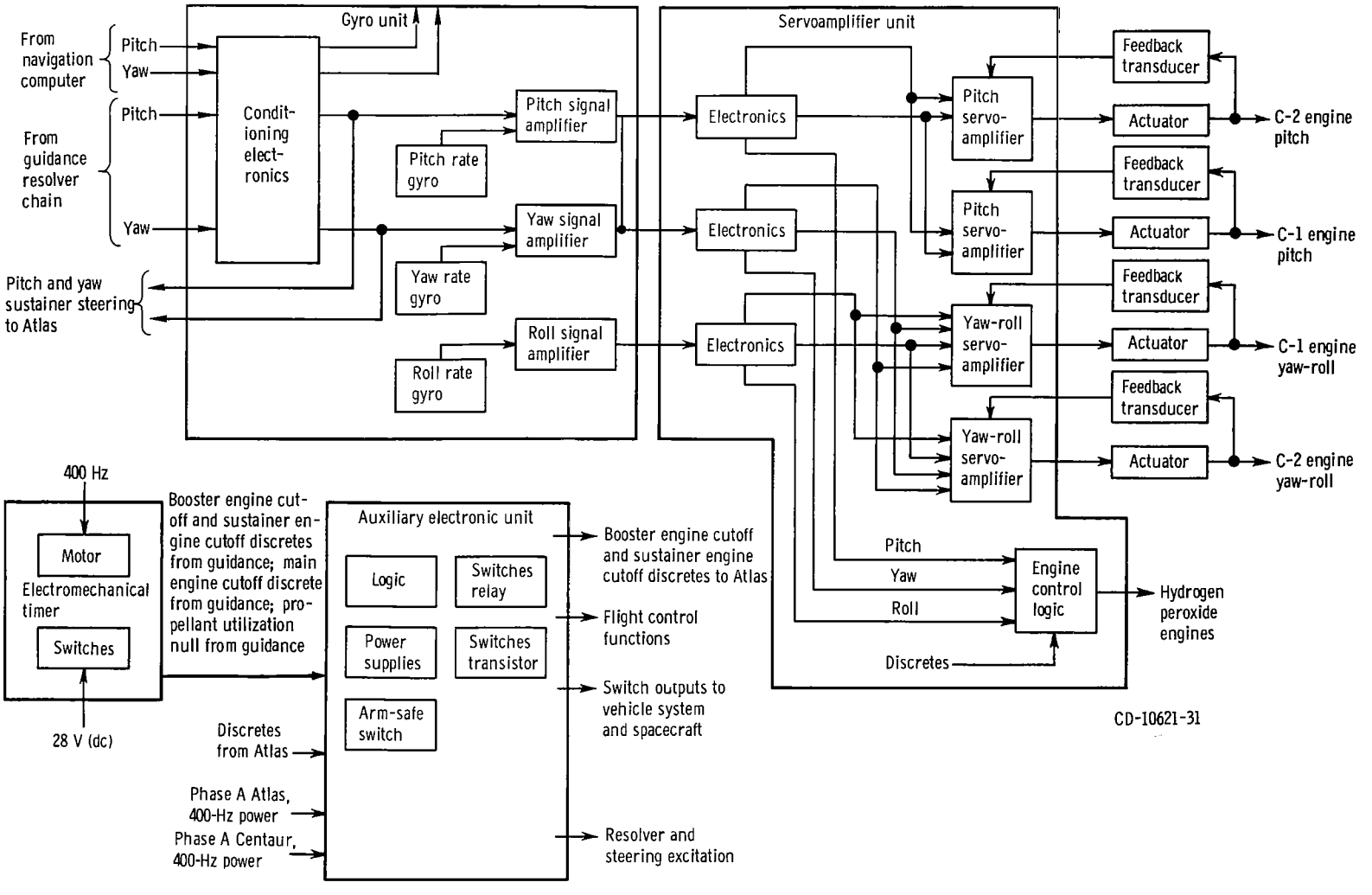

Figure VI-87. - Centaur flight control system, AC-20 and AC-19.

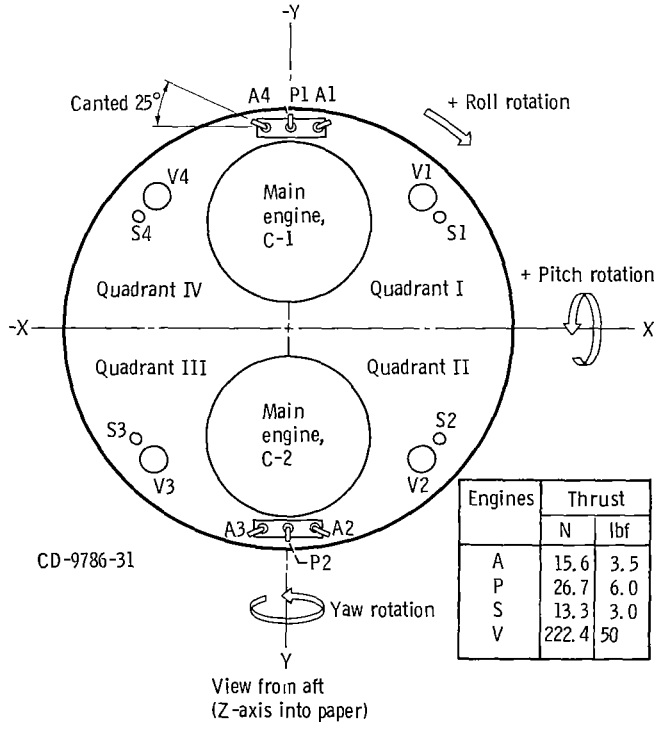

Engines	Thrust	
	N	lbf
A	15.6	3.5
P	26.7	6.0
S	13.3	3.0
V	222.4	50

Figure VI-88. - Attitude engines alphanumeric designations and locations, AC-20 and AC-19. Signs of axes are convention for flight control system.

VII. CONCLUDING REMARKS

The AC-20 and AC-19 launch vehicles successfully placed Mariner VI and Mariner VII spacecraft onto the proper transfer orbits for flying by the planet Mars. Mariner VI made an equatorial pass near the Martian surface and Mariner VII made a pass near the Martian southern polar ice cap 5 days later. These orbits were selected in order to obtain data as different as possible on the atmospheric environment and geographic features of the planet. The spacecraft missions were successful.

Both launch vehicles used the direct-ascent mode to place Mariners VI and VII on type I heliocentric transfer trajectories to the planet Mars. Orbital insertion on these flights was accurate. In terms of launch vehicle injection accuracy, the midcourse correction (miss distance plus time of arrival) required to meet target specifications was 2.18 meters per second for Mariner VI and 2.01 meters per second for Mariner VII. These corrections were well within the maximum allowable correction of 13.5 meters per second.

The configuration of the launch vehicles was similar for both flights. All launch vehicle systems performed satisfactorily except that booster engine cutoff occurred approximately 5 seconds early on the Mariner VI flight. Because of the early booster engine cutoff on AC-20, sustainer engine cutoff occurred 18.5 seconds later than expected. The total launch vehicle performance was not significantly affected by the early booster engine cutoff anomaly, and all mission objectives were achieved.

Lewis Research Center,
National Aeronautics and Space Administration,
Cleveland, Ohio, December 11, 1970,
491-02.

REFERENCES

1. Gerus, Theodore F.; Housely, John A.; and Kusic, George: Atlas-Centaur-Surveyor Longitudinal Dynamics Tests. NASA TM X-1459, 1967.

2. Foushee, B. R.: Liquid Hydrogen and Liquid Oxygen Density Data for Use in Centaur Propellant Loading Analysis. Rep. AE62-0471, General Dynamics Corp., May 1, 1962.

3. Pennington, K., Jr.: Liquid Oxygen Tanking Density for the Atlas-Centaur Vehicles. Rep. BTD65-103, General Dynamics Corp., June 3, 1965.

NASA-Langley, 1971 —— 31 E-6013